Model-based process design and solvent selection for the efficient recovery of homogeneous catalyst in chemicals production

Dissertation
zur Erlangung des akademischen Grades

Doktoringenieur
(Dr.-Ing.)

von: Dipl.-Ing. Kevin McBride
geb. am: 22. Juli 1986
in: Hayward, CA, USA

genehmigt durch die Fakultät für Verfahrens- und Systemtechnik
der Otto-von-Guericke-Universität Magdeburg

Betreuer: Prof. Dr.-Ing. Kai Sundmacher
Gutachter: Prof. Dr. rer. nat. Arno Behr
                Prof. Dr.-Ing. Jens-Uwe Repke

eingereicht am: 1. Juni 2017
Promotionskolloquium am: 25. August 2017

Summary

Interest in homogeneous transition metal catalyzed (HTMC) reactions has led to the development of many interesting catalysts for a plethora of new, exciting reactions. However, one of the problems with homogeneous catalysis is their inherently difficult separation and recovery after the reaction. This is especially true when using expensive transition metals, such as rhodium, which owing to its relatively high activity, is used frequently in HTMC. If not adequately recovered, the economics of the process can become quickly infeasible.

This is the case for the hydroformylation of 1-dodecene, a reaction that has received much attention in the last few years as part of a wider research collaboration. The catalyst complex consists of a rhodium transition metal core with the phosphite ligand biphephos has been used in the majority of this research due to its high selectivity for linear aldehyde products. The downside to using this catalyst complex is, again, related to the small amounts lost through leaching in the downstream separation. One prominent method used to recover the catalyst is by implementing a phase separation strategy using thermomorphic solvent systems (TMS). The catalyst is recovered in the polar phase after liquid-liquid phase separation upon cooling the post-reaction mixture and recycled for further use. However, the small amount of catalyst that distributes into the nonpolar phase can lead to substantial replacement costs rendering the process uneconomical.

The first part of this thesis addresses the economical aspects of TMS composition and catalyst recovery for a simplified process example of the hydroformylation of 1-dodecene. Previous process design problems for this reaction have ignored the cost of catalyst leaching, assuming complete recovery of the catalyst. This does not actually represent the reality of the situation and the work presented in this thesis shows that catalyst leaching comprises a solid majority of the process costs for the conventional TMS based process. Several areas for improvement in reducing catalyst leaching were identified as a result.

The second section of this work introduces a framework for designing TMS systems using quantum chemical tools, based on COSMO-RS. This computer-aided method integrates solvent solubility predictions into the TMS design procedure with the goal of designing TMS systems that more adequately recover the catalyst compared to the current system. Using this newly developed method, several TMS systems were identified

and successfully implemented experimentally in the hydroformylation of 1-dodecene and subsequent catalyst recovery. However, the top TMS identified using this methodology is the currently used mixture of dimethylformamide and decane, which was already shown to perform sub-optimally in the first part of this thesis.

Since the computer-aided TMS design did not improve upon the current solvent used, it is clear that a new separation strategy is required for improving catalyst recovery. In the third part of this thesis, a new extraction cascade is proposed to accomplish exactly this. Accurate surrogate models are developed to describe the LLE conditions and catalyst partitioning within a process-wide optimization problem. In this manner, the complete process including the reactor and extraction cascade can be simultaneously optimized to find the best economical conditions for the hydroformylation of 1-dodecene. It is shown that by using an extraction technique that catalyst recovery is improved and both investment and production costs are drastically reduced compared to the conventional TMS process.

Zusammenfassung

Das Interesse an mit Hilfe von Übergangsmetallen homogen katalysierten Reaktionen (im englischen HTMC) führte zur Entwicklung vieler, interessanter Katalysatoren. Diese ermöglichen die Durchführung einer Vielzahl neuer vielversprechender Reaktionen. Ein Problem homogener Katalysatoren stellt jedoch deren inhärent schwierige Abtrennung und Rückgewinnung nach der Reaktion dar. Dieser Umstand tritt besonders bei der Verwendung teurer Übergangsmetalle in HTMC ein. Ein Beispiel stellt Rhodium dar, welches aufgrund seiner relativ hohen Aktivität häufig eingesetzt wird.

Aufgrund der hohen Kosten dieser Katalysatoren ist die Wirtschaftlichkeit des Prozesses nur gewährleistet, wenn der Katalysator in ausreichendem Maße zurückgewonnen wird. Dies ist der Fall bei der Hydroformylierung von 1-Dodecen, einer Reaktion, die im Rahmen einer breit aufgestellten Forschungskollaboration des SFB/TR 63 in den letzten Jahren viel Aufmerksamkeit erfahren hat. Der Katalysatorkomplex besteht aus einem Rhodiumkern mit dem Phosphitliganden Biphephos, welcher wegen seiner hohen Selektivität für das lineare Aldehydprodukt bevorzugt eingesetzt wird. Der Nachteil der Verwendung dieses Katalysatorkomplexes besteht in kleinen Verlustmengen, die in der nachgeschalteten Trennung auftreten. Die Implementierung einer Phasentrennungsstrategie durch den Gebrauch eines thermomorphen Lösungsmittelsystems (TML) stellt eine bekannte Methode für die Rückgewinnung des Katalysators dar. Der Katalysator wird durch die Flüssig-Flüssig-Phasentrennung, die durch das Abkühlen der Reaktionsmischung erfolgt, in der polaren Phase gewonnen und zur weiteren Verwendung zurückgeführt. Allerdings können schon geringe Mengen Katalysator, die sich in der unpolaren Phase lösen, zu erheblichen Kosten durch die Nachführung frischen Katalysators führen, welche die Wirtschaftlichkeit des Prozesses stark beeinträchtigt.

Der erste Teil der Dissertation beschäftigt sich mit den wirtschaftlichen Aspekten der TML-Zusammensetzung und der Katalysatorrückgewinnung für ein vereinfachtes Prozessbeispiel der Hydroformylierung von 1-Dodecen. Bisherige Prozessentwürfe für diese Reaktion haben die Kosten des Katalysatorverlustes außer Acht gelassen und stattdessen die vollständige Rückgewinnung des Katalysators vorausgesetzt. Dies spiegelt nicht das reale Verhalten des Prozesses wieder. Die in dieser Arbeit durchgeführte Kostenanalyse zeigt, dass der Katalysatorverlust bei Nutzung des herkömmlichen TML-Systems einen erheblichen Teil der Prozesskosten ausmacht. Im Endeffekt konnten verschiedene Verbesserungsmöglichkeiten in Bezug auf den Katalysatorverlust identifiziert werden.

Im zweiten Teil der Dissertation wird ein methodischer Rahmen für die Gestaltung von TML-Systemen entwickelt, in welchem COSMO-RS basierte quantenchemische Berechnungsansätze genutzt werden. Diese computergestützte Methode kann Lösungsmittellöslichkeitsvorhersagen integrieren, um TML-Systeme zu entwerfen, die den Katalysator im Vergleich zum aktuellen TML-System, bestehend aus Dimethylformamid und n-Decan, besser zurückgewinnen. Verschiedene TML-Systeme wurden durch die Anwendung dieser neu entwickelten Methode identifiziert und für die Hydroformylierung von 1-Dodecen experimentell untersucht. Sowohl die Rückgewinnung des Katalysators als auch die Reaktion in den neu entwickelten TML-Systemen waren erfolgreich. Das vielversprechendste TML-System, das sich durch die Anwendung dieser Vorgehensweise herauskristallisiert hat, ist das momentan genutzte Gemisch aus Dimethylformamid und n-Decan, welches schon im ersten Teil dieser Doktorarbeit vorgestellt wurde.

Da mit Hilfe des computergestützen TML-Entwurfsverfahrens das bisherige Lösungsmittelsystem bestätigt werden konnten, ist eine neue Trennstrategie zur Verbesserung der Katalysatorrückgewinnung erforderlich. Im dritten Teil dieser Dissertation wird eine optimierte Trennstrategie entwickelt, um durch verbesserte Katalysatorrückgewinnung einen wirtschaftlicheren Prozess zu erhalten. Adäquate Ersatzmodelle wurden entwickelt, um das Flüssig-Flüssig-Gleichgewicht und die Aufteilung des Katalysators zwischen den entstehenden Lösungsmittelphasen innerhalb eines prozessweiten Optimierungsproblems quantitativ zu beschreiben. Der gesamte Prozess einschließlich des Reaktors und der Trennapparatestruktur kann in diesem Zusammenhang simultan optimiert werden, um die besten wirtschaftlichen Bedingungen für die Hydroformylierung von 1-Dodecen zu finden. Es wird aufgezeigt, dass die Rückgewinnung des Katalysators durch den Einsatz einer mehrstufigen Extraktionsprozesses verbessert wird und sowohl die Investitionskosten als auch die Produktionskosten im Vergleich zu einem konventionellen TML-Prozess drastisch reduziert werden.

To my family

Acknowledgements

Contents

List of Figures

List of Tables

1. Introduction

Research Vision

The chemical industry is faced with increasing demands for improved sustainability in chemical feedstocks and process design or methodology. A new paradigm of thought is required in order to restructure and reorient the conventional methods of process design towards these goals. One of these new development areas involves the use of process intensification strategies. These prioritize reducing the utility consumption of a process, increasing atom efficiency of reactions, improving economics, and various other criteria as outlined in the work by Lutze et al. [85].

One of the key technologies enabling the design of new processes with high selectivity and efficiency is homogeneous transition metal catalysis (HTMC). Not only does homogeneous catalysis offer milder reaction conditions in addition to improved performance, it also enables a plethora of new and different reactions to become industrially feasible (Behr and Johnen [9]). One of these important reactions is the hydroformylation of alkenes, the oldest and first reported HTMC reaction (Behr et al. [20]).

One area where HTMC can play an important role is in the functionalization of renewable feedstocks previously overlooked for industrial use. This is one of the major areas of inquiry within the *Sonderforschungsbereich Transregio 63* (SFB TRR/63), a joint research effort between the universities TU Berlin, TU Dortmund, and OvGU Magdeburg [2]. Here the desire is to increase the accessibility of renewable feedstocks within the chemical process industry by enabling concentrated research on potential reaction pathways, such as hydroformylation and hydroaminomethlylation. In the initial funding period of the SFB TRR/63, the hydroformylation of long-chain terminal alkenes was selected to be the primary reaction investigated. The hydroformylation of long-chain alkenes offers its own challenges in overcoming mass transfer limitations, achieving high reaction performance and regio-selectivity of the desired product, selecting the catalyst structure, and obtaining high catalyst recovery. A significant effort was placed into understanding these issues by targeted analysis of the hydroformylation

of 1-dodecene. This reaction was also considered in a subsequent funding period for further inquiry, leading expectedly to a large body of research which in turn gave rise to copious amounts of data, experience, and insights. Although this led to many innovations in how this reaction works in the presence of the chosen catalyst, one caveat remained: catalyst leaching and its economic burden.

Although homogeneous catalysis can deliver many benefits to a process such as high activity, good selectivity, robust catalyst systems, etc., separation and recycling of the catalyst can be quite cumbersome (Behr and Neubert [10]). In fact, about one in ten of all industrial reactions are homogeneously catalyzed, a trend that continues to increase. This growing interest is leading researchers towards focusing more effort on recovering the catalyst from the post-reaction mixture in downstream processes. This can be seen in the extensive amount of literature in the last few decades dealing with this issue.

Usually catalyst leaching is an issue due to the high price of the transition metal core, which frequently consists of palladium or rhodium. Efficient retention of rhodium is extremely important in many processes in order to maintain reasonable and competitive production costs (Fang et al. [43]). In the hydroformylation of long-chain alkenes, one of the most promising catalysts found consists of rhodium as the transition metal core coupled with the bidentate phosphite ligand biphephos. This is due to its high isomer selectivity for linear to branched aldehydes without a significant reduction in alkene conversion when compared to using only rhodium nano-particles (Behr et al. [17]). Despite the high performance of biphephos, one significant drawback is its price; even low levels (on the order of several ppm) of catalyst loss can lead to substantial process costs (McBride and Sundmacher [88]). Thus, not only is the rhodium metal leaching important, but the ligand leaching as well. In many hydroformylation studies, it is normally the rhodium leaching that is of primary (and often singularly) concern. These high costs lead to an economic bottleneck that needs to be overcome before practical use of this efficient catalyst can be considered industrially (Behr and Neubert [10]). In this case, process design and research efforts should prioritize the economical performance of the process by reducing catalyst leaching.

This is the reason for designing hydroformylation processes around either thermomorphic solvent systems (TMS) or surfactant based micelles solvent systems (MSS), the two main vehicles studied for catalyst recovery within the SFB. However, much of the initial work in catalyst recovery by the research collective was considered to be sufficient early on and more effort was spent in other key areas, such as reaction kinetics and miniplant development. Although the primary goal of the TMS is to recover the catalyst complex, it was assumed to perform its task successfully and the effects of catalyst loss were ignored in later reactor and process optimization schemes. This lead to an unclear picture of the true economically optimal process configuration and several questions about the feasibility of the process using this catalyst emerged from this dilemma. This thesis attempts to answer these questions.

Research Goals and Motivation

The primary objective of the work presented in this thesis is to find methods to improve catalyst recovery in the hydroformylation of 1-dodecene when using a TMS. This is to be accomplished using computational methods supported by performing experiments to collect data and to validate model-based predictions. The flow of this work does not follow an outlined plan developed at the onset. Instead, each subsequent project came about as an extension of the previous investigation's results and therefore the direction took on several different routes.

The initial part of this work undertakes the task of including catalyst leaching for both the rhodium metal and the catalyst ligand used within the current research collaborative in an economically driven process optimization problem. It has been widely discussed that catalyst leaching is expensive, particularly due to the use of rhodium as part of the catalyst complex. Therefore, discussions about catalyst loss are usually concerned about rhodium leaching levels. Many studies include catalyst ligand leaching but usually have ignored its cost or have briefly mentioned it as a future point to consider. Thus, an effort is made to include the cost of ligand leaching into the objective function. This is explored by using a simplified hydroformylation process in order to find areas that can be targeted for improvement.

One of these areas for improvement is the choice of the solvents used in the TMS. Therefore, the second step is to reevaluate the binary TMS system from a solvent design perspective. The most important criterion for solvent selection is the solubility of the catalyst in the designated catalyst phase or solvent. This also applies to the miscibility gap and general LLE behavior of the solvent system. It may be that the current solvents are suboptimal due to the absence of this consideration in their selection as TMS solvents. Thus, a method for solvent selection based on catalyst solubility is developed within an overall framework for TMS design. This is accomplished using quantum chemical representations of the catalyst ligand in solution in order to identify potential solvents based on catalyst solubility as well as other physical properties. Using the developed methodology, several potential solvent pairs are identified using purely computational means. Several candidate binary solvent systems are then validated experimentally for catalyst retention and reaction performance. It is shown that very similar solvents are found to those already considered for use in the hydroformylation of 1-dodecene.

Based on the results found in the solvent design practice, it became necessary to improve the TMS functionality prescribed on more than simply solvent selection. The single stage separation is the raison d'être for using a TMS but so far has not been economically sufficient for hydroformylation using the rhodium-biphephos catalyst. The third stage of this work is then to develop new separation techniques that reduce the amount of catalyst leaching and thus the utility cost of the process. This is realized using a series of decanters with additional catalyst, or polar, solvent used to further recover catalyst by means of extraction. The resulting arrangement is in essence a series of extraction stages. Additional capital costs must be compared to the expected decreasing

utility costs, leading to some optimal configuration. In order to accomplish this task a surrogate model is generated to predict phase equilibrium and catalyst leaching within the optimization environment. This allows for a much more complete picture of the effects of catalyst leaching on the process than in the original work using the simplified process model.

Also of interest is the fate of reactor performance within the context of the entire process when catalyst leaching is considered. This is included in the final section of this thesis using the extraction cascade for enhanced catalyst recovery. The impact of the separation sequence on the optimal reactor performance is found to be quite satisfactory when compared to previously identified optimal reactor designs using the EPF method developed in our group. Convincingly, it is shown that perhaps reactor performance is not as critical as the separation and that for high levels of catalyst leaching, at least economically, the reactor design becomes secondary. For this reason, high levels of catalyst recovery are necessary before targeted reactor optimization can be considered.

In short, the general objective of this work is to investigate the role the solvent mixture, or TMS, plays in catalyst recovery, the economic impact of this on the process and how this affects process design, how to optimize the two solvents used in the TMS using modern, quantum chemical tools, and how to further improve process economics through innovative separation techniques. Several of the results shown in this work reveal that much improvement can be made in the hydroformylation of 1-dodecene and for other long-chain alkenes by improving the catalyst recovery for economic reasons. These results and newly developed methods should also interest those working with expensive homogeneous catalysts where solvents or solvent systems are used in their recovery and recycling. This is especially true for those working on combining separation unit operations to enhance the quality of catalyst recovery when incorporating a TMS into the separation strategy. This is also noteworthy for those who have disregarded or overlooked extraction as a tool for achieving this goal.

The results and methods developed and presented in this work should show that it is possible to design a solvent mixture for homogeneous catalyst recovery using ab initio models. This provides a basis for solvent selection and greatly reduces the number of experiments required, which is still necessary owing to the difficulty in predicting liquid-liquid equilibrium using the currently available thermodynamic models. It also shows that downstream processing can have an important effect on reactor performance, but that this dependency is greatly reduced when increasing the number of separation steps used in catalyst recovery, such as by using extraction instead of simply using a single stage separation engendered by a TMS. Perhaps the most critical aspect of this work is that the effect of catalyst leaching on the process economics has been thoroughly investigated. This important aspect which has been ignored previously is now addressed and the methods developed in this work can be applied to new, homogeneously catalyzed reactions.

Goal of this Thesis

The core work of this thesis is the investigation how to identify optimal methods of reducing catalyst leaching when following the TMS principle for catalyst recovery and recycling. Since TMS usage is a primary component of the current research conducted within the SFB/TRR 63 research collaborative, it is of great importance to establish the use of a TMS as an economically feasible method for catalyst recovery. This work shows that current methods do not meet this standard and that by targeted design of the TMS or by extending and enhancing the separation process, that an economical process becomes theoretically possible.

Structure of the Thesis

This document is separated into several sections. Starting with Chapter 2, the current methods used to separate homogeneous catalysts will be discussed. In Chapter 3, a discourse about the importance of including catalyst leaching into the cost optimization of a simplified hydroformylation process is given. A framework for TMS design is then presented in Chapter 4. This approach involves a novel method for solvent screening using quantum chemical predictions using COSMO-RS. This allows one to include solvent effects on catalyst ligand solubility in TMS design with the intention of identifying better TMS systems for increased catalyst recovery. In Chapter 5, limitations encountered in catalyst leaching reduction by means of single-stage TMS separation are addressed and a method is suggested for circumventing this impediment by using an extraction cascade. Additionally, the influence of the separation performance on optimal reactor design is combined for a process-wide cost optimization problem. The thesis ends with the concluding remarks in Chapter 6 which also includes several challenges and tasks that remain in TMS design and in the recovery of homogeneous catalysts.

2. Background

2.1 Fundamentals of Chemical Processes

This work falls under the umbrella of the chemical process hierarchy developed in the Process Systems Engineering group of Prof. Kai Sundmacher. Using this concept, a chemical process is divided into four distinct levels commonly encountered in the chemical engineering discipline. These include the molecuar, phase, unit-operation, and plant levels along with relevant design variables and analysis at each corresponding level (see Figure 2.1). Information gathered at one level is then interconnected with others in the hierarchy in an attempt to facilitate process intensification or to unconventionally uncover new, potential process improvements.

In this thesis, methods for increasing the recovery of homogeneous catalysts through the use of a TMS are of primary concern. Due to this and the nature of the separation phenomena inherent when using a TMS, the phase level is considered in all aspects of this work. Solvents are obviously developed at the molecular level but successful solvent selection depends on the performance of solvent systems at the phase level. Once a TMS is shown to be effective, other process levels need to be integrated into the design problem in order to provide a more comprehensive picture of overall process performance. Thus, in addition to the phase level, choice of unit-operation arrangement, such as decantation versus extraction, will also depend on the solvents used. All of this information comes together to provide suggestions as to the best possible process design respective to the quality of the available knowledge and information.

Developed from this mindset is the Elementary Process Function (EPF) methodology developed by Freund and Sundmacher [48]. This idea takes a standard volume of a mixture, otherwise known as a fluid element, and optimizes the composition, temperature, pressure, etc. at each point in time. For example the dynamic optimization of reaction profiles potentially leads to new, process specific reactor designs based on the resulting heating or cooling strategies, dosing points, and other characteristics affecting the

fluid element. This method was further developed primarily for optimal reactor design (Peschel et al. [95, 96]), and applied to the hydroformylation of 1-octene in biphasic solvents systems by Peschel et al. [98] and for ethlyene oxide production by Peschel et al. [97]. The EPF method is important to mention because in the last few years it has been implemented to find optimal reactor trajectories for various hydroformylation reactions (Hentschel et al. [60, 61, 62], Kaiser et al. [69], Peschel et al. [98]). These results are part of the inspiration for this work, especially the cost optimizations performed in the work by Hentschel et al. [61] and the possible effect of catalyst leaching on process economics.
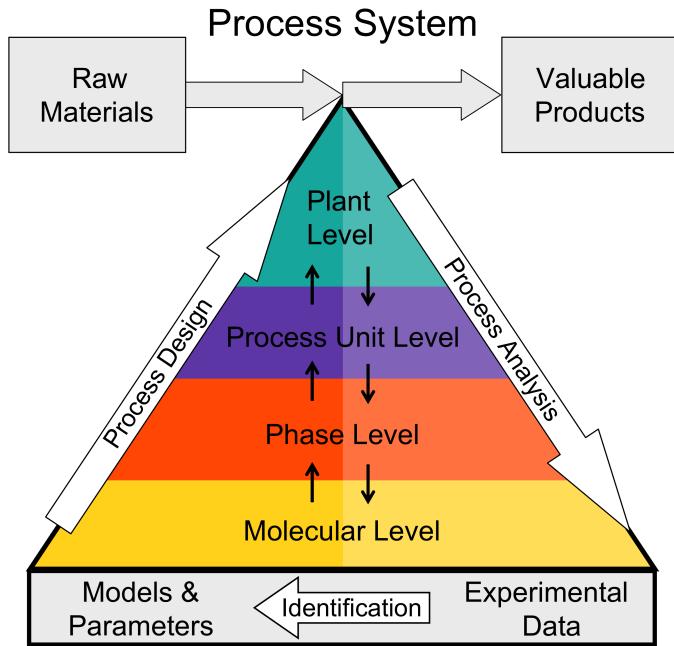
Figure 2.1: Elementary Process Function Method.

The different sections outlined in the following chapters cover various areas within the PSE pyramid. As one can see, various levels and their interactions need to be considered simultaneously in order to acquire the whole picture of possible design elements.

In Chapter 3 attention is given to the phase and unit operation levels. Here, the nature of the separation in the decanter is of primary importance based on process economics, hence the importance of the phase level. Secondarily, the performance variables of several fixed unit operations are also optimized leading to a symbiosis between the two levels. The plant level is not considered here, as the flowsheet only contains three unit operations that can be considered as an isolated case. There is no alteration of the plant that needs to be treated. Here a great importance is placed on experimental data and parameterized models. The correlations for catalyst leaching are taken directly from the literature and used to estimate the cost due to leaching in the optimization based on TMS composition.

In Chapter 4 new TMS systems are designed using quantum chemically based calculations. This extensively uses the influence at the molecular level to identify potential solvents from a large database of molecules based on modeled inter-molecular interactions used to predict catalyst solubility. Afterwards, binary solvent systems need to be checked for appropriate phase behavior. To use the molecular level alone would lead to many unusable TMS systems and can therefore not be dissociated from the phase level. Experimental validation of the highest ranking TMS designs is used to ensure that the methodology successfully performs in finding TMS component solvents *a-priori*.

For the extraction modeled in Chapter 5, the phase, process unit, and plant levels are combined for an all-encompassing look at economic performance. This is important in that the trade-offs between reactor performance, catalyst recovery, and downstream processing need to be considered simultaneously. The results indicate that regarding optimal reactor design alone leads to suboptimal solutions and that catalyst recovery is, again, economically the most important aspect the process.

2.2 Homogeneous Catalysis

The chemical industry is faced with increasing demands for sustainable processes. A key technology in designing new processes with high selectivity and efficiency is homogeneous catalysis. A homogeneously catalyzed reaction is one that occurs within a single fluid phase containing a dissolved catalyst species, reactants, products, and other inert species such as solvents. This catalyst consists of either a transition metal or an augmented complex with the addition of organic ligands. This is referred to as homogeneous transition metal catalysis (HTMC). Not only does homogeneous catalysis offer milder reaction conditions in addition to improved performance than conventional heterogeneously catalyzed reactions, it also enables a plethora of new and different reactions with industrial applicability that may have been previously inaccessible by other means Behr and Johnen [9]. Many of these new reactions can make use of renewable feedstock not dependent on petroleum based derivatives. Also, multifarious varieties of products can be designed by selective use of distinctive ligands.

As explained in the introduction, the negative characteristic of homogeneous catalysts is their subsequent, post-reaction separation and/or deactivation. For this, many different solutions have been proposed which are usually dependent upon the cost of the catalyst to be recovered. This thesis is concerned with the recovery of homogeneous catalysts from the post-reaction mixture using the TMS principle.

2.3 Hydroformylation

One of the most important industrially used reactions of the last century is the hydroformylation of alkenes, where the use of homogeneous catalysts is common practice. In fact, the first reported use of HTMC was for hydroformylation (Behr et al. [20]). This reaction is the addition of a hydrogen to one side of a carbon-carbon double bond and a formyl group to the other, where the additional reactants are usually provided as some

mixture of hydrogen and carbon monoxide or a 1:1 mixture thereof known as synthesis gas or, for short, syngas. In some cases, carbon dioxide can also be used as a reactant. A simple reaction schematic for alkene hydroformylation is shown in Figure 2.2. Aldehydes are important intermediates for alcohols, carboxylic acids, and amines leading to the production of detergents, plasticizers, surfactants, and other functionalized molecules. A very extensive review covering hydroformylation was recently provided by Franke et al. [46].

Interest in hydroformylation is based on the large variety of products that can be generated by the unconventional reactants available. Simple alkenes are not the only substrates that can be used. Other compounds containing carbon-carbon double bonds can be used, such as dienes and alkynes. Additionally, renewable and sustainable substrates such as terpenes and oleos can be also used to create new and interesting products and intermediates (Behr et al. [16]). These areas of hydroformylation research allow for processes to move away from conventional petroleum based feedstocks.
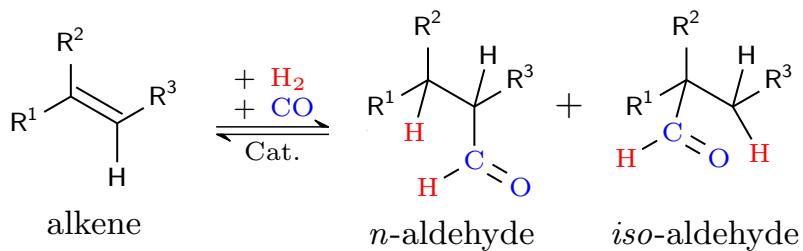
Figure 2.2: Hydroformylation of alkenes.

The first catalysts for hydroformylation were based on cobalt which require high operating pressures from 200 to 350 bar and reaction temperatures around 150 to 190 ^{o}C. Later on, rhodium was introduced as an alternative transition metal catalyst that provided a higher activity, but also milder reaction conditions with typical pressures being between 15 to 18 bar at temperatures ranging from 85 to 95 ^{o}C (Bohnen and Cornils [24]). High selectivity for linear aldehydes was also discovered using rhodium nanocatalysis by Behr et al. [17]. Despite the high activity of rhodium for the hydroformylation, its relatively high and volatile prices generally discourage its wider industrial adaptation. Even low levels of leaching usually considered acceptable for other catalysts are still too expensive for the industrial realization of many rhodium based processes.

One obvious method to reduce the use of rhodium is to search for alternative metals. A significant amount of research involving hydroformylation is actually concerned with the search for alternative transition metals for catalysis. The commonly accepted order of reactivity was defined for specific reaction conditions using unmodified metal carbonyl complexes. This lead to an inaccurate assumption that certain (and much cheaper) transition metals, such as iridium and ruthenium for example, cannot be effectively used. Jennerjahn et al. [68] investigated the use of palladium in the hydroformylation of

1-octene using a wide range of different ligands. They mention, however, that including low concentrations of acid is necessary in order to achieve high selectivity of the linear aldehyde product. Platinum based catalysts have been used for the hydroformylation of 1-octene and 4-octene using a platinum and tin metal core with diphosphine ligands by van Duren et al. [123]. A good review in the German language about the use of ruthenium, iridium, palladium, and iron in various hydroformylation reactions can be found by Pospech et al. [100]. The hydroformylation of 1-octene in a miniplant using iridium and ruthenium based catalysts has been successfully implemented, although this work has not yet been published (Behr et al. [20]). Of interest here is also that the authors mention that recycling of the catalyst is accomplished using a TMS of DMF and isooctane.

With an ever growing demand for environmentally benign chemicals, biodegradability has also become a determining factor in product design. Due to the higher biodegradability of linear aldehydes they are considered to be more valuable than their branched isomer variants (Wiese and Obst [128]). These isomers, where the formyl group becomes attached to the second carbon atom of a terminal alkene, are normal byproducts of the hydroformylation reaction and their selectivity is often highly dependent upon the catalyst used. It is then desirable to reduce the amount of branched aldehydes produced and to maximize the amount of linear aldehyde product. Not only is the linear product usually more valuable, but more efficient chemical reactions with high selectivity for the linear aldehyde are preferable to an intensive downstream isomer separation usually accomplished by distillation. This ensures a lower energy demand for product purification and a higher atom efficiency in the reactor.

This high selectivity for the terminal aldehyde is possible using special homogeneous catalysts comprised of active transition metals cobalt or rhodium enhanced with ligands (Cornils and Herrmann [36]). More specifically, rhodium based catalysts with phosphine ligands show the highest levels of activity in the hydroformylation, leading to high product yield and selectivity for linear aldehydes. Generally, the ratio of linear (or normal) to branched (or iso) aldehydes produced in a reaction is used to rate the quality of the catalyst, in addition to other attributes such as turn over rates and deactivation. It is for this reason that rhodium based catalysts would be preferable to those utilizing cobalt or other metals for the hydroformylation of long-chain alkenes at this time. This is especially true when using recently developed phosphine ligands (Brunsch [28]).

Although changing the metal catalyst shows promise in reducing the cost of the catalyst complex, the specialized ligands required may increase the cost of the process and its development considerably. Regioselectivity and stereoselectivity are important characteristics to consider in product design, especially in the development of pharmaceuticals or other specialty chemicals (Franke et al. [46]). The design of the ligands used in HTMC can play a critical role in the regioselectivity of the product aldehyde in hydroformylation. For this reason the phosphite ligand biphephos has been used quite frequently in homogeneous catalysis for hydroformylation (Behr et al. [17], Brunsch and Behr [29]). This is due to its high isomer selectivity for linear to branched aldehydes without a significant reduction in alkene conversion (Behr et al. [17]). Despite the high

performance of biphephos, one significant drawback is its price; even low levels (on the order of several ppm) of catalyst loss can lead to high process costs, as will be shown in Chapter 3. Thus, not only does the transition metal catalyst play an important role in the hydroformylation, but the nature and cost of the ligand do as well.

So, after settling on the use of a rhodium biphephos catalyst, the leaching of these higher performing, homogeneous rhodium-phosphite catalysts still remains a problem. The cost associated with even minute levels of catalyst loss can be economically limiting such that the process becomes uncompetitive. Thus the problem of catalyst recovery becomes significant even for exceptionally small amounts of catalyst leaching. Cobalt based catalysts are relatively cheap compared to those comprising rhodium and higher catalyst leaching levels are not seen as being economically critical (Fang et al. [43]). But because of the promising increase in performance as mentioned above, research has been conducted in order to develop processes and methods that can better implement rhodium-based catalysts. Many of these works focus on catalyst recovery and not just on reaction performance. This bottleneck needs to be overcome before practical use of this efficient catalyst can be considered industrially (Behr and Neubert [10]). It is for this reason that the idea of integrating catalyst retention into process design with the goal of ensuring economical feasibility developed. The priority is the catalyst recycling strategy.

2.4   Homogeneous Catalyst Recycling

As mentioned in the previous section, recovery of the catalyst in homogeneously catalyzed reactions can be of critical economical importance. Whereas heterogeneous catalysts are usually solid and the reactants and products are fluid in nature, homogeneous catalysis contains the reactants, products, and catalyst in one uniform, liquid phase. Homogeneous catalyzed reactions often show superior performance when compared to heterogeneous catalysis through higher activity, better selectivity, more robust catalyst systems, etc. Despite these positive characteristics and performance of these catalysts, their separation and recycling can be quite cumbersome, limiting potential usages (Behr and Neubert [10]). Since about one out of every ten industrial reactions is homogeneously catalyzed, it is economically important to recover and recycle the usually expensive transition metal catalysts. Not only are the precious metal cores usually made from rhodium, palladium, or platinum of high importance to recover, but also the valuable organic ligands that accompany them. Understandably, several methods to recover homogeneous catalysts from solution have been developed.

Separation techniques can be categorized as follows according to the outline presented by Behr and Fängewisch [7]:

1. Thermal or chemical recovery such as in the Wacker-Hoechst-Process and Monsato-process

2. Immobilization strategies such as solid support, liquid support, aqueous support

3. Membrane processes where the catalyst is in a membrane or where a membrane filters out the catalyst

4. Multi-phase systems including phase-transfer catalysis, thermo-regulated phase-transfer catalysis, liquid-liquid two-phase techniques, and temperature-dependent solvent systems

Of these, only recovery methods 1 and 4 are typically used industrially. In thermal or chemical recovery, commonly encountered procedures such as distillation or precipitation are used to recovery the catalyst. Two prominent examples thereof are the Wacker-Hoechst process and the Monsato process where distillation is used. The most widely employed methods involve multi-phase systems, except for phase-transfer catalysis and thermo-regulated phase-transfer catalysis.

Liquid-liquid two-phase techniques often employ polar solvents to solvate the catalyst thereby effectively separating it from the normally non-polar products that form their own, separate phase. In this procedure, the polar solvent is usually aqueous in nature. One of the shining industrial examples of the liquid-liquid two-phase technique is the Ruhrchemie-Rhône Poulenc process, which uses a rhodium transition metal homogeneous catalyst in the hydroformylation of 1-butene (Kohlpaintner et al. [77]). Owing to the difference in solubility between the predominantly non-polar aldehyde product and the polar catalyst, leaching levels are very low. This method is however restricted to shorter alkenes, those with four or fewer carbon atoms, because of decreasing water solubility of the alkene reactants with increasing chain length. Although this procedure greatly simplifies catalyst recovery it unfortunately cannot be applied to processes involving longer alkene substrates. For this reason, cobalt catalysts are still commonly used with longer alkenes, despite their lower isomer selectivity.

2.4.1 Examples of Homogeneous Catalyst Recovery

Application of hydroformylation to long-chain alkenes using modern catalysts still remains challenging and much research has been done in order to find suitable methods of catalyst recovery. There are many aspects to consider: reactant solubilities, catalyst solubility, catalyst stability, energy efficiency, industrial feasibility, etc. Many approaches to homogeneous catalyst recovery have been published in the literature including gas expanded liquids and supercritical fluids, micellar sysetms or mass transfer agents, ionic liquids and membrane filtration. In the last decade, Cole-Hamilton [35] reviewed various methods proposed to recover or retain homogeneous catalysts used in several different hydroformylation reactions. Several relevant examples of these methods are briefly reviewed in the following paragraphs. It should not, however, be considered a full review of catalyst recovery methods, as this is outside the scope of this thesis.

Several of these new techniques center around immobilization of the catalyst. An effective method for immobilizing the homogeneous catalyst is by using supported ionic liquid phases (SILP), where a thin layer of ionic liquid containing a the catalyst is

applied to high surface area structure (Riisager et al. [106]). This has been used successfully in various continuous processes utilizing homogeneous catalysts. An example of this where it proved to be an effective method for the reaction and catalyst retention was in several hydroformylation experiments performed by Hintermair et al. [63]. In a slight variation, Hintermair et al. [64] performed the continuous hydroformylation of 1-octene with considerable success in the presence of compressed CO_2. The reaction rate performance was comparable to those found in conventional organic solvents and rhodium leaching was very low, reaching only 0.2 ppm. A similar process using a rhodium complex as the homogeneous catalyst for the hydrogenation dimethyl itaconate was accomplished using SILP and supercritical CO_2 by Hintermair et al. [65]. The goal here was high enatioselectivity with low catalyst leaching. Catalyst stability was, however, found to be highly sensitive to the surface properties of the support structure.

In fact, various groups have immobilized the catalyst within a stationary ionic liquid phase and have used a continuous phase of super critical CO_2 to bring reactants and products out of the ionic liquid phase. Kunene et al. [80] explored the hydroformylation of 1-octene in a supercritical fluid-ionic liquid system. They experienced good linear to branched ratios of up to 92% linear aldehdyes and very low rhodium leaching, down to 170 ppb in some cases. They experienced a problem with oxygenation of the ligands, which decreased both the reaction performance and increased catalyst leaching. They discovered that by adding additional ligand, the effect of oxygenation could be reduced. Webb et al. [125] successfully performed the hydroformylation of various long-chain alkenes in SCF-IL. They found that good operation depends on careful choice of the IL, the catalyst, and the reaction parameters. Comparable production rates to commercial systems were found with very low levels of leaching, but the desired linear selectivity of the process was less than desirable.

Other immobilization strategies involve physically tethering the catalyst to a support structure. Song et al. [114] attempt to restrict catalyst loss in the hydroformylation of 1-octene using rhodium complexes by attaching the catalyst complex to mesoporous silica, effectively creating semi-heterogeneous catalysts. Although they achieve very low levels of catalyst leaching, a relatively high amount of branched aldehydes result due to poor selectivity. The works by van den Broeke et al. [122] and Goetheer et al. [52] present a method of using super critical CO_2 as the solvent with the homogeneous catalyst immobilized on a microporous silica membrane using the hydrogenation of 1-butene as an example reaction. Reactants and products dissolved in the scCO$_2$ can diffuse through the membrane, leaving the catalyst in the reactor.

Others have focused on the use of membranes, usually for filtration, to limit catalyst leaching. Fang et al. [44] use membrane filtration to effectively recover the catalyst in the continuous hydroformylation of 1-octene using specially designed polymer-catalysts whose bulky nature reduces the permeability of the catalyst through the membrane. They achieved constant steady state conditions with about 50% alkene conversion, an aldehyde selecitivty of 98%, and a linear to branched ratio of 3.5 for more than 22 hours. Rhodium concentrations in the post reaction mixture remained relatively stable

at approximately 20 ppb during this time. A cross-flow ceramic nanofiltration membrane reactor coupled with polyhedral oligiomeric silsesquioxane (POSS) augmented triphenylphosphine ligands were used by Janssen et al. [67] in order to reduce leaching of the homogeneous rhodium complex in the hydroformylation of 1-octene. They were able to observe stable activity of this catalyst during a two week period of operation. Xie et al. [130] demonstrated the continuous operation of the hydroformylation of 1-octene using PDMS modified rhodium complexes in combination with a nanofiltration membrane. They achieved steady conversion and selectivity for a 120 hour run, with a decrease in activity from 68% to 60%. Catalyst leaching remained relatively constant at around 2 ppm with equal amounts of phosphorous leaching. This suggests that the complete catalyst complex is leaching and not simply free rhodium or ligand.

Kunna et al. [81] report using polystyrene-based latices to act as phase-transfer agents in the aqueous-phase hydroformylation of 1-octene to overcome the issues in catalyst recovery when using long alkene substrates and standard two-phase techniques. These microsuspensions are thermodynamically stable dispersions of sub-micron polymer particles in water. The authors do not report the effectiveness of this method for catalyst recovery, however. At this time, there seemed to be a trend in the literature to not report rhodium and ligand leaching in papers describing the advantage of biphasic catalysis in hydroformylation, especially those using phase-transfer agents.

Citing this trend, Nowothnick et al. [93] investigated polystyrenes further in the hydroformylation of 1-octene using a catalyst complex comprised of $Rh(acac)(CO)_2$ and the bindentate ligand SulfoXantPhos. They also considered the hydroformylation of 1-dodecene using nonionic surfactants to create micelles in order to effectively trap the catalyst within an aqueous phase. It was shown that the reaction proceeds in a similar manner as other, current methods for catalyst recovery when using the surfactants. The reaction was much slower when using the polystyrene latices, which also experienced higher catalyst leaching, roughly an order of magnitude higher than for the surfactant systems. The authors concluded that the use of polystyrene latices is unsuitable for the reaction due to its instability at the high reaction temperatures, but that other polymers may possibly be used.

Micelles have also been used as a medium for catalyst retention. Schwarze et al. [112] investigated reaction performance and product separation using aqueous micelles in rhodium based hydrogenation reactions. Here, quantum chemical predictions of substrate partitioning using COSMO-RS (Klamt et al. [75]) were used to predict surfactant performance. Schwarze et al. [113] introduced the use of membrane filtration to recover the rhodium catalyst used in micellar hydrogenation. Rhodium leaching could be nearly eliminated when the triphenylphosphine ligand was present. Hamerla et al. [58] show that a mixture of water, 1-dodecene, and non-ionic surfactants is a feasible reaction mixture for the hydroformylation of 1-dodecene. These results led to the design of a miniplant as outlined by Rost et al. [107] and Müller et al. [92]. The successful, continuous operation of this plant for 130 hours is presented by Pogrzeba et al. [99]. They achieved a relatively high linear to branched selectivity with over 99.99% retention

of the rhodium catalyst in its active form. Thus, microemulsion systems are feasible reaction media for the rhodium-catalyzed hydroformylation of 1-dodecene.

Fang et al. [43] suggest through simulations that the hydroformylation of 1-octene using rhodium phosphine catalysts and carbon dioxide expanded liquids in the reaction phase is economically feasible when compared to conventional methods using cobalt catalysts. An interesting aspect of this study is the high sensitivity of process cost due the high cost of rhodium makeup. They state that rhodium recovery must be at least 99.8% for the process to be economically competitive with conventional cobalt based processes. Xie et al. [129] later confirmed experimentally the conclusions of Fang et al. using carbon dioxide expanded liquids for the hydroformylation of 1-octene with rhodium based catalysts with an additional membrane filtration step to enhance its recovery. They observed low levels of rhodium and ligand leaching, losing around 4.6% and 5%, respectively. This corresponds to around 0.5 ppm for both rhodium and the ligand. They mention that absorbents can be used to recover this small remaining leached rhodium or that *in situ* nano-filtration may be used. Subramaniam et al. [117] provide a thorough review on the use of supercritical fluids and gas expanded liquids as tunable solvent media for several homogeneously catalyzed reactions.

Another practical method for homogeneous catalyst recovery is with convenient temperature controlled phase separation using a thermomorphic solvent system, or TMS. The idea to use this separation principle in liquid-liquid biphasic separation should have been obvious, but it is still a relatively new method for product separation. This method of catalyst recovery is discussed in more detail in the next section.

2.4.2   Thermomorphic Solvent Systems

Behr and Fängewisch [7] proposed a new method that combines the positive qualities of the two-phase separation technique and thermo-regulated phase transfer catalysis. Both of these approaches are not directly suitable for the hydroformylation of long-chain alkenes as they possess little to no solubility in the polar phase, greatly limiting the reaction rate due to mass-transfer limitations. The process necessitates the use of a homogeneous phase for the reaction. In thermo-regulated phase transfer catalysis, the homogeneous catalyst acts as a surfactant requiring special ligand modification for each specific reaction. Also, the polar solvent is often water, leading to the same problem of low substrate solubility as in the two-phase separation technique. As a rule, the use of strongly polar solvents is generally not recommended in two-phase methods. Thus the aim was to find an improved method that allows for a single reaction phase followed by simple product and catalyst separation in a resulting multi-phase mixture.

The method Behr et al. [14] proposed is that of using temperature-dependent multi-component solvent systems (often referred to as thermomorphic solvent systems, or TMS). Basically, these multi-component systems with temperature sensitive miscibility gaps should fulfill the following requirements:

1. they should eliminate mass transfer resistances during the reaction by forming a homogeneous phase

2. they should facilitate separation of the catalyst from the post-reaction mixture through liquid-liquid phase splitting similar to biphasic catalysis

The original, or classical, TMS is comprised of three solvents of differing polarities, from polar (A) to non-polar (B), and one solvent (C) of intermediate polarity miscible in both. Usually the catalyst is recovered in the polar phase rich in A while the product is ideally recovered in the non-polar phase heavy in B. The mediator solvent C is implemented to control the miscibility of the mixture which is primarily dependent on temperature but is also strongly influenced by the mixture composition. At reaction conditions, the temperature is expected to be high enough that a single or homogeneous phase exists. After the reaction is complete, a biphasic mixture develops as the mixture is cooled. The polar, catalyst containing phase is recycled back to the reactor and the non-polar phase containing the product is then purified downstream.

These three component TMS mixtures are labeled as being type I if the miscibility gap of the heterogeneous state is closed and as being type II if the miscibility gap is open. Naturally, the type II system is preferred, as very little catalyst is expected to be contained within the non-polar, product phase due to the low presence of polar solvent.

The authors present a third TMS classification, type III, that uses only a polar catalyst solvent and a non-polar product solvent. Here there is no mediator solvent, simplifying the process by eliminating the requirement of one mass transfer agent. In Figure 2.3 a representative example of a type III TMS is presented. At the reaction temperature T_1 the operating point of the system is found above the binodal curve (for a representative ternary mixture). One should notice that the intermediate solvent at this point is the reactant, which is commonly the case. Once the reaction is terminated, the mixture is cooled to a specified separation temperature at T_2. Here, the new operating point, or more specifically the overall composition of the mixture, should be located underneath the binodal curve. The mixture has now separated into at least two phases. Product formation may lead to changes in the miscibility of the resulting mixture, especially when it itself acts as a mediator solvent. As is normally the case, the more polar catalyst complex is expected to be recovered in the polar phase. In the non-polar phase the majority of the products and unconverted reactants are anticipated. Since the type III TMS is often implemented in hydroformylation examples in the literature, especially for the hydroformylation of 1-dodecene, only type III systems are investigated in this work.

2.4.3 Examples of TMS Usage

Experiments using TMS systems have been investigated in several homogeneously catalyzed reactions including hydroaminomethylation (Behr and Roll [11]), hydroformylation (Behr and Roll [12], Behr et al. [14]), and cooligomerization (Behr and Fängewisch [8], Bergbreiter et al. [21]) where low levels of catalyst loss were realized. There are many more examples, especially from the research done by the group of Prof. Behr where
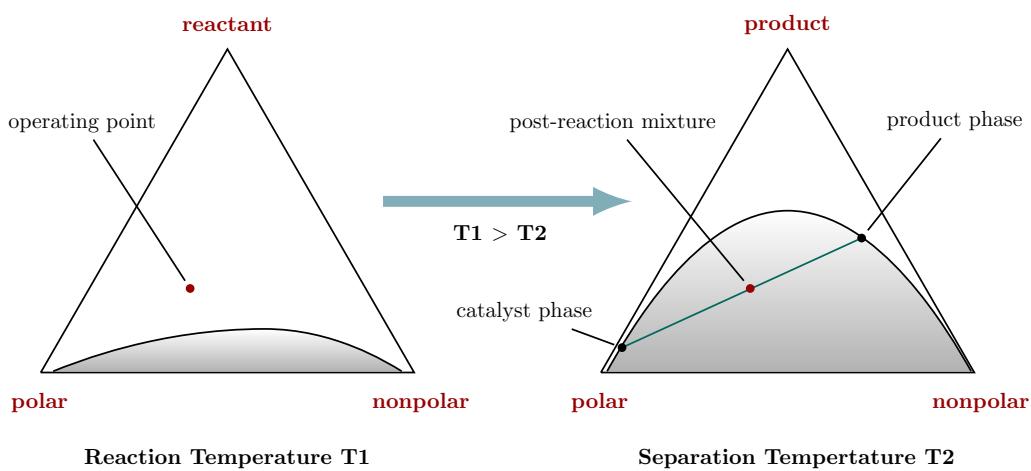
Figure 2.3: TMS functionality

the importance and practicality of TMS usage for catalyst recovery is well established. Several recent cases are summarized in the following paragraphs.

In the work presented by Behr et al. [16], the authors explore the telomerization of the industrially used terpene myrcene as a potential renewable feedstock. Myrcene is already used in the manufacturing of a variety of chemical products such as polymers, pharmaceuticals, fragrances, vitamins, biodegradable surfactants, and more. Here, homogeneous catalysts based on several palladium complexes are investigated to determine their reaction performance. In reactions involving a TMS, the polar solvents DMF, methanol, and acetonitrile were combined with nonpolar solvents heptane or octane. The UCST for all systems are already published in the literature and thus it was known that all considered TMS designs would potentially function well for catalyst and product separation in the telomerization reactions. A TMS of DMF and heptane (40:60) was finally found to perform quite well for the reaction with a 93% conversion of myrcene and a selectivity for the desired tt-telomer product of 91% after four hours of operation. Catalyst leaching was low at around 3 ppm of Pd and 4 ppm of phosphorous, which is the generally used gauge to represent ligand leaching.

In a subsequent work, the potential of myrcene is investigated further, this time in the hydroamination of myrcene with morpholine using a homogeneous catalyst complex based on the $Pd(CF_3CO_2)_2$ precursor with DPPB ligands (Behr et al. [15]). The TMS systems studied were composed of DMF or acetonitrile as the polar component and heptane as the nonpolar component. These TMS configurations were found to provide good activity for the reaction. One of the goals of this work was to comprehensively explore the composition effects of the TMS systems on the reaction. They assumed that certain transition states of the catalyst would favor different composition regions of the TMS. The reaction results showed that significant conversion and yield differences could be observed simply by changing the ratio of the component solvents of the TMS. For

example, higher amounts of polar solvent led to increased yields in telomers instead of the desired 1,4 adducts. In all cases, catalyst leaching stayed below 8 ppm for Pd and less than 0.1 ppm for phosphorous. Similar leaching values were measured using either acetonitrile or DMF, suggesting that catalyst recovery is less affected than is the reaction selectivity. This difference in reaction performance arises due to coordination effects of acetonitrile with the catalyst. Acetonitrile also led to better product extraction, a TMS characteristic of secondary, yet high, importance. A downside in this reaction is that the recovered catalyst becomes deactivated, drastically limiting the application of a TMS in this case.

In the work by Vorholt et al. [124], the authors examine catalytic functionalization through the hydroaminomethylation of oleyalcohols in a TMS for the synthesis of potential biotensides and biomonomeres. The reaction is carried out in a TMS in order to recover the expensive rhodium containing catalyst. Several TMS systems were investigated using methanol as the polar solvent and cyclooctane, n-decane, or n-dodecane as the nonpolar solvent. They found that the presence of the product leads to higher miscibility of the post-reaction mixture causing the TMS using cyclooctane to remain homogeneous upon cooling. TMS systems using the other two alkanes led to very high leaching levels due to poor phase separation, with rhodium leaching being 116 and 176 ppm and phosphorous leaching being 113 and 154 ppm, for n-dodecane and n-decane respectively. For this reaction, the TMS systems used were found to be inadequate for catalyst recovery.

The authors also studied a second reaction involving the hydroesterification of myrcene. Again, a TMS was used to recover the homogeneous palladium catalyst complex. Similar TMS compositions were investigated as in the hydroaminomethylation in that methanol was used as the polar solvent with cyclooctane, octane, n-decane, or n-dodecane as the nonpolar solvent. Interestingly, reaction performance was found to be comparable to that found in single phase experiments. However, the authors observed very long separation times, on the order of 24 hours before separation could be observed. Using octane, no separation was seen within this period. The difficulty of the separation lies with the enhanced miscibility of the system with increasing concentrations of the product. Longer chain alkanes led to lower catalyst leaching levels with 54, 229, and 541 ppm leaching of palladium and 50, 166, and 572 ppm leaching of phosphorous, for n-dodecane, n-decane, and cyclooctane respectively. Another negative aspect of product formation here is that it acts as a surfactant drawing catalyst into the nonpolar phase, thereby further increasing the amount of catalyst lost to leaching. They conclude that another reaction/separation medium is required.

The work of Behr et al. [19] continues the work being done on homogeneously catalyzed products from renewable sources. This work provided the first example of an efficient method for recycling a homogeneous catalyst in the hydroesterification of fatty compounds. This is achieved using a palladium complex catalyst coupled with XANTphos ligands in a TMS comprised of methanol and either octane or n-decane. Several TMS compositions consisting of methanol and either octane or n-decane in equal parts volume were used in reaction experiments. In one case with three consecutive reactions

using recycled catalyst, no change in activity was noticed. Conversions were between 65 and 76% with yields for the branched products reaching 50% in the experiments using both TMS configurations. Leaching levels resulted in around 3 ppm loss for both palladium and phosphorous. Thus, a TMS of methanol and either octane or n-decane is suitable for this reaction, possibly due to the high stability of the XANTphos palladium catalyst. The results in this work are important for new reactions using renewable resources.

The next two examples of TMS usage are significantly related to the work reported in this thesis. The research done by Schäfer et al. [110] involves detailed phase equilibrium measurements and hydroformylation experiments using a TMS for catalyst recovery. Here, a TMS of DMF and n-decane was used for the hydroformylation of 1-dodecene in the presence of a rhodium biphephos catalyst. Several LLE measurements were made at different temperatures for ternary systems comprised of DMF/n-decane/1-dodecene, and DMF/n-decane/1-dodecanal. 1-dodecanal is used here in place of 1-tridecanal most likely due to its simpler handling and availability, but significant deviations in phase behavior are not expected to be observable. The phase equilibrium behavior of a TMS is of critical importance to its functionality. To more easily predict the phase behavior of this system, parameters for PCP-SAFT (Gross and Vrabec [55]) were fitted to the newly collected LLE data. In the second part of their work, TMS composition effects on the reaction were investigated. They report that the reaction takes place in both pure DMF and pure n-decane solvents which surprisingly show identical reaction performances. This is also the case for a similar reaction conducted in a TMS with a 1:1 mass ratio of DMF and n-decane. However, later in the same paper, the effects of TMS solvent composition are shown to affect reaction performance and catalyst recovery under the same experimental conditions. Important here is that multiple subsequent reactions were conducted using the recycled catalyst for up to eight runs. However, fresh catalyst needed to be added after the fifth cycle.

Similar hydroformylation experiments were conducted in the dissertation by Brunsch [28], where the results for catalyst leaching deviate significantly from those published in the previously considered work. The reason for this is also not known at this time to the author, but may be related to impurities in the 1-dodecene reactant procured for the experiments discovered years later. The results found in this dissertation were later used in the catalyst leaching correlations developed in Chapter 3.

Brunsch and Behr [29] performed the hydroformylation of 1-dodecene using rhodium biphephos in various TMS with different operating conditions in order to find ways of reducing catalyst leaching. Three different TMS blends were studied using propylene carbonate, acetonitrile, or DMF as the polar solvent with n-decane as the nonpolar solvent. Substrate concentrations were varied between 10 and 30%. This naturally has an influence on the separation quality due to the product tridecanal's effect on increasing the miscibility of the post-reaction mixture, thereby limiting the amount of reactant that can be included in the reactor feed. This also means that a substantial amount of solvent is required. They found that leaching of the rhodium metal is equimolar with the phosphite ligand, suggesting that the catalyst complex is partially dissolved

in the product phase. The authors also observed the positive effect of lower separation temperatures on catalyst leaching.

They found that by reducing the temperature, the amount of polar solvent in the product phase also decreased, which directly relates to lower levels of leaching. Lower concentrations of catalyst also lead to overall lower leaching of the complex. They also checked the impact the polarity of the mixture has on leaching by increasing the length of the alkane used as the nonpolar solvent. Naturally, longer alkanes lead to lower levels of leaching due to the higher non-polarity of the product phase, resulting in larger miscibility gaps. For example, using hexane, 25% of the rhodium was found in the resulting product phase compared to 2% for hexa*n*-decane in a similar experiment. In Chapter 4 a comparison of alkane length and catalyst leaching in *a-priori* quantum chemical predictions is included based on these results. Additionally, the authors found that the size of the alkane had no effect on the reaction performance. In continuous operation using a TMS composed of DMF and *n*-decane, 30 consecutive reactions were performed with a steady decline in activity after about ten runs. After the 30th run, leaching of rhodium reached 1.7 ppm (1%) and that of phosphorus content reached 14 ppm (1%). This shows the viability of this TMS for the hydroformylation of long-chain alkenes for both the reaction and separation in a semi-continuous process. It also succeeded in improving the catalyst retention and activity than in the previous work by Schäfer et al. [110].

One of the difficulties seen in using a TMS is the choice of the component solvents. In several of the examples mentioned in this section, the choice of solvent plays an important role in catalyst stability, conversion, yield, and catalyst recovery. If the trend towards utilizing renewable sources as chemical feedstock, more research on catalyst retention and selectivity is necessary. At the moment there is no comprehensive methodology that can be used to select solvents for a TMS. One area of improvement mentioned by Hugl and Nobis [66] is that, "expert systems for the design of the solvent mix should be further developed." Methods should aim at reducing the solvent search space to a few candidates that can be quickly evaluated in the laboratory. Recovery of the solvents used should also be considered in the solvent design stage. The current methods for TMS solvent selection are discussed in Section 2.4.4.

2.4.4 Methods of TMS Solvent Selection

The component solvents of the TMS need to fulfill several requirements in order to function as desired. A methodology for solvent selection is then useful in helping design a TMS for a specific reaction. This section presents detailed accounts of previous design methods in order to provide a good background on TMS design before the introduction of a new design method in Chapter 4.

The developed solvent selection methods were originally based on the liquid phase separation behavior of two or three solvents and their respective polarities as measured using Hansen solubility parameters (Behr and Roll [12], Behr et al. [14], Hansen [59]). A more comprehensive guide to solvent selection was elaborated by Behr and Wintzer

[13] where criteria for TMS solvent selection for two (type III) and three (type I and II) component systems were presented. Taken from this work, the two most important attributes that need to be considered when selecting solvents are still the upper critical solution temperature (UCST) of the solvent blend and the solvents' respective Hansen solubility parameters. However, other decisive aspects of solvent selection include environmental factors and a specie's compatibility during the reaction. A more detailed review of the desired solvent characteristics is given below.

The simplest form of a TMS is that which consists of two component solvents. These two solvents must form two phases at a temperature above the separation temperature and below the reaction temperature. The phase separation, and hence the catalyst and product recovery, is aided by significant differences in the densities between the two phases. Therefore, solvent densities should be dissimilar. The reactants and products will have an important impact on the phase behavior of the resulting mixture. This requires knowledge of complex phase behavior and thus experiments should encompass several concentrations of species and TMS compositions around the expected reaction conditions. The polarity of the solvents must differ considerably, in that the polar catalyst should be removed in the polar phase and the product in the nonpolar phase. Solvents can be selected based on their Hansen solubility parameters with the polar solvent ranging from 22.1 to 50 $MPa^{-0.5}$ and the nonpolar solvent from 10 to 22 $MPa^{-0.5}$. A large miscibility gap with low levels of polar solvent in the nonpolar phase should exist at the separation temperature. The formation of this miscibility gap should occur with a low energy expenditure for cooling. The TMS should not be too dependent upon composition due to possible composition effects on reaction selectivity.

If the mixture is not miscible at the reaction temperature using a TMS with two component solvents, implementation of a TMS with three solvents can be used instead. A third solvent can act as a mediator solvent and should have a polarity somewhere between the other two solvents already used for the catalyst and product. Ideally, this third solvent is already present in the reaction as a reactant in excess as to avoid the addition of extra mass separating agents to the process. An open miscibility gap is a desirable trait of the ternary solvent mixture. This denotes a very low amount of polar solvent in the nonpolar phase, which directly relates to low levels of catalyst leaching. High temperature sensitivity is beneficial in order to reduce the amount of energy required to mix or separate the mixture. As with two phase systems, the density of each resulting phase should be quite different in order to more easily facilitate separation. The recommended solvent polarities as given by Hansen solubility parameters are from 26.5 to 50 $MPa^{-0.5}$ for the polar solvent, from 20 to 29.9 $MPa^{-0.5}$ for the mediator solvent, and from 10 to 19 $MPa^{-0.5}$ for the nonpolar solvent. Care must be taken when selecting the nonpolar, product solvent as its ability to extract the product may become problematic with increasing non-polarity. This is due to the slightly polar nature of the product after its functionalization.

Behr et al. [18] expanded upon their methods for solvent selection and a framework for selecting a mediator solvent in the hydroaminomethylation (HAM) of 1-octene was recently developed. The goal was to minimize catalyst leaching by finding TMS systems

with expedient liquid-liquid equilibrium behavior. This method dealt more rigorously with the pros and cons of using solvent descriptors and predictive thermodynamic models in selecting suitable solvent candidates than did previous ones.

Most importantly, the method is primarily concerned with the thermodynamic properties of the mediator solvent in the chosen mixture of 1-octene and water. In this case, 1-octene is both the nonpolar solvent and one of the reactants while water is the polar solvent. The framework begins with a pre-selection of the potential mediator solvents. Several characteristics were used here: the mediator must have a polarity between water and 1-octene, be liquid at 20 °C and 1 bar, contain no miscibility gap with water, and be inert in both condensation and hydroformylation reactions. Starting with a search space constrained to those organic compounds known to be useful as a solvent or for extraction, widely used industrially, and after applying the pre-selection rules, the authors compiled a list containing a total of 17 solvents.

Using this list of polar solvents, a pair of screening steps were used to identify potential solvents for use in the TMS. The miscibility gap of each solvent with 1-octene was checked experimentally. If the miscibility gap was found to be closed, the UCST was checked to see whether or not it is above the reaction temperature, in this case 130 °C. If the miscibility gap is closed and the mixture has an UCST above the reaction temperature it was excluded from the selection process. Of the 17 initial solvents only nine showed promising miscibility behavior. It is important to mention that the authors found that by comparing solubility parameters or by simulating the phase behavior, results accurate enough to identify feasible mediator solvents were not obtainable. This also did not allow them to determine an ideal composition of the solvent system that enables them to employ the full benefit of the TMS.

The second and final criteria for determining which solvents to use depends on the partion coefficients of the mediator in a mixture of water and 1-octene. Here, the affinity of the mediator for the polar phase and the nonpolar phase are compared. It is important in the HAM that the partition coefficient of the mediator is larger than one, according to Equation (2.1), with a binodal curve residing close to the edge of the ternary diagram. The mediator should be found predominantly in the polar phase as higher amounts of mediator found in the nonpolar phase leads to higher levels of catalyst leaching. Only five of the nine solvents at this point showed the desired partitioning performance.

$$K = \frac{X^{Mediator}_{polar}}{X^{Mediator}_{nonpolar}} \tag{2.1}$$

Three of the promising mediator solvents were experimentally tested in the HAM reactions using a rhodium (the precursor is $[Rh(cod)Cl]_2$) complex with TPPTS ligands. These mediators were ethanol, acetonitrile, and NMP. Only the TMS using acetonitrile formed a biphasic mixture after the reaction, although initially in the reactor it formed three phases. The TMS successfully lead to low levels of rhodium leaching, with a loss measuring 5 ppm. This is, however, still too high for industrial adaptation. This is

with over 99% conversion of 1-octene and desired product formation reaching a mole percentage of 53% of all produced species.

The influence that the TMS component solvents have on the reaction could not be predicted at this point and was not included in the framework. It is, however, seen in the experimental validation completed after the solvent screening phase that there were significant deviations in performance depending on which mediator solvent was used. This is due to the complexity of the single-step hydroaminomethylation of 1-octene which combines three different reaction steps that occur simultaneously. The first reaction is the hydroformylation of an alkene catalyzed by a catalyst complex with a rhodium core. The aldehyde product then reacts with an amine through condensation forming an enamine and water. In the third reaction, the newly formed enamine is hydrogenated to form the amine product. This last reaction is catalyzed using the same homogeneous rhodium catalyst as in the hydroformylation step. With such a complicated reaction network, it is no surprise that there are many side reactions that occur and opportunities for solvent effects to impact selectivities. Thus, not only is the TMS design important for catalyst recovery, but it also plays an important role in the selectivity of the reaction as well. This is an effect that was also seen in several of the previously mentioned TMS examples.

Thus, as is often the case in solvent selection, experimental validation is still very much necessary. Although some issues are found in predictive methods for phase equilibrium, still no aspect of predicting catalyst solubility in component solvents has been discussed at this point. This will be the primary criteria for the solvent screening method developed in Chapter 4.

2.4.5 Hydroformylation of 1-dodecene

One area that has received much attention within our research collaboration in the SFB/TRR 63 is the use of thermomorphic solvent systems (TMS) and micellar solvent systems (MSS) as means for recovery of the rhodium based catalyst used in the hydroformylation of 1-dodecene. This reaction is depicted in Figure 2.4 and the specific ligand, biphephos, which is extensively employed in our research, is shown in Figure 2.5. As a result of this research project spanning three universities for several years, there has been an abundance of research performed on this specific reaction in the past few years, much of which is still ongoing. Several examples of work done in this area were already mentioned in Section 2.4.1 and Section 2.4.3.

The work in this thesis focuses on extending and improving the use of a TMS consisting of dimethylformamide (DMF) as the polar solvent and n-decane as the nonpolar solvent in the hydroformylation of 1-dodecene. Previous studies had already found that a TMS of DMF and n-decane was satisfactory for both the reaction and subsequent separation for this reaction (Behr et al. [17]). As a result, Schäfer et al. [110] performed a series of experiments on the hydroformylation of 1-dodecene in a TMS of DMF and n-decane focusing on liquid-liquid phase equilibrium measurements, reaction performance, and catalyst recycling. This successful implementation of the reaction and acquisition of
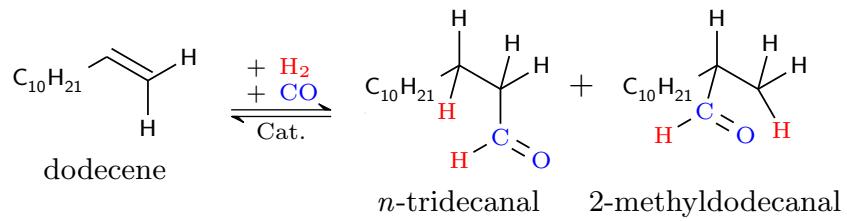
Figure 2.4: Simplified reaction scheme of the hydroformylation of 1-dodecene.
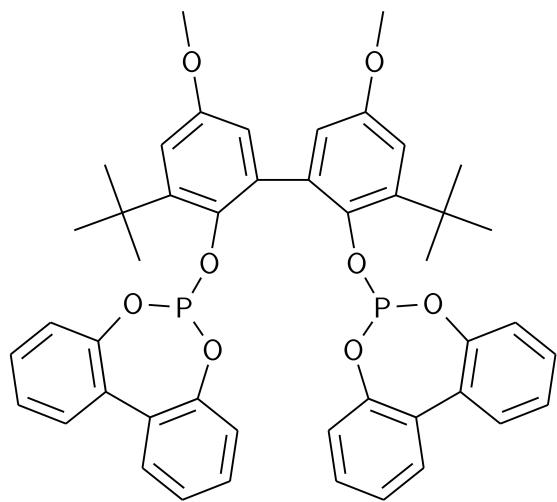
Figure 2.5: The bidentate phosphite ligand biphephos commonly used in our research activities.

useful information regarding phase behavior led to an investigation into the reaction network by Markert et al. [86] and the reaction kinetics by Kiedorf et al. [70]. These kinetics were then further improved and modified through experimental validation of optimal reaction routes in studies done by Hentschel et al. [62].

The reaction network of the hydroformylation of 1-dodecene is quite complex with many variables such as reaction temperature, parital pressures of the hydrogen and carbon monoxide reactant gases, component concentrations, potential dosing, catalyst concentration, etc. Taking this complexity into account, reactor design can be an intimidating task, especially when an optimal configuration is desired. For these reasons, the elementary process function (EPF) methodology outlined by Freund and Sundmacher [49] was applied to this reaction in the work of Hentschel et al. [61].

In the work of Hentschel et al. [61] it was emphasized that the type of plant-wide optimization performed by Peschel et al. [98], although showing significant improvements in process cost, would benefit from including investment costs into the objective function. Investment or capital costs are important in process design in order to keep the process within feasible and realistic bounds (such as keeping vessels or columns from being exceptionally large). The work of Hentschel et al. successfully showed that the impact of the investment costs on the total process are quite important, leading to a decrease in both utility and investment costs for an optimized reactor compared to a CSTR control.

In the aforementioned work, it is assumed that all of the catalyst is ideally separated in the polar phase of the biphasic post-reaction mixture and recycled. Although the importance of catalyst leaching on the process economics is well known, it was not included in the integrated reactor and process design due to the absence of a model for describing the catalyst leaching. Under this assumption, no catalyst leaching is expected although it is well known that small amounts of leaching do occur (Brunsch [28], Brunsch and Behr [29], Schäfer et al. [110]). Due to the high economical burden for even low levels of leaching, catalyst leaching is expected to have significant effects on the reactor and process design. They postulated that were catalyst loss to be taken into account that the optimal process design would attempt to reduce the loss of catalyst by tuning the outlet composition of the reactor to one more conducive towards better phase separation. This is important because the tridecanal product enhances the miscibility of the DMF/n-decane mixture thereby reducing the effectiveness of the TMS with higher conversion and selectivity. For these reasons, the work presented in this thesis attempts to address this issue. It will be shown that several other aspects of reactor design are also strongly affected by the catalyst recovery rate.

More recently, Kaiser et al. [69] present a full probabilistic orthogonal collocation approach based on the EPF methodology. This new approach accounts for parameter uncertainty, non ideal reactor behavior, and imprecisions in realizing the optimal reactor configuration. As an example, they tested their method in the optimal reactor design for the hydroformylation of 1-dodecene. They, however, also do not consider the effect of catalyst leaching on reactor design or process economics. Once coupled

with an effective method for predicting catalyst leaching, a much clearer picture of the robustness of the process can be weighed against the total process costs for varying degrees of uncertainty.

3. Economic Analysis of Catalyst Leaching with a Thermomorphic Solvent System

3.1 Introduction

Despite the aforementioned efforts used to recover the catalyst, the problem with catalyst leaching still persists. This relatively small amount of catalyst lost in the product phase is not recovered and is ultimately removed from the process in one of the final product streams. In order to ensure that an economically feasible process is designed, it becomes quite important to minimize this leaching amount (Fang et al. [43]).

The solvents that compose the selected TMS used to recover the catalyst and separate out the products has a significant impact on the performance of the process in the hydroformylation of 1-dodecene. Although it is known that these solvent effects on catalyst leaching are important, they have yet to be included in a detailed cost analysis to rate process performance. The reasons for this are the limited conditions for which the reaction kinetics and catalyst leaching levels are measured. Only a single TMS comprised of 60 w% n-decane and 40 w% DMF is used experimentally in the kinetic data collected by Kiedorf et al. [70]. As a result, the optimal reactor trajectories determined by Hentschel et al. [61] are only considered using this fixed composition of the TMS. Additionally, the effect of catalyst leaching on the process performance is ignored in the optimization. Instead it is simply assumed that catalyst leaching does not occur and that the catalyst is completely recovered in the polar phase formed in the decanter. In reality, catalyst leaching does take place and different compositions of the TMS have been shown to significantly affect reactor performance and catalyst leaching amounts (Brunsch [28], Brunsch and Behr [29], Schäfer et al. [110]).

These works also reveal that using higher molecular weight alkanes as the non-polar solvent and operating the decanter at lower temperatures both have a beneficial effect

in reducing catalyst leaching. The amount of this data is, however, quite low making it difficult to use in a process model within the complete, allowable range for TMS compositions. At this stage of development, it is rather difficult to explore the entire realm of possible configurations in order to find a more suitable route to improve catalyst recovery based on economic analysis. Therefore, the following analysis will be limited to presently obtainable information.

This section will explore the actual cost burden the rhodium-biphephos catalyst leaching has on a fixed hydroformylation of 1-dodecene process based on the existing process information. Despite the limited experimental data at the time of this work, a simple correlation fitted to the available data can be used to estimate catalyst leaching rates within a process model. This can then be incorporated into an optimization problem that is constrained to the conditions of the experiments from which the data was collected. This restricts the separation and recovery to a TMS consisting of DMF/n-decane with a decantation temperature of 25 °C. Although lower temperatures would lead to better catalyst recovery, not enough information is available to include temperature effects into the correlation. Also, since reaction kinetics are only available for a TMS composition ratio (Equation (3.6)), represented here as Ψ_{TMS}, of 0.4, a similar correlation for TMS composition dependent conversion is generated using ratios of DMF to n-decane ranging from 0.3 to 0.7, which are the bounds of known experimental investigation. Using these correlations, a process model flowsheet can be designed and optimized with the ratio of DMF to n-decane left as an optimization variable allowing for solvent-dependent process performance to be investigated, albeit in a limited manner.

Before process optimization can proceed, the issue of solving the LLE within the decanter needs to be addressed. Frequently chemical engineers encounter phase equilibrium calculations when designing new processes and evaluating flowsheets. The general methods of calculating the phase equilibrium are to find a single point based on the conditions of thermodynamic equilibrium, such as the minimum of the Gibbs enthalpy or the maximization of the mixture entropy. One such method to solve for equilibrium is by using the rate-based method developed by Steyer et al. [116], however these methods cannot be used within an optimization problem. Usually good initialization values for the start of the iterative method used to find LLE compositions are required to find a non-trivial solution, which is only made more difficult during optimization. Thus, the task of solving LLE within a process-wide optimization becomes almost impossible. To avoid this problem, a surrogate model or external functions may be used. The solutions from an activity coefficient model can be fitted to a surrogate model that is more easily implemented into the optimization environment. External functions can also be used but are placed outside of the problem and are essentially blind to the solver. Thus, derivatives must be passed from the external functions to the solver in order for deterministic optimization to be possible. This means that although it is not simple to estimate LLE in the optimization, it is decisively not impossible.

In this work, the LLE of the decanter used in the flowsheet is evaluated using a linear regression model. Phase equilibrium data is first calculated using an activity coefficient

model and the results then fit to the regression model. This relatively simple equation can be easily integrated into an optimization problem, where first and second derivatives of the surrogate functions can be determined with minimal effort.

Combining the correlations for conversion and catalyst leaching based on TMS compositions, the linear phase equilibrium model, and a simplified process model allows for the process performance based on the TMS composition to be efficiently evaluated. An optimization problem using an economical objective function is then developed based on the total annualized cost of the process over a three year period. This model should allow one to observe the trade-offs involved between energy requirements, capital costs, reactor performance, and the separation performance, now including catalyst leaching, in the overall process. The results of the optimization should present one with a clearer picture of how catalyst leaching affects the hydroformylation of 1-dodecene. This in turn will enable one to identify potential areas for process improvement. The consequences and significance of ignoring catalyst leaching in process design and optimization is also brought to light.

3.2 Process Model

The proposed flowsheet depicted in Figure 3.1 is a simplified hydroformylation example of the process evaluated by Hentschel et al. [61]. The reactor does not need to be detailed as extensively due to the lacking flexibility in the available reaction kinetics. Instead, many of the variables in the reactor are fixed according to the experimental conditions the TMS dependent conversion data is taken from. One noticeable absence from the flowsheet is the second distillation column used to separate the aldehyde isomers from one another. Since this column is highly dependent upon the linear to branched ratio, it is more directly associated with reactor performance and to a lesser degree the influence of the separation process directly before. More importantly, due to our assumption that the reaction does not produce unwanted byproducts there is no need for an isomer column for product purification. Thus, a process consisting of a reactor, decanter, and single distillation column is used to evaluate the process economics including the catalyst leaching.

Another aspect to mention is that due to the limited nature of the mixture composition, some assumptions are made regarding the components used in this analysis. The only components considered are the TMS solvents DMF and n-decane alongside the reactant 1-dodecene and the main product tridecanal. The primary byproducts typically include discernible amounts of 2-methyldodecanal, iso-dodecene, and n-dodecane which are excluded from the current analysis. The byproducts 2-methyldodecanal and iso-dodecenes are very similar thermodynamically to their isomers and will not impact the phase equilibrium assumptions in the decanter. This is essentially unavoidable when using first order group contribution methods, such as the modified UNIFAC Do. (Weidlich and Gmehling [126]) model for LLE calculations, as they cannot usually distinguish between isomers. The remaining byproduct n-dodecane, although seen in higher quantities than the other byproducts, behaves similarly to n-decane which is found in much larger

quantities and thus its effect is also negligible. Additionally, these compounds are also found in much lower concentrations than their isomers. These assumptions are also valid for the separation in the distillation column.

Process Description

A more detailed description of the process shown in Figure 3.1 is given in this section. The feed (S_1) is mixed with the two recycle streams and heated to the reaction temperature in a heat exchanger (HX_1) before being fed into the reactor (R). After the reaction, the mixture is cooled in a subsequent heat exchanger (HX_2) before being fed into the decanter (D) where phase splitting occurs as expected via the TMS. A biphasic mixture is now found here: the denser, catalyst phase, occupies the lower region of the decanter and is recycled (S_6) and mixed with the feed while the less dense, product phase found above the catalyst phase (S_7) is fed into a heat exchanger (HX_3) where the mixture is brought to its bubble point before being fed into the distillation column (C) as stream (S_8). This column separates the product as the bottoms (S_{10}) and the TMS solvents and reactant are recovered as the distillate (S_9). The distillate is then split into a recycle stream (S_{11}) and a purge (S_{12}). The recycle stream is fed back to the mixer in front of the reactor to be combined with the feed and catalyst recycle stream.

Two other reactants include carbon monoxide and hydrogen. These gases are an integral part of the reaction and are considered in more detail elsewhere (Hentschel et al. [61, 62]). The separation of unreacted synthesis gas is considered to be relatively simple and they are assumed to be removed in a flash stage directly after the reactor and are therefore not included in the downstream processing considered in this work.

The effect that the solvent mixture has on the process based on the three year averaged TAC is then investigated. This consists of the utility cost per kmol product and on the capital cost for a process that produces approximately 0.1 kmol of product per hour of operation. In order to find the solvent mixture that leads to the lowest process cost, an NLP optimization problem is developed. In the following sections, more comprehensive descriptions of each unit operation are discussed.

Reactor Model

As mentioned briefly above, the reaction kinetics for the hydroformylation of 1-dodecene were measured and calculated in a TMS mixture using a mass ratio of DMF to n-decane of 0.4 (Hentschel et al. [62], Kiedorf et al. [70]). Currently, research is being done to explore how the solvent composition affects the conversion and selectivity of the reaction. At this time, no concrete information or model is available, but some experimental data using different mixtures of the TMS for the reaction and separation are available from Brunsch [28]. The author presents a series of reactions using TMS ratios from 0.3 to 0.7 where changes in the conversion and selectivity are seen as a result of the changing solvent composition. She also presented catalyst leaching levels measured as the amount of rhodium and phosphorous found in the nonpolar phase after each separation of the post-reaction mixture. This data provides the basis for developing a simplified
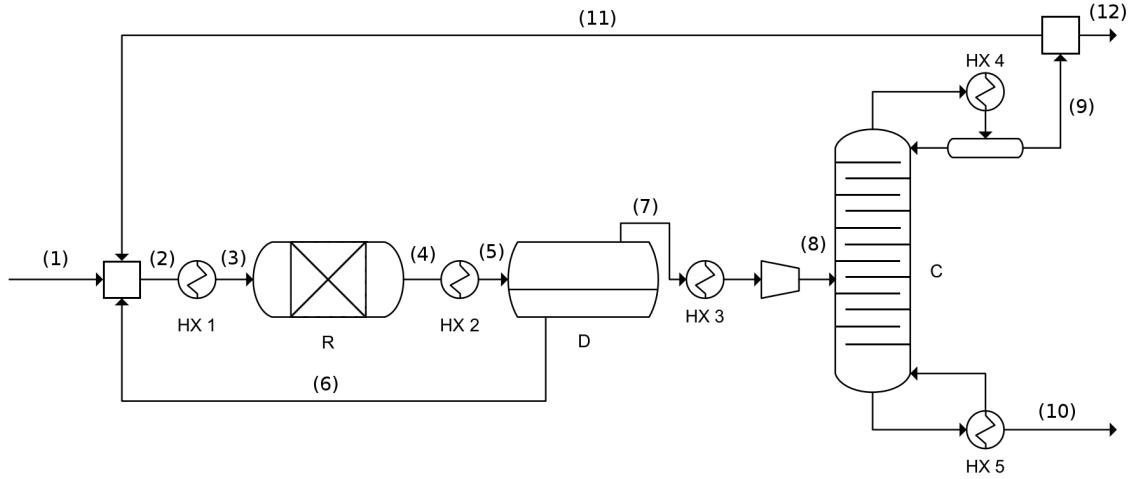
Figure 3.1: Flowsheet of the considered, simplified hydroformylation process [88].

black-box reactor governed only by conversion. This will be used instead of the complex reaction network developed by Kiedorf et al. [70]. The conversion of 1-dodecene can still be left as a degree of freedom. Conversion will affect the separation in the decanter due to the tridecanal product being a miscibility enhancer for the mixture leaving the reactor and entering the decanter. The LLE of the ternary mixture tridecanal, DMF, and n-decane (Schäfer and Sadowski [109]) has a much smaller miscibility gap than the system comprised of 1-dodecene, DMF, and n-decane (Schäfer et al. [110]). Thus, with higher conversion more product is produced leading to a lower degree of separation in the decanter. This may be associated with higher catalyst loss, higher recycle of product, and/or poor product recovery.

The conversion of 1-dodecene is shown to be weakly dependent on the composition of the TMS where higher ratios of DMF to n-decane are shown to lead to lower conversion (Schäfer et al. [110]). On the contrary, selectivity remained basically unaffected for all TMS compositions. A simple black-box model will take the composition of the feed stream to the reactor, S3, and simply calculate a conversion based on the TMS composition as represented by the TMS ratio, Ψ_{TMS}. A quadratic function (Equation (3.1)) is used to describe the maximum conversion of 1-dodecene to tridecanal based on this TMS ratio (Equation (3.2)) using data collected from Brunsch [28] (Figure 3.2).

All reaction conditions used in this study are necessarily fixed to the experimental parameters used by Brunsch: the overall mass fraction of the TMS is fixed at 0.85, the molar ratio of 1-dodecene to the rhodium precursor of the catalyst is 1000:1, the molar ratio of biphephos to the rhodium precursor is 5:1, and the reaction temperature is constant at 373.15 K. The reactor is then otherwise completely described by molar mass balances (Equation (3.4) and Equation (3.5)) and the heat of reaction is not taken into account. The TMS composition as represented by Ψ_{TMS} varies bewtween 0.3 and 0.7

(Equation (3.6)). The total sum of the mass fractions of the TMS component solvents (the combination of n-decane and DMF) is accordingly fixed to 0.85 (Equation (3.7)).
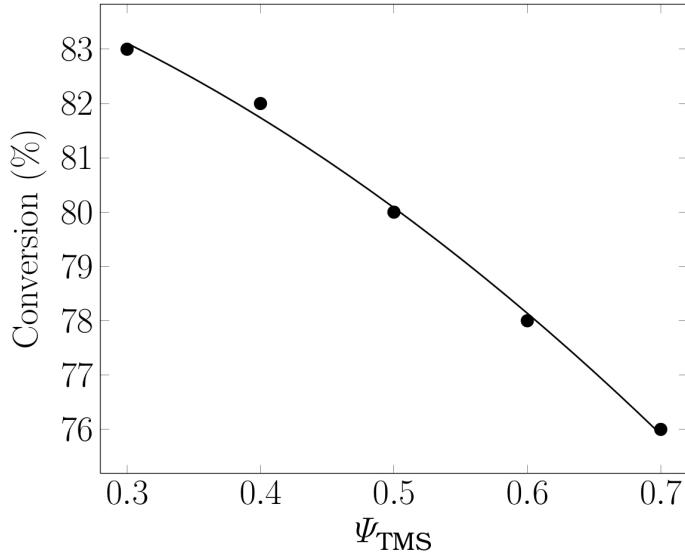
Figure 3.2: Correlation of the maximum conversion in the reactor to Ψ_{TMS} [88].

$$X_{\mathrm{nC12en}} = -0.1429 \cdot \Psi_{\mathrm{TMS}}^2 - 0.03714 \cdot \Psi_{\mathrm{TMS}} + 0.8551 \tag{3.1}$$

$$\Psi_{\mathrm{TMS}} = \frac{\dot{m}_{\mathrm{DMF},4}}{\dot{m}_{\mathrm{DMF},4} + \dot{m}_{\mathrm{C10an},4}} \tag{3.2}$$

$$\dot{n}_{i,3} = \dot{n}_{i,3} \qquad\qquad i \in \mathrm{DMF}, \mathrm{C10an} \tag{3.3}$$

$$\dot{n}_{\mathrm{nC13al},4} = (\dot{n}_{\mathrm{nC13al},3} + \dot{n}_{\mathrm{nC12en},3}) \cdot X_{\mathrm{nC12en}} \tag{3.4}$$

$$\dot{n}_{\mathrm{nC12en},4} = (\dot{n}_{\mathrm{nC13al},3} + \dot{n}_{\mathrm{nC12en},3}) \cdot (1 - X_{\mathrm{nC12en}}) \tag{3.5}$$

$$0.3 \leq \Psi_{\mathrm{TMS}} \leq 0.7 \tag{3.6}$$

$$0.85 = w_{\mathrm{DMF},4} + w_{\mathrm{C10an},4} \tag{3.7}$$

Decanter Model

Recovery of the expensive homogeneous catalyst is critical for good process economics and takes place in the decanter following the reaction. Here, the second and most important function of the TMS occurs: the formation of a biphasic mixture. From an economic standpoint, this liquid phase separation is perhaps the most significant event in the process. An accurate model for this separation event is required to ensure decent optimization results are obtainable.

The description of the separation begins with an accurate representation of the liquid-liquid equilibrium of the system. First, a model for determining the phase equilibrium

needs to be chosen. The idea for using the modified UNIFAC Dortmund activity coefficient model (Weidlich and Gmehling [126]) began with liquid-liquid phase equilibrium modeling of the same TMS system in the work by Hentschel et al. [61]. Usually group contribution methods such as the modified UNIFAC Dortmund model discussed here are used for predicting activity coefficients and phase equilibrium when experimental data is unavailable. However, the predictions made with the currently available binary interaction parameters vary significantly to experimental results for the system of DMF, n-decane, and 1-dodecene at temperatures higher than around 25°C and for the system of DMF, n-decane, and dodecanal at temperatures in the range from -10^oC to 25°C. This leads to over estimated miscibility gaps as long as these original parameters are used. This is especially the case for the predicted miscibility gap of the system containing DMF, n-decane, and dodecanal, where the size of the miscibility gap is more critical. Using this model, the amount of aldehyde product allowed in the decanter could well exceed the 20% mass constraint required in real systems. In practice, a maximum of around 15% mass is maintained to ensure liquid-liquid separation occurs. Therefore, a more accurate representation of the phase separation is required.

Dodecanal is mentioned here instead of tridecanal because the only LLE data for the ternary mixture involving tridecanal is at 25°C (Schäfer and Sadowski [109]). However, ternary LLE data for dodecanal in a mixture of DMF and n-decane at various temperatures is available from Schäfer et al, who use it in place of tridecanal for phase-equilibrium measurements presumingly due to its easier handling (Schäfer et al. [110]). Even though dodecanal is also included instead of only tridecanal, the results are not expected to differ significantly when using group methods to predict activity coefficients of the longer aldehyde when exploring the temperature dependence of the phase separation on the system. This can be seen in the LLE results for DMF, n-decane, and various aldehydes in Schäfer and Sadowski [109], where the differences in phase behaviors between dodecanal and tridecanal are very small.

The work mentioned above by Schäfer et al. [110] also included various pure-component and binary interaction parameters for PCP-SAFT (Gross and Vrabec [55]) for the currently used system. Although parameters exist for this advanced equation of state, it was found that by modifying certain binary interaction parameters of the modified UNIFAC Dortmund activity coefficient model, very accurate results at a fraction of the computational cost were obtainable. This is realized by fitting new binary interaction parameters to the experimental data obtained from Schäfer et al. [110]. Some of these parameters were originally fitted by Ye [132], but the binary interaction parameters for HCO-DMF and HCO-CH$_2$ are modified here to more accurately describe the phase behavior of the ternary system of DMF, n-decane, and dodecanal. This is done using the parameter estimation feature embedded in the Aspen Plus software suite (ASPEN Tech, Cambridge, MA). Phase diagrams comparing experimental data to the predictions made using the new parameters (Table 3.1) are shown in Figures 3.3 and 3.4. It is clear that the newly fitted parameters provide good predictability of the phase splitting behaviors for both systems. Thus for the quaternary system of DMF, n-decane, 1-dodecene, and tridecanal explored in this work, more reliable predictions are assured.
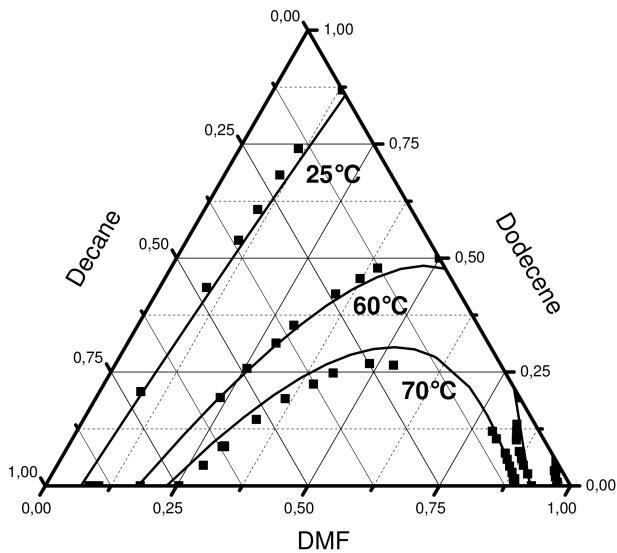
Figure 3.3: Ternary LLE diagram for the system DMF/n-decane/1-dodecene with regressed binary interaction parameters. The solid lines represent the predicted LLE and the points represent the experimental data [88].
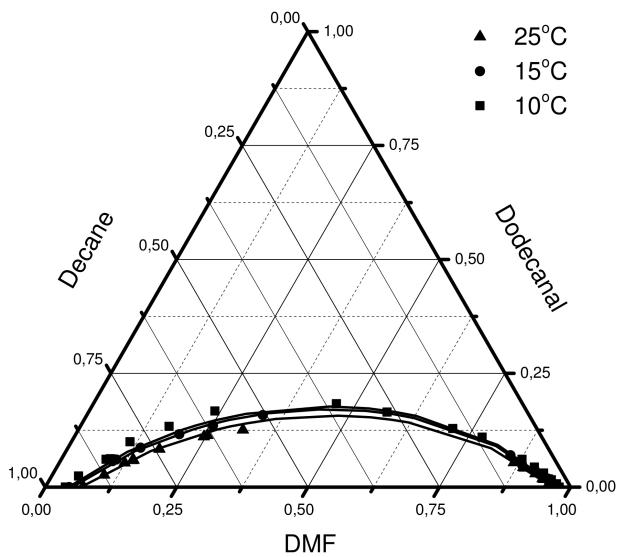
Figure 3.4: Ternary LLE diagram for the system DMF/n-decane/dodecanal with regressed binary interaction parameters. The solid lines represent the predicted LLE and the points represent the experimental data.

Table 3.1: Regressed (italics) binary interaction parameters (A_{ij} above, B_{ij} below) for use with modified UNIFAC Do [88].

	CH$_2$	HCO	DMF	CH$_2$=CH
CH$_2$	0	*639.581004*	*871.437927*	189.66
	0	0	*-0.9515929*	-0.27232
HCO	*-504.63464*	0	*-549.81302*	202.49
	0	0	0	0
DMF	*114.342456*	*92.889318*	0	*-55.044021*
	-0.7540952	0	0	*-0.3573974*
CH$_2$=CH	-95.418	476.25	*1033.73782*	0
	0.061708	0	*-2.1595105*	0

An issue encountered by Hentschel et al. [61] was in the difficulty in calculating the phase separation during the optimization. Converging to a non-trivial solution for LLE on its own is already a challenging task. Once compounded within a process optimization problem where equilibrium may be calculated many hundreds or thousands of times, ensuring a convenient, internal solution becomes impossible. Their solution was to calculate partition coefficients (Equation (3.8)) using regressed second order linear equations with conversion as the independent variable, similar to the reactor model discussed in the previous section. This correlation was found to provide a very agreeable description of the phase separation as calculated using the standard modified UNIFAC Dortmund model described in the literature. Albeit this model did not use the system specific parameters calculated in this thesis.

A similar idea is used in this work, but instead of basing the model on conversion, it is based instead on the composition of the inlet to the decanter, allowing for greater flexibility in the TMS composition. The TMS composition in this model is however more complicated than that of Hentschel et al. [61] because Ψ_{TMS} is no longer considered constant at 0.4. To take the varying TMS compositions into account, conversion is no longer valid and must instead rely on the overall composition of the mixture. To maintain the ease of solving the LLE conditions within the decanter, this new model is also linear in respect to its coefficients. The benefit of using a linear regression model lies in its simplicity and uncomplicated differentiation. Such models can then be smoothly incorporated into an optimization problem to avert the difficulties inherent in phase equilibrium convergence.

Phase equilibrium is represented here using partition coefficients, θ_i^α, defined in Equation (3.8). By using partition coefficients, the number of moles of each species in each phase as well as the total size of each phase can be calculated using the minimum amount of input data. The surrogate linear regression model will use the mole fraction vector of the decanter inlet ($\mathbf{x}_3$) as the independent variables. The predicted partition coefficients, $\hat{\theta}_i^\alpha$, can now be calculated simply using the linear regression models, as

represented in Equation (3.9). For each component in the mixture, a separate linear function is required. Thus, four surrogate models are needed.

$$\theta_i^\alpha = \frac{n_i^\alpha}{n_i^\alpha + n_i^\beta} \qquad\qquad i \in \text{COM} \qquad\qquad (3.8)$$

$$\hat{\theta}_i^\alpha = f_i(\mathbf{x}_3) \qquad\qquad i \in \text{COM} \qquad\qquad (3.9)$$

To generate data for the linear regression model, the phase equilibrium for ten thousand randomly initialized compositions are calculated at 298.16 K using the rate based method developed by Steyer et al. [116]. Roughly 51% of the initial compositions are predicted to form biphasic mixtures. It is very important to ensure that only compositions forming two phases are used to fit the linear models. Otherwise, obscure values larger than one or less than zero for the partition coefficients will be returned, leading to unacceptable models for use in the optimization. As long as the systems being incorporated into the surrogate models are well defined and constrained to the biphasic region, no significant problems should be encountered or expected. So, using only the biphasic compositions, four linear regression models are calculated using the statistics toolbox in MATLAB (version R2012b). This allows one to conveniently remove insignificant terms or add significant terms to the regression models. In future models, a smaller feasible region based on composition constraints may be used to simplify the model further.

The linear regression models created predict the partition coefficients very well for all mixtures that do not contain coefficients with values close to zero. However, this is very unlikely to occur during the optimization at the given compositions investigated. Using these models, accurate descriptions of the liquid-liquid equilibrium can be easily calculated within an optimization problem. The linear regression models and their corresponding parameters are found in Appendix A.3.

As seen in Table 3.2, when partition coefficients close to zero are removed from the regression, the average percent error decreases substantially. In contrast, the relative error changes less drastically. This simply means that for components with very low partition coefficients, the error can be quite large, which is more so reflected in the percent error than in the absolute error. Since the optimization will not encounter values close to zero, the models are found to be satisfactory for the present need. Figure 3.5 depicts the the partition coefficients as predicted using the linear regression model with the data calculated using modified UNIFAC Dortmund with the fitted parameters presented in Table 3.1. In this figure, all of the biphasic compositions used in the regressions are represented. It can be seen that a reasonable number of outliers is present, suggesting that a linear model may not be suitable for describing the LLE, but overall the models accurately reflect the phase splitting behavior of the system. It is interesting to note that these outliers primarily represent high fractions of non-polar components in the polar phase.

Since two phases are generated in the decanter, the recycle and product phases need to be accurately identified. This can be simply done using the density of each phase. These

Table 3.2: Linear regression model errors for acceptable ranges of θ (Equation (3.9)).

θ Range	0.0-1.0	0.01-1.0	0.02-1.0	0.03-1.0
MAPE (%)	22.13	7.92	4.92	3.48
MAE	0.0068	0.0056	0.0049	0.0046
Data Points	5056	4586	3965	3414
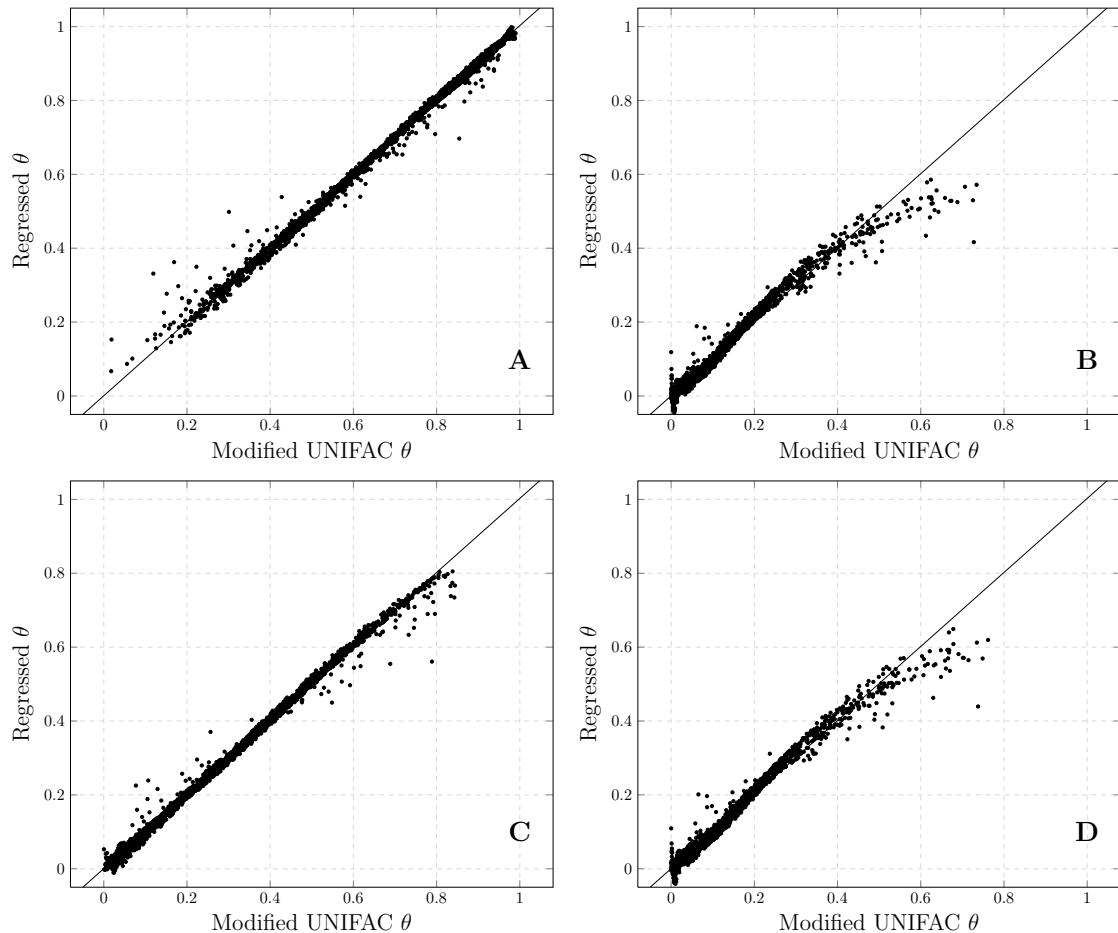
Figure 3.5: Parity plot of partition values for the quaternary system consisting of DMF (A), n-decane (B), tridecanal (C), and 1-dodecene (D) at 25°C [88].

densities are calculated using the summation of each component density multiplied by its respective weight fraction (Equation (3.13)). Correlations for density and the appropriate parameters are found in Appendix A.1. The lower density phase is primarily comprised of the nonpolar components, which includes the product, and is thus fittingly assigned as the product phase. The higher density phase is the more polar phase consisting mainly of the polar solvent DMF. This phase also contains a majority of the recovered catalyst from the reactor that is to be recycled. This procedure to differentiate the phases based on density is necessary because the linear regression model does not return partition coefficients specific to one of the phases. It is, however, possible to apply this phase determining step to the data used to generated the surrogate models, eliminating the phase determining step done here. This may also improve the accuracy of the model, but was not performed at this time. The decanter is then described by the following system of Equations (3.10) to (3.14) in addition to the linear regression models (Equation (3.9)) mentioned above:

$$\dot{n}_{\text{dec,i,p}} = \theta_i^\alpha \cdot \dot{n}_{\text{i,5}} \qquad\qquad i \in \text{COM} \qquad\qquad (3.10)$$

$$\dot{n}_{\text{dec,i,np}} = (1 - \theta_i^\alpha) \cdot \dot{n}_{\text{i,5}} \qquad\qquad i \in \text{COM} \qquad\qquad (3.11)$$

$$\rho_i = a_{\rho,0,i} + a_{\rho,1,i} \cdot T_d \qquad\qquad i \in \text{COM} \qquad\qquad (3.12)$$

$$\rho_{\text{dec,j}} = \sum_{i \in \text{COM}} w_{\text{dec,i,j}} \cdot \rho_i \qquad\qquad j \in \text{PHASE} \qquad\qquad (3.13)$$

$$\rho_{\text{dec,p}} \geq \rho_{\text{dec,np}} \qquad\qquad\qquad\qquad (3.14)$$

Catalyst Leaching

The purpose behind using a TMS is to economically recover the catalyst by simply inducing phase separation through cooling after the reaction step is complete. The small remnant of catalyst complex and excess ligands found in the nonpolar product phase are deactivated in the subsequent distillation column and are removed from the process as part of the product stream. Since the concentration of catalyst is quite small, in the range of a few ppm or less, its effect on the tridecanal purity is negligible.

In order to evaluate the effectiveness of the chosen TMS system, the effect of catalyst leaching must be included in the optimization problem. This is especially important owing to the high cost of the the catalyst complex. For example, one quote from a major specialty chemical company priced biphephos as high as around 140,000 € for a single kilogram!

As previously mentioned, Hentschel et al. [61] do not consider catalyst leaching in their reactor and process optimization problem. They assumed that catalyst leaching does not occur and that it is completely recovered in the polar phase and recycled back to the reactor. This is known to be not realistic and that catalyst leaching does indeed occur for this system (Brunsch and Behr [29], Schäfer et al. [110]), hence the current investigation. The amount of catalyst lost also depends strongly on the TMS

composition due to its influence on the miscibility gap size. Although there is some information about the catalyst leaching available, it too sparse for greater analysis of this problem, such as for other solvents or separation temperatures. The restrictions on the mixture composition are thus the same as those used for the reaction conversion.
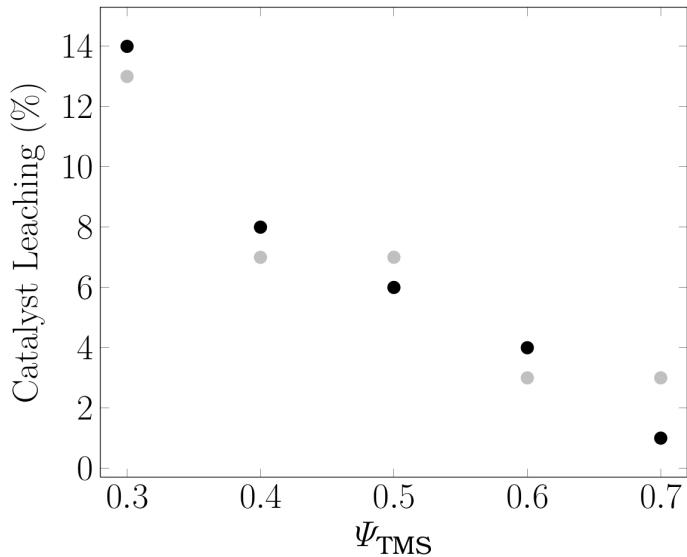
Figure 3.6: Catalyst leaching represented by rhodium (black) and phosphorus (gray) loss relative to TMS composition [88].

Figure 3.6 depicts relative levels of leaching for rhodium and biphephos for various TMS compositions in the same reaction systems used in the correlation for reaction conversion. With increasing levels of DMF in the TMS, the leaching amounts for both rhodium and biphephos decrease at a very similar rate. If one assumes that the leaching rate of rhodium is the same as that of biphephos, within the experimental margin of error, a single correlation to determine leaching rates for both catalyst components can be used instead of two separate ones. The simple average of each component's respective leaching amount is considered to be the overall magnitude of catalyst leaching, $w_{cat,leaching}$. This average is then correlated to Ψ_{TMS} as done for conversion and an adequate fit is observed (see Figure 3.7). The correlation is represented by a quadratic equation presented as Equation (3.15). A linear representation is unsuitable due to large underestimations of catalyst loss when using higher ratios of DMF to n-decane in the TMS. This correlation can then be used with the total mass of the catalyst in the reactor to predict catalyst leaching amounts. The amount of catalyst in the reactor is itself dependent upon the amount of 1-dodecene found in the reactor feed. Using this new variable, the percent of catalyst leaching can be incorporated into the cost optimization of the process. With more experimental data, it may be necessary to fit separate correlations for rhodium and ligand leaching levels if larger deviations between their respective leaching amounts are observed.

$$\text{w}_{\text{cat,leaching}} = 0.4643 \cdot \psi_{TMS}^2 - 0.7493 \cdot \psi_{TMS} + 0.3133 \tag{3.15}$$
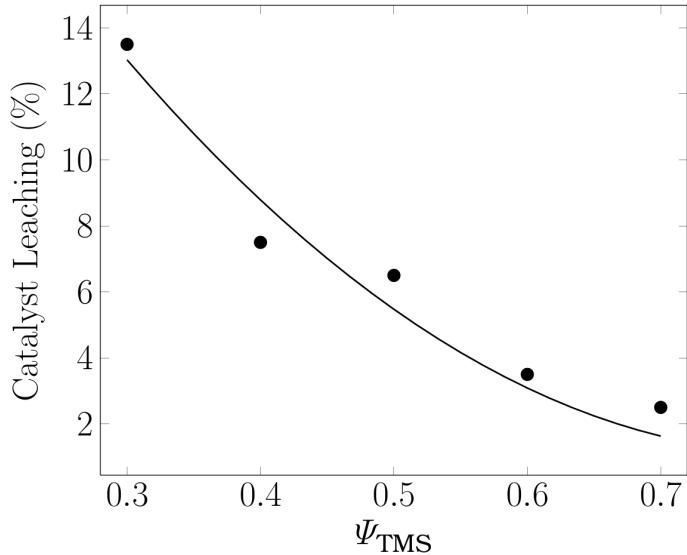
Figure 3.7: Correlation between combined catalyst leaching and Ψ_{TMS} [88].

Distillation Column

As seen in Figure 3.1, the non-polar phase leaving the decanter is fed to a distillation column. The primary goal of this column is to separate the tridecanal product from the TMS solvents and unconverted 1-dodecene. The behavior of this column is very similar to the solvent recovery column discussed by Hentschel et al. [61]. The product is to be separated at a high purity of at least 99.9% from the solvents and remaining 1-dodecene and will be recovered as the bottoms, S_{10}, due to its lower vapor pressure. The other components are condensed and form the distillate. A small purge is separated from the distillate and the remaining stream, S_{11}, is recycled to the mixer and combined with the feed stream, S_1, and with the catalyst recycle stream leaving the decanter, S_6.

The energy requirements for the distillation column consist of the heating and cooling duties of the reboiler and condenser which are related to the reflux and boilup ratios. The flows in the column are modeled using the Underwood correlation (Underwood [120] and [121]), assuming constant molar overflow and constant relative volatilities. The temperature of the column is restricted to a maximum of 453.16 K in the reboiler in order to avoid degradation of the tridecanal product. Since the normal boiling point of tridecanal lies well above 453.16 K the column must be operated under vacuum and a pressure drop of 50% from the top to the bottom of the column is assumed. This fixes a maximum bottoms pressure of 88 mbar, leaving the pressure at the top of the column to be 59 mbar according the assumed pressure drop.

The correlations and methods used to design the distillation column used in this flow-sheet are included in Appendix A.4. The required vapor pressure correlations and parameters are found in Appendix A.1.

3.2.1 Flowsheet Design

In this section, all of the stream balances and stream temperatures for the process are presented.

The mass of the catalyst is based on the amount of 1-dodecene in the reactor. In the work by Brunsch [28], from which the catalyst leaching and reaction performance data are taken, the amount of rhodium precursor was set at one-thousandth of a mole relative to that of 1-dodecene present at the start of the reaction. Since the ratio of biphephos to rhodium was set at five to one, the amount of each catalyst component can be found by Equation (3.16) and Equation (3.17).

$$\dot{m}_{\text{Rh}} = 1 \cdot 10^{-3} \cdot \dot{n}_{\text{nC12en,2}} \cdot M_{\text{Rh}} \tag{3.16}$$

$$\dot{m}_{\text{BPP}} = 5 \cdot 10^{-3} \cdot \dot{n}_{\text{nC12en,2}} \cdot M_{\text{BPP}} \tag{3.17}$$

The flowsheet has several constraints that are not included in the model section above. These constraints are used to ensure that the mass balances are correct.

$$\dot{n}_{\text{nC13al,1}} = 0 \tag{3.18}$$

$$\dot{n}_{i,2} = \sum_{s\in\{1,6,11\}} \dot{n}_{i,s} \qquad\qquad i \in \text{COM} \tag{3.19}$$

$$\dot{n}_{i,s+1} = \dot{n}_{i,s} \qquad\qquad s \in \{2,4,7\} \tag{3.20}$$

$$\dot{n}_{i,6} = \dot{n}_{\text{dec},i,\text{p}} \qquad\qquad i \in \text{COM} \tag{3.21}$$

$$\dot{n}_{i,7} = \dot{n}_{\text{dec},i,\text{np}} \qquad\qquad i \in \text{COM} \tag{3.22}$$

$$\dot{n}_{\text{C,in},i} = \dot{n}_{i,8} \tag{3.23}$$

$$\dot{n}_{i,9} = \dot{n}_{\text{C,D},i} \qquad\qquad i \in \text{COM} \tag{3.24}$$

$$\dot{n}_{i,10} = \dot{n}_{\text{C,B},i} \qquad\qquad i \in \text{COM} \tag{3.25}$$

$$0.01 \leq x_{\text{purge}} \leq 0.1 \tag{3.26}$$

$$\dot{n}_{i,12} = x_{\text{purge}} \cdot \dot{n}_{i,9} \tag{3.27}$$

$$\dot{n}_{i,11} = (1 - x_{\text{purge}}) \cdot \dot{n}_{i,9} \tag{3.28}$$

Stream temperatures are defined as the following:

$$T_s = T_D = 298.16 \text{ K} \qquad\qquad s \in \{1,5,6,7\} \tag{3.29}$$

$$T_3 = T_{\text{R}} \tag{3.30}$$

$$T_4 = T_{\text{R}} \tag{3.31}$$

$$T_R = 353.16 \text{ K} \tag{3.32}$$

$$T_D = T_{\text{dew,C,D}} \tag{3.33}$$

$$T_8 = T_{\text{bub,C,F}} \tag{3.34}$$

$$T_s = T_{\text{bub,C,D}} \qquad\qquad s \in \{9, 11, 12\} \tag{3.35}$$

$$T_{10} = T_{\text{bub,C,B}} \tag{3.36}$$

The temperature of the stream exiting the mixer (S_2) is calculated using the energy balance around the mixer consisting of the feed and recycle streams. The correlation for enthalpy is given by Equation (A.2) in Appendix A.1.

$$\sum_{i \in \text{COM}} \left(\dot{n}_{i,2} \cdot h_{i,2}(T_2) \right) = \sum_{s} \sum_{i \in \text{COM}} \left(\dot{n}_{i,s} \cdot h_{i,s}(T_s) \right) \tag{3.37}$$
$$s \in \{1, 6, 11\}$$

3.2.2 Production and Investment Costs

The objective of this work is to determine the cost optimal solution for the process described in this section in order to produce a specified amount of tridecanal. The objective function seen later in Equation (3.71) contains two parts, namely the annualized cost of the capital investment and the continuing production costs. In this section, the complete cost model for the optimization is included, starting with the production costs and followed by the investment costs.

3.2.2.1 Production Costs

Utility costs are composed of feedstock or make-up, steam, and cooling water costs. Prices for each component are listed in Table 3.3. Prices for materials are based on a molar or mass basis and utility prices are based on an energy basis. More specifically, a constant heat capacity for cooling water ($c_p = 75.3 J/mol/K$) and a constant heat of vaporization for steam ($h_{\text{vap,st}} = 1888 kJ/kg$) are used in determining the energy based cost. These values, as well as the material costs excluding biphephos, were originally used by Hentschel et al. [61].

For the work considered in this chapter, a kilogram price of \$38.5k is adopted for the Biphephos ligand based on past purchase information from 2010 (MOLISA GmbH). The cost of the Rhodium(I) dicarbonyl acetylacetonate precursor is estimated using the spot price of rhodium at the time of the Biphephos acquisition, \$2648 per troy ounce (Spring 2010). Of course, the cost of the finished rhodium precursor will have a higher cost than the spot metal price, but this is not considered here. Care must also be taken when using rhodium due to its highly volatile price as this may have a significant effect on process economics. Some may notice that the price of the ligand and rhodium have changed considerably since 2010 when the prices above were adopted. These values are used due to the acquisition time of the initial components used within

the SFB TRR/63 research consortium. At the time of writing this document, the price of rhodium has fallen significantly. To account for these changes, a price sensitivity analysis where the price of the ligand and rhodium both vary by $\pm 50\%$ is included in the analysis.

Table 3.3: Prices of raw materials and utilities.

Utility	Price Φ	Unit
DMF	73.1	$/kmol$
C10an	71.4	$/kmol$
nC12en	661.5	$/kmol$
Catalyst(Rh)	85150	$/kg$
Catalyst(BPP)	38500	$/kg$
Cooling water	2.54e-6	$/kJ$
Steam	1.41e-5	$/kJ$

Heating and Cooling Duties

There are five units in the flowsheet that require heating or cooling, and their respective heat duties need be quantified. Two heat exchangers, HX_2 and HX_4, require cooling and are supplied with cooling water. The three remaining heat exchangers, HX_2, HX_3, and HX_5, are used to raise the temperature of their respective streams and are supplied with steam.

Two heat exchangers, HX_4 and HX_5, are the condenser and reboiler for the distillation column, respectively. To calculate the heat and/or cooling duties of the condenser and reboiler for a distillation column using the short cut method used here, the reflux ratio must be known. The reflux ratio is determined using the methods outlined in Appendix A.4 and is ultimately left as an optimization variable.

This model uses a total condenser and the distillate is assumed to be a saturated liquid. Thus, calculating the heat to be removed from the distillate requires the heat of vaporization at the dew point temperature of the mixture. A correlation (Equation (A.3)) taken from Yaws [131] is used for the heat of vaporization for DMF, n-decane, and 1-dodecene. The vapor pressure correlation (Equation (A.4)) for tridecanal is taken from Hentschel et al. [61]. The parameters for both equations are listed in Table A.4. Thus, the heat duty for the condenser can be calculated using Equations (3.38) to (3.40).

$$\dot{Q}_{\text{con}} = (R+1) \cdot \dot{n}_{\text{D}} \cdot \sum_{i \in \text{COM}} \left(x_{\text{D},i} \cdot h_{\text{vap},i}(T_{\text{dew}}) \right) \tag{3.38}$$

$$p_{\text{vap,LK}}(T_{\text{dew}}) = p \cdot \sum_{i \in \text{COM}} \left(\frac{x_{\text{D},i}}{\alpha_{i,\text{LK}}} \right) \tag{3.39}$$

$$h_{\text{vap},i}(T) = a_{1,i} \cdot \left(1 - \frac{T}{a_{2,i}}\right)^{a_{3,i}} \tag{3.40}$$

Similar to the condenser, a total reboiler is used in this model. The vapor pressure correlation is used again but in conjunction with the bubble point temperature of the mixture in the bottoms. Equation (3.41) is used to find the boilup ratio for the bottoms needed to determine the required heat duty in the reboiler. Since the feed is always assumed to be a saturated liquid, q is always equal to one. Once known, the heat duty of the reboiler can be found using Equations 3.42 and 3.43.

$$S = \frac{R + q}{\frac{\dot{n}_D}{\dot{n}_B} + q - 1} \tag{3.41}$$

$$\dot{Q}_{\text{reb}} = S \cdot \dot{n}_B \cdot \sum_{i \in \text{COM}} (x_{B,i} \cdot h_{\text{vap},i}(T_{\text{bub}})) \tag{3.42}$$

$$p_{\text{vap,HK}}(T_{\text{bub}}) = (p + \Delta p) \cdot \sum_{i \in \text{COM}} \left(\frac{x_{B,i}}{\alpha_{i,\text{HK}}}\right) \tag{3.43}$$

More specifically to the model at hand, the heat duties for the condenser and rebolier are described using Equations 3.44 and 3.45, respectively.

$$\dot{Q}_9 = -\dot{n}_D \cdot (R + 1) \sum_{i \in \text{COM}} (x_{D,i} \cdot h_{\text{vap,D},i}) \tag{3.44}$$

$$\dot{Q}_{10} = \dot{n}_B \cdot S \sum_{i \in \text{COM}} (x_{B,i} \cdot h_{\text{vap,B},i}) \tag{3.45}$$

Heat duties for the three remaining heat exchangers are calculated using a simple enthalpy difference between the inlet and outlet streams, (Equation (3.46)). Heat exchangers where heating takes place will have a positive heat flux and coolers will have negative heat flux. This is taken into consideration when sizing the heat exchanger surface areas.

$$\dot{Q}_s = \sum_{i \in \text{COM}} (\dot{n}_{i,s+1} h_{i,s+1} - \dot{n}_{i,s} h_{i,s}) \qquad s \in \{2, 4, 7\} \tag{3.46}$$

The cooling water and steam utilities calculated previously are now used to find the overall amount of cooling water and steam required for the process. In total, two heat exchangers require cooling, namely to cool the post-reaction mixture down to the separation temperature (HX_2 with duty $\dot{Q}_4$) and for the condenser (HX_4 with duty $\dot{Q}_9$). The three remaining heat exchangers need to be heated with steam and include heating the reactor feed (HX_1 with duty $\dot{Q}_2$), increasing the column feed to its bubble point temperature (HX_3 with duty $\dot{Q}_7$), and the column reboiler (HX_5 with duty $\dot{Q}_{10}$). Now

the cooling water costs can be calculated using Equation (3.47) and the steam costs by Equation (3.48) in conjunction with their respective unit utility costs.

$$C_{\text{cw}} = -\Phi_{\text{cw}} \cdot \sum_{s\in\{4,9\}} Q_s \tag{3.47}$$

$$C_{\text{st}} = \Phi_{\text{st}} \cdot \sum_{s\in\{2,7,10\}} Q_s \tag{3.48}$$

The feed costs in this simplified model are only constituted by the 1-dodecene feed and the replenishing of DMF and n-decane. The total cost associated with the feed, excluding the catalyst makeup, C_{feed}, is then given by Equation (3.49).

$$C_{\text{feed}} = \sum_{i \,\in\{\text{DMF,C10an,nC12en}\}} \Phi_i \cdot \dot{n}_{i,1} \cdot 10^{-3} \tag{3.49}$$

The cost associated with catalyst leaching (Equation (3.50)) is determined by the catalyst leaching factor found in Equation (3.15), by the total mass of both catalyst components found in the reactor, and their respective prices.

$$C_{\text{cat}} = \text{w}_{\text{cat,leaching}} \cdot \sum_{i \,\in\, \{\text{Rh,BPP}\}} \Phi_i \cdot \dot{m}_{i,2} \tag{3.50}$$

Production Cost Function

Once the various production costs have been calculated, the overall production cost is simply the summation of each component (Equation (3.51)).

$$C_{\text{production}} = C_{\text{feed}} + C_{\text{cw}} + C_{\text{st}} + C_{\text{cat}} \tag{3.51}$$

3.2.2.2 Investment Costs

To be able to estimate the capital cost of the process, the size of each unit must be calculated. Once known, the capital required can be estimated using specific dimensions of the unit that are correlated to cost functions. In this work, the correlations developed by Guthrie [56] are used.

Reactor

In order to be able to estimate the size of the reactor, the volume must be known which requires knowledge of the residence time, τ_r. Since the proposed reactor model is simply based on conversion without consideration of reaction kinetics or trajectories, a residence time must be chosen. The reactor used in this model is thus fixed to

a residence time of three hours in order to maintain consistency between the results found in this work and those obtained by Brunsch [28]. The volume of the reactor is then mainly influenced by the size of the recycle streams and the changing density of the mixture when the TMS composition is altered. As done by Hentschel et al. [61], the volume of the reactor is doubled to allow room for the gas phase. The dimensions of the reactor are restricted as such that the length of the reactor is four times that of the diameter (Biegler et al. [23]). The length and diameter of the reactor can then be found using Equations (3.52) to (3.54).

$$V_{\text{r,liq}} = \tau_{\text{r}} \cdot \sum_{i \in \text{COM}} \frac{\dot{n}_{i,4} M_i}{\rho_i(T_4)} \tag{3.52}$$

$$D_{\text{r}} = \sqrt[3]{\frac{2V_{\text{r,liq}}}{\pi}} \tag{3.53}$$

$$L_{\text{r}} = 4D_{\text{r}} \tag{3.54}$$

Decanter

Decanter dimensions are described similar to the reactor except that the residence time is reduced to 20 minutes as was previously assumed by Hentschel et al. [61]. The length and diameter of the decanter are found using Equations (3.55) to (3.57).

$$V_{\text{d,liq}} = \tau_{\text{d}} \cdot \sum_{i \in \text{COM} \backslash \text{GAS}} \frac{\dot{n}_{i,5} M_i}{\rho_i(T_{\text{d}})} \tag{3.55}$$

$$D_{\text{d}} = \sqrt[3]{\frac{2V_{\text{d,liq}}}{\pi}} \tag{3.56}$$

$$L_{\text{d}} = 4D_{\text{d}} \tag{3.57}$$

Heat exchangers

Table 3.4: Heat transfer coefficients of heat exchangers (Equation (3.58)).

Unit	$U[W/m^2/K]$	Type
HX 1	283.9	organic solvents (shell)/water (tube)
HX 2	283.9	organic solvents (shell)/water (tube)
HX 3	283.9	organic solvents (shell)/water (tube)
HX 4	113.56	high boiling hydrocarbons (shell)/water (tube)
HX 5	1419.5	water (shell) / steam condensing (tube)

Heat exchangers are priced based on the surface area available for heat transfer. Using Equation (3.58), the areas of each heat exchanger can be estimated using heat duties,

log-mean temperature differences ΔT_{lm}, and the heat transfer coefficients, U, which are taken from Guthrie [56]. Table 3.4 contains the heat transfer coefficients used in this work and the reasoning for each selection.

$$A_{\mathrm{hex},s} = \left| \frac{\dot{Q}_s}{U_s \Delta T_{\mathrm{lm},s}} \right| \tag{3.58}$$

To calculate the log mean temperature difference, the temperatures of the steam and cooling water must be known. The conditions for these utilities are a steam temperature of 600 K, a cooling water temperature of 298 K, and a decanter cooling water stream of 278 K, due to the lower temperature needed in the decanter. For each cooling case, the cooling water is assumed to increase by 10 K ($\Delta T_{\mathrm{cw}} = 10$ K). The heat exchangers used are counter-current and the log mean temperature differences are calculated depending on whether the heat exchangers use steam (Equation (3.59)), cooling water (Equation (3.60)), or sub-cooled decanter cooling water (Equation (3.61)).

$$\Delta T_{\mathrm{lm,st}}(T_{\mathrm{h}}, T_{\mathrm{c}}) = \frac{T_{\mathrm{h}} - T_{\mathrm{c}}}{log(\frac{T_{\mathrm{st}}-T_{\mathrm{c}}}{T_{\mathrm{st}}-T_{\mathrm{h}}})} \tag{3.59}$$

$$\Delta T_{\mathrm{lm,cw}}(T_{\mathrm{h}}, T_{\mathrm{c}}) = \frac{(T_{\mathrm{h}} - T_{\mathrm{cw}}) - (T_{\mathrm{c}} - (T_{\mathrm{cw}} + \Delta T_{\mathrm{cw}}))}{log(\frac{T_{\mathrm{h}}-T_{\mathrm{cw}}}{T_{\mathrm{c}}-(T_{\mathrm{cw}}+\Delta T_{\mathrm{cw}})})} \tag{3.60}$$

$$\Delta T_{\mathrm{lm,cw,D}}(T_{\mathrm{h}}, T_{\mathrm{c}}) = \frac{(T_{\mathrm{h}} - T_{\mathrm{cw,D}}) - (T_{\mathrm{c}} - (T_{\mathrm{cw,D}} + \Delta T_{\mathrm{cw,D}}))}{log(\frac{T_{\mathrm{h}}-T_{\mathrm{cw,D}}}{T_{\mathrm{c}}-(T_{\mathrm{cw,D}}+\Delta T_{\mathrm{cw,D}})})} \tag{3.61}$$

Since there are only five heat exchangers the five log mean temperature values in the model can easily be shown. These are calculated using their respective inlet and outlet temperatures given in Equations (3.62) to (3.66).

$$\Delta T_{\mathrm{lm},1} = \Delta T_{\mathrm{lm,st}}(T_3, T_2) \tag{3.62}$$
$$\Delta T_{\mathrm{lm},2} = \Delta T_{\mathrm{lm,cw,D}}(T_4, T_5) \tag{3.63}$$
$$\Delta T_{\mathrm{lm},3} = \Delta T_{\mathrm{lm,st}}(T_8, T_7) \tag{3.64}$$
$$\Delta T_{\mathrm{lm},4} = \Delta T_{\mathrm{lm,cw}}(T_{\mathrm{dew,D}}, T_{\mathrm{bub,D}}) \tag{3.65}$$
$$\Delta T_{\mathrm{lm},5} = \Delta T_{\mathrm{lm,st}}(T_{\mathrm{bub,B}}, T_{\mathrm{dew,B}}) \tag{3.66}$$

Distillation Columns

As mentioned previously, correlations for designing the distillation column can be found in Appendix A.4. This includes the methods used to determine the average diameter of the rectification and stripping sections as well as the overall height of the column. These are the two design criteria required to estimate the investment cost of the column comprised of the vessel and stack (trays).

Table 3.5: Cost parameters for the bare cost (BC) correlation (Equation (3.68)), material and pressure factors (MPF), module factors (MF), and the CE index used to estimate the bare module cost using Equation (3.69).

Unit	a_0	a_1	a_2	a_3	a_4	MPF	MF	CE_{base}
VES R	1e3	1.2192	0.81	0.9144	1.05	1.45	4.23	115
VES D	690	1.2192	0.78	0.9144	0.98	1	3.18	115
VES C	1e3	1.2192	0.81	0.9144	1.05	1	4.23	115
STA C	180	3.048	0.97	0.6096	1.45	2.8	1	115
HX 1	5e3	37.1612	0.65	1	0	1.87	3.29	115
HX 2	5e3	37.1612	0.65	1	0	1.87	3.29	115
HX 3	5e3	37.1612	0.65	1	0	1.35	3.29	115
HX 4	5e3	37.1612	0.65	1	0	1	3.29	115
HX 5	5e3	37.1612	0.65	1	0	1.35	3.29	115

Cost Functions

Capital costs are found using correlations that estimate the base price for each unit known as the bare cost (BC). These are then modified using a material and pressure factor (MPF) to account for the use of different materials (carbon steel, stainless steel, etc) at different pressures, a module factor (MF) that takes installation costs into account, and an update factor (UF) that adjusts for inflation. The bare cost depends on one or t wo (S_1 and S_2) size characteristics specific to each unit. Decanters, reactors, and column shells can be modeled as horizontal or vertical vessels which require the height or length as S_1 and the diameter as S_2. Column trays also depend on the height and the diameter of the column. Heat exchangers only require the surface area available for heat transfer as S_1. These values can been calculated using the equations presented previously in this section. Consulting the "Chemical Engineering Index" published by Chemical Engineering is required to ascertain the current monthly index in order to determine the update factor required in Equation (3.67). However, the value chosen by Hentschel et al. [61], where CE is equal to the 2011 average of 585, is used here for comparison reasons.

$$UF_u = \frac{CE}{CE_{\text{base}}} \tag{3.67}$$

$$BC_u = a_{0,u} \left(\frac{S_1}{a_{1,u}} \right)^{a_{2,u}} \left(\frac{S_2}{a_{3,u}} \right)^{a_{4,u}} \tag{3.68}$$

$$BMC_u = UF_u \cdot (MPF_u + MF_u - 1) \cdot BC_u \tag{3.69}$$

$$C_{\text{invest}} = \sum_u BMC_u + \Psi_{\text{cat}} \dot{n}_{\text{cat}} M_{\text{cat}} \tau_R \tag{3.70}$$

Table 3.5 lists the values of BC, MPF, MF, and CE_{base} used for this model. The module factors are determined based on the bare cost of the unit (here they are all the maximum

as the BC for each unit remains low). Material and pressure factors (MPF) are chosen based on the expected conditions within the respective unit. The bare module cost (BMC) is the final price for the unit to be integrated into the plant (Equation (3.69)) after considering all other cost factors. Thus, the total capital investment is the summation of all bare module costs in the proposed plant (Equation (3.70)).

3.3 Optimization

The goal of this work is to identify the cost optimal process considering catalyst leaching for the previously described model. The results gathered allow for a detailed analysis of where process improvement or process intensification measures should be applied. The major trade-off expected is the lowered conversion in the reactor and larger recycle streams competing with lower levels of catalyst leaching when using higher ratios of DMF to n-decane in the TMS. Using cost functions is the ideal approach to ensure that the best, economical compromise is made.

The objective function is based on the three year total annualized cost of production. This includes the depreciation of the capital equipment, all utilities, feedstock, and make-up solvent and catalyst. Two slightly different optimizations will take place: one with catalyst lost based on rhodium alone and a second that takes both rhodium and biphephos leaching into account. This is done to show the importance of ligand loss when compared to only focusing on rhodium. It is expected that the increased cost of the ligand will have significant effects on the process design and cost.

Optimization variables in this process include the feed composition ($\dot{n}_{i,1}$), the composition of the TMS in the reactor (ψ_{TMS}), recovery fractions of the distillate and bottoms ($\xi_{1-\text{dodecene}}$), and the reflux ratio of the distillation column (R_{factor}). The product specifications are for 10,000 tons n-tridecanal produced annually with at least 99.9% purity and plant operation for 330 days annually. The objective function is then summarized in Equation (3.71).

All optimization problems are implemented in AMPL and optimized using the solver CONOPT 3.14V on a PC with one Intel Core$^{\text{TM}}$ i5-3570 CPU at 3.40 GHz, a memory of 8 GB, and running on the Kubuntu 12.04 operating system. Therefore, global optimality cannot be guaranteed and all minimums are considered to be local solutions.

$$\min \text{TAC} \left[\frac{\$}{\min} \right] = (C_{\text{invest}}/3 + C_{\text{production}}) \tag{3.71}$$

s.t. Reactor: Equations (3.1) to (3.5)
      Solvent composition: Equations (3.6) to (3.7)
      Decanter: Equations (3.8) to (3.14)
      Catalyst Leaching: Equation (3.15)
      Catalyst Amount: Equations (3.16) and (3.17)
      Flowsheet: Equations (3.18) to (3.37)
      Production Cost: Equations (3.38) to (3.51)
      Investment Cost: Equations (3.52) to (3.67) and (A.18) to (A.47)
      Product specifications: $\dot{n}_{\text{tridecanal},10} = 0.1 kmol/min$

3.4 Discussion and Results

In both optimization problems, the optimal operating point is found to be the point with the highest allowable DMF, when Ψ_{TMS} is equal to 0.7. The considerably high cost that results due to catalyst leaching is responsible for a very large majority of the overall process cost. In order to reduce the amount of catalyst lost, a TMS with higher ratios of polar DMF to n-decane are used to enhance the phase separation in the decanter. This leads to higher levels of catalyst retention, which more than off-sets the slight reduction in conversion. The lowered conversion and larger recycle streams that occur with higher values of Ψ_{TMS} lead to higher specific capital and utility costs that are minuscule in comparison to the amount saved due to a reduction in catalyst makeup. This alone proves that catalyst loss and its relevance to solvent selection are the most important criteria for further study.

In the remaining sections, the TMS ratio is fixed at several points between the upper and lower bounds of 0.3 and 0.7 to compare different aspects of the cost optimal process.

3.4.1 Catalyst Leaching

Due to the importance of catalyst leaching in the hydroformylation of 1-dodecene, an entire section is devoted to its discussion.

It was mentioned above that the optimal TMS composition is that which contains the maximum amount of polar solvent DMF. With higher levels of polar solvent, more catalyst can be recovered after separation in the decanter. Therefore, the optimization result is not surprising when considering the high cost of the catalyst in comparison to the other utility costs. For example, with Ψ_{TMS} equal to 0.3, the catalyst makeup is 97.6% of the utility cost and with Ψ_{TMS} equal to 0.7, this fraction of the utility cost reduces only to 86.8%. This is met, however, with a substantial decrease in the overall process cost as can be seen in Figure 3.8. This shows one that by increasing Ψ_{TMS}, the total cost of the process decreases significantly.

A simple procedure then to reduce the cost of the process is to simply change the TMS composition from the commonly used mixture ($\Psi_{\text{TMS}} = 0.4$) to one containing the maximum feasible amount of DMF. Again, this is the common composition of the TMS mixture used by Hentschel et al. [61] and Kiedorf et al. [70]. It is useful at this point

to compare the economic performance of this TMS composition to the optimal solution found here.

In the first optimization where the catalyst loss is restricted to rhodium, the optimal TAC is equal to \$3214/kmol product when Ψ_{TMS} is equal to 0.4. As Ψ_{TMS} increases to 0.7, the total cost drops significantly to \$1373/kmol product, a reduction of 57.3%. The results of the second optimization, which include the cost of ligand leaching, show a much more pronounced effect on the process cost. One can see that the cost increases by at least an order of magnitude when the price of biphephos make-up is included in the objective function (see Figure 3.8). It is again possible to make a direct comparison as before. The cost of this process considering ligand loss is \$20020/kmol product with Ψ_{TMS} equal to 0.4 which reduces to \$5307/kmol product when Ψ_{TMS} increases to 0.7. This means that a 73.5% reduction in total process cost could be expected simply by using a different composition of the TMS without significant changes being made to the unit operations in the process.

Much discussion revolves around the loss of metal catalyst due to its cost, such as in Fang et al. [43], but the results presented here suggest that the same if not more attention should be given to the biphephos ligand. Not only does the ligand show similar leaching levels as rhodium, it has a higher concentration in the mixture (in this work it is five times the mole number of metal) and about three times the molecular mass of the precursor. Based on our assumptions, then for every unit mass of rhodium lost due to leaching, roughly 15 times as much biphephos is also lost. As seen in Table 3.6, the cost of biphephos at the optimal point is about 76% of the total process TAC while rhodium loss accounts for only 11%. When the cost of biphephos is not considered, rhodium loss still remains significant but constitutes only 45% of the total cost. It would seem more focus should be made on ligand retention (or on reducing the ligand price) in addition to efforts at improving rhodium recovery.

Table 3.6: Cost breakdown of the optimal points ($\Psi_{TMS} = 0.7$) for catalyst costs excluding and including Biphephos (BPP) leaching cost. Values given are percent TAC.

	Rhodium	Dodecene	Utilities/Solvents	Biphephos	TAC
Excl. BPP	45.4%	53.0%	1.6%	-	\$1373/kmol
Incl. BPP	10.6%	12.8%	0.4%	76.2%	\$5307/kmol

It is not unexpected that more polar solvent would lead to better separation of the catalyst. This is previously discussed in the work by Brunsch and Behr [29]. The significance of how a simple change in the TMS would affect the process cost was, however, unanticipated. These results suggest that before investigating detailed kinetics and downstream processing, the economical bottleneck of the process should be thoroughly considered beforehand. These results show that maximizing conversion, even for the simplified reaction here, would only benefit (or worsen due to increased miscibility
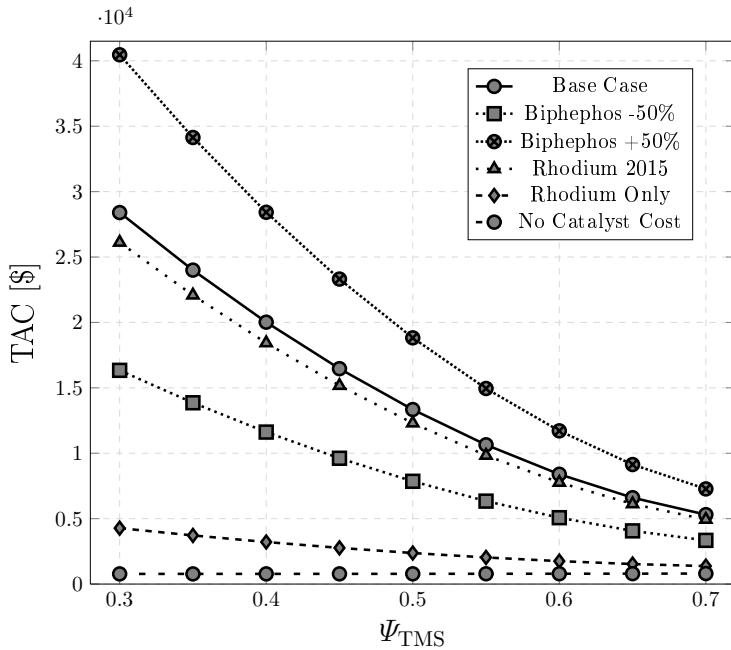
Figure 3.8: Total cost per kmol tridecanal produced with respect to the TMS composition, Ψ_{TMS}.

of the resulting mixture) the process insignificantly if the catalyst leaching problem is not addressed beforehand.

Optimizations performed excluding catalyst costs only showed slight differences in the total annualized cost, with the maximum difference being around 0.51%. This simply reflects the expected increased conversion when higher levels of n-decane are used in the TMS. It also shows the very small influence this change in conversion has on the TAC. In this scenario, the cost optimal process uses a Ψ_{TMS} equal to 0.3 and a TAC of $776/kmol product and the cost continues to rise with increasing levels of DMF to a maximum of $803/kmol product with Ψ_{TMS} equal to 0.7. The majority of this cost is the 1-dodecene feed. As seen above, the overwhelming impact of catalyst leaching on the cost of the process makes the increased capital and utility costs associated with lower conversion negligible. If we optimize the process without taking the catalyst leaching into account, the optimal configuration provided may be quite the opposite of what one initially expects.

3.4.1.1 Price Sensitivity

Due to the volatile changes in the price of rhodium, it is worth comparing the optimization results for different spot prices. This work was originally conducted using a rhodium price taken at the time of the original biphephos acquisition, a relatively high $85150/kg. The price of rhodium has fallen quite significantly since then with the 2015 average being $29563/kg, a decrease of 63.7%. The optimizations are repeated

using this updated rhodium price and the results are included in Figure 3.8 labeled as Rhodium 2015. It can be seen that the overall change in the TAC is low, reinforcing the lower significance of the rhodium metal leaching compared to that of the biphephos ligand.

Comparatively, changing the price of the biphephos ligand from -50 to 50% of the price given in Table 3.3 results in much larger deviations in the TAC. These changes are probably best explained using the TAC of the optimizations considering only the cost of rhodium and the process where catalyst costs are ignored. In the rhodium only example, the original, higher price for rhodium is used. Any decrease in the price of rhodium will decrease the TAC effectively approaching the lower bound where no catalyst cost is considered. Thus, the TAC cannot be reduced further below this line. The amount of room for improvement for the catalyst ligand is much larger. Thus, changes in price or recovery of the ligand will more significantly and effectively lower the TAC. Therefore, efforts should be made to lower the cost of the ligand in addition to improving its retention in the system. Perhaps even the substitution of the biphephos ligand with another, albeit poorer performing, ligand would be economically preferable. In general, even if the prices of the catalyst ligand and the rhodium metal core both fell by more than 50% each, efforts to reduce catalyst leaching would still need to be prioritized.

3.4.2 Captial costs

Although accounting for a very small percentage of the overall process costs (0.34% at $\Psi_{\text{TMS}} = 0.3$ to 2.23% at $\Psi_{\text{TMS}} = 0.7$ when considering the cost of biphephos), it is interesting to see how the individual capital costs of each unit vary with TMS composition.

The unit capital costs for the five heat exchangers are shown in Figure 3.9 and in Figure 3.10 for the reactor, decanter, and distillation column. Increasing amounts of polar solvent lead to a larger catalyst recycle stream (S_6) which is seen in the increasing size of the reactor and the heat exchangers before (H_{X1}) and after (H_{X2}) the reactor. The size of the decanter increases only slightly with respect to TMS composition. An increase in DMF in the post-reaction mixture leads to a larger polar phase forming in the decanter. As the amount of DMF in the system increases, the amount of n-decane and 1-dodecene in the nonpolar phase decreases while the amount of DMF and tridecanal remains relatively constant. So, as the separation of the catalyst in the decanter improves, less n-decane enters the distillation column, decreasing the overall flowrate and hence its required size. This reduction in the amount of material entering the distillation column also reduces the amount of material to be vaporized, leading to lower steam duties for the reboiler and cooling water duties for the condenser. However, due to the increased amount of mass within the system with higher amounts of DMF in the TMS, the overall heating and cooling duties increase due to the requirements of HX_1 and HX_2. This is also seen in the decrease in size of the condenser, the largest heat exchanger in the flowsheet.

Considering the relatively low capital cost of this process, any increase in process size or extra units used that help to improve catalyst retention would be beneficial. One

possible strategy may be to increase the residence time in the reactor while lowering the catalyst concentration in order to reduce the amount of catalyst lost in the product phase. This would also increase the total volume of each remaining vessel and the amount of the utilities used, but would open up new, potential areas for process optimization. Integrated separation processes may also be considered as the additional cost of extra separation units would be expectedly economical. In contrast to the reduced catalyst leaching, these increased costs would be very small in comparison. It is therefore recommended to investigate such schemes in future process designs utilizing this catalyst complex and TMS system for catalyst recovery.
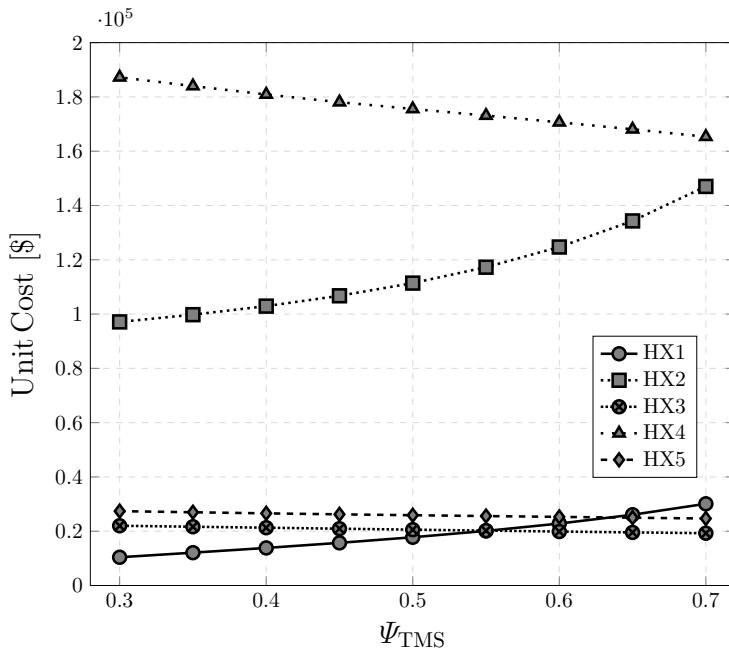
Figure 3.9: Total capital cost for the five heat exchangers for various TMS compositions [88].

3.4.3 Utility costs

In Figure 3.11 the relative utility costs for the feedstock, cooling water, steam, and catalyst are presented. The largest variation is in the relative catalyst cost. As this is by far the largest fraction of the total process cost, this large deviation has a sizable impact on the overall utility cost. This is why as Ψ_{TMS} increases, the cost of the catalyst significantly decreases in a similar manner as the total annualized process cost. All other utilities increase with increasing values of Ψ_{TMS} except for n-decane which, by design, decreases. Due to the increase in reactor size, there is a parallel increase in heating and cooling duties which results in higher usage of steam and cooling water. Only the amount of 1-dodecene remains almost unchanged as the DMF fraction
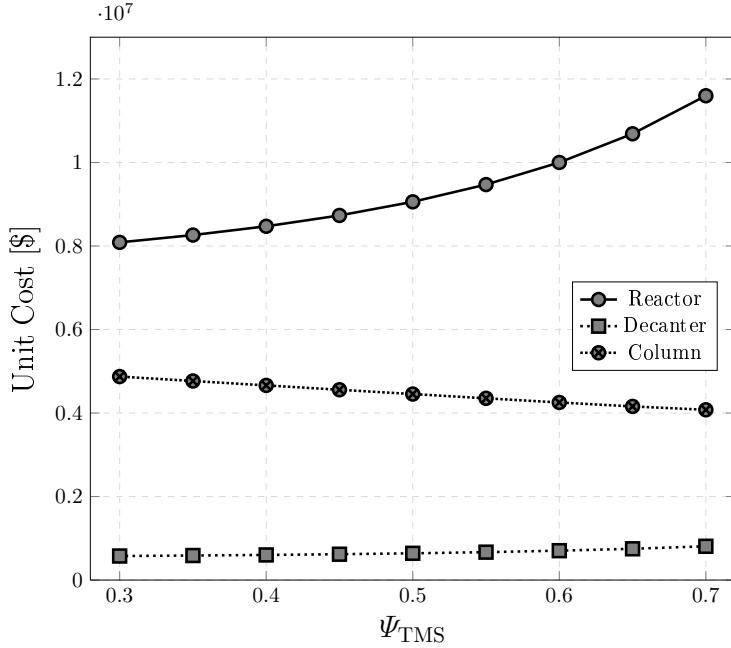
Figure 3.10: Total capital cost for the reactor, decanter, distillation column shell, and distillation trays for various TMS compositions [88].

in the TMS increases. This is a result of the required product constraint and also that most unconverted 1-dodecene is recycled back to the reactor feed. When considering byproduct formation in a more realistic process model, a large portion of the uncoverted 1-dodecene would be isomerized in the reactor forming various iso-dodecenes. As shown by Hentschel [61], recycling iso-dodecene benefits the process by reducing the amount of fresh 1-dodecene that is isomerized thereby increasing the overall selectivity and conversion to tridecanal. In a real process at steady state, the required amount of 1-dodecene in the feed would probably not vary significantly with changing TMS compositions.

The recovery fraction of 1-dodecene in the distillate is optimal at very high ratios. With Ψ_{TMS} equal to 0.3, the recovery fraction of 1-dodecene is 0.999503 and reduces ever so slightly to 0.998816 with Ψ_{TMS} being equal to 0.7. This very high recovery fraction means that almost no tridecanal is found in the distillate. The almost negligible differences in the recovery fractions when using different TMS compositions shows that the recovery rate is an insignificant optimization variable in this problem. It would be a good assumption to model the column as an indirect separation with a non-distributing bottoms product, simplifying the model further, as long as the assumption of an ideal system is valid.

The effect of the reflux ratio is to decrease the size of the column by finding the balance between the diameter and the height of the column. In this case, the reflux ratio remains relatively constant, staying at 0.287 for each value of Ψ_{TMS}. The reflux rate
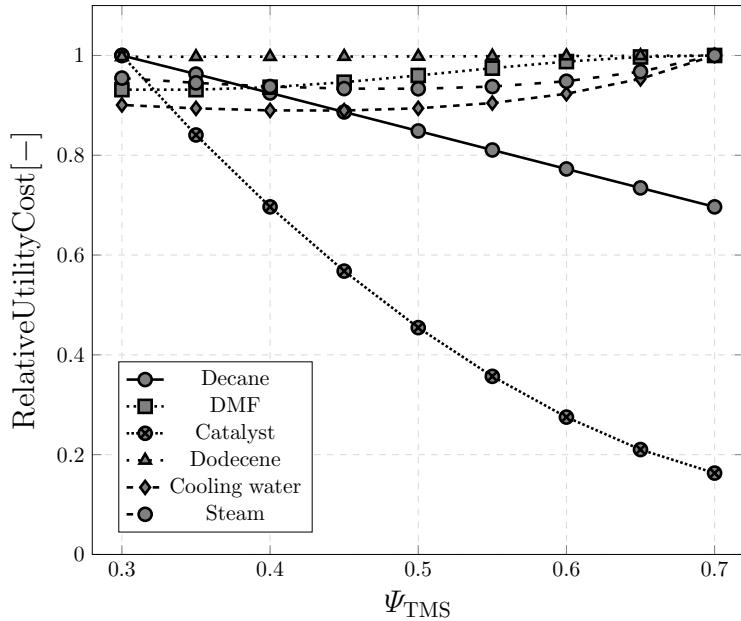
Figure 3.11: Relative utility costs for various TMS compositions [88].

is as insignificant in this process as the recovery rate is. With a more dynamic model including advanced reaction kinetics with consideration of byproducts, the separation in the distillation columns would probably take on more importance. This must, however, first be met with higher levels of catalyst recovery.

3.5 Conclusion

A complex process is simplified in order to focus on the importance that catalyst recovery has on the hydroformylation of 1-dodecene. By incorporating catalyst leaching into the process design problem using correlations developed using limited data, significant effects of catalyst loss on the total annualized cost become visible. A similar method is implemented for the reaction system by replacing the complex reaction kinetics with a correlation taken from the same experimental data. The complex, liquid-liquid equilibrium behavior is also successfully implemented into the optimization problem by using the linear surrogate models developed in this work. These allow for an efficient and simpler optimization problem that allow one to focus on the solvent composition aspect in the hydroformylation of 1-dodecene. Results from the optimization show that a strong dependency of process economics on the TMS composition due to catalyst leaching exists and suggests that new cost reduction strategies should focus on reducing the cost of the catalyst or decreasing the incidence of leaching to less than negligible levels.

The solvent composition has a large effect on process costs. With the current levels of catalyst leaching, altering almost all other design variables, such as reactor design, bring about negligible changes. This is exactly the result seen when optimizing the process

while excluding catalyst leaching costs, where only a small change in TAC is seen due to the small change in conversion. The most immediate action that can be taken as a result of this work is to increase the DMF ratio in the TMS to the maximum allowable amount that still produces a biphasic mixture upon cooling. Another strategy would be to increase the size of all units in the flow sheet if this would lower the catalyst cost due to leaching. For example, increasing the size of the reactor, in order to increase the residence time of the mixture during the reaction, could reduce the required catalyst concentration. This would in turn lower the overall amount of leaching. Due to the very large differences between catalyst and capital costs, it would be beneficial for the economical viability of the process to decrease operating costs at the expense of increasing investment costs. This may entail not only increasing the size of the reactor, but also the addition of catalyst separation units.

It was previously discussed that, as shown by experimental data, there are other avenues that lead to better recovery of the catalyst. The effect of lowering the temperature in the decanter also has a large positive influence on reducing catalyst leaching. However, more data is required before a reasonable model or even correlation including temperature effects based on experimental data can be made. Using different temperatures would also require a more capable surrogate model for phase separation. Using different compositions that are not limited to the restricted amount of data used in this work would also lead to a better understanding of the catalyst leaching problem. It may be that higher compositions of overall solvent (more than the 85% total mass in the reaction mixture) may reduce leaching further at the expense of larger process units, a strategy that may prove feasible.

Another point to consider is that the solvents comprising the TMS may be suboptimal. Thus, it may be worthwhile to investigate methods for selecting component solvents for the TMS in order to find mixtures that better facilitate recovery of the catalyst. This would require detailed studies into the solubility of the catalyst complex or ligands in different mixtures. As it clearly seems to be the most important aspect of this process, this course of action is highly recommended. Such a method is developed and explored in the next chapter.

4. Computational Thermomorphic Solvent System Design

4.1 Introduction

As seen in the last chapter, the currently used TMS of DMF and n-decane does not separate the dissolved catalyst of rhodium and biphephos economically. One of the conclusions reached was to find a better solvent system that delivers higher catalyst retention while still adhering to TMS principles. A methodology for solvent selection is required to ensure that suitable solvent candidates are identified. The work presented in this chapter describes a method developed for selecting TMS solvents for recovering the rhodium biphephos catalyst in the hydroformylation of 1-dodecene.

The current solvent selection methods have been so far based on the liquid phase separation behavior of two or three solvents and their polarities as measured using Hansen parameters (Behr and Roll [12], Behr et al. [14], Hansen [59]). A more detailed framework that rigorously dealt with the particulars of using solvent descriptors and predictive thermodynamic models in selecting suitable mediator solvents was developed by Behr et al. [19]. The authors' goal was to select a mediator solvent for the hydroaminomethylation of 1-octene in a three component TMS. A brief description of this procedure is outlined in Section 2.4.4. Although such methods for solvent selection can sometimes lead to satisfactory candidate solvents, predictions of phase behavior or solubility are disappointingly too inaccurate to be considered reliable. This is exactly the scenario Behr et al. encountered with several of the predicted solubilities compared to those found experimentally. They advised, as is usually the case when using predictive models in solvent selection, that experimental validation is still very much required. This has much to do with issues in predicting liquid-liquid phase equilibrium, where the miscibility gap temperature dependency is still difficult to describe.

Another point to consider is that until now, no aspect of catalyst solubility is discussed during TMS design. The current methods for solvent selection take for granted that the

catalyst (which is usually polar, unless specially modified) will be recovered in the polar phase and that the product will be recovered in the non-polar phase, due to its much lower polarity. It is proposed that the design of the TMS system should preferably incorporate some predictions of the thermodynamic behavior of the catalyst during the initial stage of solvent selection or design. This would help to ensure, at least on some fundamental level, that the TMS will perform as desired.

The intention is to minimize catalyst leaching by designing a new TMS based on predicting the thermodynamic properties of the catalyst ligand. Unfortunately, there is a drought when it comes to thermodynamic and experimental data regarding solvent effects on the rhodium-biphephos catalyst. Therefore, the *ab initio* COSMO-RS model (Klamt [71]) is used as the basis for thermodynamic predictions. Molecules are to be carefully chosen as TMS component solvents based on catalyst complex solubilities, represented by the biphephos ligand, and predicted phase equilibrium characteristics. Knowing the difficulty in predicting LLE behaviors, it will be seen if the COSMO-RS model actually helps in this regard. A framework aimed at TMS design is developed to systematically screen solvents from a database list and then to deliver a shortlist of promising TMS systems. However, as noted before, experimental validation is still necessary. Several candidate TMS systems are then investigated experimentally in order to validate the ability of the methodology in designing them. Additionally, several of the potential TMS systems are evaluated under reaction conditions to ensure process feasibility.

4.2   Motivation

The currently used TMS for the hydroformylation of 1-dodecene may be suboptimal. As seen in Chapter 3, the cost of catalyst leaching in a TMS of DMF and *n*-decane is still economically prohibitive. This is in light of the fact that the TMS functions as intended and usually recovers around 95% of the catalyst. Here, the TMS is examined in more detail and the goal of finding an optimal TMS configuration explored.

4.2.1   Thermomorphic solvent systems

The primary method to recover the rhodium biphephos catalyst complex is by using the previously mentioned thermomorphic solvent system (TMS). These special mixtures are composed of solvents with varying degrees of polarity allowing for simple temperature induced phase switching. A more detailed description of TMS functionality and its implementation in various examples can be found in Section 2.4.2 and Section 2.4.3, respectively. Some key points are briefly repeated here.

In Figure 2.3, the basic principle of the TMS is outlined. At a specific reaction temperature, T1, the mixture of solvents should enable the formation of a single, homogeneous phase that allows the reaction to proceed unhindered by mass transfer limiting effects. After the reaction is finished, the resulting mixture should form two phases when cooled to the desired separation temperature, T2. In the ideal case, the catalyst is recovered

in the polar phase and the product along with the unconverted reactant are recovered in the non-polar phase.

Several TMS compositions were investigated for the hydroformylation of 1-dodecene by Behr et al. [14]. One TMS system that showed good performance in both the reaction and separation was the TMS composed of the polar solvent DMF and non-polar solvent n-decane, which was covered in Chapter 3. This solvent mixture enables decent recovery of the rhodium biphephos catalyst while still separating out modest amounts of the tridecanal product into the nonpolar phase. These positive results prompted further investigations by Brunsch [28] to find how different reaction conditions and solvent compositions using this TMS could lead to lower levels of catalyst leaching. A continuous mini-plant was also designed by Behr and Neubert [10] and operated by Zagajewski et al. [133] using this TMS of DMF and n-decane TMS in equal weight percentages. Since this TMS system is well analyzed and still the target of current, ongoing research, it will serve as a good benchmark for other TMS systems found in the TMS design approach that follows.

A TMS of this nature, consisting of a binary pair of polar and non-polar solvents without an explicit mediator solvent, was labeled as a Type III TMS (Behr et al. [14]). In the present contribution, a method is proposed to identify an optimal Type III TMS system, exemplified on the hydroformylation of 1-dodecene using the rhodium-biphephos catalyst. The goal is to find a pair of solvents that exhibit desirable TMS characteristics: a polar, catalyst solvent used to extract the catalyst complex and a non-polar, product solvent in which catalyst solubility is low and product solubility is relatively high. This is shown in Figure 4.1, a slightly modified version of Figure 2.3. Proper miscibility at the operating point for the reaction (homogeneous) and for the overall composition of the post-reaction mixture (heterogeneous) are also required.
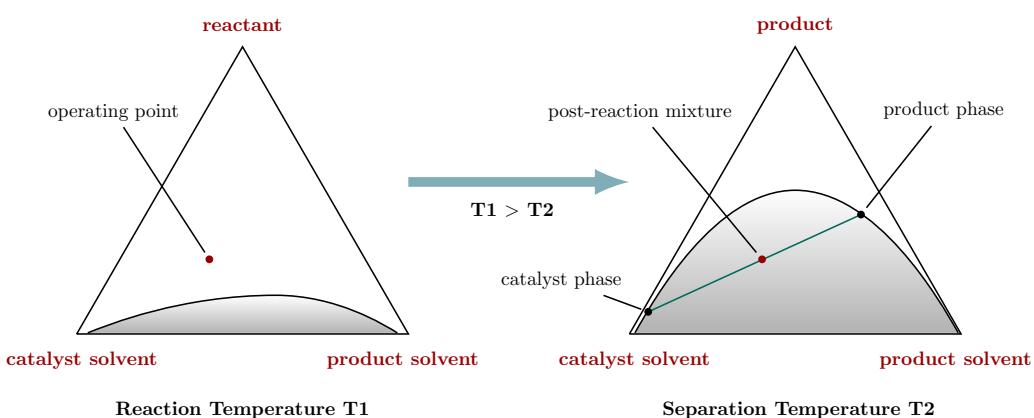
Figure 4.1: Type III TMS design goals: identify a catalyst solvent and a product solvent [89].

4.2.2 Thermodynamic Predictions

The component solvents' respective solubilities of the catalyst are the primary characteristics in the proposed TMS design methodology. Other thermodynamic properties such as melting point, boiling point, polarity, phase equilibrium characteristics, etc. are secondary although critical in TMS design. The primary method of solvent screening is thus to estimate the solubility of the biphephos ligand in various candidate solvents.

The available data in the literature concerning the physical properties of the biphephos ligand in different solvents is non-existent. In order to gain reliable thermophysical data about this catalyst ligand, time consuming experiments must be conducted. This would also restrict the TMS design space to a small subset of available and common solvents. Most of these methods are based on fitting parameters to theoretical models based on available empirical data. These are the commonly used excess Gibb's energy models such as NRTL (Renon and Prausnitz [104, 105]) and UNIQUAC (Abrams and Prausnitz [4]). More advanced equations of state, such as PC-SAFT (Gross and Sadowski [54]), may also be applicable.

Many theoretically based computational methods have been developed to estimate missing thermophysical data. Some of these methods allow for the properties of new molecules to be investigated allowing for a much larger design space to be explored. When less data is at hand, predictive group contribution methods such as modified UNIFAC Dortmund (Weidlich and Gmehling [126]), mentioned eariler, are available. However, group contribution methods do not provide accurate predictions for very large molecules and for systems containing molecules with large differences in molecular weight. Both of these conditions apply to the system at hand and group contribution methods cannot be used in this work. Unfortunately, the lack of thermophysical data for the catalyst complex and the catalyst ligand leaves one with few remaining options. Also, the complexity of the biphephos ligand does not allow one to use group contribution methods due to the inaccuracies in such models when molecules with high molecular masses are considered. Another method used to select solvent based on solubility is through the use of solubility descriptors, such as Hansen parameters (Hansen [59]). Again, for predictions of catalyst solubility this method cannot be used due to missing data for the ligand.

For these reasons, predicting the thermodynamic properties of the catalyst ligand in solution using the COSMO-RS method developed by Klamt [71] is of high interest. COSMO-RS is a quantum chemical based model that predicts thermodynamic properties based on the segment-segment interaction of molecular surfaces. This method can be used for making thermodynamic predictions of pure components or of mixtures. To begin, each modeled molecule is cast into a perfect conductor in order to determine its screening charge. This is done using the efficient continuum solvation model COSMO (Klamt and Schüürmann [74]). In the "Real Solvent" extension (-RS), the three dimensional surface information is condensed into a histogram, the σ-profile, detailing the amount of each surface segment type within a certain polarity interval. COSMO-RS then combines the σ-profile data unique to each molecule with a statisti-

cal thermodynamics approach where the chemical potentials of pair-wise interactions of surface segments (from single component mixtures or of those with multiple species) are calculated using important molecular interactions such as electrostatic misfit and hydrogen bonding energies. Therefore, only the energetically optimized molecular structure of each molecule considered is necessary to make a wide variety of thermodynamic predictions, such as phase behavior and solubility. This reduces the thermodynamic handling of complex molecules and functionalities to the same level as with simple organic molecules. A recent review covering both COSMO and COSMO-RS models is presented by Klamt [73].

The alluring feature of using COSMO-RS for solvent screening is the absence of required experimental data. This is naturally interesting for predicting the solubility of large and complex molecules that are difficult to model using other methods. The use of COSMO-RS based methods for predicting the solubility of active pharmaceutical ingredients (APIs) in various solvents has found much interest lately. Naturally, conducting experiments on API solubility can be quite costly and time consuming. Thus, the use of COSMO-RS based methods are welcomed within the pharmaceutical industry due to its ability to identify candidate solvents *a priori*. Although this work does not consider APIs, the predicament with modeling the catalyst ligand is similar.

A handful of research groups have investigated the use of the several existing COSMO-RS variants in the prediction of API solubility for use in crystallization. Tung et al. [118] compared the solubility predictions for four different APIs in nine common solvents using NRTL-SAC (Chen and Song [34]) and COSMO-SAC (Lin and Sandler [84]). The authors found that NRTL-SAC produces a smaller error and better predictions for solubility than the *ab-initio* COSMO-SAC, although the results calculated from the latter were considered to provide reasonable estimations. API solubilities based on solid-liquid-equilibrium predictions made using the group contribution methods UNIFAC (Fredenslund et al. [47]) and modified UNIFAC Dortmund (Weidlich and Gmehling [126]) with the COSMO-RS variant COSMO-RS (Ol) (Grensemann and Gmehling [53]) were performed by Hahnenkamp et al. [57]. Here, the SLE of aspirin, paracetamol, and ibuprofen in various solvents and temperatures were measured to use in validating their predicted values. They found that out of all three methods, modified UNIFAC Dortmund performed the best, having the lowest overall percent error in solubility prediction and in its ability to rank solvents accordingly. However, the performance of COSMO-RS(Ol) was shown to provide a good ranking of solvents based on solubility despite its overall higher percentage error. In a report from Pfizer by Pozarska et al. [101], it was shown that the COSMO-RS version from Klamt [72] performed well in ranking solvents for use in crystallization for new APIs, leading to a reduction in their required experimental burden.

More work on comparing several predictive models for use in SLE predictions for APIs was conducted by Bouillot et al. [25]. This work focused on UNIFAC, modified UNIFAC Dortmund, COSMO-SAC, and NRTL-SAC and concluded that no model was accurate enough to qualitatively predict solubilities, especially due to poor results when considering the temperature dependency of the SLE. Later works by Bouillot et al. [26, 27]

looked at improving the COSMO-SAC models by optimizing parameters using experimental data. They were successful in improving the solubility predictions but still had problems with several interactions such as hydrogen bonding, dipole-dipole, and weaker electrostatic interactions.

Perhaps the most advanced COSMO-RS implementation is still the version provided by COSMOlogic with the software package COSMOtherm (Eckert and Klamt [41]). This is the version of COSMO-RS that is used throughout the work presented in this thesis. A relevant article on the use of this software is the short review by Wichmann and Klamt [127], who give a detailed description of the COSMO-RS method when used in solvent screening for an API in pure solvents, solvent mixtures, and in estimating heats of reaction. For the examples presented, a relatively accurate qualitative ranking of solvents was achieved and several estimates were also quantitatively accurate as well.

A general consensus can be made that predictive methods cannot ensure quantitatively accurate predictions of actual solubilities. However, the qualitative ranking of solvents, especially when using COSMO-RS methods, leads to better selection of more promising candidates without necessitating experimental data. Thus, it can be said that COSMO-RS can qualitatively predict the solubility of large and complex molecules in various solvents. Also, in those articles that used UNIFAC and modified UNIFAC Dortmund the APIs were of smaller sizes suitable for use with group contribution methods. Larger molecules cannot be represented adequately or reliably with such models and require a different approach, leaving basically the COSMO-RS method as one of few options. Therefore, it seems suitable to adopt this method for the task of qualitatively predicting catalyst ligand solubility in various solvents that can then be uniquely applied to TMS design. For the proposed TMS design procedure in this chapter and the catalyst extraction problem consdiered in Chapter 5, this is the thermodynamic model used for predicting catalyst solubility and partitioning.

4.3   Framework

The procedure used to screen for component solvents for use in a Type III TMS is outlined in Figure 4.2. This framework consists of two major components: the computational solvent screening of TMS systems and the empirical investigation and validation of candidate solvent mixtures. In the solvent screening section several steps are presented in order to come to feasible TMS compositions.

Computational Screening

1. The COSMO file of the biphephos ligand is created.

2. The entire database of molecules provided with COSMObase (version 1301) is reduced using a pre-screening step based on physical property constraints such as boiling temperature, melting temperature, charge, size, elemental composition, etc.

3. The relative solubility of the biphephos ligand is calculated for the remaining solvent candidates.

4. Two lists of solvents are now generated: one for catalyst solvents and one for product solvents. Two solvents, one from each list are to be combined to form binary TMS systems.

5. The phase behavior of the binary solvent systems are checked for miscibility gap formation at the chosen separation temperatures.

6. The partition coefficient of the product is now estimated for remaining binary systems as a rough estimate of product separation quality.

7. Various characteristics of the remaining solvents such as reactivity, toxicity, etc. are checked.

8. TMS Systems are ranked according to their ability to recover the catalyst.

Experimental Validation

1. The catalyst partitioning behaviors of top performing TMS systems are experimentally determined.

2. The hydroformylation of 1-dodecene is carried out in the chosen TMS systems to evaluate TMS composition effects on reaction performance and real-world separation abilities.

After the first steps to generate the COSMO file of the catalyst ligand and the simple pre-screening of molecules to reduce the search space are complete, the remaining procedures are primarily active in predicting solvent behaviors related to the solubility of biphephos, in product recovery, in miscibility, and in their process feasibility. After the computational solvent screening procedure is finished, promising TMS designs are experimentally investigated in the second stage of the framework. Here predictions made about partition coefficients based on catalyst ligand solubilities are investigated as well as performing the hydroformylation of 1-dodecene in each chosen mixture. Each step is explained in more detail in the following sections.

4.3.1 Generate COSMO file of catalyst ligand

The first task is to create the COSMO file of the catalyst ligand used in the process. In this case the catalyst is the biphephos ligand used as part of the catalyst complex for the hydroformylation of 1-dodecene. In this screening work only the catalyst ligand is considered due to its usually higher concentration in the solution. Additionally, catalyst leaching has been shown to have similar levels in both rhodium and phosphorous, as reported by Brunsch and Behr [29]. This means that it can safely be assumed that by representing the catalyst as the ligand no significant error should be expected.

Solvent Selection Framework

Computational TMS Design
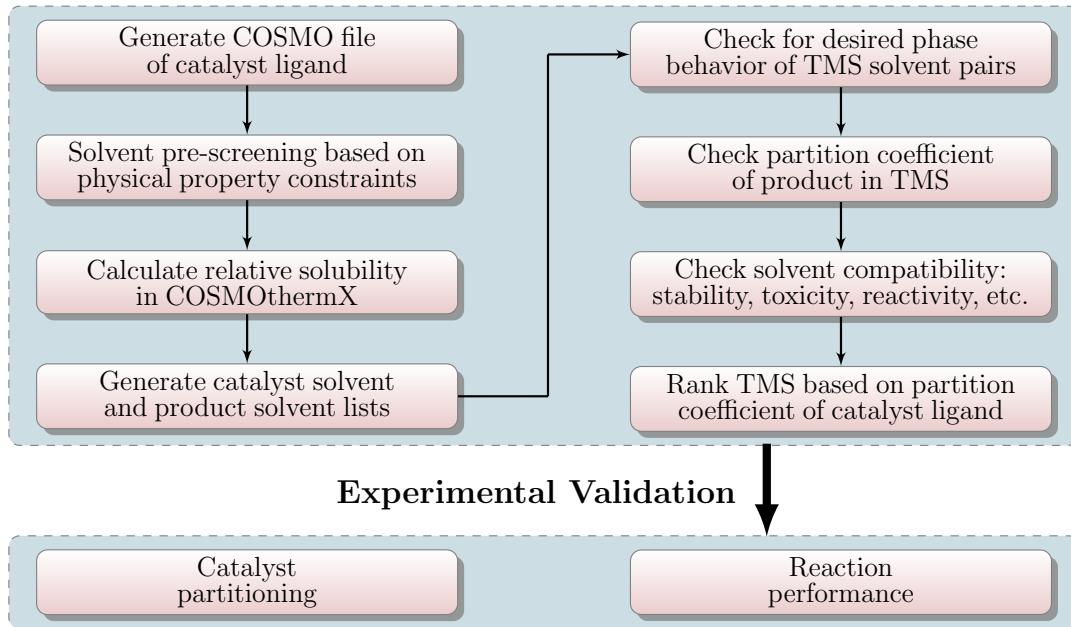
Figure 4.2: Computer-aided procedure for TMS design with experimental validation

The molecular model is developed using TURBOMOLE [119], at the RI-DFT level of theory (Eichkorn et al. [42]) using the def-TZVP basis set (Schäfer et al. [108]). The structural formula of biphephos (A) and the resulting structure with its surface charge density (B) are presented in Figure 4.3. The COSMO file created here contains all the required information needed for predicting the thermodynamic properties of biphephos in the forthcoming solvent screening tasks using COSMOtherm (Eckert and Klamt [41]).
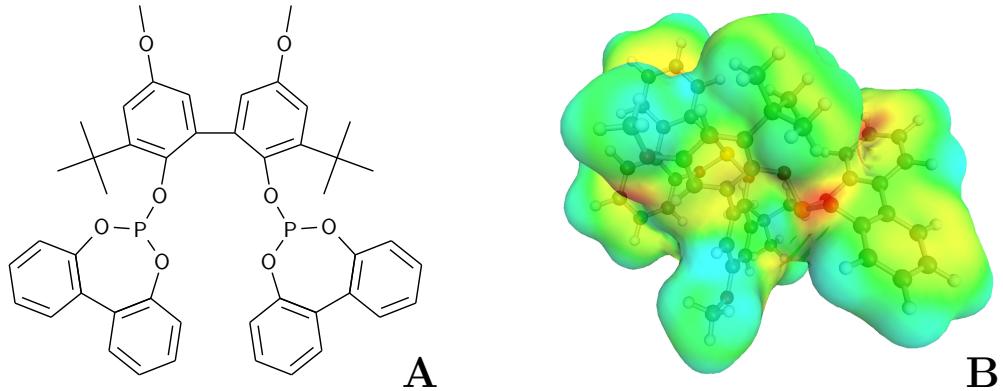
Figure 4.3: Structural formula of biphephos (A) and its surface charge in a perfect conductor (B) as calculated using TURBOMOLE [89].
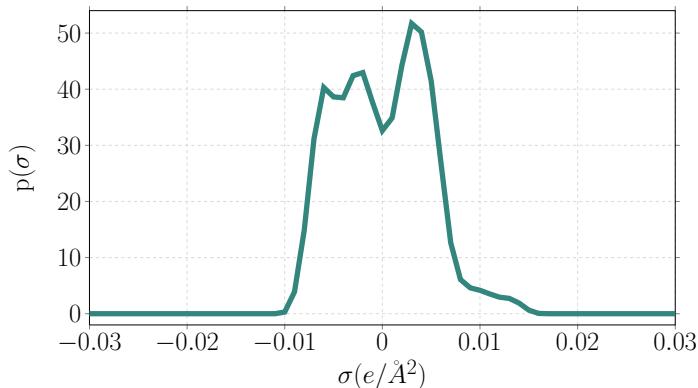
Figure 4.4: Sigma profile of the biphephos ligand [89].

At a glance, it is possible to obtain a significant amount of information about a molecule simply by noticing its σ-profile, which is provided for biphephos in Figure 4.4. It can be easily seen that a tall, wide non-polar region is located between -0.01 and 0.01 e/Å, which are usually the accepted boundaries for hydrogen bonding (see Klamt [72]). Segments located outside of this region can form strong hydrogen bonds and are quite

visible for polar molecules. However, most non-polar molecules do not usually depict such a wide non-polar profile as biphephos. This is due to the negative p-orbitals and positive carbons of the phenyl groups giving two distinct peaks instead of one, typical for compounds containing aromatic ring structures, of which biphephos has six. The small shoulder extending from 0.01 to about 0.015 e/Å results from the negative charge of the oxygen and phosphorous atoms which suggests that the catalyst may prefer to be in solution with solvents exhibiting hydrogen bond donor characteristics. It is therefore expected that biphephos will have a higher affinity for polar solvents and those having broad profiles between the hydrogen bonding borders to strictly non-polar ones.

4.3.2   Pre-screening of candidate solvents

Before screening can take place, a database of potential solvents needs to be sourced. This is done using the existing database of COSMO files in the COSMObase (ver. 1301, COSMOlogic GmbH) add-on to the COSMOtherm software package. This enables one to immediately begin solvent screening without the need to invest copious amounts of time in generating a database of potential solvents. Instead, the opposite problem exists in that too many molecules are included in the database that are for one reason or another unsuitable for the desired purpose. For example, if a potential solvent is found that has a high relative solubility of the catalyst but is unfortunately solid at the separation temperature, it cannot be used. To reduce the number of potentially unsuitable molecules from the initial database list, about 7700 in total, certain molecular properties, such as molecular weight, melting temperature, boiling temperature, screening charge, and component atoms can be used as constraints to prescreen solvent candidates. Within the files of the database are several molecular properties that can be accessed using a regular expression search tool, such as grep, for example. A large spread sheet containing all of the relevant information is generated allowing one to easily create a reduced set for the TMS design sequence.

In this work, a large search space is purposely maintained, using only boiling temperature, molecular weight, and charge as the initial, pre-screening constraints. The boiling temperature of each solvent is limited to temperatures between 273.16 and 533.16 K. The upper bound is chosen to be 20 K lower than the boiling point of the desired product tridecanal in order to avoid possible azeotrope formation in a subsequent distillation step. The molecular weight of each solvent is arbitrarily chosen not to exceed 200 g/-mol in order to keep the molecules small. Solvents are preferably small owing to better solvent functionality and that large molecules usually have higher boiling and melting temperatures. Since the database contains several ions, all species with an non-zero charge are removed. If boiling point temperatures were not available, the compounds were also excluded from the search space. Using these three constraints, the solvent search space is reduced to a list containing 2831 molecules.

One primary reason for this step is to reduce the computational time required in the following steps. Since most of the molecules contained within the COSMObase database cannot be used in the considered hydroformylation process, it is simply inefficient to

consider every molecule in the database as a possible solvent in the TMS. It will be seen later that further restrictions of the initial search space can be made without changing the final results, leading to a decreased computational cost in the screening procedure. This may be useful for subsequent TMS design problems.

4.3.3 Solvent screening: catalyst solubility

The next step, and perhaps the most important one, is to predict the solubility of biphephos in each of the candidate solvents. This is done using the relative solubility of the catalyst in each solvent, which reduces the complexity of the calculation without necessarily reducing the qualitative, predictive accuracy. Relative solubility is determined in COSMOtherm using only the chemical potential, $\mu_i^{solvent}$, of the solute (in this case biphephos) at infinite dilution in a pure solvent. This chemical potential is calculated by COSMO-RS (Equation (4.1)) using the statistical thermodynamic approach mentioned previously using the sigma profiles of the involved components (a good reference for a detailed description of how COSMO-RS calculates potentials is found in Klamt [72]). Relative solubilities are calculated for each candidate solvent, allowing for direct comparison of every considered molecule. Once all calculations are complete, the solvents are ranked in descending order by relative solubility. The maximum solubility is represented by a value of zero and the relative solubility of all remaining molecules decreases therefrom. All relative solubility calculations were performed assuming a temperature of 298.16 K.

$$\ln(x_i) = \mu_i^{solvent}/RT \tag{4.1}$$

Once the relative solubility for all 2831 components have been calculated, they are ranked accordingly. These ranked relative solubilities are shown in Figure 4.5.

4.3.4 Solvent screening: generation of two lists

From this list of ordered solubilities, two new lists are to be created: one with solvents having the highest predicted relative solubilities of biphephos, designated as HRSC, and the other containing those solvents having the lowest relative solubilities of the catalyst ligand, designated as LRSC. For each TMS system, two solvents will be used in order to create the desired Type III system. The solvent used to recover the catalyst is chosen from the HRSC list and the counter solvent to recover the product is chosen from the LRSC list. This is pictorially shown in Figure 4.6, where the two unknown solvents shown in Figure 4.1 are each selected from their respective lists. In this manner, a very large number of TMS designs is possible.

The size of each solvent list determines the overall number of binary systems that will need to be investigated in the subsequent screening steps. Suppose there are $\boldsymbol{m}$ solvents in the HRSC list and $\boldsymbol{n}$ solvents in the LRSC list. This leads to a total of $\boldsymbol{m} \times \boldsymbol{n}$ binary systems to consider. Therefore, the more solvents considered in each list, the larger the computational effort required in the remaining screening tasks.

However, their are still several problems with the solvents found in each list. As an example, two short lists are generated using the top five solvents predicted as having the
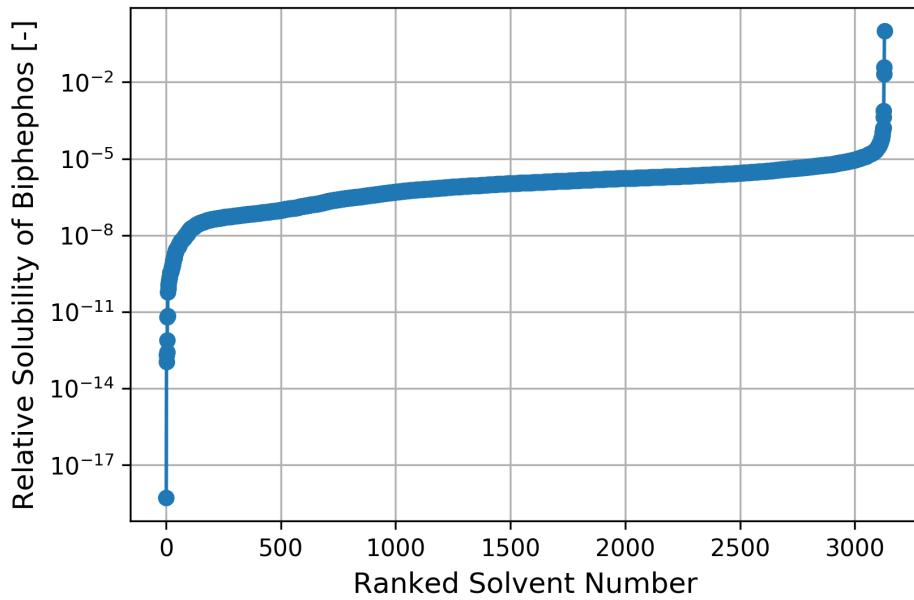
Figure 4.5: Solvents ranked according to their relative solubilities of the biphephos ligand.
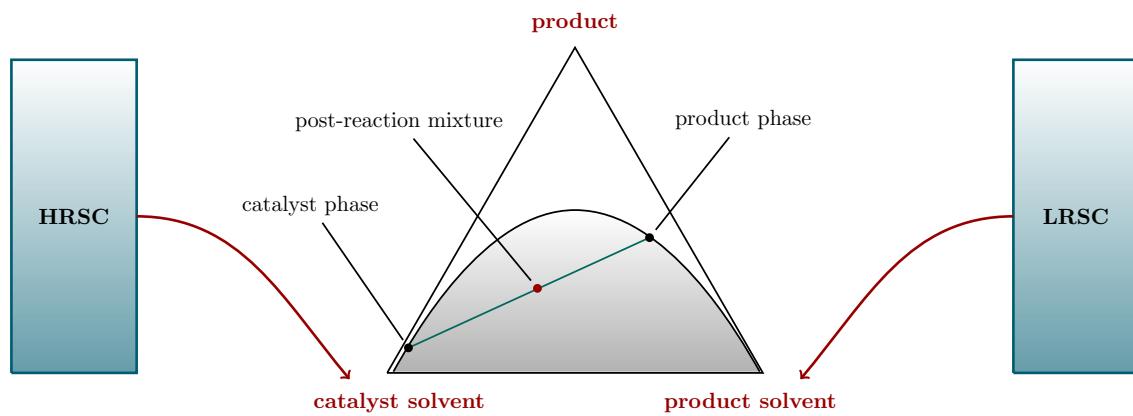
Figure 4.6: TMS design: A solvent from the HRSC list is chosen as the catalyst solvent and one from the LRSC list as the product solvent.

highest solubility alongside the five having the lowest predicted solubility of biphephos. These are presented in Table 4.1. Here, hydrofluoric acid is predicted as having the highest solubility for biphephos while water is predicted to have the lowest solubility, being about 18 orders of magnitude less than that of hydrofluoric acid. Of course this TMS design is not feasible for several reasons and it should be quite obvious that all candidate solvents shown in Table 4.1 are quite unsatisfactory. All of the HRSC solvents listed in this representative list are, unfortunately, either highly reactive acids, strong oxidizers, or CFCs. This presents a potential problem in solvent selection that is handled later in the screening procedure. The solvents found in the LRSC list are also problematic, with the exception of water, due to their respective reactivity or toxicity. However, it is already known that water is a poor solvent for the reaction due to its abysmal miscibility with the reactant and also due to its low solubility of the tridecanal product. This problem will also be addressed at a later point in the screening process. That several of the LRSC solvents are polar, the convention of naming the catalyst solvent as the polar solvent should probably be dropped. This is the primary reason for why the two components of the TMS to design are labeled as either the catalyst or the product solvent.

Table 4.1: List of top five high (HRSC) and low (LRSC) relative solubility catalyst solvents

HRSC	$\log_{10}(x_i)$	LRSC	$\log_{10}(x_i)$
Hydrofluoric acid	0.0000	H_2O	-18.4128
Selenic acid	-1.0582	Formamide	-12.7388
Chlorosulfonic acid	-1.2406	Hydroxyacetonitrile	-12.2432
ClO_2	-2.6015	Butanedinitrile	-12.1521
1,1,1-Trifluoro-2-bromoethane	-3.0996	Dicyanomethane	-11.6746

It would seem prudent to perform a stricter pre-screening of candidate solvents to avoid this issue. This may be done by removing those structures containing reactive functional groups or those that are acids, etc. At this point there is no really efficient method for performing this task for the structures contained within the COSMObase database. For other aspects, such as deciding the environmental, health, and safety aspects of solvents, there are methods such as the one developed by Koller et al. [78]. However due to the limited availability of information for many of the solvents in this list and the small size of the EHS tool database (Capello et al. [32]), this tool was not suitable for the current task. The selection and exclusion of solvents is instead based on heuristics, relying more on expertise and process knowledge (such as no carbon-carbon double bonds). This manual screening step, as seen in Figure 4.2, comes near the end of the process when the number of candidate solvents remaining is much lower, greatly reducing the workload.

It is for this reason that a sizable number of candidate solvents needs to be selected for both the HRSC and LRSC lists, effectively leading to a trade-off in computation time and the assurance that feasible TMS systems will be obtainable. For the HRSC list an arbitrary number of solvents, 100, is chosen. These 100 solvents are again those solvents having the highest relative solubility for biphephos. For the LRSC list, the selection of solvents is performed differently. This is due to the availability of experimental data comparing the performance of different TMS systems consisting of DMF and alkanes of various chain lengths for rhodium-biphephos catalyst recovery in the hydroformylation of 1-dodecene. It is desirable to include several of these alkanes into the LRSC list, as well as other similarly performing solvents (Brunsch and Behr [29]). Therefore, octane is chosen as the cut-off point for the LRSC list instead of an arbitrary number as with the HRSC solvents. These solvents, numbering 403 altogether, are those solvents having the lowest solubility for the catalyst. These solvent list boundaries are shown in Figure 4.7 to more easily see the regions of solvents selected compared to the entire data set. This leads to a total of 40,300 binary pairs that are examined in the next screening step.
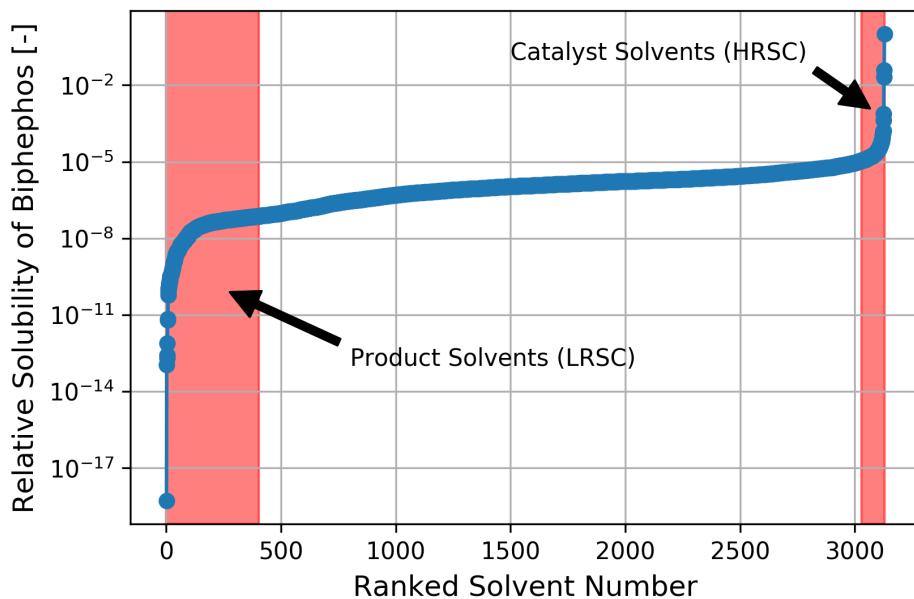
Figure 4.7: In comparison to Figure 4.5, the areas for catalyst and product solvents are now marked.

4.3.5   Miscibility gap formation

The basis of a functioning TMS relies upon the fact that after the reaction, a biphasic mixture is formed that separates the polar, catalyst containing phase from the less polar, product phase. This means that for each binary TMS system an estimation of the LLE or miscibility gap size must be made. Again using COSMOtherm, liquid-liquid

equilibrium calculations are made for each possible binary pair of solvents, each with one from the HRSC list and and one from the LRSC list. As mentioned in the last section, this leads to 40,300 binary systems in total. This represents a large computational load that can take several hours to solve. The separation temperature for each LLE prediction was chosen to be 248.16 K. This temperature is selected for two reasons: the lower limit for planned LLE experiments is around this temperature and that predictive methods for thermodynamic equilibrium (especially for predicting LLE) are not very reliable, something encountered previously by Behr et al. [19]. Unreliable phase equilibrium predictions, especially LLE at higher temperatures, may potentially eliminate interesting TMS systems during screening due to faulty miscibility ggap predictions, such as those made at ambient conditions. Therefore, to avoid these reliability issues and bring the predictions more in line with our experimental limits, the low temperature of 248.16 K is used. Binary TMS systems that are predicted to be feasible at lower temperatures (good miscibility gap) can be observed at higher temperatures at a later time as part of the final process design stage.

Basically a larger screening net is used to ensure that TMS systems are not excluded due to inaccurate predictions of LLE. Additionally, and for a similar reason, the screening criteria is based simply on the predicted formation of a miscibility gap in the binary mixture. The size of this gap is not considered at this time. After applying this single constraint, 5225 potential TMS compositions from the initial 40,300 remain.

4.3.6   Product Distribution

The secondary, but also critical, function of a TMS is its ability to separate the product from the mixture by means of the less polar phase. Therefore it is also necessary to perform some check as to whether or not the TMS can selectively remove the tridecanal product from the post-reaction mixture. Remember that although water should be a great LRSC solvent due to its unequally poor solubility of the catalyst, this characteristic also applies to the slightly polar tridecanal. This renders water as unsuitable for the process as a product solvent, as its use would lead to practically all of the product being recycled back into the reactor; no feasible separation would take place. In order to circumvent this issue and to remove such TMS systems from consideration, some measure of the ability of the TMS to remove the product must be included as part of the screening process.

This is considered in a manner similar to that as was done with biphephos, but because the screening process now involves binary solvent systems, partition coefficients as predicted by Equation (4.2) are used instead to predict the tridecanal distribution.

$$\log_{10}(P_j^{(2,1)}) = \log_{10}(\exp((\mu_j^{(1)} - \mu_j^{(2)})/RT) \cdot V_1/V_2) \tag{4.2}$$

Here, $\mu_j^{(i)}$ is the chemical potential of species j at infinite dilution in species i, where j stands for the reaction product tridecanal, 1 for the HRSC solvent, 2 for the LRSC solvent, and V for the estimated solvent volume. For tridecanal partition coefficients,

Table 4.2: Unfiltered list of top 30 TMS mixtures.

Rank	HRSC	LRSC	$\log_{10}(P_{tridecanal})$	$\log_{10}(P_{biphephos})$
1	Iodomethane	Propanal,2-(hydroxyimino)-,oxime	0.1460	3.6040
2	Bromomethane	Propanal,2-(hydroxyimino)-,oxime	−0.0749	3.4292
3	Iodoethane	Propanal,2-(hydroxyimino)-,oxime	0.2419	3.3888
4	Bromoethane	Propanal,2-(hydroxyimino)-,oxime	0.1770	3.3865
5	1-Bromo-1,2-difluoroethylene	Choralhydrate	−0.0339	3.2778
6	Ethylisocyanate	Propanal,2-(hydroxyimino)-,oxime	0.1255	3.2460
7	Iodoethene	Propanal,2-(hydroxyimino)-,oxime	0.0737	3.2343
8	Iodomethane	Resorcinol	0.1454	3.2080
9	Bromomethane	Resorcinol	−0.0754	3.0331
10	Iodoethane	Resorcinol	0.2413	2.9928
11	1-Bromo-1,2-difluoroethylene	4-Methyl-1,3-benzenediol	0.1482	2.9927
12	Bromoethane	Resorcinol	0.1765	2.9905
13	Iodomethane	Methylhydroquinone	0.0589	2.9670
14	1-Bromo-1,2-difluoroethylene	Difluoroaceticacid	−0.2472	2.9523
15	Bromomethane	2,2,2-Trifluoroethanol	−0.0589	2.9509
16	Bromomethane	Pentafluoro-1-propanol	−0.1543	2.9265
17	3-Bromo-3,3-difluoro-1-propene	Pentafluoro-1-propanol	0.2062	2.9130
18	Bromoethane	2,2,2-Trifluoroethanol	0.1930	2.9082
19	Ethyleneoxide	Hexahydroindene	0.2220	2.8928
20	Bromoethane	Pentafluoro-1-propanol	0.0976	2.8838
21	Iodomethane	Orcinol	−0.0620	2.8765
22	Iodoethene	Resorcinol	0.0731	2.8383
23	Acetaldehyde	n-Tetradecane	0.2308	2.8324
24	Sulfurylchlorideisocyanate	Orcinol	0.2445	2.8260
25	Iodomethane	Cyclohexanemethanol	0.1229	2.8076
26	Acetaldehyde	n-decaneTridecane	0.2060	2.8038
27	Acetaldehyde	1-Tridecanol	0.1235	2.7985
28	Bromomethane	Methylhydroquinone	−0.1620	2.7922
29	Acetaldehyde	Dodecanol	0.1046	2.7905
30	2-Butyne	Methylhydroquinone	0.2250	2.7898

the volume quotient of the solvents as estimated using the liquid density/volume QSPR method from COSMOtherm is included. The use of this method basically assumes that the tridecanal product is also at infinite dilution. This is known not to be the case and that the presence of tridecanal is in high enough quantities to effect the LLE of the resulting mixture. The purpose of this screening step is not to evaluate the ternary LLE of each candidate TMS design due to the computational demand that would impose, but to screen out those TMS designs where the catalyst solvent has a high affinity for tridecanal.

Instead, this simple partitioning coefficient is compared to that of tridecanal in the the currently used TMS of DMF and n-decane. This value is considered as a rough starting value for choosing the maximum value of allowable partition coefficients used in this screening step. The exact cut-off value is arbitrarily chosen based roughly on doubling the predicted partition coefficient of tridecanal between DMF and n-decane, which is found to be 0.118. Thus, a chosen maximum of 0.25 is used. This ensures that the qualified TMS designs should have a somewhat similar performance in tridecanal separation as the current TMS. Meanwhile, all systems with poor tridecanal solubility in the less polar phase should be eliminated. After applying this criteria for the remaining TMS designs, only 928 potential solvent pairs are left.

4.3.7 Elimination of Unsuitable Solvents

As stated in Section 4.3.4 there are potentially many solvents that cannot be used for a multitude of reasons from reactivity to toxicity. The goal of this screening step is to manually remove these solvents in the most efficient method possible. This is again necessary, because this step cannot be reliably completed computationally and is the bottleneck in this screening process.

The top 30 TMS systems at this point are shown in Table 4.2. TMS systems are ranked according to biphephos recovery measured using the partition coefficients that are explained in the next section (Section 4.3.8). The majority of listed HRSC solvents are small alkanes that contain halogens, mainly bromine and iodine. The LRSCs they are frequently paired with are either large alcohols or molecules containing several functional groups. Upon closer inspection, many of these solvents are infeasible as TMS solvents based only on melting temperature. For example, resorcinol has a melting temperature of 384 K. Others seem quite suitable, such as cyclohexanemethanol which melts at 230 K. This suggests that including a melting temperature constraint in pre-screening could help to reduce the number infeasible molecules and make the screening more efficient.

What is really interesting is that many of these LRSC solvents have polar characteristics. This is not really expected and is unlike the non-polar solvents envisioned for product recovery. However, there are several problems with these TMS designs in addition to melting temperatures and polarity. The predicted top two performing HRSC solvents iodomethane and bromomethane are both common pesticides with bromomethane being known to damage the ozone layer. It was already phased out completely in 2005

in accordance with the Montreal Protocol and the Clean Air Act [3]. Thus it is rec-ommended that such molecules are removed for these reasons as well as for the various arguments mentioned below.

Solvents are individually screened according to several characteristics:

1. Species containing halogens (may be included in pre-screening)

2. Highly reactive species that are considered too unstable

3. Solvents with carbon-carbon double or triple bonds likely to react in the hydro-formylation

4. Extremely toxic species otherwise not eliminated according to the above criteria

Since there are by far fewer HRSC solvents left in the remaining TMS designs, only 33 compared to 158 LRSC solvents, this screening step starts with HRSC solvent elimina-tion. After a portion of the HRSC solvents have been removed from consideration, the total number of TMS systems and the corresponding LRSC solvents are reevaluated. In this way, a reduction in the number of LRSC solvents to investigate is expected.

In all, 13 solvents are removed for due the presence of halogens, seven for containing a carbon-carbon double or triple bond, and five for either being highly reactive, highly toxic, or both. In all, eight solvents remain in the new HRSC list, shown in Table 4.3. Some of these chemicals are still somewhat toxic, including the currently used DMF (it is known to cause reproductive problems). Thus, they require special care in handling and exposure, but are commonly used as solvents or intermediates in industry and can be used in the laboratory without extraordinary or unprecedented caution.

Table 4.3: Remaining HRSC solvents.

HRSC Solvent
acetaldehyde
DMF
acetone
N,N-dimethylacetamide
N-methyl-2-pyrrolidone
methylacetate
N,N-diethylformamide
N-formylpiperidine

After eliminating the 25 HRSC solvents from consideration, and the TMS systems that contained them, only 324 TMS pairs remain. This means that about two-thirds of

all TMS systems up until now cannot be used for reasons other than their predicted ability to recover the catalyst while removing the product. This again shows room for improvement in the initial pre-screening task (such as including halogen screening). This elimination of various HRSC solvents also reduces the list of remaining LRSC solvents from 158 down to 65 unique molecules in the 324 remaining systems. Of these, 62 are branched, linear, or cyclic alkanes and can be used without problem. The three remaining solvents are dodecanol, tridecanol, and hexahydroindene. Hexahydroindene is removed due to it having a carbon-carbon double bond. With the removal of this single LRSC solvent, five TMS pairs are removed leaving 319 TMS pairs remaining.

For some LRSC solvents, 21 in total, the melting temperature is not included in the COSMObase database; however, these solvents are all C_9 or C_{10} alkanes and should have melting temperatures much lower than the process temperatures considered here and are therefore retained. Several of the remaining LRSC solvents have melting temperatures higher than -25 °C, which may not be problematic, considering that they are in a mixture. These include tridecanol, dodecanol, n-tetradecane, n-triradecane, n-dodecane, bicyclohexyl, 2,2,5,5-tetramethylhexane, and cyclodecane. However, to ensure that the predicted liquid-liquid equilibrium is still valid, each TMS system consisting of one of these solvents is recalculated again at the melting temperature of the LRSC instead. Only 25 TMS pairs are affected by this. In eight of these systems no miscibility gap is predicted, leaving 311 solvent pairs in our final list of potential TMS systems. It is again obvious from these results that boiling point constraints are not satisfactory alone for the pre-screening step and that it would be desirable to also add a melting temperature constraint.

It is also of interest to check the phase behavior at a reaction temperature of 373.16 K, considering this is an often used reaction temperature for the present reaction system (Schäfer et al. [110]). Here, five TMS systems are predicted to form heterogeneous mixtures: DMF with n-dodecane, n-triradecane, and n-tetradecane, and acetaldehyde with n-triradecane and n-tetradecane. Although these miscibility gaps are small, they may effect the process in a negative way if the operating point is found within the biphasic region. Therefore, the temperature is slightly increased to 393.16 K to check if all TMS systems were homogeneous, which they are predicted to be. Due to these systems all having upper critical solution temperatures predicted as being below 393.16 K, they were considered acceptable for further evaluation, as this is still within the acceptable temperature range for the reaction.

4.3.8 Analysis

The final 311 TMS designs are now ranked according to their partition coefficients for biphephos as measured between the HRSC and LRSC solvents. In this case partition coefficients are calculated using Equation (4.3), with j representing biphephos. The volume quotient of the solvents is not included in these calculations to ensure consistency with the relative solubility calculations performed during second screening step. When the solvent volume is ignored in Equation (4.2), it reduces to Equation (4.3)

which is simply the logarithm of the ratio of the relative solubilities calculated using Equation (4.1).

$$\log_{10}(P_j^{(2,1)}) = \log_{10}(\exp((\mu_j^{(1)} - \mu_j^{(2)})/RT)) = \log_{10}(x_j^{(1)}/x_j^{(2)}) \qquad (4.3)$$

Using the partitioning of biphephos between the two phases should provide an adequate yardstick as to which designs are most suited for use as a TMS relative to catalyst recovery. Since product partitioning has already been constrained below a specific performance criteria, each remaining TMS design should feasibly function as a Type III TMS for the hydroformylation of 1-dodecene. That is, as long as tridecanal does not strongly affect the miscibility gap. The results are presented in the next section.

4.4 Screening Results

The top 30 TMS from the remaining 311 systems based on catalyst partition coefficients are presented in Table 4.4. TMS systems composed of catalyst solvents acetaldehyde or DMF coupled with large alkanes as product solvents seem to provide good catalyst recovery and satisfactory product separation. As the size of the alkane increases, the catalyst recovery capacity also increases due to the enlargement in the number of non-polar segments of the product solvent's σ-profile. This leads to the prediction that the amount of catalyst that is soluble in the non-polar phase decreases. For the same reason, the partition coefficients of tridecanal also increase, due to its reduced solubility in the product phase. This is because of the dominant apolar hydrocarbon backbone of tridecanal. It is true that the carbonyl group of the aldehyde provides some polar characteristics and possibilities for hydrogen bonding, but its surface is still mostly non-polar. Thus, there exists a trade-off between catalyst recovery and the efficiency of product separation, which should be kept in mind when designing a TMS. Though as seen in Chapter 3, the solvent effect on catalyst recovery is economically of greater importance.

4.4.1 Catalyst Solvent Comparison

As mentioned in Section 4.3.7, all LRSC solvents are large alkanes up to C_{14} in size. Since all of the remaining LRSC solvents are thermophysically similar, it is therefore convenient to compare the HRSC solvents paired with a single LRSC solvent. Naturally, n-decane is chosen as the representative LRSC solvent. It has already been extensively used in ongoing research for the hydroformylation of 1-dodecene. Therefore, some experimental data is already available and it can be easily considered to be the benchmark product solvent.

Catalyst partition coefficients for biphephos and tridecanal in each TMS system using one of the remaining HRSC solvents paired with n-decane are provided in Table 4.5. Acetaldehyde is, expectedly, predicted to form TMS with the highest performance because of its higher relative solubility of the catalyst ligand over DMF and other HRSC solvents. An explanation for this based on COSMO-RS analysis, may be that a slight

Table 4.4: List of top 30 TMS mixtures

Rank	HRSC	LRSC	$\log_{10}(P_{tridecanal})$	$\log_{10}(P_{biphephos})$
1	Acetaldehyde	n-Tetradecane	0.2308	2.8324
2	Acetaldehyde	n-Tridecane	0.2060	2.8038
3	Acetaldehyde	n-Dodecane	0.1750	2.7655
4	Acetaldehyde	Bicyclohexyl	0.0663	2.7507
5	Dimethylformamide	n-Tetradecane	0.2427	2.7245
6	Acetaldehyde	n-Undecane	0.1445	2.7231
7	Acetaldehyde	n-Hexylcyclopentane	0.0953	2.7151
8	Acetaldehyde	2-Methyldecane	0.1423	2.7099
9	Acetaldehyde	Pentylcyclohexane	0.0896	2.6978
10	Dimethylformamide	n-Tridecane	0.2180	2.6959
11	Acetaldehyde	4-Methyldecane	0.1415	2.6850
12	Acetaldehyde	Pentylcyclopentane	0.0522	2.6754
13	Acetaldehyde	n-Decane	0.1061	2.6713
14	Acetaldehyde	2-Methyl-nonane	0.1047	2.6643
15	Dimethylformamide	n-Dodecane	0.1870	2.6577
16	Acetaldehyde	1-Isopropyl-4-methylcyclohexane	0.0360	2.6495
17	Acetaldehyde	$trans$-Decalin	−0.0164	2.6443
18	Dimethylformamide	Bicyclohexyl	0.0783	2.6428
19	Acetone	Bicyclohexyl	0.2485	2.6421
20	Acetaldehyde	2,3-Dimethyloctane	0.0989	2.6407
21	Acetaldehyde	Butylcyclohexane	0.0437	2.6380
22	N,N-Dimethylacetamide	Bicyclohexyl	0.1786	2.6365
23	Acetaldehyde	2,7-Dimethyloctane	0.0997	2.6339
24	Acetaldehyde	2,2-Dimethyloctane	0.0866	2.6334
25	Acetaldehyde	3-Methyl-nonane	0.1041	2.6306
26	Acetaldehyde	4-Methyl-nonane	0.1043	2.6277
27	Acetaldehyde	1-Methyl-3-propylcyclohexane	0.0412	2.6247
28	Acetaldehyde	5-Methyl-nonane	0.1036	2.6218
29	Acetaldehyde	1-Methyl-2-propylcyclohexane	0.0391	2.6218
30	Acetaldehyde	2,2,4,6,6-Pentamethylheptane	0.1305	2.6202

Table 4.5: List of high relative solubility solvents and n-decane TMS candidates

HRSC	LRSC	$\log_{10}(P_{tridecanal})$	$\log_{10}(P_{biphephos})$
Acetaldehyde	n-Decane	0.1061	2.6713
Dimethylformamide	n-Decane	0.1180	2.5635
Acetone	n-Decane	0.2882	2.5627
N,N-Dimethylacetamide	n-Decane	0.2184	2.5572
N-Methyl-2-pyrrolidone	n-Decane	0.3017	2.5193
Methyl acetate	n-Decane	0.1777	2.2222
N,N-diethylformamide	n-Decane	0.1880	2.2166
N-Formylpiperidine	n-Decane	0.2487	2.1614

increase in excess entropy is observed when comparing acetaldehyde to DMF in a binary mixture of each solvent with n-decane including biphephos at infinite dilution. Both solvents are also predicted to form approximately ideal solutions with biphephos. The solvents DMF, acetone, and N,N-dimethylacetamide (DMA) all have very similar predicted catalyst distributions. The major difference between these solvents is the predicted tridecanal partitioning, which should be considered more prone to error than that of the catalyst. N-Methyl-2-pyrrolidone (NMP) also has a slightly lower catalyst distribution than the previous three solvents and should be expected to behave in a similar manner as DMF. The last three solvents methyl acetate, N,N-diethylformamide (DEF), and N-formylpiperidine (NFP) come in at the end of the list with a significant deviation in catalyst distribution when compared to the other five solvents. The inclusion of DEF and NFP in this list are not surprising. DEF is structurally similar to DMF containing two ethyl groups instead of the two methyl groups leading to a higher non-polar segment area. This larger non-polar region results in the lower catalyst solubility and probably is also responsible for the increase in tridecanal's partition coefficient. NFP is known to be a common replacement solvent for DMF, but has a higher alkane solubility. This can also be seen in its lower catalyst and higher tridecanal partitioning coefficients when compared to DMF.

Also of interest is the noticeable difference in tridecanal solubility (as seen in the partion coefficient) from solvents having similar biphephos solubilities. For example, DMF and acetone possess comparable heats of mixing with tridecanal, but acetone is predicted as forming a mixture with lower excess entropy leading to a slightly more favorable solution. This should reduce the ability of the TMS with acetone in separating the product. Also, the TMS systems of acetone/n-decane and NMP/n-decane would have been eliminated as possible TMS systems because of their relatively high tridecanal partition coefficients (> 0.25). Thus, concentration effects may play an important role in the estimation of product removal suggesting that the more time consuming ternary LLE calculations may become necessary in future TMS design problems.

Table 4.6: Comparison of TMS composed of DMF and linear alkanes

HRSC	LRSC	$\log_{10}(P_{tridecanal})$	$\log_{10}(P_{biphephos})$
Dimethylformamide	n-Octane	0.0267	2.4158
Dimethylformamide	n-Nonane	0.0759	2.4982
Dimethylformamide	n-Decane	0.1180	2.5635
Dimethylformamide	n-Undecane	0.1565	2.6152
Dimethylformamide	n-Dodecane	0.1870	2.6577
Dimethylformamide	n-Tridecane	0.2180	2.6959
Dimethylformamide	n-Tetradecane	0.2427	2.7245

4.4.2 Product Solvent Comparison - Alkane Size

The reason for generating a large LRSC list, containing the original 403 solvents, was to be able to compare the TMS performance of DMF with several linear alkanes. In this case, the lower bound was chosen to be n-octane and the upper bound n-tetradecane, as taken from the screening results. This results in seven TMS systems to investigate. Each of the catalyst and tridecanal partition coefficients for these systems are evaluated and listed in Table 4.6. As expected, the solubility of the catalyst and of tridecanal worsen in the product phase as the length of the alkane chain increases. This is probably a result of the predicted increase in the heat of mixing brought about by the additional non-polarity of the system. The change in excess entropy is small from mixture to mixture, as the molecular order is not drastically influenced by more of the same non-polar interactions. The size of the molecule may also play a more direct role than simply the surface charge density. The results of this alkane comparison are in qualitative agreement with the experiments conducted by Brunsch [28], where similar trends are observed. In her work, catalyst leaching measurements were conducted post reaction for TMS mixtures of DMF and alkanes from n-hexane up to n-hexadecane. This more clearly shows the previously suggested trade-off between catalyst recovery and product separation performance characteristics of the TMS.

4.5 Experimental Validation

Now that the computational portion of TMS design is finished, the second part of the proposed framework begins. Experimental validation can be considered a requirement due to the inaccuracies inherent in any predictive model or method. This is especially true in regards to predictions about thermodynamic properties, particularly in calculating liquid phase equilibrium. Related to this is also the assumption that tridecanal partitioning could be predicted using infinite dilution based predictions as a general estimate for product removal in each TMS. Thus, the results from solvent screening need to be empirically investigated.

This examination is done using a two-step process that begins with simple biphephos ligand partitioning experiments. Since the primary assumption of the developed screening method is to design TMS systems based on catalyst solubility, this first experimental portion is of great importance in order to directly compare predictions made using COSMOtherm and actual partitioning performance measured in the laboratory. This begins with biphephos being added to binary solvent mixtures where the amount of biphephos in the product phase is then measured. Not only does this deliver information about potential quality of the TMS systems with regard to catalyst leaching, but also allows for the LLE of each system to be partially validated as well.

The second step is then to take each of the TMS systems examined in the first stage and to perform the hydroformylation of 1-dodecene in each mixture using a standard procedure. This allows for an evaluation of the influence of the reactants and products on the phase behavior as well as the effect of solvent selection on reaction performance. This also covers another weakness and difficulty inherent in the framework: there is no consideration of the solvent effects on the reaction. At this point there is no developed predictive method for this and the experiments done here are the only confirmation at this point.

Since the screening results reveal that large alkanes should be used as LRSC solvents, it is preferable to again fix the LRSC solvent to n-decane, as is done previously in the screening result comparisons. Additionally, the effect of using different size alkanes in this reaction has already been confirmed experimentally where no effect of alkane size on the hydroformylation was observed (Brunsch and Behr [29]). This makes the selection of the LRSC less importannt than when choosing the HRSC, where different structures and functional groups have a stronger effect on various physical properties such as boiling temperature, phase characteristics, syngas solubilities, or coordination effects with the catalyst. In light of these arguments, the systems investigated experimentally are chosen from those listed in Table 4.5.

Of these potential TMS mixtures, only six of the eight systems are experimentally observed. Acetaldehyde is not empirically considered due to its low boiling temperature of 293.16 K, making experimental validation and analysis difficult. No experimental analysis of NFP is conducted as it only appeared in one predicted TMS design. This stems from its much higher solubility in alkanes than DMF, for which it is often used as a replacement solvent. Since this is an undesirable quality for the TMS, its performance is expected to be worse than DMF and its exclusion is justified.

4.5.1   Experimental methods

The experiments described in this section were performed by colleagues in the Department of Technical Chemistry headed by Prof. Behr at TU Dortmund as part of a collaborative effort published in McBride et al. [89]. The members of this group are experts in the area of homogeneous catalysis and have many years of experience working with the hydroformylation of long-chain alkenes. The following description of the experimental methods are of those undertaken in Dortmund.

All phase partitioning and hydroformylation experiments are carried out under an argon atmosphere using standard Schlenk techniques. The chemicals used are all commercially available and used without further purification.

4.5.1.1 Catalyst Ligand Partitioning

Each phase partitioning experiment was conducted using a binary mixture of each TMS system with a 1:1 mass ratio of the polar (15 g) and the non-polar (15 g) solvent *n*-decane being added to a double-walled 100 mL separating funnel. An amount (116.9 mg, 0.149 mmol) of biphephos was added to the mixture and thoroughly mixed before being cooled to a temperature of 253.16 K. After 20 minutes, the phases were separated. Samples for Inductively Coupled Plasma Optical Emission Spectrometry (ICP-OES) measurements were prepared using 0.230 g of the non-polar phase weighted into a Teflon cup. A mixture of 2.5 mL of nitric acid (65%) and 4 mL of sulfuric acid (96%) was then added to the solution and the digestion conducted in a Micro mPrep A microwave (MWS GmbH, Switzerland). Subsequently 2 mL of distilled water and 1 mL of hydrogen peroxide solution (30-32%, optima grade, Fisher Chemical) were added to the solution. Finally, the samples were analyzed with an IRIS Intrepid optical emission spectrometer (Thermo Fisher Scientific GmbH) and the phosphorous content determined.

4.5.1.2 Reaction Performance

The experiments for the hydroformylation of 1-dodecene in each TMS follow a similar process with the addition of the reaction step. In a typical reaction set-up, the catalyst precursor $Rh(CO)_2$acac (3.8 mg, 0.0149 mmol) and the ligand biphephos (58.4 mg, 0.0745 mmol) were weighed in a 40 mL steel autoclave. The autoclave was evaporated and flushed with argon three times. The polar solvent (6.25 g), *n*-decane (6.25 g), and 1-dodecene (2.5 g, 14.9 mmol) were then transferred into the autoclave also under an argon atmosphere. Afterwards, the reactor was pressurized to 20 bar using syngas, a (1:1) mixture of CO/H_2, and heated to 373.16 K The stirrer was adjusted to 600 rpm. After 90 minutes the reaction was stopped by cooling the reactor with ice. After depressurization through removal of the remaining synthesis gas, the reaction mixture was cooled down to 253.16 K in a double-walled 100 mL separating funnel, as done in the partition experiments. The temperature was controlled by a cooling circulation thermostat (HAAKE K40, Thermo Electron Corporation HAAKE DC50, internal temperature regulation) using ethylene glycol/water (1:1) as the cooling medium. The mixture was allowed to settle at this temperature for 20 minutes before both phases were separated and analyzed using gas chromatography and ICP-OES. For quantitative analysis of the reaction mixture an Agilent Technologies 6890N Network gas chromatograph equipped with an HP-5 column (30 m x 0.320 mm x 0.25 mm film thickness, Agilent J&W GC Columns) and an FI-Detector was used. Leaching values of rhodium and phosphorus in the product phase were measured using an IRIS Intrepid ICP-OES spectrometer (Thermo Fisher Scientific GmbH). The identification of the products was carried out by NMR spectroscopy (Bruker model DPX 500) and using a GC-MS (Agilent Technologies 5977A MSD, 70 eV). The same procedure for preparing analysis samples was used here as in the phase separation experiments.

4.5.2   Experimental Results

4.5.2.1   Catalyst Ligand Partitioning

In five of the six TMS systems examined, two phases are observed at the separation temperature of 253.16 K. The TMS comprised of methyl acetate and n-decane remained homogeneous. This is regrettable considering that methyl acetate is predicted by COS-MOtherm as forming at least some kind of miscibility gap with n-decane in a binary mixture at this temperature. This result is similar to the ternary LLE experiments and model comparisons conducted by Casás et al. [33], where the ternary LLE of the system methyl acetate, methanol, and n-decane is investigated at temperatures from 278.16 to 308.16 K. They reveal that several group contribution models used to predict phase behavior show miscibility gap formation for the binary system methyl acetate and n-decane. However, all experiments show the opposite to be true. This seems to probably be the case with COSMO-RS as well and may result from an exaggeration of the polar nature of the sp2 oxygen of the otherwise weakly polar methyl acetate. In fact the σ-profile of methyl acetate is found to be quite comparable to the more polar acetone, due to its own carbonyl group.

Therefore, the careful approach taken to miscibility gap formation chosen in solvent screening is insufficient in identifying systems with proper TMS characteristics. This shows the weakness of COSMO-RS in predicting LLE, a trait shared by all thermodynamic models. Another aspect to consider is that with the higher predicted polarity of methyl acetate, its relative solubility of biphephos is also most likely exaggerated. It may be possible that by using other mixtures of methyl acetate and n-decane instead of the 1:1 mass ratio used here would lead to a biphasic mixture at this temperature; this is however unlikely.

The amount of biphephos recovered in each phase is determined from the amount of phosphorous in each phase, seen in Table 4.7 as the distribution of phosphorous, D_P. In each of our TMS systems, the catalyst ligand is the only species that contains phosphorous, allowing for this standard procedure to be used. For example, in the mixture of DMF and n-decane, 99% of biphephos is found in the catalyst phase and 1% is lost in the product phase. All solvents forming two phases had leaching levels of approximately one percent except for acetone which had around three percent. This TMS of acetone and n-decane possessed a smaller miscibility gap as evidenced by the higher distribution of each solvent. Results indicate that COSMO-RS can, in this case, provide good predictions of biphephos partitioning for those systems actually forming biphasic systems based on the very low leaching of the catalyst in each HRSC solvent. It must be noted, however, that many of the results for catalyst leaching are near the lower limit of detectability of the ICP-OES resolution making it difficult to exactly define the performance of each solvent system. This makes a qualitative analysis and comparison with the results produced in COSMO-RS somewhat problematic.

When the ratio D_P is equal to 1/99, this correlates to a partition coefficient of 1.996. It must be noted that the partition coefficients estimated in Section 4.3.8 were made using

pure components and not the resulting mixtures of the LLE formation seen in Table 4.7. However, the predicted partition coefficients were very similar and most likely within the expected margin of error for such calculations using COSMOtherm. With higher precision measurements, such as those from a ICP-MS possessing higher resolution, more detailed analysis of the experimental results compared to their predicted values could be made. This is something considered for the third phase of the SFB/TRR 63 as part of the new B9 project led by Prof. Sundmacher.

Table 4.7: Phase Partitioning with biphephos: D_{HRSC}, D_{dec}, and D_P are the distributions of the HRSC solvent, n-decane, and phosphorous (biphephos) by mass between the product and catalyst phases, respectively.

HRSC	LRSC	D_{HRSC}	D_{dec}	D_P
Dimethylformamide	n-Decane	2/98	94/6	1/99
Acetone	n-Decane	10/90	75/25	3/97
N,N-Dimethylacetamide	n-Decane	5/95	91/9	1/99
N-Methyl-2-pyrrolidone	n-Decane	1/99	93/7	1/99
Methyl acetate	n-Decane	/	/	/
N,N-diethylformamide	n-Decane	4/96	82/18	1/99

4.5.2.2 Reaction Performance: Hydroformylation in each TMS

In Section 4.5.2.1 five of the six TMS designs showed positive results in catalyst recovery and phase separation. The successful separation in a pure, binary TMS does not necessarily confirm that the TMS will function when applied to real-world reaction conditions. Thus, the final point to conclude solvent screening for the hydroformylation of 1-dodecene is to check whether the final TMS designs can facilitate the reaction and still provide adequate phase separation and catalyst recovery.

For each of the six systems investigated in the catalyst partitioning experiments, a reaction based on the procedure outlined in Schäfer et al. [110] is developed. The experimental method is described in Section 4.5.1.2.

One of the most important aspects to notice is that tridecanal is a miscibility enhancer and that the degree of separation between the two phases is expected to worsen with its accumulation in the system. This is the trade-off between conversion and yield with catalyst leaching as seen in the economic evaluations shown in Chapter 3. The degree of separation seen in the partitioning experiments is expected to decrease due to tridecanal and is also expected to negatively affect the catalyst recovery.

Also, solvent effects on the reaction in regard to conversion and selectivity need to be evaluated, something the screening method does not take into account. There are several aspects that may have a strong effect on the reaction such as the solubility of the synthesis gas components carbon monoxide and hydrogen in the TMS, which is known

to have significant effects on the active state of the catalyst (Hentschel et al. [62]). This in turn influences the reaction performance showing a direct dependency on the solvent composition. The reaction performance not only depends on the gas solubilities, but also on the coordination effects of each solvent with the catalyst complex. This is, however, something not possible to predict using the proposed screening process at this time.

Table 4.8: Hydroformylation results for each selected TMS system: n/iso is the ratio of linear to branched aldehyde product, Y_{tri} is the tridecanal yield, and D_{tri}, D_{dod}, D_{HRSC}, D_{dec}, D_P, and D_{Rh} are the distributions of tridecanal, 1-dodecene, the HRSC solvent, n-decane, phosphorous (biphephos), and Rh by mass between the product and catalyst phases, respectively. All values are given in percents.

	n/iso	Y_{tri}	D_{tri}	D_{dod}	D_{HRSC}	D_{dec}	D_P	D_{Rh}
N,N-Dimethylformamide	99/1	80	74/26	94/6	4/96	95/5	1/99	1/99
Acetone	99/1	81	/	/	/	/	/	/
N,N-Dimethylacetamide	98/2	77	68/32	89/11	11/89	90/10	1/99	1/99
N-Methyl-2-pyrrolidone	98/2	79	70/30	91/9	12/88	92/8	1/99	1/99
Methyl acetate	98/2	80	/	/	/	/	/	/
N,N-Diethylformamide	97/3	62	43/57	53/47	28/72	58/42	3/97	5/95

0.1 mol% Rh(CO)$_2$acac, 0.5 mol% biphephos, 14.9 mmol 1-dodecene, 6.25 g polar solvent, 6.25 g n-decane, T=100 °C, pCO/H$_2$= 20 bar, t = 90 min, 600 rpm, yield (Y), ratio of linear and branched hydroformylation products (n/iso) and distribution of the solvents, products and subtrate are determined by GC-FID, distribution of biphephos and Rh is determined by ICP-OES

Results from the reaction experiments are shown in Table 4.8. It can immediately be seen that all but on of the TMS systems lead to similar levels of conversion of 1-dodecene and selectivity of the linear product tridecanal. The variation in the n/iso ratio is very small and shows that the selectivity of the biphephos ligand is not significantly affected by the choice of polar solvent. The only significant deviation in reaction performance is seen in the yield of tridecanal when using DEF as the HRSC solvent. A lower yield is observed when using this TMS, which may be caused either by a significant change in synthesis gas solubility or by a more pronounced coordination effect with the catalyst that inhibits the reaction. This suggests that multiple TMS designs are required when using the screening method not just because of the thermodynamic uncertainties, but also for the unknown effects on the reaction.

As expected, the miscibility gaps formed in each post-reaction mixture after cooling are much smaller than in the simple binary LLE experiments. This is seen by the higher distribution of polar solvent between both phases and is a result of the miscibility enhancing effect of the tridecanal product. In the systems using DMF, DMA, and NMP as the HRSC solvent, the distribution of n-decane between the two phases remains relatively constant; however, the distribution of the polar solvents worsen as seen by the higher percentage of polar solvent found in the nonpolar, product phase. In the case of DEF as the HRSC solvent, the distribution of n-decane is much larger than in the

binary LLE seaparation experiment whereas the distribution of DEF to the nonpolar phase, albeit fairly large compared to the other polar solvents, changes less drastically. When using acetone as the HRSC solvent no phase separation occurs, even upon cooling to an extra low separation temperature of 243.16 K.

The behavior of the uncoverted reactant 1-dodecene is unremarkable. The slight polar character of the carbon-carbon double bond in 1-dodecene does not affect its phase behavior strongly as seen in its very similar distribution to n-decane.

When considering the predicted tridecanal partition coefficients, no general comparison between the distribution of tridecanal in the reaction experiments can be made. DMA is predicted as having a higher distribution of tridecanal than DEF but performs much better in this regard experimentally. The product distribution with this solvent is almost on par with the distribution when using NMP, which had the highest predicted tridecanal partition coefficient of all HRSC solvents in Table 4.5. In fact, the TMS with DEF contains more tridecanal in the catalyst phase than in the product phase indicating a much larger partition coefficient than that predicted by COSMO-RS. Although, this could be based on the fact that these partition coefficients do not show much variation and may well be within the average error in partition coefficients predictions made using COSMO-RS. This suggests that no significant differences in tridecanal affinity can be made therefrom. However, it may be that concentration effects of tridecanal are significant and cannot be effectively predicted using the partition coefficients which assumes a dilute mixture. To compensate, the partition coefficient constraint should be increased to a higher value than used in this screening example. This would allow more, potentially effective candidate solvents to be considered later in the screening process. Perhaps a more detailed LLE calculation for all remaining systems could be calculated thereafter. This would provide the most conclusive predictions using this method.

A very interesting aspect of the reaction results are found when observing the catalyst leaching levels. Very similar levels of biphephos leaching are seen here as in the phase separation experiments. This is not only true for the catalyst ligand but for rhodium as well. Interestingly enough, even in the case of the TMS using DEF and n-decane, seemingly low levels of catalyst leaching are observed, being roughly only about five times that of the benchmark TMS of DMF and n-decane. Catalyst loss is very similar for the systems containing DMF, DMA, and NMP, each with catalyst leaching equal to around one percent (remember though, this is near the resolution limit for measuring leaching). It can be concluded that the amount of leaching is only roughly comparable to the quality of the distribution of the HRSC solvent between the two phases, showing that LLE behavior does not necessarily correlate as strongly with catalyst leaching as previously thought.

Also noticeable is that the leaching levels of rhodium and biphephos are quite similar. Thus the assumption that rhodium and biphephos leaching would be analogous and that predictions of catalyst leaching only require the ligand structure seem to be valid for this case. For other systems, however, this may not be the rule and such assumptions may not hold for other catalyst complexes. However, caution is again to be used as the

leaching levels reported here are near the lower boundary of the ICP-OES resolution used. With higher accuracy, more definite comparisons between the predicted and measured leaching values could be made.

4.6 Conclusion

An innovative method for computational TMS design based on quantum chemical COSMO calculations developed around a reaction specific catalyst is successfully implemented. For the hydroformylation of 1-dodecene, it is shown that by selectively screening for solvents based primarily on the biphephos catalyst ligand solubility and secondarily on product recovery through partition coefficients, functioning TMS systems can be identified. The benefit of using such a model is that when experimental data is absent or sparse, solvent selection decisions can still be made at an initial stage of process development.

In addition to the screening framework developed, the necessary experimental validation of the catalyst ligand's partitioning between the two solvents is also evaluated. This important step in the process allows for the validation of the TMS systems identified during computational screening. Here, it is seen that using thermodynamic models to predict phase equilibrium is still problematic for LLE. This is most vividly seen in methyl acetate's inclusion as a feasible solvent in a TMS with n-decane. This is erroneous as in reality they are completely soluble in one another at the investigated temperatures. Also, predicted partition coefficients between the solvents are found to be inaccurate in predicting which solvent systems would be most affected by tridecanal, although concentration effects were not considered. These problems illustrate the reasons why it is important to forge an ample group of potential TMS designs that can then be experimentally validated.

Another aspect that is not covered in the screening methodology is how the different solvent species influences the reaction. Fortunately, for the hydroformylation of 1-dodecene, the solvents selected here have a minimal effect on the reaction performance. This would mean that the identified solvents have very similar coordinating effects and/or synthesis gas solubilities. The one exception was the lower yield of tridecanal when using DEF as the catalyst solvent. In four of the five remaining TMS systems that did form biphasic mixtures after the reaction (acetone is the one the failed to do so), it would be quite feasible to perform the hydroformylation of 1-dodecene. The catalyst leaching levels predicted in the in the partitioning calculations were qualitatively consistent with the actual leaching levels found.

Finally to conclude, four functioning TMS systems identified using the solvent selection framework presented here are successfully implemented in the hydroformylation of 1-dodecene. It is found that the importance of the solvent mixture depends significantly on the polar solvent chosen and less so on the product solvent. The several limitations that appeared in the screening methods are also evaluated and should provide guidance for when applying the method for TMS design in other homogeneously catalyzed reactions. It is also worth noting that the quantum chemical COSMO-RS method employed

for thermodynamic predictions is being continuously revised and upgraded. Therefore, the screening methodology presented here will also continue to improve with time as the theory and methods become more reliable, robust, and accurate.

A silver lining found when applying this method is that DMF was one of the qualitatively best solvents for catalyst recovery. It can then be stated that the method is successful in identifying solvents already known to be suitable for this process. However, there is a downside, considering that expectations were high that new, better functioning TMS designs would be found. Perhaps by using a larger search space (by extending the database) or by considering a larger batch of HRSC solvents (more than 100), other interesting TMS designs can be found. It may also be possible to design a new solvent based on catalyst solubility using new CAMD techniques such as the method developed recently by Scheffczyk et al. [111].

Considering the margin of error using this method, future screening examples should also relax or eliminate some constraints to increase the number of solvents considered. However, any increase in the number of solvents in the search space may lead to a larger batch of possible TMS systems, increasing the experimental time and cost.

5. Integrated Reaction and Extraction Cascade

5.1   Introduction

Despite the promise of using a TMS for catalyst recovery and product separation, there are still several issues with its implementation in the hydroformylation of 1-dodecene. It was shown in Chapter 3 that a TMS composed of DMF and n-decane does not satisfactorily recover the rhodium biphephos catalyst in a single separation stage. In Chapter 4, a new framework was developed for TMS design using quantum chemical calculations in order to identify potentially better TMS candidates based on their ability to recover the catalyst ligand. It was found that mixtures of DMF with large alkanes (C_8-C_{14}) were predicted as being top performing TMS systems for catalyst recovery. The fact that a practical TMS design better suited for catalyst recovery than one consisting of DMF and n-decane was not found strongly suggests that the single stage separation following the TMS principle is not adequate enough for economical recovery of the rhodium-biphephos catalyst. Therefore, the TMS must either be replaced by another method for catalyst recovery or it must be enhanced with subsequent separation stages.

A similar conclusion was reached by Dreimann et al. [39] who developed an integrated reactor-separator system for the hydroformylation of 1-dodecene using a coupled TMS and organic solvent nanofiltration (OSN) approach. This was presented as a possible mechanism to increase retention of the rhodium-biphephos catalyst, where the membrane would retain the leached catalyst found in the product phase after phase separation in a preceding decanter. They showed that improved retention occurs with the addition of the membrane leading to low levels of leaching (<1 ppm) exemplified in a batch process. Afterwards, they investigated the continuous operation of the hydroformylation of 1-dodecene using toluene as the only solvent and OSN for catalyst recovery [40]. Note here that no TMS is used in the reaction or separation and that

catalyst recovery is completely determined by the retention performance of the membrane. They found that the membrane successfully recovers the catalyst, leading to very low levels of leaching, but that after one day of operation catalyst deactivation occurs leading to an undesirable decrease in activity and selectivity.

The idea of combining separation unit operations for increasing the catalyst retention is still fundamentally sound and, at least in our case, necessary. The question becomes then, which combination of separation practices to implement? Instead of establishing a completely new method for enhancing catalyst recovery, it is proposed that by including subsequent extraction stages with fresh catalyst solvent (DMF), catalyst leaching levels can be economically reduced. In this way the functionality of the TMS is maintained and simply extended by recovering leached catalyst found in the nonpolar phases separated in previous stages. From a process design perspective, the introduction of extraction stages is straightforward. This is still the case here although additional mass separating agents and unit operations are required.

The suggestion of using extraction to recover the catalyst is not completely new, however. In the work by Dreimann et al. [39], the authors considered the possibility of extraction but disregarded it as an option due to expected thermal degradation of the catalyst. The distillation temperatures required are simply too high and would lead the deactivation of any catalyst recovered in the subsequent stages. This can be circumvented by using vacuum distillation which would lower the column temperature to a practical level, preventing catalyst deactivation. Such techniques are already necessary for the downstream separation of the reaction solvents, unconverted reactant, and aldehyde products.

To investigate the effectiveness of extraction in catalyst recovery, a model capable of predicting the partitioning behavior of the catalyst must be created. A major difference between the proposed model here and the one used previously in Chapter 3 is the inclusion of catalyst partitioning and the temperature effects on phase separation. By including these two components, the design space for the TMS composition increases and provides one with the ability to model the proposed extraction cascade. This model must also be able to provide LLE solutions within an optimization problem. Once the LLE and catalyst partitioning can be reasonably predicted within the optimization, the feasibility of an extraction or decanter cascade can be incorporated into a process design problem.

Although the importance of catalyst leaching on the process economics is well known (as shown in Chapter 3), it was not included in the integrated reactor and process design conducted by Hentschel et al. [61]. This was due to the absence of a model for describing the catalyst leaching. The authors then assumed that the catalyst was completely recovered in the polar phase after separation in the decanter in order to simplify their process model. Since the primary goal was to investigate optimal reactor trajectories, especially with the influence of recycle streams and process economics, this assumption is acceptable. They postulated, however, that were catalyst loss to be taken into account that the optimal process design would attempt to reduce the loss of catalyst

by tuning the outlet composition of the reactor to one more conducive towards better phase separation in the following decanter. This is important due to the miscibility enhancing effects of the product tridecanal in the primarily DMF/n-decane mixture. Thus, higher conversion and selectivity of the reaction lowers the effectiveness of the TMS in catalyst recovery. This shows that a trade-off between the reactor performance and phase separation quality exists.

Thus, the proposed extraction design procedure would need to include the effects on the reactor in order to be considered complete. Once a model describing the thermodynamics of the process is complete, the effect of integrated catalyst recovery and reactor performance can be evaluated by optimizing the total annualized cost of the process. This would advance the previous work done on reactor design by finally combining catalyst leaching effects into the design stage. This proposed process should offer more flexibility in process conditions, lower overall energy usage, reduce waste, and drastically sink the operational costs.

The work presented in this chapter is taken primarily from the recently accepted article by McBride et al. [90].

5.2 LLE Surrogate Model

The object outlined here is to establish a model that can be used to calculate the LLE equilibrium of a mixture given its molar composition and temperature. The model must also be able to provide LLE solutions inside an optimization problem. Using the original thermodynamic models is not an option, as any such problem requiring convergence on its own is almost guaranteed to fail during optimization. For this reason a surrogate model is developed and used to solve the LLE internally during optimization, similar to the procedure adopted in Section 3.2.

Whereas a linear surrogate model is used to alleviate a similar problem by McBride and Sundmacher [87], a Kriging model (Krige [79]) is chosen for this work. Such a model should hopefully provide better accuracy than the linear model used in Chapter 3. The use of Kriging surrogate models for chemical engineering tasks is not new, as they have been the focus of much interest in chemical process simulation (Kleijnen [76]). For example, Kriging models have been successfully used in process optimization, such as in modular flowsheet optimization by Caballero and Grossmann [31] and distillation column design by Quirante et al. [102]. Whereas these examples used surrogate models to represent entire unit operations, this work focuses simply on using a surrogate model to describe the LLE conditions within units in the process model. In the specific case at hand, the desired model must also include predictions of catalyst leaching. This is the key component that has been missing in previous optimal process design work on the hydroformylation of 1-dodecene. Use of this model to describe the biphasic separations will alleviate the problem of solving the LLE within an optimization problem and also deliver the much needed catalyst partitioning information as well.

In the remainder of this section, the procedure used to develop the model is described in detail. To help visualize how the thermodynamic model used to describe the phase

equilibrium and catalyst partitioning is generated, the primary steps used are depicted in Figure 5.1.
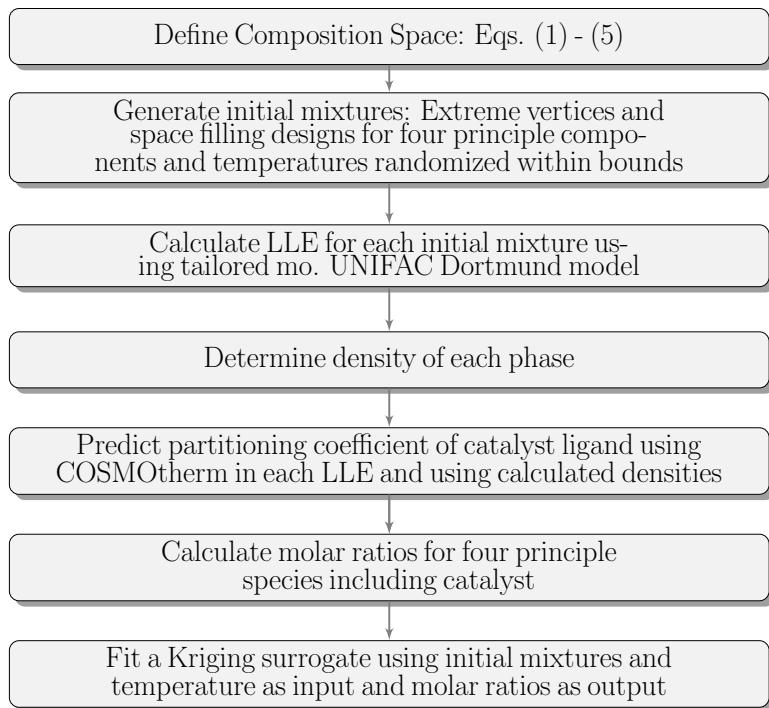
Figure 5.1: Method used to generate thermodynamic model including catalyst leaching for optimization.

5.2.1   Phase Equilibrium

The mixture considered here for phase separation consists of reactants, products, byproducts, and TMS solvents encountered in the hydroformylation of 1-dodecene. In total, there are eight components that need to be considered: DMF, n-decane, n-dodecane, 1-dodecene, iso-dodecene (a mixture of various internal 1-dodecenes), tridecanal, 2-methyldodecanal, and the catalyst ligand biphephos. It was shown in Chapters 3 and 4 that catalyst leaching can be estimated quite well using only the ligand. This is the primary reason for why the entire catalyst complex is not considered here.

In this work, the liquid-liquid equilibrium is modeled using the modified UNIFAC Dortmund (Weidlich and Gmehling [126]) activity coefficient model with several of the binary interaction parameters refit to experimental data. This is the same model previously described in Section 3.2. This tailored thermodynamic model is very accurate in predicting LLE for mixtures containing the four principle components found in the system considered: DMF, n-decane, 1-dodecene, and tridecanal. Two of the remaining components, iso-dodecene and 2-methyldodecanal, are isomers of 1-dodecene and tridecanal, respectively, and are predicted to have the same phase equilibrium behavior as their

isomers. The small amount of n-dodecane is considered to behave similarly to n-decane. Thus, out of the seven non-catalyst components considered, only four are necessary to effectively describe the phase equilibrium beahvior. The catalyst is assumed to be at infinite dilution and to have no effect on the phase behavior.

5.2.2 Catalyst Leaching

Another main objective of the surrogate thermodynamic model is its capability in predicting the partitioning behavior of the catalyst, as represented by the ligand biphephos. As in Chapter 4, only the catalyst ligand is considered in partitioning calculations. This is due to its commonly higher concentration in the reaction mixture (in this case the ligand to Rh ratio is 5:1) and that the leaching of rhodium and the ligand are found to be similar (Brunsch and Behr [29]). Also, the economical burden of biphephos was found to be more significant in affecting the total process costs than the rhodium metal, as seen in Figure 3.8 in Section 3.4.1.

A key factor why a model for catalyst leaching does not exist is the lack of data or an available method to thermodynamically model the catalyst in solution. The use of modern quantum chemically based tools such as COSMO-RS allows for the thermodynamic modeling of large, complex molecules like biphephos (Klamt et al. [75]), as used previously in Chapter 4. The molecular structure is developed using TURBOMOLE [119] at the RI-DFT level of theory [42] using the def2-TZVPD basis set (Rappoport and Furche [103]). The resulting COSMO file encompasses all the necessary information for making solubility predictions of the biphephos ligand using the software COSMOtherm (Eckert and Klamt [41]). A similar procedure was used for modeling the catalyst ligand in Chapter 4.

The concentration of the catalyst in the reaction mixture is very low and is usually determined by the amount of 1-dodecene in the reactor feed, being somewhere between four or five orders of magnitude smaller. Therefore COSMOtherm can be used to estimate biphephos partitioning coefficients by assuming that the solute is at infinite dilution. The distribution of the catalyst ligand can be directly determined using these partitioning coefficients. Since only the ratio between the two phases is required, absolute values are not necessary. Thus, this prediction of partitioning is sufficient for the model used in the following reaction-extraction optimizations.

5.2.3 Data Generation

As done in Chapter 3, only compositions ensured to form miscibility gaps can be taken into account for the surrogate model. At the moment, it is not possible to describe the transition between a homogeneous mixture and a heterogeneous mixture using a surrogate model. This means the composition of the initial mixtures must be selected carefully to ensure that each overall composition remains below the binodal curve for the specified temperature. By using the experimental data from Schäfer and Sadowski [109], the approximate location of the binodal curve for the ternary system DMF, n-decane, and tridecanal at 298.15 K can be ascertained. In reference to this known LLE

behavior, a fixed region is chosen for typical compositions used in the TMS that are ensured to form biphasic mixtures at all contemplated separation temperatures in the range of 253.15 to 293.15 K. This region representing the established composition space is shown in Figure 5.2. Equations (5.1) to (5.5) are the composition constraints used to define this area. Since 1-dodecene is not a miscibility enhancer of DMF and n-decane to the extent that tridecanal is, its effect on the phase behavior is not considered to be critical in ensuring that the post-reaction mixtures form two liquid phases. Additionally, all of the tridecanal found in the post-reaction mixture is converted from 1-dodecene, making the concentration of the two species dependent. For these two reasons, the composition constraints that apply to tridecanal are also implemented for 1-dodecene.
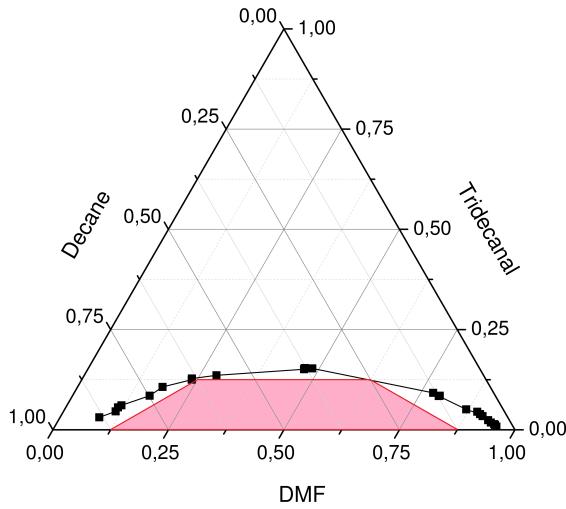
Figure 5.2: Post-reaction mixture constraints shown for a ternary mixture of DMF, n-decane, and tridecanal (within the shaded region under the binodal curve) used in modeling the surrogate model for determining LLE and catalyst partitioning [90]. Experimental data at 298.15 K taken from Schäfer and Sadowski [109].

$$x_{\text{DMF}} - x_{\text{tridecanal}} \geq 0.125 \qquad (5.1)$$
$$x_{\text{DMF}} + 2 \cdot x_{\text{tridecanal}} \leq 0.875 \qquad (5.2)$$
$$x_{\text{DMF}} - x_{1-\text{dodecene}} \geq 0.125 \qquad (5.3)$$
$$x_{\text{DMF}} + 2 \cdot x_{1-\text{dodecene}} \leq 0.875 \qquad (5.4)$$
$$x_{\text{tridecanal}} + x_{1-\text{dodecene}} \leq 0.125 \qquad (5.5)$$

The first step in fitting the surrogate model is to generate the initial compositions within the fixed composition space. This is accomplished by finding the extreme vertices of the composition space and by using a space-filling design that ensures adequate spacing between sample points, which is important when fitting a Kriging model. A total of 29 extreme vertices are used in combination with a space-filling plan consisting of

500 additional compositions. To prevent possible extrapolation by the Kriging model at compositions near the boundaries of the composition space, the LLE for each composition at the extreme vertices are calculated at five different temperatures: 253.15, 273.15, and 293.15 K (the lower temperature bound, the center point, and the upper temperature bound, respectively) as well as for two random temperatures within this range. This generates a total of 145 points. The LLE of each composition produced by the space-filling design is evaluated at three different random temperatures between 253.15 and 293.15 K. This additionally adds 1500 LLEs to the data set.

The LLE for each composition and temperature is now estimated using the specially fitted modified UNIFAC model developed in Chapter 3. Once the compositions of the two liquid phases in equilibrium for each of the initial compositions have been determined, the density (Equation (A.1)) of each phase is calculated using correlations published by Yaws [131]. This is done to ensure that more accurate densities are used in COSMOtherm than the simple linear method used by default. The paritioning coefficient (see Equation (5.6)) of biphephos can now be predicted using COSMOtherm for each biphasic system with their specific densities.

$$
\begin{aligned}
\log_{10}(P_j^{(2,1)}) &= \log_{10}(\exp((\mu_j^{(1)} - \mu_j^{(2)})/RT)) \\
&= \log_{10}(x_j^{(1)}/x_j^{(2)})
\end{aligned}
\tag{5.6}
$$

$$
\theta_i^\alpha = \frac{n_i^\alpha}{n_i^\alpha + n_i^\beta} \qquad i \in \text{COM}
\tag{5.7}
$$

The molar ratios (the θ values first seen in Chapter 3) for the four principle components used in the LLE calculations and for the catalyst ligand can now be calculated according to Equation (5.7).

5.2.4 Kriging Surrogate

A Kriging model with a second order polynomial regression model and a Gaussian correlation model is chosen as the surrogate. The model was fit using the DACE toolbox for Matlab [1], and a very detailed description of how the Kriginig model functions and how it is regressed are included on the author's website. In our preliminary investigations, the Kriging surrogates provided better results than when using linear functions; this is especially true when including temperature as an input variable. Gaussian correlations also showed the lowest average error for all correlations tested. This allows for an almost seamless integration of the separation temperature as a variable into the surrogate instead of using a fixed temperature in the decanter, as done in the previous linear model. Not only for that reason, but when consulting Section 3.2, it can be seen that for a single temperature, significant deviations in the predicted partition coefficients occur when using a linear regression model. The Kriging model used here should not show such high deviations.

Linear regression models and response surface maps were not the only surrogate model formulations tested. The surrogate model generating software ALAMO (Cozad et al. [37, 38]) was implemented in a battery of tests, in order to see if a simple, yet accurate surrogate model could be created. This, however, also did not produce accurate results for LLE predictions. It must be stated that this software is still very new and does not yet have the ability to implement the necessary mixture constraints needed for simulation of the phase separation. Future editions of the software may prove useful in creating surrogate models for LLE predictions.

$$\hat{\theta}_i^\alpha = KR(\hat{x}_j, T) \tag{5.8}$$
$$i \in \{\text{DMF}, \text{C10an}, \text{nC13al}, \text{nC12en}, \text{BPP}\},$$
$$j \in \{\text{DMF}, \text{C10an} + \text{C12an}, \text{nC13al} + \text{iC13al}\}$$

The surrogate model uses the mole fractions of DMF, n-decane, and tridecanal and the target separation temperature as input variables. In the final optimization, one must also consider the complete mixture used. Therefore, several mole fractions are added together: the mole fractions of n-decane and n-dodecane, those of tridecanal and 2-methyldodecanal, and those of 1-dodecene and iso-dodecene. This reduces the number of components to consider down to four, however, due to the summation rule for mole fractions, only three of these four components are necessary as input. The output consists of five molar fractions: those of the four principle components and that of the catalyst ligand. This is represented by the vector $\hat{\theta}_i^\alpha$ shown in Equation (5.8). As before, the outputted molar fraction of iso-dodecene is assumed to equal that of 1-dodecene, 2-methyldodecanal to that of 1-tridecanal, and n-dodecane to that of n-decane.

If one decided to use the full space-filling design with the additional points generated to capture temperature effects, it would lead to a surrogate model that requires an unnecessarily large number of data points. This may also lead to over fitting of the model which is undesirable. Therefore it is not convenient to use the full space-filling design to fit the model. It would be wiser to incorporate only those points needed in the model and to use the remaining data set for validation as a compromise.

An iterative process is used to fit the Kriging model. It starts with only the inital set of extreme vertices (145 compositions and temperatures) to fit an initial model. The entire remaining data set (1500 compositions and temperature at this point) is then used for validation. To speed up the fitting process, the ten points in the validation set with the highest sum of relative errors are added to the sample set and a new Kriging model is generated in the subsequent iteration step. This process continues until either the overall relative error is less than 10^{-4} or the number of data points reaches the chosen maximum limit, in this case 550. This value was chosen due to preliminary work that showed only small deviations in error after around 500 to 600 data points were included in fitting the Kriging model. The overall relative error used here is the summation of the absolute relative errors for all five predicted molar ratios by the Kriging model.

This iterative procedure stopped after reaching the maximum allowable number of data points, 550, and had a maximum overall relative error of 0.0117 with an average overall relative error of 0.0021. After around 400 data points, very little change in overall error was observed, suggesting that fewer data points may be used. The importance of this realization would only become important if the sample set included expensive data. However, the LLE and biphephos partitioning calculations performed here require low computational effort.

A parity plot comparing the calculated molar ratios using the uniquely parameterized Modified UNIFAC Dortmung model and COSMOtherm for biphephos partitioning coefficients with the predictions made using the Kriging surrogate is shown in Figure 5.3. It is quite obvious that the fit is very good for the 5475 individual molar ratios in the validation set plotted here. In the inset, a magnified view of the predicted molar ratios found near unity are shown in more detail. During optimization, the Kriging surrogate must accurately predict the molar ratios for the catalyst which are often very close to unity. If the surrogate is ill-fitted to such a degree that molar ratios greater than or equal to one are predicted for the catalyst, the solver would select these compositions and temperatures erroneously leading to an unreasonable solution for the process. To ensure again that the model does not predict values above one, a second validation using randomly generated inlet compositions and temperatures within the boundaries of the sample data was performed. A similar procedure was done for partition coefficients approaching zero.
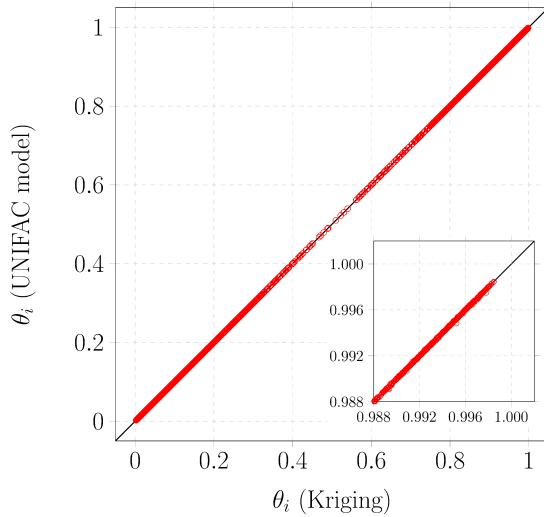
Figure 5.3: Comparison of calculated molar ratios using the predicted molar ratios from the Kriging surrogate model. The inset shows that Kriging model can also accurately reproduce the critical results near unity [90].

Now that a reliable surrogate model for catalyst leaching and phase equilibrium has been developed, the effect of catalyst separation using a TMS and extraction in the hydroformylation of 1-dodecene can be included in process wide design problems.

5.3   Process Model

This work considers an integrated reaction and extraction design problem. Two primary aspects for the process flow sheet are the reactor and the complete downstream separation including the proposed decanter cascade.

This section begins with descriptions of the important process units: the reactor, the decanters and extraction cascade, and the distillation columns. Also, the balance equations for the proposed flowsheet are presented along with utility and equipment sizing functions.

It is noted here that the following sections: Section 5.3.1, Section 5.3.2, and Section 5.3.3 are very similar to the descriptions given in McBride et al. [90], as it concerns the same process. Thus, the mentioned sections have been only slightly modified for minor content and editing and to adapt the references to this document.

5.3.1   Reaction

The most important component for designing an optimal reactor are reliable reaction kinetics and correlations (gas solubilities, for example). In the hydroformylation of 1-dodecene, reaction pathways were determined by Markert et al. [86] and reaction kinetics were originally developed by Kiedorf et al. [70]. Since the original kinetics were only fit using data collected from batch experiments with low partial pressures of CO, they were found to deviate substantially for systems operating at conditions other than those used in the batch cases. To account for this, additional batch, semi-batch, and perturbed batch experiments were performed by Hentschel et al. [62] in order to collect new data and to increase the robustness and accuracy of the reaction kinetics. Several parameters were updated and an additional, sixth reaction, that of the direct hydroformylation of 1-dodecene to 2-methyldodecanal, was amended to the reaction network. The catalyst complex equilibrium was also updated to better reflect the influence of CO concentration. The resulting reaction network is shown in Figure 5.4.

Reaction kinetic data and accompanying equations are located in Appendix A.2. The reaction kinetics are represented by Equations (A.5) to (A.10), the temperature dependency of the reaction rate constants by Equation (A.11), and the equilibrium constants used in reactions 2 (Equation (A.6)) and 3 (Equation (A.7)) are found using Equation (A.12) and Equation (A.13). The catalyst equilibrium is represented by Equation (A.14). The correlations for H_2 and CO solubility in the liquid phase are based on predictions made using PC-SAFT (Gross and Sadowski [54]) are also adapted from the work by Hentschel et al. [62]. The equilibrium gas concentration is given by Equation (A.15) and the liquid phase gas solubility by Equation (A.16). The kinetic parameters for the reaction are listed in Table A.6, the parameters for determining the

equilibrium constants in Table A.7, and the gas solubility parameters in Table A.8. The mass fraction of DMF and n-decane at the reactor inlet are maintained at 0.32
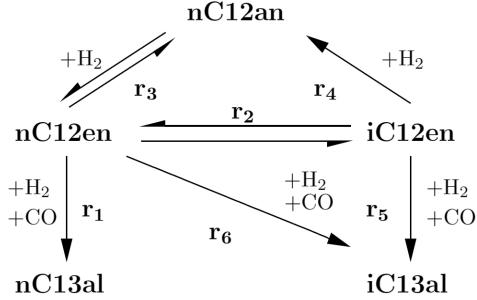
Figure 5.4: Updated reaction network for the hydroformylation of 1-dodecene proposed by Hentschel et al., from whom this figure is adopted [62].

and 0.48, respectively. These are fixed for the given reaction kinetic data. The reaction kinetics are valid for specific temperatures and pressures which form the bounds in the following optimizations:

$$10 \text{ bar} \leq P \leq 20 \text{ bar} \tag{5.9}$$
$$368.15 \text{ K} \leq T \leq 388.15 \text{ K} \tag{5.10}$$

5.3.2 Reactor

The reactor trajectories optimized using the elementary process function (EPF) methodology (Freund et al. [50]) lead to non-intuitive control strategies for temperature and H_2/CO pressures along the reactor. In the hydroformylation of 1-dodecene, two major reaction zones could be identified: initially a region for quick formation of the desired linear aldehyde and the second region being dominated by reverse-isomerization of iso-dodecene, leading to additional linear and branched aldehyde formation. However, the regio- and chemo-selectivity behaviors are contrary. Hence, a cost optimization of the overall process was carried out by Hentschel et al. [61] to evaluate the optimal reactor operation and the trade-offs with the downstream energy and unit size demands. In addition to the two identified reactions zones, seemingly high reaction times were also characteristic for optimal reactor configurations due to the lower significance of capital investment on the TAC.

With the updated kinetics, the same two reaction sections are again identified (see Hentschel et al. [62] for more detail). The first region with high 1-dodecene concentration is preferably operated at the lower temperature bound and the reisomerization region at the upper temperature bound in order to accelerate the conversion of iso-dodecene back into 1-dodecene. Optimal pressure profiles for the new kinetics indicate

that the first reaction zone is enhanced by an excess of CO to inhibit side reactions and an excess of H_2 in the second reaction zone to reduce this inhibition in order to support the reverse-isomerization. Note, that this reactor arrangement is only optimal in case of a stand-alone reactor not coupled with recycle streams. One can see that the impact of the optimal gas profiles in each reaction zone on reactor performance is rather small and that the ratio of CO and H_2 partial pressures are more important than their absolute values. Furthermore the second reaction zone, namely the reverse-isomerization, is enhanced by back-mixing for high conversions.

For these reasons, the proposed reactor design is considered as a series of two reactors: a differential sidestream reactor (DSR) for the first reaction zone with low temperature and excess CO and a continuously stirred tank reactor (CSTR) for the second reaction zone with higher temperatures and excess H_2 (see Figure 5.5). The CSTR is assumed to have a comparatively longer residence time because of the relatively slow reverse-isomerization. For optimization purposes the DSR is modeled as a series of equal volume CSTRs with gas reactant dosing to maintain the pressure at the optimal level. In this manner, the proposed reactor series is modeled using Equations (5.11) to (5.16).

$$C_{out,r,i} = C_{in,r,i} + C_{cat,r}\tau_r M_{cat} \sum_{j \in \text{RCT}} v_{i,j} r_j \tag{5.11}$$

$$C_{in,r,i} = \frac{\dot{n}_{liq,r,i}}{\dot{V}_{liq,r}} \tag{5.12}$$

$$\dot{V}_{liq,r} = \sum_{i \in \text{COM}} \frac{\dot{n}_{liq,r,i} M_i}{\rho_i} \tag{5.13}$$

$$\rho_i = a_{\rho,0,i} + a_{\rho,1,i} T \tag{5.14}$$

$$\tau_r = \frac{V_r}{\dot{V}_{liq,r}} \tag{5.15}$$

$$Q_r = \sum_{i \in COM} \left(n_{out,r,i} \cdot h_{out,i} - n_{in,r,i} \cdot h_{in,i} \right) \tag{5.16}$$

5.3.3   Separation

5.3.3.1   Decanters

The separation processes are perhaps the most important in the flowsheet, especially the decanters. It is in the decanters where the expensive catalyst is to be recovered. Now that a model is available for the LLEs within each decanter, the strong temperature and composition effects on catalyst leaching can be included in the optimization. The complete phase compositions formed within each decanter are determined using the Kriging model described in the previous section, given by Equation (5.17) and Equation (5.18).

$$\dot{n}_{\text{out,i,s,p}} = \theta_{\text{i,s}}^{\alpha} \cdot \dot{n}_{\text{i,s}} \qquad\qquad i \in \text{COM}, s \in \{d1,..,dn\} \tag{5.17}$$
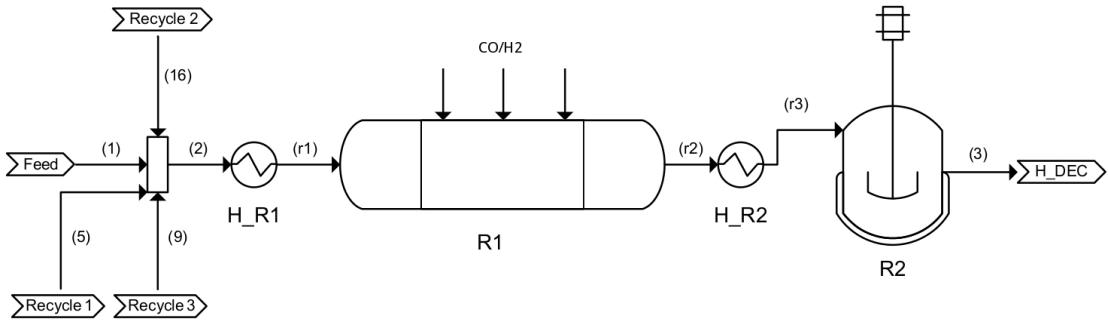
Figure 5.5: Depiction of the proposed reactor arrangement. This unit comes before the decanter feed shown in Figure 5.6 or Figure 5.7. The recycle streams shown in Figure 5.6 and Figure 5.7 are integrated into the flowsheet at this point [90].

$$\dot{n}_{\text{out},i,s,\text{np}} = (1 - \theta_{i,s}^{\alpha}) \cdot \dot{n}_{i,s} \qquad\qquad i \in \text{COM}, s \in \{d1,..,dn\} \qquad (5.18)$$

Here, p and np represent the polar and nonpolar phases, respectively. The inlet streams to each decanter are specially designated as $d1$, $d2$, etc. Since the number of decanters is theoretically infinite, the stream dn represents the inlet to the final decanter in the cascade.

The upper and lower bounds for the mixture compositions in each decanter in the cascade must be congruent with those used to generate the thermodynamic model (Equations (5.1) to (5.5)). The temperature in each decanter is the same except for that in the first decanter which is not part of the cascade.

$$253.16 \text{ K} \leq T_s \leq 293.16 \text{ K}, \qquad s \in \{d1,..,dn\} \qquad (5.19)$$

There are two different separation scenarios to consider: a separation following the TMS principle using a single decanter (case 1), and several cases using a counter current decanter cascade that requires extra polar solvent to be mixed with the inlet stream to the final decanter in the series. In the latter cases, an extra distillation column to recover the extraction solvent is required. The separation of the CO and H_2 from the post reaction mixture is assumed to occur in a flash unit which is not modeled here. This gas is assumed to be recycled back to the reactor and only the reactant gas consumed during the reaction is considered replaced.

5.3.3.2 Scenario 1: Single Decanter

The process considered in this analysis is shown in Figure 5.6. The post-reaction mixture (S_3) is fed to a heat exchanger (H_{DEC}) where the temperature is cooled from the reactor temperature to 300 K and then cooled further to the required separation temperature using a refrigerated coolant in a second heat exchanger (H_{D1}). The more polar of the two phases formed in D1 is to be eventually recycled (Recycle 1, S_5) back to the

reactor feed and contains the majority of the catalyst used in the reaction. The non-polar phase leaving the decanter is then heated (H_{CF2}) to its bubble point temperature and fed to the reaction solvent distillation column (C2) where the unreacted reactants, various byproducts, and solvents are separated as the distillate from the aldehyde products which form the bottoms. The distillate of C2 is to be recycled (Recycle 2, S_{14}) back to the reactor feed and the aldehyde bottoms is cooled (H_{CF3}) to its bubble point and fed to the isomer column (C3) where the desired product n-tridecanal is separated as the bottoms from 2-methyldodecanal which forms the majority of the distillate. Altogether this separation process contains six heat exchangers, two columns, one decanter, and one refrigeration unit (not shown).

This has been the commonly used arrangement developed in previous process design concepts for the hydroformylation of 1-dodecene using a TMS for catalyst recovery, as seen in Chapter 3. A similar process is used in the optimization work done by Hentschel et al. [61] and in the operation of a miniplant by Zagajewski et al. [134].
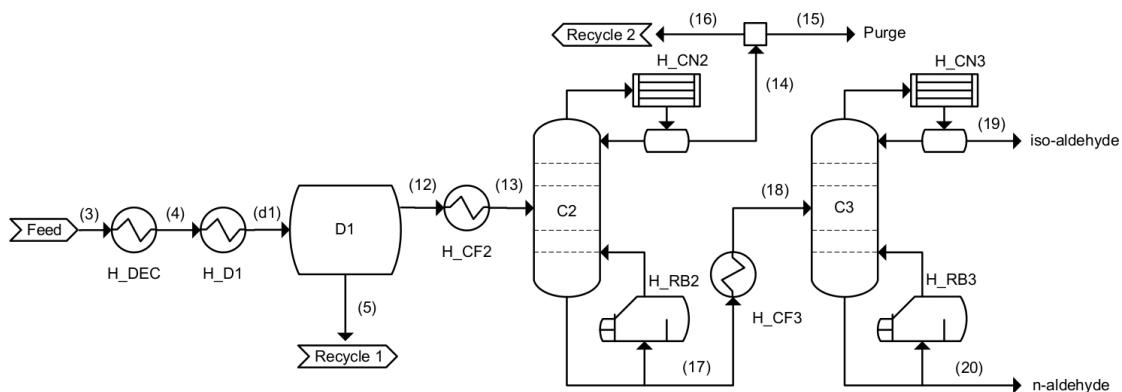
Figure 5.6: Flowsheet for the separation using a single decanter (D1). Distillation columns for the unreacted reactants and solvents (C2) and for the aldehyde separation (C3) are shown [90].

5.3.3.3   Scenario 2: Liquid-Liquid Extraction

The addition of extra separation stages in the form of decanters with excess polar solvent leads to a slightly more complicated process flowsheet. In Figure 5.7, the necessary changes to the flowsheet using a counter current cascade are shown. The cascade stages are labeled as D2 through DN, which is the final stage. Except for the additional decanters, heat exchangers, and extraction solvent column (C1), the rest of the downstream processing remains the same as in Scenario 1.

As before, the post-reaction mixture is initially cooled to the separation temperature using two heat exchangers. The polar phase in D1 is to be recycled (Recycle 1, S_5) back

to the mixer preceding the reactor feed. The non-polar phase leaving D1 is now cooled (H_{D2}) to the cascade temperature and fed to the next decanter (D2) in the cascade. The polar phase from decanter D3 is also fed to D2 forming a new mixture which now separates into two phases. This process is applied to all subsequent decanters in the cascade except for the final decanter, where the non-polar phase is then fed to C2 (see DN in Figure 5.7 for clarification). Also, the fresh polar, extraction solvent is added here to DN. The polar phase of D2 is heated (H_{CF1}) to its bubble point temperature before being fed into the extraction solvent column (C1). This column is designed such that the distillate contains exactly the amount of solvent added to the cascade in order to avoid accumulation of extraction solvent in the system. The bottoms of C1 contains valuable catalyst recovered in the extraction and is to be recycled (Recycle 3, S_9) back to the reactor feed. The extraction solvent added to the final decanter in the cascade is not necessarily pure DMF but may contain a small amount of other components, particularly *n*-decane. This may occur because the purity and recovery of the extraction solvent are left as degrees of freedom in the optimization.
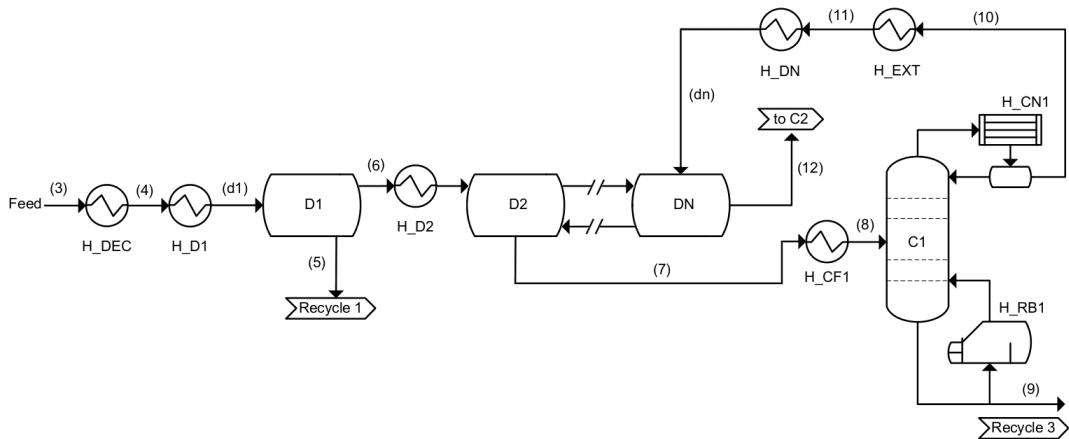
Figure 5.7: Counter current LL separation cascade and a solvent column (C1) to recover extraction solvent. The non-polar phase leaving the last decanter in the cascade is fed to column C2 as seen in Figure 5.6. The extra catalyst recovered using the cascade is recycled back to the reactor feed (Recycle 3) [90].

5.3.3.4 Distillation Columns

The proposed flowsheets contain two or three distillation columns depending on which scenario is being considered. The first column, C1, is the extraction solvent column that separates the extra DMF heavy extraction solvent added to the decanter cascade as the distillate. The bottoms of this column contains a mixture of all remaining components, most importantly recovered catalyst. The light key is DMF and the heavy key is *n*-decane. Naturally in Scenario 1, this column is not included in the flowsheet. The second column, C2, is the reaction solvent column where the remaining reaction solvents, unreacted reactants, and *n*-dodecane and iso-dodecene byproducts are separated from

the aldehydes and recycled back to the reactor feed. The light key in this column is iso-dodecene and the heavy key is 2-methyldodecanal. The third column, C3, is the isomer column used to separate 2-methyldodecanal, the light key, from the product tridecanal, the heavy key.

All columns are modeled using the Fenske-Underwood-Gilliand correlations which are used to estimate column sizes and flowrates (Fenske [45], Gilliland [51], Molokanov et al. [91], Underwood [120, 121]). The column pressure in C1 is assumed to be 246 mbar, as the catalyst becomes deactivated at temperatures above 393.15 K. Because the tridecanal product will degrade at temperatures higher than 453 K, the maximum pressure in C2 and C3 is limited to 88 mbar. The pressure drop is assumed to be 50% from the top to the bottom of the column, as done in the previous studies performed in our group (Hentschel et al. [61], McBride and Sundmacher [88]). All models used for the column design, vapor pressure correlations, mass balances, parameters, etc. are found in Appendix A.4.

5.3.4 Flowsheet Constraints

Depending on the case considered, the flowsheet will vary. Scenario 1 only uses a single decanter based on the TMS priciple and will not utilize a solvent column (C1). Several streams, 6-11, are not used in Scenario 1 and the connectivity is seen as in Figures 5.5 and 5.6.

The amount of 1-dodecene in the reactor feed stream determines how much catalyst should be in the reactor. In this work, the amount of rhodium precursor is taken as being one ten thousandth of a mole for each mole of 1-dodecene in the reactor inlet (Equation (5.20)). The biphephos ligand is then given at five times the concentration of the rhodium precursor (Equation (5.21)). Note that the amount of catalyst is one-tenth that used in Chapter 3. In the work by Hentschel et al. [61], a reactant to catalyst ratio of 1:10000 was used in place of the 1:1000 used in the experiments conducted by Brunsch [28] and the correlating process model in Chapter 3.

$$\dot{m}_{\text{Rh}} = 1 \cdot 10^{-4} \cdot \dot{n}_{\text{nC12en,2}} \cdot M_{\text{Rh}} \tag{5.20}$$

$$\dot{m}_{\text{BPP}} = 5 \cdot 10^{-4} \cdot \dot{n}_{\text{nC12en,2}} \cdot M_{\text{Biphephos}} \tag{5.21}$$

5.3.4.1 Flowsheet for Scenario 1

This section contains briefly the connectivity constraints and the stream temperatures for the flowsheet used in Scenario 1. Note again that streams 6 - 11 are not used in this model.

$$\dot{n}_{i,1} = 0 \qquad\qquad i \in \{\text{nC13al}, \text{iC13al}, \text{iC12en}, \text{C12an}\} \tag{5.22}$$

$$\dot{n}_{i,2} = \sum_{s \in \{1,5,16\}} \dot{n}_{i,s} \qquad\qquad i \in \text{COM} \tag{5.23}$$

$$\dot{n}_{i,s+1} = \dot{n}_{i,s} \qquad\qquad i \in \text{COM}, s \in \{3, 12, 17\} \tag{5.24}$$

$$\dot{n}_{C_2,\text{in},i} = \dot{n}_{i,12} \qquad\qquad i \in \text{COM} \qquad (5.25)$$

$$\dot{n}_{C_3,\text{in},i} = \dot{n}_{i,18} \qquad\qquad i \in \text{COM} \qquad (5.26)$$

$$\dot{n}_{i,14} = \dot{n}_{C_2,D,i} \qquad\qquad i \in \text{COM} \qquad (5.27)$$

$$\dot{n}_{i,17} = \dot{n}_{C_2,B,i} \qquad\qquad i \in \text{COM} \qquad (5.28)$$

$$\dot{n}_{i,19} = \dot{n}_{C_3,D,i} \qquad\qquad i \in \text{COM} \qquad (5.29)$$

$$\dot{n}_{i,20} = \dot{n}_{C_3,B,i} \qquad\qquad i \in \text{COM} \qquad (5.30)$$

$$\dot{n}_{i,15} = x_{\text{purge}} \cdot \dot{n}_{i,14} \qquad\qquad i \in \text{COM} \qquad (5.31)$$

$$\dot{n}_{i,16} = (1 - x_{\text{purge}}) \cdot \dot{n}_{i,14} \qquad\qquad i \in \text{COM} \qquad (5.32)$$

Stream temperatures are defined as the following:

$$T_1 = 293.16 \text{ K} \qquad\qquad (5.33)$$

$$T_3 = T_{R_2} \qquad\qquad (5.34)$$

$$T_4 = 300 \text{ K} \qquad\qquad (5.35)$$

$$T_s = T_{d1} \qquad\qquad s \in \{5, 12\} \qquad (5.36)$$

$$T_{13} = T_{\text{bub},C_2,F} \qquad\qquad (5.37)$$

$$T_s = T_{\text{bub},C_2,D}, \qquad\qquad s \in \{14, 15, 16\} \qquad (5.38)$$

$$T_{17} = T_{\text{bub},C_2,B} \qquad\qquad (5.39)$$

$$T_{18} = T_{\text{bub},C_3,F} \qquad\qquad (5.40)$$

$$T_{19} = T_{\text{bub},C_3,D} \qquad\qquad (5.41)$$

$$T_{20} = T_{\text{bub},C_3,B} \qquad\qquad (5.42)$$

The temperature of the stream exiting the mixer (S_2) is calculated using the energy balance around the mixer consisting of the feed and recycle streams (Equation (5.43)). The correlation for enthalpy (Equation (A.2)) is found in A.1.

$$\sum_{i \in \text{COM}} (\dot{n}_{i,2} \cdot h_{i,2}(T_2)) = \sum_s \sum_{i \in \text{COM}} (\dot{n}_{i,s} \cdot h_{i,s}(T_s)) \qquad s \in \{1, 5, 16\} \qquad (5.43)$$

5.3.4.2 Flowsheet for Scenario 2

Due to the inclusion of the extraction cascade, the connectivity constraints and stream temperatures in Scenario 2 differ in some instances from those in Scenario 1. This also means that several of the equations shown here to define the flowsheet are similar to those found in Scenario 1.

$$\dot{n}_{i,1} = 0 \qquad\qquad i \in \{\text{nC13al}, \text{iC13al}, \text{iC12en}, \text{C12an}\} \qquad (5.44)$$

$$\dot{n}_{i,2} = \sum_{s \in \{1,5,9,16\}} \dot{n}_{i,s} \qquad\qquad i \in \text{COM} \qquad (5.45)$$

$$\dot{n}_{i,6} = \dot{n}_{out,i,2,np} \qquad\qquad i \in \text{COM} \qquad (5.46)$$

$$\dot{n}_{i,7} = \dot{n}_{out,i,2,p} \qquad\qquad i \in \text{COM} \qquad (5.47)$$

$$\dot{n}_{i,s+1} = \dot{n}_{i,s} \qquad\qquad i \in \text{COM}, s \in \{3,7,10,12,17\} \qquad (5.48)$$

$$\dot{n}_{\text{C}_1,\text{in},i} = \dot{n}_{i,7} \qquad\qquad i \in \text{COM} \qquad (5.49)$$

$$\dot{n}_{\text{C}_2,\text{in},i} = \dot{n}_{i,12} \qquad\qquad i \in \text{COM} \qquad (5.50)$$

$$\dot{n}_{\text{C}_3,\text{in},i} = \dot{n}_{i,18} \qquad\qquad i \in \text{COM} \qquad (5.51)$$

$$\dot{n}_{i,10} = \dot{n}_{\text{C}_1,\text{D},i} \qquad\qquad i \in \text{COM} \qquad (5.52)$$

$$\dot{n}_{i,9} = \dot{n}_{\text{C}_1,\text{B},i} \qquad\qquad i \in \text{COM} \qquad (5.53)$$

$$\dot{n}_{i,14} = \dot{n}_{\text{C}_2,\text{D},i} \qquad\qquad i \in \text{COM} \qquad (5.54)$$

$$\dot{n}_{i,17} = \dot{n}_{\text{C}_2,\text{B},i} \qquad\qquad i \in \text{COM} \qquad (5.55)$$

$$\dot{n}_{i,19} = \dot{n}_{\text{C}_3,\text{D},i} \qquad\qquad i \in \text{COM} \qquad (5.56)$$

$$\dot{n}_{i,20} = \dot{n}_{\text{C}_3,\text{B},i} \qquad\qquad i \in \text{COM} \qquad (5.57)$$

$$\dot{n}_{i,15} = x_{\text{purge}} \cdot \dot{n}_{i,14} \qquad\qquad i \in \text{COM} \qquad (5.58)$$

$$\dot{n}_{i,16} = (1 - x_{\text{purge}}) \cdot \dot{n}_{i,14} \qquad\qquad i \in \text{COM} \qquad (5.59)$$

Stream temperatures are defined as the following:

$$T_1 = 293.16 \text{ K} \qquad\qquad\qquad (5.60)$$

$$T_3 = T_{\text{R}_2} \qquad\qquad\qquad (5.61)$$

$$T_s = 300 \text{ K} \qquad\qquad s \in \{4,11\} \qquad (5.62)$$

$$T_s = T_{\text{d1}} \qquad\qquad s \in \{5,6\} \qquad (5.63)$$

$$T_7 = T_{\text{d2}} \qquad\qquad\qquad (5.64)$$

$$T_8 = T_{\text{bub},\text{C}_1,\text{F}} \qquad\qquad\qquad (5.65)$$

$$T_9 = T_{\text{bub},\text{C}_1,\text{B}} \qquad\qquad\qquad (5.66)$$

$$T_{10} = T_{\text{bub},\text{C}_1,\text{D}} \qquad\qquad\qquad (5.67)$$

$$T_{12} = T_{\text{dn}} \qquad\qquad\qquad (5.68)$$

$$T_{13} = T_{\text{bub},\text{C}_2,\text{F}} \qquad\qquad\qquad (5.69)$$

$$T_s = T_{\text{bub},\text{C}_2,\text{D}}, \qquad\qquad s \in \{14,15,16\} \qquad (5.70)$$

$$T_{17} = T_{\text{bub},\text{C}_2,\text{B}} \qquad\qquad\qquad (5.71)$$

$$T_{18} = T_{\text{bub},\text{C}_3,\text{F}} \qquad\qquad\qquad (5.72)$$

$$T_{19} = T_{\text{bub},\text{C}_3,\text{D}} \qquad\qquad\qquad (5.73)$$

$$T_{20} = T_{\text{bub},\text{C}_3,\text{B}} \qquad\qquad\qquad (5.74)$$

The temperature of the stream exiting the mixer (S_2) is again calculated using the energy balance around the mixer consisting of the feed and recycle streams, which now includes the bottoms from the extraction solvent column (Equation (5.75)).

$$\sum_{i \in \text{COM}} (\dot{n}_{i,2} \cdot h_{i,2}(T_2)) = \sum_{s} \sum_{i \in \text{COM}} (\dot{n}_{i,s} \cdot h_{i,s}(T_s)) \qquad s \in \{1,5,9,16\} \qquad (5.75)$$

5.3.5 Production and Investment Costs

The objective functions in this work depend on the cost optimal separation process following the TMS principle with a single decanter and the cost optimal integrated reaction-extraction process proposed in this chapter. As done previously in Chapter 3, the objective functions take the annualized cost of the capital investment and the production costs into account. In this section, all required cost models for the optimization are included, starting with the production costs and secondly the investment costs.

5.3.5.1 Production Costs

This section contains the functions used to determine the required utilities and other production costs in the proposed processes. The utilities considered here include steam, cooling water, refrigeration (electricity) with the remaining production costs consisting of the 1-dodecene feed, replenishment of the TMS solvents, and replenishment of the catalyst complex. The prices for each production component are listed in Table 5.1. Materials are based on either a molar or a mass basis. The heating and cooling duties using steam and water are based on a cost per unit energy basis, assuming a constant heat capacity for cooling water ($c_p = 75.3$ J/mol/K) and a constant heat of vaporization for steam ($h_{\mathrm{vap,st}} = 1888$ kJ/kg). Electricity costs are also based on an energy basis. Many of these costs are the same as those used in Chapter 3. Based on past purchase information, the biphephos ligand is assumed to be priced at \$38.5k per kilogram (MOLISA GmbH). The cost of the Rhodium(I) dicarbonyl acetylacetonate precursor is estimated using the average spot price of rhodium for 2015 at \$29562.70 per kilogram.

Table 5.1: Prices of raw materials and utilities (McBride et al. [90]).

Utility	Price Φ	Unit
DMF	73.1	$\$/kmol$
Decane	71.4	$\$/kmol$
1-Dodecene	661.5	$\$/kmol$
CO	4	$\$/kmol$
H_2	4	$\$/kmol$
Catalyst(Rh)	29562.7	$\$/kg$
Catalyst(ligand)	38500	$\$/kg$
Cooling water	$2.54{\cdot}10^{-6}$	$\$/kJ$
Steam	$1.41{\cdot}10^{-5}$	$\$/kJ$
Electricity	$2.22{\cdot}10^{-5}$	$\$/kJ$

Heating and Cooling Duties

In the complete flowsheet, ten heat exchangers (including reboilers and condensers) are used for Scenario 1 (Section 5.3.3.2) and 16 heat exchangers are used in Scenario 2

with the extraction cascade (Section 5.3.3.3). If a decanter, heat exchanger, reactor, or column should be considered to be unnecessary, the unit is ignored and all related utilities are set equal to zero.

In Scenario 1, four heat exchangers require cooling with cooling water for bringing the decanter feed down to the 300 K temperature limit for cooling water (H_{DEC}), for cooling the aldehyde column feed to its bubble point temperature (H_{CF3}), and for the two condensers found in the present distillation columns (H_{CN2} and H_{CN3}). One heat exchanger, H_{D1}, requires refrigerated coolant to bring the decanter feed down to the desired separation temperature in D1. Four heat exchangers require steam for heating the column feed of C2 (H_{CF2}), for the column reboilers (H_{RB2} and H_{RB3}), and for heating the feed to the first reactor (H_{R1}). The remaining heat exchanger H_{R2} may be either heated with steam or cooled with cooling water depending on the optimal temperature for the second reactor.

In Scenario 2 six additional heat exchangers are found in addition to the ten required in Scenario 1. Two of these require cooling water for cooling the extraction solvent down to the 300 K limit (H_{EXT}) and for the condenser found on the extraction solvent column (H_{CN1}). An additional heat exchanger (H_{DN}) requires refrigerated coolant for cooling the extraction solvent down to the initial cascade temperature, T_{DN}. Another (H_{D2}) also requires refrigerated coolant to decrease the temperature of stream 6 down to the cascade temperature found in D2. Two additional heat exchangers, one for heating the feed to C1 (H_{CF1}) and the other being the reboiler for C1 (H_{RB1}) require heating with steam. The other heat exchangers remain as before.

Several heat exchangers are coupled to distillation columns either as condensers or reboilers. To calculate the heat and cooling duties of the condenser and reboiler for a distillation column using the short cut method mentioned previously, the reflux ratio must be known (Equation (A.31)).

This model uses a total condenser and the distillate is assumed to be a saturated liquid. Thus, calculating the condenser duty (Equation (5.76)) requires the heat of vaporization at the dew point temperature of the mixture to be condensed (Equation (5.77)). A correlation Equation (5.78) taken from Yaws [131] is used to determine the heat of vaporization. The parameters for this equation are listed in Table A.4.

$$\dot{Q}_{CN,c} = (R_c + 1) \cdot \dot{n}_{c,D} \cdot \sum_{i \in COM} (x_{c,D,i} \cdot h_{\text{vap},i}(T_{\text{dew},c,D})) \quad c \in COL \quad (5.76)$$

$$p_{\text{vap},c,LK}(T_{\text{dew},c,D}) = p_c \cdot \sum_{i \in COM} \left(\frac{x_{c,D,i}}{\alpha_{c,i,LK}} \right) \quad c \in COL \quad (5.77)$$

$$h_{\text{vap},i}(T) = a_{1,i} \cdot \left(1 - \frac{T}{a_{2,i}} \right)^{a_{3,i}} \quad i \in COM \quad (5.78)$$

Similar to the condenser, a total reboiler is used with each column. The boilup ratio, S_c, is found using a simple mass balance around the column (Equation (5.79)). Since

the feed is considered to be saturated, the value of q is always set equal to one. Now, this ratio is used in conjunction with the bubble point temperature (Equation (5.81)) of the bottoms of each column to calculate the reboiler duties (Equation (5.80)).

$$S_c = \frac{R_c + q}{\frac{\dot{n}_{c,\mathrm{D}}}{\dot{n}_{c,\mathrm{B}}} + q - 1} \qquad\qquad c \in \mathrm{COL} \qquad (5.79)$$

$$\dot{Q}_{RB,c} = S_c \cdot \dot{n}_{c,\mathrm{B}} \cdot \sum_{i \in \mathrm{COM}} (x_{c,\mathrm{B},i} \cdot h_{\mathrm{vap},i}(T_{\mathrm{bub},c,B})) \qquad c \in \mathrm{COL} \qquad (5.80)$$

$$p_{\mathrm{vap},c,\mathrm{HK}}(T_{\mathrm{bub},c,B}) = p_{c,b} \cdot \sum_{i \in \mathrm{COM}} \left(\frac{x_{c,\mathrm{B},i}}{\alpha_{c,i,\mathrm{HK}}}\right) \qquad c \in \mathrm{COL} \qquad (5.81)$$

The set {COL} contains C2 and C3 for Scenario 1 and additionally C1 in Scenario 2.

The heat duties for the remaining heat exchangers are calculated using enthalpy balances around their respective inlet and outlet streams. Below are the balances used for determining the heat duties of the six heat exchangers in Scenario 1 not defined above.

$$\dot{Q}_{\mathrm{DEC}} = \sum_{i \in \mathrm{COM}} (\dot{n}_{i,3} \cdot (h_i(300\ \mathrm{K}) - h_i(T_3))) \qquad (5.82)$$

$$\dot{Q}_{\mathrm{CF2}} = \sum_{i \in \mathrm{COM}} (\dot{n}_{i,13} h_{i,13} - \dot{n}_{i,12} h_{i,12}) \qquad (5.83)$$

$$\dot{Q}_{\mathrm{CF3}} = \sum_{i \in \mathrm{COM}} (\dot{n}_{i,18} h_{i,18} - \dot{n}_{i,17} h_{i,17}) \qquad (5.84)$$

$$\dot{Q}_{\mathrm{R}_1} = \sum_{i \in \mathrm{COM}} (\dot{n}_{i,s} \cdot (h_i(T_{R_1}) - h_i(T_2))) \qquad (5.85)$$

$$\dot{Q}_{\mathrm{R}_2} = \sum_{i \in \mathrm{COM}} (\dot{n}_{i,r_2} \cdot (h_i(T_{R_2}) - h_i(T_{R_1}))) \qquad (5.86)$$

$$\dot{Q}_{\mathrm{D1}} = \sum_{i \in \mathrm{COM}} (\dot{n}_{i,6} \cdot (h_{i,s} - h_i(300\ \mathrm{K}))) \qquad (5.87)$$

In Scenario 2, there are four additional heat exchangers not counting the condenser (H_{CN1}) and reboiler (H_{RB1}) for the extraction solvent column. The balances for these supplementary heat exchangers are given below:

$$\dot{Q}_{\mathrm{CF1}} = \sum_{i \in \mathrm{COM}} (\dot{n}_{i,8} h_{i,8} - \dot{n}_{i,7} h_{i,7}) \qquad (5.88)$$

$$\dot{Q}_{\mathrm{EXT}} = \sum_{i \in \mathrm{COM}} (\dot{n}_{i,11} \cdot (h_i(300\ \mathrm{K}) - h_i(T_{10}))) \qquad (5.89)$$

$$\dot{Q}_{\mathrm{DN}} = \sum_{i \in \mathrm{COM}} (\dot{n}_{ini,s} \cdot (h_{i,s} - h_i(300\ \mathrm{K}))) \qquad (5.90)$$

$$\dot{Q}_{\mathrm{D2}} = \sum_{i \in \mathrm{COM}} (\dot{n}_{i,6} \cdot (h_i(T_{D2}) - h_i(T_{D1}))) \qquad (5.91)$$

Refrigeration

The electricity costs used in the process model depend only on the amount of refrigeration. In this process, a single temperature for the refrigerated coolant, T_{cd}, is used to cool all streams requiring temperatures below 300 K. The correlations for sizing the refrigeration unit is taken from Biegler et al. [23]. A typical value for the coefficient of performance, CP, is taken as four. The refrigeration is then designed as follows:

$$N_{\text{stages}} = (300 \ K - T_{\text{cd}})/30 \tag{5.92}$$

$$Q_{\text{RF}} = \sum_{s \in \{D1,D2,DN\}} Q_{s} \tag{5.93}$$

$$W_{\text{ref}} = ((1 + 1/\text{CP})^{N\text{stages}} - 1) \cdot Q_{\text{RF}} \tag{5.94}$$

$$W_{\text{b}} = (W_{\text{ref}}/0.72) \tag{5.95}$$

$$Q_{\text{c}} = (1 + 1/\text{CP})^{N\text{stages}} \cdot Q_{\text{RF}} \tag{5.96}$$

$$S_{\text{c}} = -Q_{\text{c}} \cdot \left(\frac{3.412 \ BTU}{J} \cdot \frac{1 \ ton}{12000 \cdot BTU} \right) \tag{5.97}$$

The electricity consumption is represented by W_{b} and the refrigeration duty used for sizing, represented as tons BTU, is given as S_{c}, which is used later for calculating the capital investment. The cost of the electricity utility is then given by Equation (5.98).

$$C_{\text{el}} = \Phi_{\text{el}} \cdot W_{\text{b}} \cdot 10^{-3} \tag{5.98}$$

Reactant, Solvents, and Catalyst Makeup

The amount of gas added to the reactor feed is determined based on the amount consumed during the reaction. Hydrogen gas is depleted in a one-to-one molar ratio in the hydroformylation reactions forming tridecanal and 2-methyldodecanal as well as the hydrogenation of 1-dodecene to n-dodecane. The change in the amount of hydrogen can then be determined by the molar balance of these compounds around the reactor (Equation (5.99)). Carbon monoxide consumption is found in only the hydroformylation reactions, also in a one-to-one molar ratio. Analogous to hydrogen, the amount of CO consumed can be determined by the molar balance of the aldehydes around the reactor (Equation (5.100)).

$$\dot{n}_{\text{H}_2,1} = \sum_{i \in \{nC12an,nC13al,iC13al\}} (\dot{n}_{i,3} - \dot{n}_{i,2}) \tag{5.99}$$

$$\dot{n}_{\text{CO},1} = \sum_{i \in \{nC13al,iC13al\}} (\dot{n}_{i,3} - \dot{n}_{i,2}) \tag{5.100}$$

Additional feed costs are constituted by the 1-dodecene feed and the replenishing of DMF and n-decane. The total cost associated with the feed, excluding the catalyst makeup, C_{feed}, is then given by Equation (5.101).

$$C_{\text{feed}} = \sum_{i \in \{\text{H}_2,\text{CO},\text{DMF},\text{C10an},\text{nC12en}\}} \Phi_i \cdot \dot{n}_{i,1} \cdot 10^{-3} \tag{5.101}$$

The catalyst leaching is taken as the amount of catalyst found in the nonpolar phase leaving the final decanter in the cascade, DN, or the initial decanter, D1, in the case of Scenario 1. The cost associated with catalyst leaching is then given by Equation (5.102).

$$C_{\text{cat}} = \begin{cases} \sum_{i \in \{\text{Rh},\text{BPP}\}} \Phi_i \cdot n_{out,i,d1,np} \cdot M_i \cdot 10^{-3} & \text{for Scenario 1} \\ \sum_{i \in \{\text{Rh},\text{BPP}\}} \Phi_i \cdot n_{out,i,dn,np} \cdot M_i \cdot 10^{-3} & \text{for Scenario 2} \end{cases} \tag{5.102}$$

Steam and Cooling Water

The cooling water and steam utilities calculated previously are now used to find the overall amount of cooling water and steam required for the process as well as their costs. The heat duty for the CSTR (R2), Q_{R2}, requires either steam, cooling water, or is absent depending on the temperature profile between the two reactors. The cooling water costs are given by Equation (5.103) and the steam costs by Equation (5.104) for Scenario 1.

$$C_{\text{cw}} = \begin{cases} -\Phi_{\text{cw}} \cdot \left(\sum_{s \in \{\text{CF3},\text{CN2},\text{CN3},\text{DEC},\text{R2}\}} Q_s + Q_c + Q_r \right) \cdot 10^{-3} & \text{for } \dot{Q}_{R2} < 0 \\ -\Phi_{\text{cw}} \cdot \left(\sum_{s \in \{\text{CF3},\text{CN2},\text{CN3},\text{DEC}\}} Q_s + Q_c + Q_r \right) \cdot 10^{-3} & \text{for } \dot{Q}_{R2} > 0 \end{cases} \tag{5.103}$$

$$C_{\text{st}} = \begin{cases} \Phi_{\text{st}} \cdot \left(\sum_{s \in \{\text{CF2},\text{R1},\text{RB2},\text{RB3}\}} Q_s \right) \cdot 10^{-3} & \text{for } \dot{Q}_{R2} < 0 \\ \Phi_{\text{st}} \cdot \left(\sum_{s \in \{\text{CF2},\text{R1},\text{R2},\text{RB2},\text{RB3}\}} Q_s \right) \cdot 10^{-3} & \text{for } \dot{Q}_{R2} > 0 \end{cases} \tag{5.104}$$

Analogously, the the cooling water and steam costs for Scenario 2 are given by Equation (5.105) and Equation (5.106), respectively.

$$
C_{\text{cw}} =
\begin{cases}
-\Phi_{\text{cw}} \cdot \left(\displaystyle\sum_{s \in \{\text{CF3,CN1,CN2,CN3,DEC,EXT,R2}\}} Q_s + Q_c + Q_r \right) \cdot 10^{-3} & \text{for } \dot{Q}_{\text{R2}} < 0 \\[4ex]
-\Phi_{\text{cw}} \cdot \left(\displaystyle\sum_{s \in \{\text{CF3,CN1,CN2,CN3,DEC,EXT}\}} Q_s + Q_c + Q_r \right) \cdot 10^{-3} & \text{for } \dot{Q}_{\text{R2}} > 0
\end{cases}
\tag{5.105}
$$

$$
C_{\text{st}} =
\begin{cases}
\Phi_{\text{st}} \cdot \left(\displaystyle\sum_{s \in \{\text{CF1,CF2,R1,RB1,RB2,RB3}\}} Q_s \right) \cdot 10^{-3} & \text{for } \dot{Q}_{\text{R2}} < 0 \\[4ex]
\Phi_{\text{st}} \cdot \left(\displaystyle\sum_{s \in \{\text{CF1,CF2,R1,R2,RB1,RB2,RB3}\}} Q_s \right) \cdot 10^{-3} & \text{for } \dot{Q}_{\text{R2}} > 0
\end{cases}
\tag{5.106}
$$

Included here for cooling water are the cooling duty from the refrigeration unit, Q_c, and the integrated reactor cooling duty, Q_r, as the reaction is exothermic.

Production Cost Function

Once the various production costs have been calculated, the overall production cost is simply the summation of each individual production cost component (Equation (5.107)).

$$
C_{\text{production}} = C_{\text{feed}} + C_{\text{cw}} + C_{\text{st}} + C_{\text{el}} + C_{\text{cat}}
\tag{5.107}
$$

5.3.5.2   Investment Costs

In order to estimate the capital investment required in the process, the size of each unit must be determined. In this section the methods used to estimate the sizes of all units are detailed. As done in Chapter 3, the correlations developed by Guthrie [56] are used to predict the capital costs.

Reactor

The volume of the reactor depends on the residence time, τ_{r}, and the volumetric flowrate of the mixture through the reactor. The residence time is left as an optimization variable in this model and is not fixed to a specific value. Several factors influence the volume of the reactor such as the size of the recycle streams, the desired conversion and selectivity, etc. Similar to the process model in Chapter 3 the volume of the reactor is doubled to allow room for the gas phase. As usual, the length of the reactor is assumed to be four times that of the diameter (Biegler et al. [23]).

$$
V_{\text{r,liq}} = \tau_{\text{r}} \cdot \sum_{i \in \text{COM} \setminus \text{GAS}} \frac{\dot{n}_{i,r} M_i}{\rho_i(T_r)} \qquad r \in \{1, 2\}
\tag{5.108}
$$

Table 5.2: Heat transfer coefficients of heat exchangers (Equation (5.114)).

Unit	$U[W/m^2/K]$	Type
R1, R2	283.9	organic solvents (shell)/water (tube)
DEC, EXT	283.9	organic solvents (shell)/water (tube)
CF1, CF2, CF3	283.9	organic solvents (shell)/water (tube)
CN1, CN2	567.9	organic solvents (shell)/water (tube)
CN3	113.6	high boiling hydrocarbons (shell)/water (tube)
RB1, RB2, RB3	1419.5	water (shell) / steam condensing (tube)
D1, D2	113.6	organic solvents (shell)/organic solvents (tube)

$$D_{\mathrm{R}} = \sqrt[3]{\frac{2V_{\mathrm{r,liq}}}{\pi}} \qquad r \in \{1,2\} \qquad (5.109)$$

$$L_{\mathrm{r}} = 4D_{\mathrm{r}} \qquad r \in \{1,2\} \qquad (5.110)$$

Decanters

The decanter volumes are determined in a similar manner as with the reactors except that the residence time is again fixed to 20 minutes. Therefore the primary design variable is the volumetric flowrate through each decanter. The length and diameter of the decanters are found using Equations (5.111) to (5.113).

$$V_{\mathrm{d,liq}} = \tau_{\mathrm{d}} \cdot \sum_{i \in \mathrm{COM\backslash GAS}} \frac{\dot{n}_{i,d} M_i}{\rho_i(T_{\mathrm{d}})} \qquad d \in \{d1..dn\} \qquad (5.111)$$

$$D_{\mathrm{d}} = \sqrt[3]{\frac{2V_{\mathrm{d,liq}}}{\pi}} \qquad d \in \{d1..dn\} \qquad (5.112)$$

$$L_{\mathrm{d}} = 4D_{\mathrm{d}} \qquad d \in \{d1..dn\} \qquad (5.113)$$

Heat Exchangers

The correlations for heat exchanger investment costs are based on the surface area of the heat-transfer area of each unit. Equation (5.114) is used to estimate this heat-transfer area using the heat duty, log-mean temperature difference ΔT_{lm}, and the heat transfer coefficient, U, taken from Guthrie [56]. Table 5.2 contains the heat transfer coefficients used for the heat exchangers in this work and a brief reasoning for each selection.

$$A_{\mathrm{hex},s} = \left| \frac{\dot{Q}_s}{U_s \Delta T_{\mathrm{lm},s}} \right| \qquad s \in \mathrm{HX} \qquad (5.114)$$

Steam and cooling water temperatures must be available such that the log mean temperatures can be determined. The conditions for these utilities are chosen such that the

steam has a temperature of 600 K (T_s), the cooling water a somewhat cool temperature of 288 K (T_{cw}), and a coolant temperature somewhere between 240 and 283.16 K (T_{cd}), which is left as an optimization variable. In each instance where cooling water or coolant are used, it is assumed that they increase in temperature by 10 K ($\Delta T_{cw} = 10K$). The heat exchangers used are counter-current and the log mean temperature differences are calculated depending on which type of medium is used: steam (Equation (5.115)), cooling water (Equation (5.116)), or coolant (Equation (5.117)).

$$\Delta T_{\text{lm,st}}(T_h, T_c) = \frac{T_h - T_c}{log(\frac{T_{st} - T_c}{T_{st} - T_h})} \tag{5.115}$$

$$\Delta T_{\text{lm,cw}}(T_h, T_c) = \frac{(T_h - T_{cw}) - (T_c - (T_{cw} + \Delta T_{cw}))}{log(\frac{T_h - T_{cw}}{T_c - (T_{cw} + \Delta T_{cw})})} \tag{5.116}$$

$$\Delta T_{\text{lm,cd}}(T_h, T_c) = \frac{(T_h - T_{cd}) - (T_c - (T_{cd} + \Delta T_{cd}))}{log(\frac{T_h - T_{cd}}{T_c - (T_{cd} + \Delta T_{cd})})} \tag{5.117}$$

Distillation Columns

The procedure for sizing the distillation columns is found in Appendix A.4, which is the same method as used in Chapter 3.

Cost Functions

The investment cost is determined in a similar manner as done for the process model in Chapter 3. Capital costs are found using a correlations for the bare cost (BC) of each unit which are modified using a material and pressure factor (MPF), a module factor (MF) that takes installation costs into account, and an update factor (UF) that adjusts for inflation. The bare cost depends on one or two (S_1 and S_2) size characteristics specific to each unit. Decanters, reactors, and column shells can be modeled as vessels which require the height or length as S_1 and the diameter as S_2. The cost of the column trays also require the height and diameter as S_1 and S_2, respectively. Heat exchangers only require the surface area available for heat transfer as S_1. Refrigeration simply necessitates the cooling duty, S_c as its sizing characteristic S_1. These values can been calculated using the equations already presented in this section. Equation (5.118) depends on the Chemical Engineering Index (CE), which is used to help adjust for inflation when using the original cost correlations. The CE used here is from April, 2015 with a value of 562.9.

Table 5.3 lists the unit specific BC, MPF, MF, and CE_{base} values used in this model. The material and pressure factor adjusts for the cost of differing materials and pressures other than standard. The module factors (MF) are determined based on the bare cost of the unit and account for installation costs. The bare module cost (BMC) is the final price for the unit to be integrated into the plant (Equation (5.120)). The total capital investment is the summation of all bare module costs in the proposed plant, given by Equation (5.121).

$$\text{UF}_u = \frac{\text{CE}}{\text{CE}_{\text{base}}} \qquad\qquad \forall\, u \in \text{UNIT} \tag{5.118}$$

$$\mathrm{BC}_u = a_{0,u} \left(\frac{S_1}{a_{1,u}} \right)^{a_{2,u}} \left(\frac{S_2}{a_{3,u}} \right)^{a_{4,u}} \qquad \forall\, u \in \mathrm{UNIT} \qquad (5.119)$$

$$\mathrm{BMC}_u = UF_u \cdot (\mathrm{MPF}_u + \mathrm{MF}_u - 1) \cdot \mathrm{BC}_u \qquad \forall\, u \in \mathrm{UNIT} \qquad (5.120)$$

$$C_{\mathrm{invest}} = \sum_{\forall\, u \in \mathrm{UNIT}} \mathrm{BMC}_u \qquad (5.121)$$

Table 5.3: Cost parameters for the bare cost (BC) correlation (Equation (5.119)), material and pressure factors (MPF) and the CE index used to estimate the bare module cost using (Equation (5.120)). See Equation (5.122) for MPF_{RF}.

Unit	a_0	a_1	a_2	a_3	a_4	MPF	CE_{base}
Vessel: R1, R2	$1{\cdot}10^3$	1.2192	0.81	0.9144	1.05	1.45	115
Vessel: D1, D2, D3, D4	690	1.2192	0.78	0.9144	0.98	1	115
Vessel: C1, C2, C3	$1{\cdot}10^3$	1.2192	0.81	0.9144	1.05	1	115
Stack: C1, C2, C3	180	3.048	0.97	0.6096	1.45	2.8	115
HX: R1, R2, DEC	$5{\cdot}10^3$	37.1612	0.65	1	0	1.87	115
HX: CF1, CF2, CF3, RB1, RB2, RB3	$5{\cdot}10^3$	37.1612	0.65	1	0	1.35	115
HX: CN1, CN2, CN3, D1, D2, D3, D4	$5{\cdot}10^3$	37.1612	0.65	1	0	1	115
RF	$6{\cdot}10^4$	200	0.70	1	0	MPF_{RF}	115

Table 5.4: The module factor (MF) depends on the bare cost of the unit. Here, the typical values for MF are shown. Each unit starts in MF2 and with each increase in value of \$200k, the next level MF is used.

Unit	MF2	MF4	MF6	MF8	MF10
Vessel: R1, R2	4.23	4.12	4.07	4.06	4.02
Vessel: D1, D2, D3, D4	3.18	3.06	3.01	2.99	2.96
Vessel: C1, C2, C3	4.23	4.12	4.07	4.06	4.02
Stack: C1, C2, C3	1	1	1	1	1
HX: all	3.29	3.18	3.14	3.12	3.09
RF	1.42	1.42	1.42	1.42	1.42

The MPF for refrigeration as defined by Guthrie [56] is added to the BMC cost estimation for the refrigeration unit. This value depends on the temperature that needs to be reached by cooling. To penalize higher refrigeration usage with lower temperatures

more evenly, the values provided in the literature seen in Table 5.5 were fit to a linear function dependent on temperature to provide the correlation in Equation (5.122). This correlation is used in place of the fixed values in Table 5.5 for the optimization.

$$\text{MPF}_{\text{RF}} = -0.08098 \cdot T_{cd} + 23.4 \tag{5.122}$$

Table 5.5: The MPF for refrigeration based on the temperature required (Biegler et al. [23]).

$T_{cd}[\text{K}]$	MPF
278	1
266	1.95
255	2.25
244	3.95
233	4.54

5.4   Optimization

The goal of this work is to identify the economically optimal reaction-extraction process for each scenario mentioned in the previous section. When the number of optimization variables is large and the model is quite complex, it becomes difficult to evaluate the trade-offs between increased capital and utility costs and decreased catalyst leaching. This makes the use of cost functions necessarily mandatory. As in Chapter 3, the cost functions developed by Guthrie [56] are used with sizing estimations developed by Biegler et al. [23]. These were already presented in Section 5.3.5. The objective functions Equation (5.123) and Equation (5.124) are based on the three year total annualized cost of the process investment (Equation (5.121)) and production costs (Equation (5.107)) consisting of steam, cooling water, electricity, 1-dodecene feed, H_2, CO, and makeup solvents and catalyst. The product specifications include the production values assumed by Hentschel et al. [61]: 10,000 tons n-tridecanal produced annually with at least 99.5% purity. The plant is assumed to operate for 330 days annually.

In Scenario 1, the optimization variables are the decanter temperature, coolant temperature, recovery fractions of the distillate and bottoms in each distillation column, reflux ratios in each distillation column, reactor temperatures, CO and H_2 partial pressures in each reactor, reactor volumes, and the size of the purge stream. In Scenario 2, the optimization variables include those used in Scenario 1 and furthermore the temperatures of the additional decanters, amount of extraction solvent added to the cascade, and column variables for C1, the extraction solvent column.

Due to the differing flowsheets, the constraints used in both optimization problems are slightly different. Equation (5.123) is used for Scenario 1 (case 1 and the reference) while Equation (5.124) is used for all remaining cases involving the extraction cascade.

Optimization for Scenario 1

$$\min \text{TAC} \left[\frac{\$}{\min}\right] = (C_{\text{invest}}/3 + C_{\text{production}}) \tag{5.123}$$

s.t. Reaction kinetics: Equations (A.5) to (A.13)
Reactor: Equations (5.9) to (5.16)
Gas solubility: Equations (A.15) to (A.16)
Catalyst amount: Equations (5.20) to (5.21)
Mixture comp.: Equations (5.1) to (5.5)
Decanter: Equations (5.17) to (5.19)
Flowsheet: Equations (5.22) to (5.43)
Production Cost: Equations (5.76) to (5.87) and 5.92 to 5.107
Investment Cost: Equations (5.108) to (5.122) and A.18 to A.47
Coolant: $230 \text{ K} \leq T_{cd} \leq 283.15 \text{ K}$
Purge: $10^{-4} \leq x_{\text{purge}} \leq 0.1$
Reactor Volume: $1 \text{ m}^3 \leq V_r \leq 10^4 \text{ m}^3$, $\quad r \in \{r1, r2\}$

Optimization for Scenario 2

$$\min \text{TAC} \left[\frac{\$}{\min}\right] = (C_{\text{invest}}/3 + C_{\text{production}}) \tag{5.124}$$

s.t. Reaction kinetics: Equations (A.5) to (A.13)
Reactor: Equations (5.9) to (5.16)
Gas solubility: Equations (A.15) to (A.16)
Catalyst amount: Equations (5.20) to (5.21)
Flowsheet: Equations (5.44) to (5.75)
Production Cost: Equations (5.76) to (5.107)
Investment Cost: Equations (5.108) to (5.122) and A.18 to A.47
Mixture comp.: Equations (5.1) to (5.5)
Decanter: Equations (5.17) to (5.19)
Coolant: $230 \text{ K} \leq T_{cd} \leq 283.15 \text{ K}$
Purge: $10^{-4} \leq x_{\text{purge}} \leq 0.1$
Reactor Volume: $1 \text{ m}^3 \leq V_r \leq 10^4 \text{ m}^3$, $\quad r \in \{r1, r2\}$
Extraction Solvent: $0 \leq \sum_{i \in \{\text{COM}\}} \dot{n}_{i,11} \leq 100 \text{ moles/sec}$

All scenarios mentioned in this section are implemented as separate NLPs in AMPL and solved using the solver CONOPT 3.14V on a PC with one Intel Core™ i5-3570 CPU at 3.40GHz, a memory of 8 GB, and running on the Kubuntu 12.04 operating system.

The total number of cases to be optimized depends primarily on the trend seen in the TAC. If catalyst leaching becomes nearly zero, then further separation stages may be unnecessary. Once a minimum in the TAC has been established, additional separation stages simply add to the process costs rather than to decrease it. At this point the optimizations should be terminated. An additional case, the reference case, which is similar to case 1, but without consideration of catalyst leaching costs in the optimization, is used for comparison purposes. This allows for direct comparison the process optimizations considered by Hentschel et al. [60]. It must also be stated that all optimal solutions presented here are local optima and that better solutions may be possible. A guarantee that the global solution has been found cannot be given using the CONOPT solver.

5.5   Results and Discussion

In total seven different cases were optimized: six cases using one to six decanters and the single reference case. The optimization process ceases after six decanters because the catalyst leaching is predicted to be zero with a very slight increase in TAC over that found with the optimal arrangement using five decanters. Table 5.6 presents a detailed breakdown of the costs for all cases. All values are presented in dollars per kilo-mole of tridecanal product.
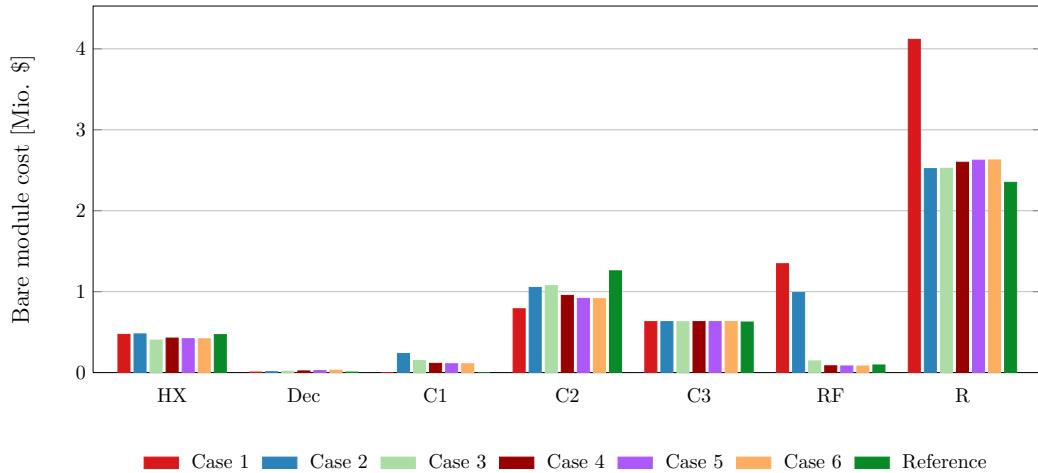
Figure 5.8: Investment cost comparison for the optimal separation process in each case. Costs are shown for the heat exchangers (HX), decanters (Dec), distillation columns (C1, C2, and C3), refrigeration (RF), and reactors (R) [90].

5.5.1   Separation Performance

It is immediately clear that the additional separation stages positively affect the process cost, decreasing it substantially in all cases where multiple extraction stages or decanters

Table 5.6: Comparison of production and capital costs for each integrated reaction-extraction case. All costs presented here are \$/kmol product except for the % Recovered referring to the amount of catalyst recovered.

	Case 1	Case 2	Case 3	Case 4	Case 5	Case 6	Reference
Decane	0.07	2.43	2.57	3.12	3.31	3.33	2.14
DMF	0.01	0.31	0.58	0.85	0.93	0.94	0.47
1-Dodecene	681.67	684.71	685.22	687.15	687.73	687.80	682.96
H_2	4.11	4.13	4.13	4.14	4.15	4.15	4.11
CO	4.09	4.11	4.11	4.12	4.12	4.12	4.10
Catalyst	334.68	6.65	2.58	0.40	0.03	0.00	1792.72
(% Recovered)	99.3595	99.9851	99.9943	99.9990	99.9999	100.0000	96.5692
Steam	26.42	25.99	23.08	20.31	19.69	19.62	24.71
Cooling water	3.64	1.82	2.37	2.10	2.02	2.01	2.90
Electricity	4.68	3.25	0.38	0.19	0.19	0.19	0.24
Production	1059.36	733.40	725.01	722.39	722.16	722.15	2511.21
Capital	49.85	40.42	33.20	31.77	31.62	31.63	31.72
Total	1109.21	773.81	758.21	754.16	753.78	753.78	2542.93
Total (no cat)							750.2

Table 5.7: Temperatures [K] in each decanter and for the coolant in each case.

	$T_{d1..dn}$	T_{cd}
Case 1	253.16	241.82
Case 2	259.16	242.33
Case 3	289.35	274.03
Case 4	293.16	276.61
Case 5	293.16	276.61
Case 6	293.16	276.61
Reference	293.16	277.41

Table 5.8: Percentage costs of catalyst in each case as part of the total TAC, the total production costs, and the production costs not including 1-dodecene.

Catalyst Cost %	Case 1	Case 2	Case 3	Case 4	Case 5	Case 6	Ref.
TAC	30.17	0.86	0.34	0.05	0.00	0.00	70.50
Production	31.59	0.91	0.36	0.05	0.00	0.00	71.39
Production w/o 1-dodecene	88.61	13.67	6.47	1.12	0.09	0.01	98.06

Table 5.9: Distillation column dimensions, recoveries, heating duties, and cooling duties.

C1	H (m)	D (m)	Recovery	Stages	Q_{reb} (kW)	Q_{con} (kW)
Case 1	/	/	/	/	/	/
Case 2	23.36	0.84	0.98501	29.93	308.14	-260.20
Case 3	20.41	0.62	0.97073	25.02	161.51	-140.97
Case 4	19.08	0.51	0.96089	22.80	109.00	-95.63
Case 5	18.86	0.49	0.95895	22.43	102.11	-89.61
Case 6	18.84	0.49	0.95873	22.39	101.34	-88.94
Reference	/	/	/	/	/	/
C2	H (m)	D (m)	Recovery	Stages	Q_{reb} (kW)	Q_{con} (kW)
Case 1	21.55	2.66	0.94607	26.92	1555.99	-1208.43
Case 2	32.55	2.52	0.99512	45.25	1411.63	-1091.72
Case 3	32.40	2.58	0.99517	45.01	1490.39	-1146.21
Case 4	30.42	2.43	0.99307	41.69	1335.07	-1023.46
Case 5	29.73	2.39	0.99209	40.56	1290.06	-988.29
Case 6	29.65	2.38	0.99197	40.42	1285.16	-984.47
Reference	34.82	2.81	0.99688	49.03	1767.40	-1361.09
C3	H (m)	D (m)	Recovery	Stages	Q_{reb} (kW)	Q_{con} (kW)
Case 1	55.98	1.06	0.99975	84.29	224.82	-223.13
Case 2	54.21	1.09	0.99951	81.35	234.58	-241.32
Case 3	54.09	1.09	0.99950	81.15	234.65	-241.37
Case 4	54.05	1.09	0.99950	81.09	235.51	-242.45
Case 5	54.04	1.09	0.99950	81.07	235.71	-242.67
Case 6	54.04	1.09	0.99950	81.07	235.73	-242.69
Reference	53.95	1.08	0.99950	80.92	233.17	-239.33

are used. This is most noticeable in the change in the production costs, which are predominantly comprised of either catalyst or 1-dodecene feed. This large decrease when using multiple decanters is primarily due to the reduction in catalyst leaching, which although quite low in case 1 ($<1\%$), contributes significantly to the cost at about 30.17% of the TAC. With only the addition of one extra extraction stage in case 2, catalyst recovery is already predicted to be above 99.98%. Here, catalyst leaching only contributes 0.86% to the TAC, which is slightly more than that of the reactant gases consumed in the reaction. Catalyst leaching continues to decrease with an increasing number of separation stages, but the overall impact on the TAC is almost insignificant after the addition of a third decanter. The cost of 1-dodecene increases as a result of the lower n/iso ratios leading to more 2-methyldodecanal product and overall lower conversion, albeit this influence is small. The increase in the cost of the TMS solvents is due to the increasing size of the purge stream split from the distillate of C2 as the number of decanters increases. Although the amount lost in the purge tends to increase with case number, the amount of 1-dodecene, iso-dodecene, and n-dodecane eliminated remains relatively constant.

In case 6 it can be seen that a near complete recovery of the catalyst leads to no significant change in the TAC over those found in cases 3, 4, and 5. Interestingly enough, as the number of separation stages increases the capital costs tend to decrease. This is not so intuitive, given that more vessels and devices are required, but is a result of the reduced need for refrigeration as the decanter temperatures increase as well due to the decrease in size of the reactor between case 1 and case 2. When using four or more decanters, the separation temperatures are found on the upper bound (see Table 5.7). As the number of possible separation stages increases, the process no longer depends upon a single separation stage for catalyst recovery. That the catalyst shows better partitioning at lower temperatures, a lower number of separation stages leads to decanters that operate at lower temperatures. Thus, the strong temperature dependency of catalyst leaching becomes irrelevant as more opportunities for recovery by extraction become available, allowing for higher temperature separations to take place. This reduction in the refrigeration utility can be seen very clearly in Figure 5.8 where it is quite high in cases 1 and 2 and falls quickly after case 3 to an almost inconsequential value. The reduction in refrigeration also leads to lower utility costs for electricity as well.

Once the cost of the leached catalyst is included in the TAC of the reference case, where its cost was not included in the objective function, the TAC is found to be quite high. The catalyst cost would constitute 70.5% of the TAC. The separation in the single decanter is not as critical due to the disregard for catalyst recovery and therefore the separation temperature is the maximum. The process is trying to reduce the amount of refrigeration utility instead. When compared to case 1, the reference case has more tridecanal in the post-reaction mixture. Since catalyst recovery is not a concern here, the poorer phase separation brought about by higher levels of tridecanal and a higher separation temperature does not significantly affect the TAC in this case. The reactor

size is also not critical because the outlet composition of the reactor does not need to consider catalyst leaching, making it much smaller than that in case 1.

After the impact of refrigeration becomes negligible after case 3, the trade-off in cost is found primarily between the size and performance of the reactor with the size and utilitly demand of the reaction solvent column (C2). This column is quite large compared to the others due to the large internal and external flow rates caused by the sheer volume of solvent that need to be vaporized (see Table 5.9). This also results in a large vapor flow that requires a wider column diameter. This also leads to a much higher heating duty in the reboiler and a much higher cooling duty in the condenser than required in the other two columns. As the number of decanters in the cascade increases, the size of C2 tends to decrease while the reactor volume increases. This is a direct result of the lower concentrations of n-dodecane found in the reactor. Since there is a constraint requiring that the TMS compromises 80% of the mass found in the reactor feed, a lower amount of n-dodecane also leads to a reduction in the amount of TMS. This is valid in that the other components do not vary as much. The overall molar flowrate of the reactor feed decreases from 45.51 mol/s in case 1 to 33.61 mol/s in case 6 as a direct consequence (see Figure 5.9). Normally one would expect that reactor volume would decrease, but because of longer residence times the reactor size actually increases. The reduction in the necessary amount of TMS solvents that need to be vaporized in C2 lead to a decrease in its size as well. The visible reduction in the amount of steam utility consumed in the process also results from this decrease in column size. Additionally, due to the increased temperature of the decanter cascade, the amount of steam necessary to bring the feed to column C2 up to its bubble point decreases. This also results in lower steam costs.

The size of the isomer column, C3, is not strongly affected from case to case as the n/iso ratio does not vary much. A very slight increase in column size can be seen as the n/iso ratio marginally decreases. This is due to a small increase in its volumetric flow rate, which requires a larger column diameter. However, this small change is insignificant and very little potential for improving the process economics remains.

When compared to the other process units, the additional investment and production costs for including the extraction solvent column, C1, are quite low. The cost of adding this process unit compared to the reduction in refrigeration costs and catalyst leaching is very economical and reduces the overall process cost. The cost of this column tends to decrease with the number of decanters used in the cascade as the amount of solvent needed for the cascade decreases, which can be seen in Figure 5.10

Another interesting aspect of the process is that the temperatures used in the first decanter and the remaining decanters in the cascade have a uniform temperature. This eliminates the use of H_{D2}, leaving only two heat exchangers that are supplied by coolant for controlling the separation temperatures. This makes sense when one considers that higher separation temperatures perform better economically once many stages are present.
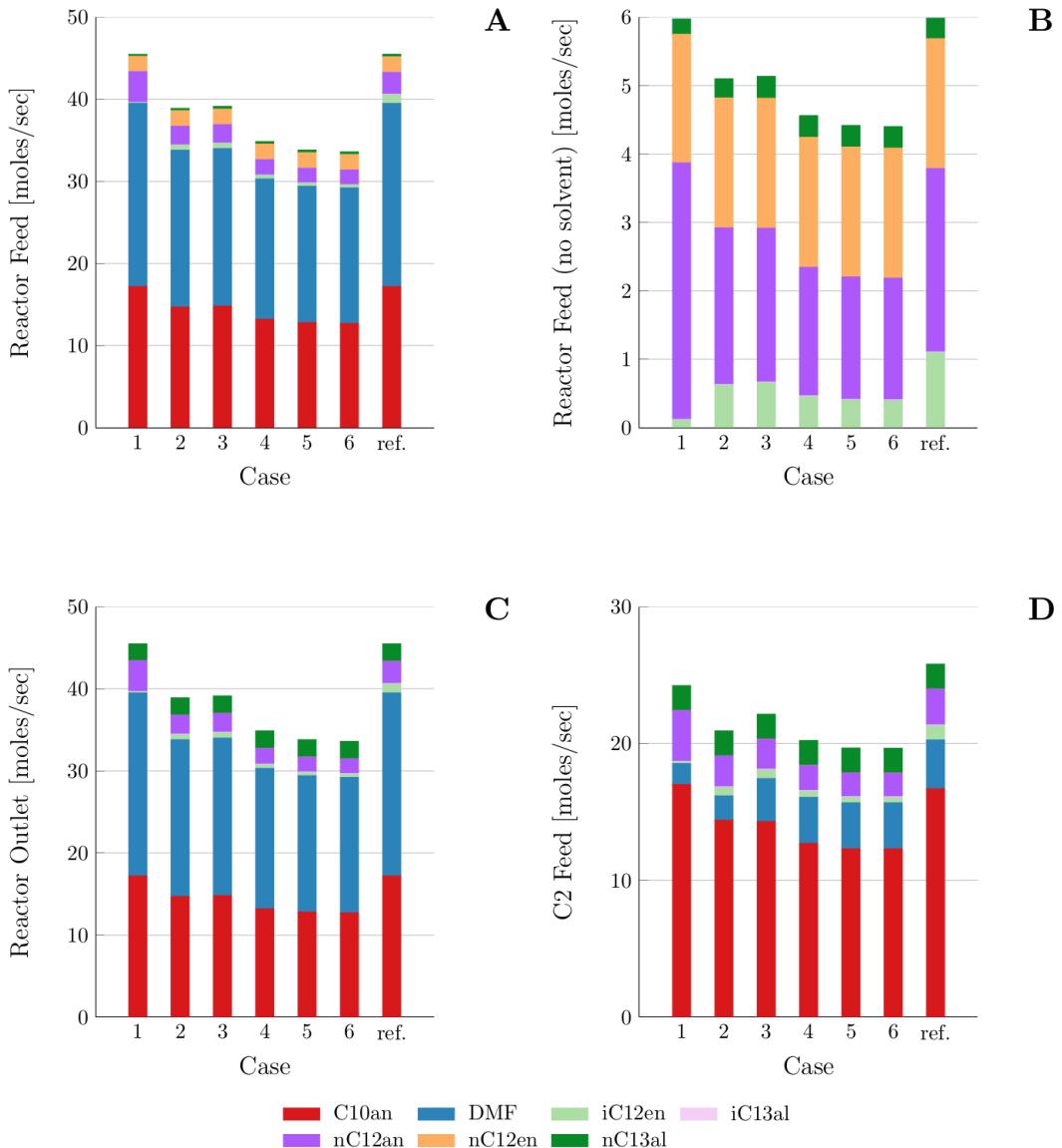
Figure 5.9: Stream compositions of the reactor feed with all components (A), the reactor feed not including the TMS solvents (B), the reactor outlet (C), and the feed to the reaction solvent column, C2 (D) [90].
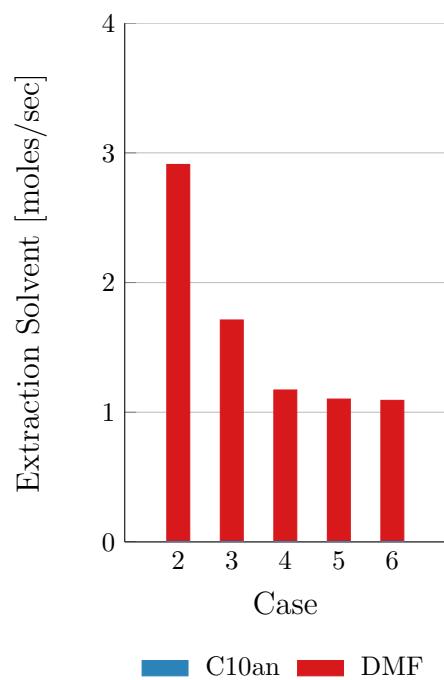
Figure 5.10: Extraction solvent added to the cascade. Notice the very small amounts of n-decane [90].

Table 5.10: Reactor performance for the cost optimal point in each case.

	τ (min)	V (m³)	X (%)	S (%)	$\frac{n}{n+iso}$	T [K]	P_{CO} [bar]	P_{H_2} [bar]
Case 1	3398	1457	99.81	97.07	97.66	388.15	16.52	3.48
Case 2	1803	660	99.26	96.66	97.44	388.15	17.17	2.83
Case 3	1793	662	99.23	96.59	97.41	388.15	17.20	2.80
Case 4	2112	694	99.41	96.32	97.19	388.15	17.15	2.85
Case 5	2217	705	99.46	96.24	97.13	388.15	17.14	2.86
Case 6	2229	706	99.47	96.23	97.12	388.15	17.14	2.86
Reference	1377	590	98.92	96.91	97.70	388.15	17.34	2.66

5.5.2 Reactor Performance

An interesting aspect of the optimization is that in each case, the second reactor R2, the CSTR, is not considered for use. Instead, both reaction zones take place in the first reactor, R1, in a single DSR with long residence times. Large reactors are a result of the high residence times which lead to the very high selectivity and conversion found in this work. Several other optimal solutions were found with higher costs where the CSTR was used for the reverse-isomerization as anticipated. Differences in cost are slight and are most likely influenced by the correlations used to predict reactor costs. In a technical realization it is, however, more reasonable to use a large CSTR for the reverse-isomerization. Although considering the overall effect of capital cost on the process, any changes in reactor configuration will lead to only minuscule differences in the resulting TAC. In fact, if the residence time is constrained to a more feasible value, say 300 minutes, both reactors are used in each case albeit at higher TACs than found here. In order to show the differences in the reactor performance more clearly, and to help in understanding the following discussion, molar flow rate profiles for all optimizations are provided. In Figure 5.11, the reactor profiles for cases 1 through 6 are shown. Afterwards, Figure 5.12 depicts the molar flow rates for the reference case.

The reaction performances for all cases are shown in Table 5.10. The general trend is for the reactor to increase slightly in size as the number of decanters increases, except for the transition between case 1 and case 2. The most important effect deciphered from the results is that it is the amount of iso-dodecene found in the feed that determines the length of the reactor due to the slow reverse-isomerization. This effect can be seen more clearly in the composition profiles for each reaction shown in Figure 5.11 and Figure 5.12. To a lesser degree, this is connected to the higher recycle rate of products to the reactor feed as a result of the additional separation stages. The multiple extraction steps also remove small amounts of the slightly polar aldehydes and 1-dodecenes from the product mixture, increasing the size of the recycle stream to the reactor. This is one reason why the extraction solvent amount added to DN is usually very small compared to the overall amount found in each decanter.

The large reactor in case 1 is not primarily designed for reactor performance but is geared towards tuning the post-reaction mixture for better catalyst recovery in the single decanter. In Table 5.8 it can be seen that the catalyst consumes almost 89% of the total production cost when excluding 1-dodecene for this case, making it the most critical cost variable in the process. Thus, it makes sense that the reactor is trying to reduce catalyst leaching by producing the best mixture for biphasic separation given the required constraints. This is seen in the outlet composition of the reactor where there is basically only DMF, n-decane, n-dodecane, and tridecanal. The reactor outlet contains very low amounts of 1-dodecene reactant and the byproducts iso-dodecene and 2-methyldodecanal. Instead, the amount of n-dodecane found in the reactor is 63 to 110% more than in all other cases, as seen in Figure 5.9. The increase in n-dodecane and the reduced amount of the components that lead to smaller miscibility gaps enhances the degree of separation in the following decanter. This desirable increase in the amount of n-dodecane found in case 1 is also reflected in the slightly higher H_2 pressure than when compared to all other cases (see Table 5.10). However, the reverse-isomerization reaction is more likely responsible for this pressure change. The separation in case 1 is so critically dependent on the composition of the post-reaction mixture, that even the total amount of 1-dodecenes is kept low. This results in a very small recycle of iso-dodecene through the system, requiring a much larger reactor to convert almost all of the iso-dodecene produced in the reaction back into 1-dodecene. This 1-dodecene is then almost completely converted to tridecanal. Tridecanal is only present at all due to the production constraint. Its concentration in the reactor outlet is also lower than in all other cases. The results seen here in the optimal reactor design for case 1 is similar to what Hentschel et al. [61] mentioned might happen with respect to optimal reactor design when taking catalyst leaching into account. This shows that targeted reactor design for optimal performance is not suitable when the catalyst leaching costs remain economically limiting.

The results discussed in the last paragraphs also explain why only a small amount of aldehyde is recycled back to the reactor feed. Case 1 has the highest amount of tridecanal recovered as product per amount leaving the reactor at 89.1%. The amount of tridecanal recovered decreases in all other cases, being somewhere in the range of 85.3% to 86.7%. In addition to the higher rates of tridecanal recycle due to the increased number of extraction stages, the overall composition in the first decanter for cases 2 to 6 is not as important as in case 1. Since the additional separation stages drastically reduce the amount of leaching, other areas of the process become targets for cost reduction. The process is no longer simply focused on tuning the post-reaction mixture.

For the remaining cases, 2 through 6, the reactor volume depends predominantly on the amount of iso-dodecene present in the feed. In each case, the amount of iso-dodecene leaving the reactor is slightly more than that in the reactor feed. The difference is mainly due to the small portion lost in the purge stream. When a higher concentration of iso-dodecene is found in the feed, the maximum, equilibrium concentration is reached relatively quickly, requiring less time for the slow reverse-isomerization to reduce the concentration to near inlet levels. For example, the reactor in case 2 is the smallest for

all cases considering the cost of catalyst leaching. It has the highest concentration of iso-dodecene found in the reactor feed. The equilibrium concentration of iso-dodecene is achieved at a faster rate than in the other cases and the time required for the reverse isomerization process does not require a comparatively long residence time. In fact, each reactor attempts to balance the amount of iso-dodecene in the process in such a way as to reduce the cost of 1-dodecene in the feed and to limit the size and utility demand of C2.

In all cases, the reaction temperature is maintained at the maximum of 388.15 K. Higher reaction temperatures lead to a faster reverse-isomerization reaction, which basically determines the size of each reactor. Lower temperatures are actually beneficial for better conversion of 1-dodecene to tridecanal, but this reaction domain is very fast compared to the reverse-isomerization and therefore not as critical. The assumption of isothermal control is considered to be satisfactory.

The partial pressures of CO and H_2 found in each case vary only slightly, as shown in Table 5.10. Since higher concentrations of CO in the liquid phase inhibit the isomerization reaction, it is not unexpected that the partial of pressure ratio of CO to H_2 is large. Equivalent conclusions were reached by Hentschel et al. [62] where the effect of high CO to H_2 ratios were investigated for this reaction. Such pressure profiles also lead to a higher tridecanal selectivity. In cases where the reverse-isomerization becomes more significant, such as in case 1, the partial pressure of H_2 tends to be higher than otherwise. This may also be responsible for the very small increase in H_2 pressures as the reactor size increases outside of case 2 and case 3.
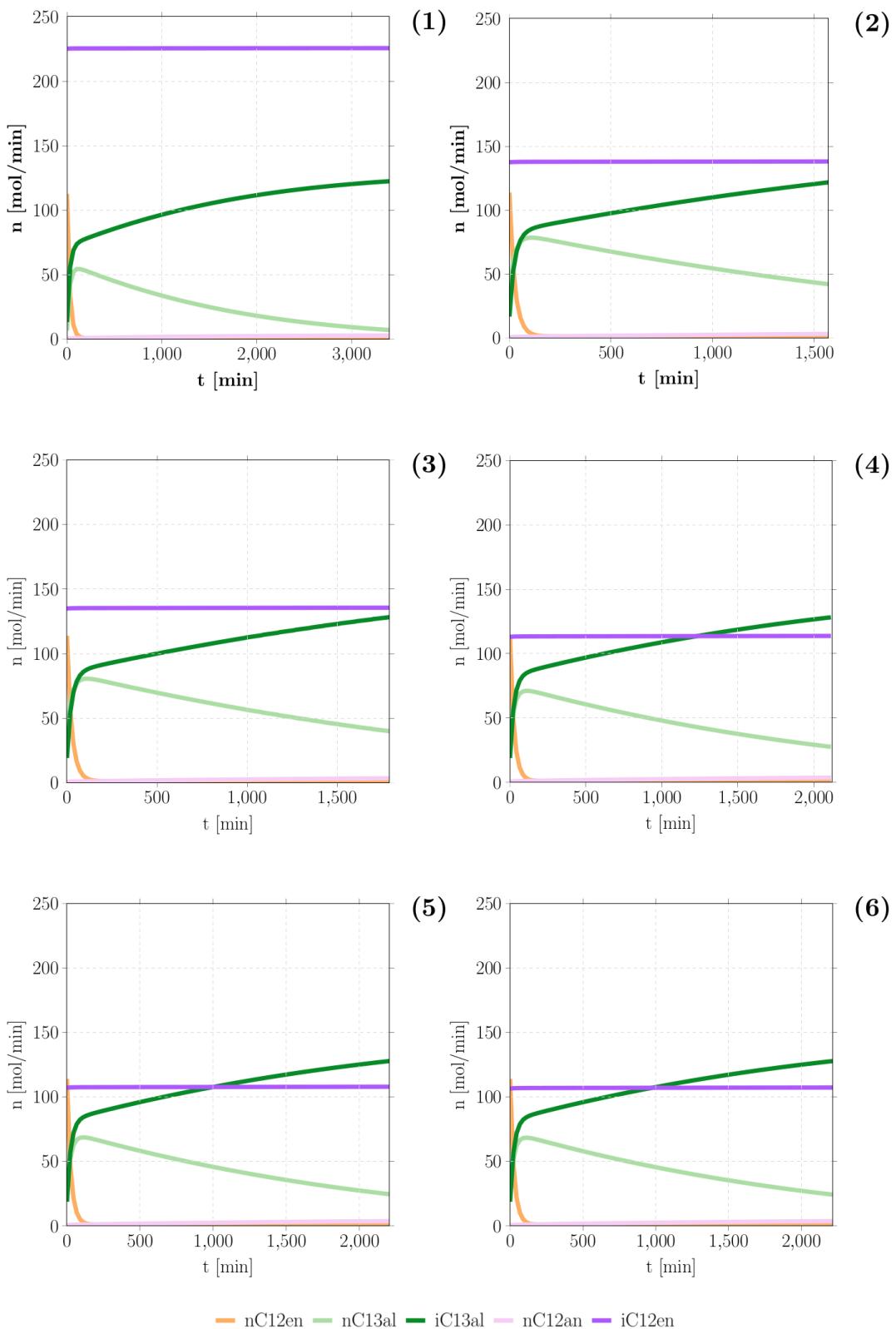
Figure 5.11: Composition profiles for the reactor in cases one through six.
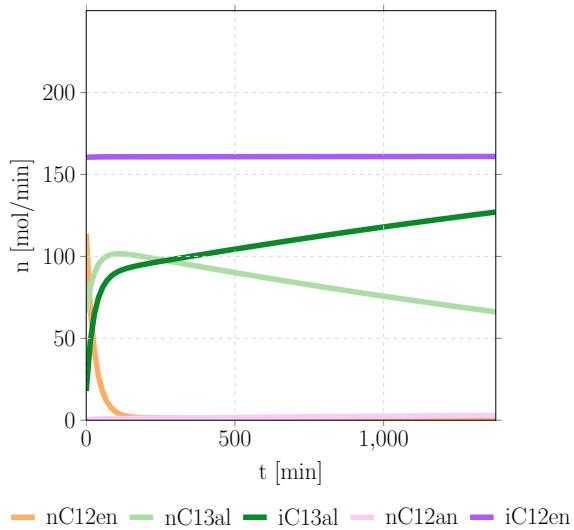
Figure 5.12: Composition profiles for the reactor in the reference case.

5.5.2.1 Elementary Process Function Comparison

The reactors modeled in this work were based on the results taken from Hentschel et al. [62] and from preliminary work on optimal reactor configurations that were mentioned in Chapter 5. This work assumed constant temperature and pressures for a reactor with recycle and were found to be reasonable approximations of the optimal control strategies for each reaction zone: one for the conversion of 1-dodecene to tridecanal and the other for the reverse isomerization of iso-dodecenes. Therefore, it was expected that both reactors would behave differently but each at relatively constant temperatures and pressures. To validate this assumption, the EPF method using variable temperature and partial pressures in the reactors is applied to the optimal case found using five decanters. Thus, the only difference is that the constraints fixing the reactor temperatures and pressures are relaxed in Equation (5.124) and the optimization is repeated. This section provides a discussion concerning the differences between the two resulting optimal process solutions.

The results from this subsequent optimization are shown in Table 5.11 in a similar manner as done in Table 5.6. In this table the results from the previously determined case 5 are placed alongside the new results using the EPF method. It is immediately clear that the EPF method delivers a process that performs better economically than in case 5. This is an expected result, considering the extra degrees of freedom of the new problem. The question is then, what can one learn from this result?

When observing the reactor trajectories of the EPF case, given in Figures 5.13 and 5.14, the two reaction zones are visible; however, the first zone transitions to the second after only a short time in the reactor. This shows that the reverse-isomerization dominates the reaction similarly to the previous cases. Again, only the DSR is used and the CSTR

ignored, which is most likely an effect of the cost functions for the reactor and not a repudiation of the reactor arrangement based per se on physical properties. The use of the EPF method did not affect this decision.

When one looks at the individual costs of the system, one can see that both production and capital costs decrease for the EPF optimal case. However, the catalyst leaching and 1-dodecene feed costs increase, but are offset by a reduction in the purge amount (seen by the amount of TMS solvent makeup) and the required steam and cooling water. This comes about as a trade-off between the reactor volume (see Table 5.12) and the height of the second column C2, which has only about half as many theoretical trays as in case 5 (see Table 5.13). When compared to the rest of the cases, C2 has a much shorter column owing to its reduced recovery fraction. This leads to a small purge and a larger recycle which in turn increases the amount of iso-dodecene in the feed as well as the TMS solvents required. This is the reason for the increased reactor size compared to case 5.

Also, the column C1 is smaller due to the smaller amount of extraction solvent that is used. In the EPF optimal process, the amount of solvent added to the first decanter in the cascade is 0.65 moles/sec when compared to 1.10 moles/sec used in case 5. In fact, all decanter, column, and heat exchanger sizes decrease in size except for H_{RB2}, which increases in size. In short, only the reactor and the reboiler of C2 slightly increase in cost due to increase in volume but are more than compensated for by a reduction in size of all other units. This leads to the reduced captial costs.

The production costs also decrease primarily due to the reduced heating and cooling duties for each unit except for a slight increase in the amount of cooling water required for H_{CF3}. However, due to the reduced size of the solvent recovery column, C2, and its poorer separation when compared to case 5 more iso-dodecene and n-dodecane enter the aldehyde column C3. These components are removed in the distillate of the column, leading to a reduction in the amount of each component recycled back to the reactor feed. This is what leads to the slight increase in the amount of 1-dodecene required in the feed.

The effect of the temperature control is minimal on the reactor performance. The reaction temperature quickly raises from the minimum to the maximum in the initial stages of the reactor, following the expected temperature profile of the two reaction zones. Instead, controlling the partial pressures of the synthesis gases is more important. The increased partial pressure of H_2 towards the end of the reactor is primarily to limit the size of the reactor by increasing the speed of the reverse-isomerization. This reverse-isomerization leads to a larger reactor, but at the same time, the reduction of the quality of the separation in C2 leads to a process that is overall more economical. This can be seen in Table 5.12, where the reactor size and residence times are larger and selectivity and the n/iso ratio lower for the EPF reactor. This is interesting in that, when considered alone, the optimal reactor using the EPF methodolgy is *worse*, than the reactor used case 5. The optimal EPF reactor is now attempting to tune its output to improve the economics of the downstream separation. This is quite ironic, considering

Table 5.11: Comparison of investment and production costs for the optimal points in case 5 and for the EPF variant thereof.

	Case 5	EPF
Decane	3.31	0.06
DMF	0.93	0.01
1-Dodecene	687.73	692.16
H_2	4.15	4.17
CO	4.12	4.13
Catalyst	0.03	0.25
(% Recovered)	99.9999	99.9992
Steam	19.69	14.16
Cooling water	2.02	1.41
Electricity	0.19	0.15
Production	722.16	716.49
Capital	31.62	29.33
Total	753.78	745.82

this is the point initially made about catalyst leaching. This is a very interesting point and something that the PSE group of Prof. Sundmacher will investigate futher. It again proves that reactor design cannot be separated from the process, especially the separation processes downstream.

The comparison presented in this section shows that a more detailed synthesis gas control strategy is recommendable. Perhaps when using both reactors (the DSR and CSTR) under constant partial pressures, a similar result as seen in the EPF example may be obtainable. Temperature control can be left constant, as in our assumption used in this chapter, without much concern. However, the EPF example does not detract from the extraction-cascade example, it simply shows that our assumed reactor configuration may not be optimal for all scenarios. It must be noted that the EPF result may have simple found a local minimum that was not obtainable using constant temperatures and pressures in the previous optimizations. Future investigations into the optimal process structure will include considerations on how to implement strategies that may help to ensure a global solution is found.

Table 5.12: Comparison of reactor performance for the optimal points in case 5 and for the EPF variant thereof.

	τ (min)	V (m³)	X (%)	S (%)	$\frac{n}{n+iso}$
Case 5	2217	705	99.46	96.24	97.13
EPF	3156	816	99.89	95.62	96.63

Table 5.13: Distillation column dimensions, recoveries, heating duties, and cooling duties.

C1	H (m)	D (m)	Recovery	Stages	Q_{reb} (kW)	Q_{con} (kW)
Case 5	18.86	0.49	0.95895	22.43	102.11	-89.61
EPF	17.19	0.37	0.94101	19.65	59.48	-52.49
C2	H (m)	D (m)	Recovery	Stages	Q_{reb} (kW)	Q_{con} (kW)
Case 5	29.73	2.39	0.99209	40.56	1290.06	-988.29
EPF	17.06	2.03	0.89124	19.44	939.91	-716.87
C3	H (m)	D (m)	Recovery	Stages	Q_{reb} (kW)	Q_{con} (kW)
Case 5	54.04	1.09	0.99950	81.07	235.71	-242.67
EPF	52.15	1.05	0.99954	77.92	221.03	-215.64
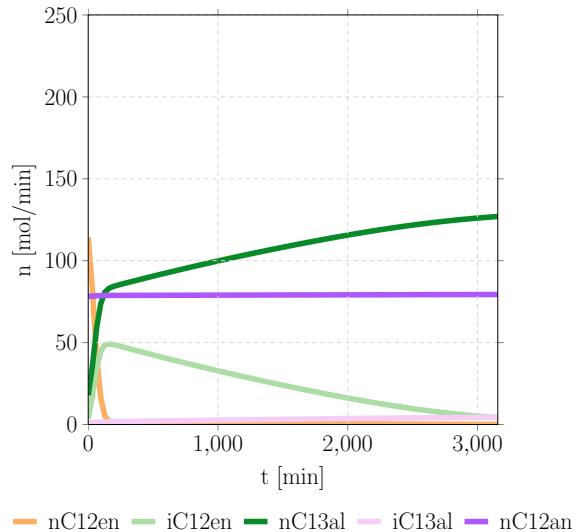
Figure 5.13: Composition profiles for the reactor in case 5 when using the EPF method for reactor design.
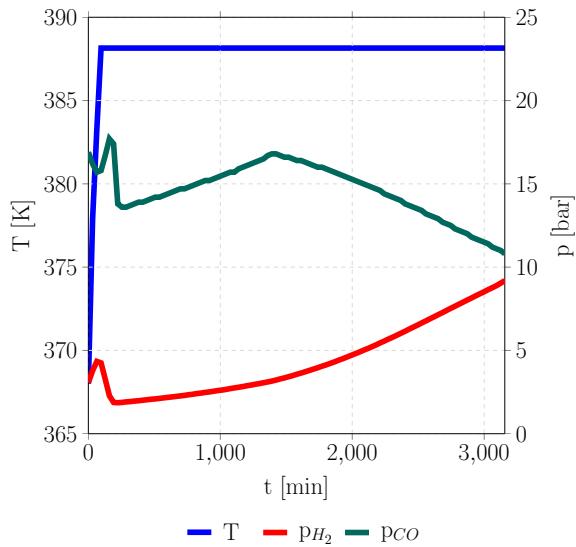
Figure 5.14: Temperature and pressure profiles in case 5 when using the EPF method for reactor design.

5.6 Conclusion

The issue of catalyst leaching in the hydroformylation of 1-dodecene has been a long-standing hindrance to reasonable economic performance. By using state-of-the-art computational techniques like COSMO-RS, the expensive catalyst ligand biphephos was modeled and partition coefficients for its distribution between the phases predicted. In order to calculate LLE and catalyst ligand partitioning in an optimization problem, phase equilibrium data and predicted catalyst partitioning ratios were integrated into a highly accurate Kriging surrogate model.

Several integrated reaction extraction optimization studies were performed showing improved process economics compared to the chosen reference case. This reference case closely resembles the conventional TMS method widely used in the hydroformylation of 1-dodecene using a single stage separation technique. The extraction cascade proposed in this work improves the process through a more efficient use of resources, especially in the expensive catalyst, and by reducing the necessary capital investment and utility consumption costs. This results in a substantial reduction in the TAC. Although the number of process units increases, a key tenet of process intensification is still seen in the enhanced catalyst separation in that the energy expenditure of the downstream separation decreases when using multiple decanters and at the same time the overall separation efficiency increases.

The optimization results show that by using extraction, in the form of a counter current cascade, catalyst leaching levels become almost negligible. The addition of supplementary decanters ultimately reduces the overall process cost to values approaching the TAC of the reference case where catalyst leaching is not included in the objective func-

tion. This work shows that extraction for catalyst recovery is a viable solution to the catalyst leaching problem in the hydroformylation of long-chain alkenes and should not be ignored. Once catalyst leaching becomes insignificant, such as after case 3, the optimization becomes a conventional reactor-separator problem. With an integrated reaction and separation process, it is not the reactor that always defines the separation, but sometimes the separation that defines the reactor. This is especially true when using expensive homogeneous catalysts. Not only does the extraction cascade increase the recovery of the catalyst, but it also increases the robustness of the process as the separation becomes less dependent on the reactor output. The process economics would no longer exclusively depend upon the separation performance of a single decanter that is itself dependent upon the composition of the post-reaction mixture. This work concludes that the hydroformylation of 1-dodecene, as well as for other long-chain alkenes, is economically feasible and more robust when implementing an extraction cascade for enhanced catalyst recovery.

6. Conclusion

This thesis is a journey through primarily economic issues surrounding the leaching of the expensive catalyst complex, more specifically the ligand biphephos, in the hydroformylation of 1-dodecene. It confronts insufficiencies in catalyst retention when using a TMS of n-decane and DMF and develops methods to increase the catalyst retention and the economic feasibility of the entire process. The main contributions in this work are summarized below.

In Chapter 3 the significance of catalyst ligand leaching on the process economics in a simplified example using correlations for catalyst leaching developed from experimental data was shown. This was the first time that the economics of catalyst leaching were included in a process design model. This initial economic evaluation shows that the current process using a single stage separation following the TMS principle is still too expensive using a TMS comprised of n-decane and DMF for catalyst recovery. Process costs were found to remain quite high, overshadowing all other production and capital costs, despite that additional DMF solvent in the TMS was found to substantially reduce the overall TAC. Such an evaluation done in the early stages of process design can help researchers decide where more effort in process development should be prioritized. In this case, catalyst recovery would have been observed at the top of the list and potentially more resources would have been directed towards solving this problem.

A framework for the computer aided design of TMS systems was developed and implemented for the hydroformylation of 1-dodecene in Chapter 4. The very high production costs due to catalyst leaching when using a TMS composed of DMF and n-decane led to the idea that perhaps this mixture was not optimally suited for biphephos recovery. It was proposed that superior TMS systems could be found by incorporating catalyst solubility into the TMS design process. Solvents were to be primarily considered based on the relative solubility of the catalyst ligand and secondarily on phase behavior, reactivity, toxicity, etc. A framework based on quantum chemical methods implemented using COSMO-RS theory was then developed. Using this method, several successful

TMS systems with good catalyst separation and reaction performance were identified. However, instead of improving the process by identifying new TMS solvents, the results showed that DMF is currently the most practical solvent identified for catalyst recovery when paired with alkanes from n-octane to n-tetradecane. This strongly suggests that a different approach to catalyst recovery other than that of a TMS is required.

Once it was concluded that finding an improved TMS system was improbable, the new integrated reaction extraction process described in Chapter 5 was developed. The objective of the process optimization here was to alleviate the issues encountered in both previous endeavors: to improve the process economics limited to using DMF as the catalyst solvent. This led to the successful implementation of previously developed methods such as the process optimization and use of surrogate models in Chapter 3 and the use of COSMOtherm for solubility estimations in Chapter 4. The complete incorporation of the TMS composition and catalyst leaching into the process-wide optimization problem was then possible. A cascade of counter-current separation stages was shown to economically recover almost all of the catalyst leading to a much more economically feasible process than before. Also, several trade-offs between reactor performance and downstream separation efficiency were illuminated, leading to a deeper understanding of the process that may have been otherwise overlooked. These results should prompt further research into this tangent of hydroformylation process design as there remains much potential for new developments.

6.1   Future Work

Naturally, this work has opened more doors than it has closed and any other result would have been unsatisfactory. Several of these ideas for improvement are suggested as topics for further research.

6.1.1   Thermodynamic Models

The choice of thermodynamic model used in predicting the LLE behaviors necessary for this work was very important for ensuring accurate modeling and results. This is the primary reason for fitting the unique modified UNIFAC Dortmund parameters presented in Chapter 3. When choosing a thermodynamic model for predictions of the catalyst ligand solubility, the selection of a model was quite restricted, being confined to a COSMO-RS based method.

There were, however, several issues mentioned when using the COSMOtherm software with respect to solubility predictions. Although the ranking results can qualitatively represent actual solvent tendencies, it is not always correct when comparing prediction results with those from real systems. However, this method is still young and is improving constantly under the eye of its creator. The benefit of this model is the absence of experimental data or binary interaction parameter fitting. As the accuracy increases, it will become a more and more useful tool in CAMD. Therefore, it can be predicted that the use of COSMO-RS will most likely play a larger role in solvent design within

the next decade. In fact, two different CAMD methods using COSMO-RS have already been developed by Scheffczyk et al. [111] and Austin et al. [5]. Our focus should also include future potential uses of this software for solvent selection.

Also of interest is the use of modern equations of state, such as the often mentioned PC-SAFT developed by Gross and Sadowski [54]. It is desirable to incorporate this model within a CAMD framework to be used in TMS solvent design. Many other world renowned research groups are currently pursuing CAMD methods using various SAFT based models (Bardow et al. [6], Burger et al. [30], Lampe et al. [82, 83], Pereira et al. [94], Stavrou et al. [115]). The new aspect that would need to be addressed is the liquid-liquid equilibrium during the optimization, which is an inherently difficult problem that was encountered in this work. Predicting liquid phase splitting behavior is also one of the most difficult properties to accurately recreate using current thermodynamic models. Therefore, a detailed investigation into different modern thermodynamic models and LLE predictions is necessary, as well as an evaluation of the various surrogate models used to represent them.

Thus, a iterative process combining optimal solvents and experimental validation is proposed. This would combine optimal solvent design using a group method equation of state such as PC-SAFT and subsequent experiments to gather real data to refine the parameters used in the model. Such a task is included in a proposal for a new subproject within the SFB/TRR 63 during the third funding period, if it should be accepted.

6.1.2 DMF Replacement

Despite its positive characteristics as a solvent, it is generally accepted that usage of DMF needs to be reduced or eliminated. The proposed decanter cascade provides a foundation for selection of new solvents. A different, potentially friendlier, solvent other than DMF could be identified for use as the extraction solvent. Although DMF is a satisfactory solvent for separating the catalyst from the post-reaction mixture as part of a TMS, high catalyst solubility is not necessarily required when using several additional catalyst extractions. Thus, solvents that do not perform as well as DMF at separating the catalyst may be used for extraction in a decanter cascade similar to the one proposed in Chapter 5. Although the solubility of the catalyst may be lower in the new solvent, several separation stages would alleviate this problem, potentially leading to a safer process. The new solvent may not even need to form a TMS, as seen in the successful hydroformylation of 1-dodecene in toluene (Dreimann et al. [40]). Naturally, the other physical properties of the new solvent would need to be investigated, such as vapor pressure for example. Thus, future work should consider identifying replacement solvents for extracting a homogeneous catalyst used in a decanter cascade.

This would naturally need include several environmentally important criteria, such as toxicity and bioaccumulation, for example. Several methods exist for estimating solvent properties to ensure "green" candidates are found for solvent replacement or in design problems, such as those outlined by Bergez-Lacoste et al. [22]. As much work has

been done in this area in the last few years, there is a possibility that such methods can be incorporated into a solvent screening method similar to the one outlined in Chapter 4 or redeveloped into a CAMD methodology that can be used as part of optimal solvent design. This would enhance the robustness of the solvent selection process and may remove several of the manual steps in the screening framework, such as manually checking the toxicity of each candidate molecule.

6.1.3   Integrated Process and TMS Design

As seen in the previous section, an obvious trade-off between solvent performance, process structure, and environmental considerations exists. Once methods for solvent selection have been refined and the thermodynamic predictions become more reasonable, it would then worthwhile to pursue the integrated process and solvent design problem. This would combine the solvent selection routines based on catalyst recovery, LLE behavior, and environmental aspects with process structure decisions. In our group, several recent papers have explored integrated process design, albeit using simple examples (Zhou et al. [135, 136, 137]). Additionally, our group is focusing on optimizing complex reactor-separator process models, including the hydroformylation reaction considered in this thesis (Kaiser et al. [69]). This strong background provides a solid foundation to innovate new methods and strategies to solve the complicated integrated process and solvent design problem for the homogeneously catalyzed hydroformylation. The methods to be developed would then be applied to another relevant process: homogeneously catalyzed hydroaminomethylation. This work is to be included as part of a proposed project during the third funding period of the SFB TRR 63.

A. Appendix

A.1 Pure substance properties

Density is calculated using the following correlation and parameters given in Table A.1.

$$\rho_i = a_{\rho,0,i} + a_{\rho,1,i} \cdot T \qquad\qquad i \in \text{COM} \qquad (A.1)$$

The enthalpy of each component is calculated using the following correlation:

Table A.1: Density correlation parameters (Equation (A.1)).

Component	a_0	a_1
C10an	981.5951	$-8.3536 \cdot 10^{-1}$
DMF	1256.5163	-1.0306
nC12en	993.8919	$-7.8875 \cdot 10^{-1}$
iC12en	993.8919	$-7.8875 \cdot 10^{-1}$
nC12an	977.0381	$-7.6743 \cdot 10^{-1}$
nC13al	1068.1228	$-8.0180 \cdot 10^{-1}$
iC13al	1068.1228	$-8.0180 \cdot 10^{-1}$

$$h_i(T) = h_{f,0,i}(T_0) + \sum_{j=1}^{4} p_{Cp,j,i}(T^j - T_0^j) \qquad (A.2)$$

Table A.2: Heat capacity correlation and enthalpy of formation parameters (Equation (A.2)).

Comp.	$h_{f,0}$	$p_{Cp,0}$	$p_{Cp,1}$	$p_{Cp,2}$	$p_{Cp,3}$	$p_{Cp,4}$
C10an	$-2.482645 \cdot 10^5$	$7.974100 \cdot 10^1$	$1.6926 \cdot 10^0$	$-4.5287 \cdot 10^{-3}$	$4.97693 \cdot 10^{-6}$	0
DMF	$-1.911874 \cdot 10^5$	$6.372700 \cdot 10^1$	$6.0708 \cdot 10^{-1}$	$-1.6163 \cdot 10^{-3}$	$1.85600 \cdot 10^{-6}$	0
iC12en	$-1.638537 \cdot 10^5$	$1.292030 \cdot 10^2$	$1.5842 \cdot 10^0$	$-4.0461 \cdot 10^{-3}$	$4.38510 \cdot 10^{-6}$	0
nC12en	$-1.638537 \cdot 10^5$	$1.292030 \cdot 10^2$	$1.5842 \cdot 10^0$	$-4.0461 \cdot 10^{-3}$	$4.38510 \cdot 10^{-6}$	0
nC12an	$-2.892453 \cdot 10^5$	$8.448500 \cdot 10^1$	$2.0358 \cdot 10^0$	$-5.0981 \cdot 10^{-3}$	$5.21860 \cdot 10^{-6}$	0
nC13al	$-3.902267 \cdot 10^5$	$7.437700 \cdot 10^1$	$2.4379 \cdot 10^0$	$-5.6713 \cdot 10^{-3}$	$5.40890 \cdot 10^{-6}$	0
iC13al	$-3.902267 \cdot 10^5$	$7.437700 \cdot 10^1$	$2.4379 \cdot 10^0$	$-5.6713 \cdot 10^{-3}$	$5.40890 \cdot 10^{-6}$	0

The vapor pressure is described using the following two correlations:

$$p_{\text{vap},i} = 10^{\left(a_0 + \frac{a_1}{T} + a_2 \log_{10}(T) + a_3 T + a_4 T^2\right)} \cdot 133.322 \cdot 10^{-5} \tag{A.3}$$
$$i \in \text{COM} \setminus \text{GAS} \setminus \{\text{iC12en, iC13al}\}$$

$$p_{vap,i} = \exp\left(a_0 + \frac{a_1}{T} + a_2 \ln(T) + a_3 T^{a_4}\right) \tag{A.4}$$
$$i \in \{\text{iC12en, iC13al}\}$$

Table A.3: Vapor pressure correlation parameters (Equation (A.3) and Equation (A.4)).

Component	a_0	a_1	a_2	a_3	a_4
C10an	26.5125	$-3.3584 \cdot 10^3$	-6.1174	$-3.3225 \cdot 10^{-10}$	$4.8554 \cdot 10^{-7}$
DMF	-47.9857	$-2.385 \cdot 10^3$	$2.88 \cdot 10^1$	$-5.8596 \cdot 10^{-2}$	$3.1386 \cdot 10^{-5}$
nC12en	-8.5899	$-3.5241 \cdot 10^3$	$1.0806 \cdot 10^1$	$-2.8161 \cdot 10^{-2}$	$1.4267 \cdot 10^{-5}$
nC12an	-5.563	$-3.470 \cdot 10^3$	9.027	$-2.319 \cdot 10^{-2}$	$1.124 \cdot 10^{-5}$
nC13al	161.5042	$-9.7660 \cdot 10^3$	$-5.5591 \cdot 10^1$	$2.1036 \cdot 10^{-2}$	$5.5498 \cdot 10^{-13}$
iC12en	75.79	$-9.964 \cdot 10^3$	-8.965	$4.940 \cdot 10^{-18}$	6
iC13al	10.420	$-6.149 \cdot 10^3$	0.197	$-2 \cdot 10^{-4}$	1

Table A.4: Heat of vaporization correlation (Equation (3.40) and Equation (5.78)) parameters taken from the literature [131].

Component	a_1	a_2	a_3
C10an	71.4282	618.45	0.451
DMF	59.355	647	0.381
nC12en	77.1658	658.2	0.407
iC12en	77.229	663	0.4025
nC12an	78.8021	657	0.437
nC13al	95.6235	700	0.414
iC13al	95.6235	700	0.414

Table A.5: Molecular weight of each component.

Component	M_i (g/mol)
C10an	142.2817
DMF	73.0938
nC12en	168.3190
iC12en	168.3190
nC13al	198.3449
iC13al	198.3449
nC12an	170.3348
H2	2.01588
CO	28.0101
BPP	786.68

A.2 Reaction System

The reaction kinetics for the six reactions shown in Figure 5.4 are shown below as Equations (A.5) to (A.10) with accompanying parameters in given in Table A.6. This system is quite complex with several competing reactions. There are three hydroformylation reactions (r_1, r_5, r_6), two hydrogenation reactions (r_3, r_4), and one isomerization of dodecene reaction (r_2). Basically, the same reaction kinetics as developed by Hentschel et al. [62] are used in this work with the one exception being that the equilibrium concentrations of the reactant gases are assumed in the liquid phase at all times.

The reactors in this work are modeled as a series of equal volume CSTRs for the PFR (R1) and one final CSTR with variable volume as the last CSTR in the cascade (R2). The gas pressures and temperature for the last CSTR are independent of the PFR.

$$r_1 = \frac{k_{1,0}(T) \cdot C_{\text{nC12en}} \cdot C_{\text{H2}} \cdot C_{\text{CO}}}{1 + K_{1,1} \cdot C_{\text{nC12en}} + K_{1,2} \cdot C_{\text{nC13al}} + K_{1,3} \cdot C_{\text{H2}}} \tag{A.5}$$

$$r_2 = \frac{k_{2,0}(T) \left(C_{\text{nC12en}} - \frac{C_{\text{iC12en}}}{K_{p,2}} \right)}{1 + K_{2,1} \cdot C_{\text{nC12en}} + K_{2,2} \cdot C_{\text{iC12en}}} \tag{A.6}$$

$$r_3 = \frac{k_{3,0}(T) \left(C_{\text{nC12en}} \cdot C_{\text{H2}} - \frac{C_{\text{nC12an}}}{K_{p,3}} \right)}{1 + K_{3,1} \cdot C_{\text{nC12en}} + K_{3,2} \cdot C_{\text{nC12an}} + K_{3,3} \cdot C_{\text{H2}}} \tag{A.7}$$

$$r_4 = k_{4,0}(T) \cdot C_{\text{iC12en}} \cdot C_{\text{H2}} \tag{A.8}$$

$$r_5 = k_{5,0}(T) \cdot C_{\text{iC12en}} \cdot C_{\text{H2}} \cdot C_{\text{CO}} \tag{A.9}$$

$$r_6 = k_{6,0}(T) \cdot C_{\text{nC12en}} \cdot C_{\text{H2}} \cdot C_{\text{CO}} \tag{A.10}$$

The temperature dependencies of the rate constants $k_j(T)$ were modeled using the Arrhenius equation based on a reference temperature. This is corrected for using a correction (Equation (A.11)) with the reference temperature $T_{ref} = 378.15 K$.

$$k_j(T) = k_{0,j} \exp \left(\frac{-E_{\text{A,j}}}{R} \left(\frac{1}{T} - \frac{1}{T_{\text{ref}}} \right) \right) \qquad j \in \text{REA} \tag{A.11}$$

Reactions r_2 (Equation (A.6)) and r_3 (Equation (A.7)) require equilibrium constants, given by Equation (A.12) and Equation (A.13), respectively. The parameters for the temperature correlation are found in Table A.7.

$$K_{p,j} = \exp \left(\frac{-\Delta G_j}{RT} \right) \tag{A.12}$$

$$\Delta G_j = a_{0,j} + a_{1,j}T + a_{2,j}T^2 \qquad j \in \{2, 3\} \tag{A.13}$$

The concentration of active catalyst (Equation (A.14)) must also be known, which depends strongly on the amount of CO in the liquid phase.

$$C_{\text{cat}} = \frac{C_{\text{cat,tot}}}{1 + K_{\text{cat},1} C_{\text{CO}}^{K_{\text{cat},3}} + K_{\text{cat},2} \frac{C_{\text{CO}}^{K_{\text{cat},3}}}{C_{\text{H2}}}} \tag{A.14}$$

Gas solubility

The amount of H_2 and CO dissolved in the liquid phase must be known for the reaction kinetics. The equilibrium gas concentrations are found using Equation (A.15) and the parameters given in Table A.8. Temperature dependency of the reactant gas solubilities are provided using Equation (A.16). Due to the high concentrations of solvent relative to the other components in the reaction mixture, the solubility is considered to be independent of change in the composition during the reaction.

$$C_i^* = \frac{p_i}{H_i} \qquad\qquad i \in \{\text{GAS}\} \tag{A.15}$$

$$H_i = H_i^0 \exp\left(\frac{-E_{A,H,i}}{RT}\right) \tag{A.16}$$

Table A.6: Parameters of reaction kinetics (Equations (A.5) to (A.10)) from Hentschel et al. [62]

Variable	Eq.	$E_A \left[\frac{kJ}{mol}\right]$	k_0	Unit	$K_1 \left[\frac{ml}{mol}\right]$	$K_2 \left[\frac{ml}{mol}\right]$	$K_3 \left[\frac{ml}{mol}\right]$
r_1	(A.5)	113.08	$4.904 \cdot 10^{16}$	$\frac{ml^3}{gminmol^2}$	574876	3020413	11732838
r_2	(A.6)	136.89	$4.878 \cdot 10^6$	$\frac{ml}{gmin}$	38632	226214	-
r_3	(A.7)	76.11	$2.724 \cdot 10^8$	$\frac{ml^2}{gminmol}$	2661.2	7100	1280
r_4	(A.8)	102.26	$2.958 \cdot 10^4$	$\frac{ml^2}{gminmol}$	-	-	-
r_5	(A.9)	120.84	$3.702\text{e} \cdot 10^{10}$	$\frac{ml^3}{gminmol^2}$	-	-	-
r_6	(A.10)	113.08	$3.951 \cdot 10^{11}$	$\frac{ml^3}{gminmol^2}$	-	-	-
C_{cat}	(A.14)	-	-	-	$3.041 \cdot 10^4$	0	0.644

Table A.7: Equilibrium constant parameters (Equation (A.12)).

Variable	$a_0[kJ/mol]$	$a_1[kJ/mol/K]$	$a_2[kJ/mol/K^2]$
ΔG_2	-11.0034	0	0
ΔG_3	-126.275	0.1266	6.803e-6

Table A.8: Solubility parameters (Equation (A.16))

Component	$H_0 \left[\frac{bar \cdot ml}{mol}\right]$	$E_{A,H} \left[\frac{kJ}{mol}\right]$
H_2	66400	-3.06
CO	73900	-0.84

A.3 Linear regression model for phase separation in Chapter 3

In total there are four regression models of the form shown in Equation (A.17). There are a total of 35 terms in each equation with the parameter set taken from Table 1 dependent upon which species is being considered. These are the equations referenced to in Equation (3.9) as a function of the mole fractions of the mixture. From the predicted partition coefficients, the phase equilibrium of the system can be quickly calculated during the optimization.

$$
\begin{aligned}
\theta_i^\alpha = {} & b_1^i \cdot x_1 + b_2^i \cdot x_2 + b_3^i \cdot x_3 + b_4^i \cdot x_4 + b_{23}^i \cdot x_2 \cdot x_3 + b_{24}^i \cdot x_2 \cdot x_4 + b_{11}^i \cdot x_1 \cdot x_1 \\
& + b_{33}^i \cdot x_3 \cdot x_3 + b_{44}^i \cdot x_4 \cdot x_4 + b_{112}^i \cdot x_1^2 \cdot x_2 + b_{133}^i \cdot x_1 \cdot x_3^2 + b_{233}^i \cdot x_2 \cdot x_3^2 \\
& + b_{224}^i \cdot x_2^2 \cdot x_4 + b_{334}^i \cdot x_3^2 \cdot x_4 + b_{222}^i \cdot x_2^3 + b_{1122}^i \cdot x_1^2 \cdot x_2^2 + b_{1133}^i \cdot x_1^2 \cdot x_3^2 \\
& + b_{2233}^i \cdot x_2^2 \cdot x_3^2 + b_{1144}^i \cdot x_1^2 \cdot x_4^2 + b_{2244}^i \cdot x_2^2 \cdot x_4^2 + b_{3344}^i \cdot x_3^2 \cdot x_4^2 \\
& + b_{1112}^i \cdot x_1^3 \cdot x_2 + b_{1222}^i \cdot x_1 \cdot x_2^3 + b_{1113}^i \cdot x_1^3 \cdot x_3 + b_{2223}^i \cdot x_2^3 \cdot x_3 \\
& + b_{1333}^i \cdot x_1 \cdot x_3^3 + b_{2333}^i \cdot x_2 \cdot x_3^3 + b_{1114}^i \cdot x_1^3 \cdot x_4 + b_{3334}^i \cdot x_3^3 \cdot x_4 \\
& + b_{1444}^i \cdot x_1 \cdot x_4^3 + b_{2444}^i \cdot x_2 \cdot x_4^3 + b_{3444}^i \cdot x_3 \cdot x_4^3 + b_{1111}^i \cdot x_1^4 \\
& + b_{2222}^i \cdot x_2^4 + b_{4444}^i \cdot x_4^4
\end{aligned}
\tag{A.17}
$$

Table A.9: Linear regression model coefficients for partition coefficient predictions used in Equation (3.9), which is shown in more detail in Equation (A.17). For each substance, i, there is a specific parameter (1-4) for each term in the regression.

Parameter	DMF (1)	Decane (2)	Dodecene (3)	Tridecanal (4)
b_1^i	14.4808	-2.3061	-1.7521	-2.6731
b_2^i	-2.5660	3.6252	2.7289	4.1332
b_3^i	-8.6201	-1.9662	-2.3920	-2.1765
b_4^i	2.4020	4.1360	3.2430	4.8296
b_{23}^i	11.2306	-0.8307	0.3163	-1.0474
b_{24}^i	-9.5867	-7.8207	-6.5538	-9.0683
b_{11}^i	-34.6745	3.0932	5.1633	2.9304
b_{33}^i	-1020.3088	-138.1630	-203.3126	-135.1988
b_{44}^i	-7.9921	-6.8150	-4.5824	-7.9643
b_{112}^i	1.0496	-6.1005	-8.0307	-5.4940
b_{133}^i	1040.9808	143.5350	199.2659	146.8331
b_{233}^i	1001.2131	140.7131	234.8855	135.9110
b_{224}^i	-1.9453	-12.7290	-8.6222	-14.4881
b_{334}^i	996.8243	137.4105	190.4944	132.7743
b_{222}^i	17.0606	5.8076	3.9847	6.6440
b_{1122}^i	2.7024	0.5069	2.1017	-0.1186
b_{1133}^i	4.9408	18.4265	12.0850	14.7777
b_{2233}^i	-95.7376	-25.0740	-69.3817	-26.2172
b_{1144}^i	-4.4483	-1.2894	-4.4478	-0.6812
b_{2244}^i	28.3694	12.0543	8.3998	13.8959
b_{3344}^i	-19.3906	5.4062	21.1133	5.0202
b_{1112}^i	31.7528	2.4096	-0.0603	2.6268
b_{1222}^i	-19.3565	-15.1061	-11.0208	-17.2047
b_{1113}^i	40.0196	7.4382	2.3922	10.1651
b_{2223}^i	-17.0907	-14.4105	-9.2882	-16.4754
b_{1333}^i	874.3016	77.2236	119.6448	46.8970
b_{2333}^i	1443.3809	250.9856	329.7378	261.1439
b_{1114}^i	27.9007	-3.7309	-7.0036	-3.1622
b_{3334}^i	602.0993	105.7394	147.6803	99.8873
b_{1444}^i	-0.6328	3.4680	1.5399	3.9433
b_{2444}^i	18.8748	5.4450	3.0795	6.4297
b_{3444}^i	-1.3634	3.3721	0.3453	3.8671
b_{1111}^i	21.1478	-0.3726	-2.3449	0.2566
b_{2222}^i	-14.2844	-9.3136	-6.6438	-10.6376
b_{4444}^i	4.7630	2.6736	1.2385	3.1428

A.4 Distillation Column Sizing

In both the processes used in Chapter 3 and Chapter 5 distillation columns are present. In each column, the same design procedure is followed and therefore a single distillation column design section is considered prudent. All columns are modeled using the Fenske-Underwood-Gilliland correlations which are used to estimate column sizes and flowrates (Fenske [45], Gilliland [51], Molokanov et al. [91], Underwood [120, 121]). All columns are assumed to have a pressure drop of 50% with the feed being the average pressure between the pressures at the top and bottom trays (see Equations (A.18) to (A.20)). Specific pressure and temperature constraints for each column are included in their respective sections.

$$p_{c,f} = 1.25 \cdot p_c \qquad\qquad c \in \text{COL} \qquad\qquad (A.18)$$

$$p_{c,d} = p_C \qquad\qquad c \in \text{COL} \qquad\qquad (A.19)$$

$$p_{c,b} = 1.5 \cdot p_c \qquad\qquad c \in \text{COL} \qquad\qquad (A.20)$$

where c is the column number, d is for the distillate, and b for the bottoms.

The relative volatilities can be calculated using a simple vapor pressure ratio, where component j is the heavy key.

$$\alpha_{c,i,j}(T) = \frac{p_{\text{vap},c,i}(T)}{p_{\text{vap},c,j}(T)} \qquad c \in \text{COL}, \; i \in \text{COM}, \; j \in \text{COM} \qquad (A.21)$$

The mean relative volatility is calculated as the geometric mean of the relative volatility of the distillate (D) and that of the bottoms (B). Each distillation feed is considered to be a saturated liquid ($q = 1$) and therefore each stream (7,12,17) requires heating to its bubble point after leaving their respective decanters.

$$\bar{\alpha}_{c,i,j} = \sqrt{\alpha_{c,i,j}(T_{c,D}) \cdot \alpha_{c,i,j}(T_{c,B})} \qquad c \in \text{COL}, \; i \in \text{COM}, \; j \in \text{COM} \qquad (A.22)$$

The minimum number of trays for the column is estimated using the Fenske equation which requires the outlet compositions of the key components.

$$N_{c,\text{min}} = \frac{\log\left(\frac{\dot{n}_{c,D,LK} \cdot \dot{n}_{c,B,HK}}{\dot{n}_{c,B,LK} \cdot \dot{n}_{c,D,HK}}\right)}{log(\bar{\alpha}_{c,LK,HK})} \qquad c \in \text{COL} \qquad (A.23)$$

Once N_{min} is known, the outlet compositions for the remaining components can be calculated using Equation (A.24) and Equation (A.25).

$$\dot{n}_{c,B,i} = \frac{\dot{n}_{c,\text{in},i}}{1 + \frac{\dot{n}_{c,D,HK}}{\dot{n}_{c,B,HK}} \cdot \bar{\alpha}_{c,i,HK}^{N_{c,\text{min}}}} \qquad c \in \text{COL}, \; i \in \text{COM} \qquad (A.24)$$

$$\dot{n}_{c,\text{in},i} = \dot{n}_{c,D,i} + \dot{n}_{c,B,i} \qquad c \in \text{COL}, \; i \in \text{COM} \qquad (A.25)$$

The recovery ratios of the key components are left as optimization variables. Recovery of each light component must be at least 80% and no greater than 99.999%. The amount of

key component recovered in each distillate and bottoms are determined by the recovery ratios $\zeta_{c,LK}$ and $\zeta_{c,HK}$ for the light and heavy keys in each column, respectively.

$$\dot{n}_{c,D,LK} = \zeta_{c,LK} \cdot \dot{n}_{c,in,LK} \qquad\qquad c \in COL \qquad (A.26)$$

$$\dot{n}_{c,D,HK} = \zeta_{c,HK} \cdot \dot{n}_{c,in,HK} \qquad\qquad c \in COL \qquad (A.27)$$

$$0.8 \leq \xi_{c,LK} \leq 0.99999 \qquad\qquad c \in COL \qquad (A.28)$$

To begin, the minimum reflux ration is determined using the Underwood correlation (Equation (A.29))

$$1 - q = \sum_{i \in COM} \left(\frac{\bar{\alpha}_{i,HK} \cdot x_{in,i}}{\bar{\alpha}_{i,HK} - \Theta} \right) \qquad\qquad (A.29)$$

$$1 \leq \Theta \leq \bar{\alpha}_{LK,HK}$$

$$R_{c,min} = \sum_{i \in COM} \left(\frac{\bar{\alpha}_{i,HK} \cdot x_{D,i}}{\bar{\alpha}_{i,HK} - \Theta} \right) - 1 \qquad\qquad c \in COL \qquad (A.30)$$

The distillation feed is always assumed to be saturated liquid, therefore q is always equal to one. The reflux ratio of the column is left as an optimization variable which is modeled as the product of the minimum reflux ratio and the variable R_{factor}.

$$R_c = R_{c,factor} \cdot R_{c,min} \qquad\qquad c \in COL \qquad (A.31)$$

The vessel cost for a distillation column depends on the height and diameter of the column. The height of the column depends on the number of trays, tray spacing, the disengaging space, the liquid reservoir, and skirt height (see Equation (A.35)). The diameter is dependent on the volumetric flowrate through the column. Using the reflux ratio calculated previously, the theoretical number of stages can be estimated using the Gilliland correlation. With an assumed tray efficiency of 0.8, the total height of the column can then be determined.

$$X = \frac{R - R_{min}}{R + 1} \qquad\qquad (A.32)$$

$$X_1 = 1 - \exp\left(\frac{1 + 54.4X}{11 + 117.2X} \cdot \frac{X - 1}{X^{0.5}} \right) \qquad\qquad (A.33)$$

$$N_{th} = \frac{N_{min} + X_1}{1 - X_1} \qquad\qquad (A.34)$$

$$H_{col} = \left(\frac{N_{th}}{\eta_N} - 1 \right) \cdot 0.6 + 1.5 + 3 + 1.5 \qquad\qquad (A.35)$$

Column diameter hinges on the flooding velocity of each tray. Technically each tray may have a different, optimally sized diameter, but due to the assumption of constant molar

overflow, a different diameter exists for each the stripping and rectification sections. The overall diameter used for sizing purposes is the average of these diameters. Bubble-cap tray vapor efficiency, ϵ_{vap}, is taken as 0.6. Determining the flooding velocity depends on several terms, such as the flooding efficiency, η_{fl}, assumed to be 0.8, a surface tension, σ, of 20 $\frac{mN}{m}$, and the flooding parameter, C_{sb}, set equal to $0.1\frac{m}{s}$. The diameter can then be found using the following set of equations:

$$D_{\text{c}} = 0.5 \sum_{s \in \{\text{B,D}\}} D_{c,s} \qquad\qquad c \in \text{COL} \qquad (A.36)$$

$$D_{\text{c},s} = \sqrt{\frac{4 \cdot \dot{m}_{\text{V},s}}{\pi \cdot u_{\text{fl},s} \cdot \epsilon_{\text{vap}} \cdot \hat{\rho}_{\text{gas},c,s}}} \qquad\qquad s \in \{\text{B,D}\},\ c \in \text{COL} \qquad (A.37)$$

$$\rho_{\text{liq},c,i,s} = a_{0,i} + a_{1,i} T_{c,s} \qquad\qquad s \in \{\text{B,D}\},\ c \in \text{COL},\ i \in \text{COM} \qquad (A.38)$$

$$\omega_{\text{liq},c,i,s} = \frac{\dot{n}_{c,s,i} M_i}{\sum_{i \in \text{COM}} (\dot{n}_{c,s,i} M_i)} \qquad\qquad s \in \{\text{B,D}\},\ c \in \text{COL} \qquad (A.39)$$

$$\hat{\rho}_{\text{liq},c,s} = \sum_{i \in \text{COM}} (\omega_{\text{liq},c,i,s} \cdot \rho_{\text{liq},c,i,s}) \qquad\qquad s \in \{\text{B,D}\},\ c \in \text{COL} \qquad (A.40)$$

$$\hat{\rho}_{\text{gas},c,\text{D}} = p \sum_{i \in \text{COM}} \left(\frac{x_{c,\text{D},i} \cdot M_i}{R_{gas} \cdot T_{\text{dew},c,D}} \right) \qquad\qquad c \in \text{COL} \qquad (A.41)$$

$$\hat{\rho}_{\text{gas},c,\text{B}} = p \sum_{i \in \text{COM}} \left(\frac{x_{c,\text{B},i} \cdot M_i}{R_{gas} \cdot T_{\text{bub},c,B}} \right) \qquad\qquad c \in \text{COL} \qquad (A.42)$$

$$\dot{m}_{\text{vap},c,s} = (R_c + 1)\dot{n}_{c,\text{D}} \sum_{i \in \text{COM}} (x_{c,s,i} M_i) \qquad\qquad s \in \{\text{B,D}\},\ c \in \text{COL} \qquad (A.43)$$

$$\dot{m}_{\text{liq},c,\text{B}} = \sum_{i \in \text{COM}} (\dot{n}_{c,\text{in},i} M_i) + R_c \cdot \dot{n}_{c,\text{D}} \sum_{i \in \text{COM}} (x_{c,\text{B},i} M_i) \quad c \in \text{COL} \qquad (A.44)$$

$$\dot{m}_{\text{liq},c,\text{D}} = R_c \cdot \dot{n}_{c,\text{D}} \sum_{i \in \text{COM}} (x_{c,\text{D},i} M_i) \qquad\qquad c \in \text{COL} \qquad (A.45)$$

$$F_{\text{fl},c,s} = \frac{\dot{m}_{\text{liq},c,s}}{\dot{m}_{\text{vap},c,s}} \cdot \sqrt{\frac{\hat{\rho}_{\text{gas},c,s}}{\hat{\rho}_{\text{liq},c,s}}} \qquad\qquad c \in \text{COL} \qquad (A.46)$$

$$u_{\text{fl},c,s} = \eta_{\text{fl}} C_{\text{sb}} \left(\frac{\sigma}{20} \right)^{0.2} \sqrt{\frac{\hat{\rho}_{\text{liq},c,s}}{\hat{\rho}_{\text{gas},c,s} - 1}} \qquad\qquad s \in \{\text{B,D}\} \qquad (A.47)$$

Nomenclature

Latin symbols

A_{hex}	=	Heat exchanger area, (m^2)
c_p	=	Heat capacity, $\left(\frac{J}{kmol \cdot K}\right)$
C	=	Total production costs, $\left(\frac{\$}{kmol}\right)$
$C_{capital}$	=	Capital costs, $\left(\frac{\$}{kmol}\right)$
$C_{production}$	=	Utility costs, $\left(\frac{\$}{kmol}\right)$
C_{sb}	=	Flooding parameter, $\left(\frac{m}{s}\right)$
D	=	Diameter, (m)
D	=	Distribution, $(-)$
F_{fl}	=	Flooding flow factor, $(-)$
H	=	Height, (m)
h	=	Molar enthalpy, $\left(\frac{kJ}{kmol}\right)$
K	=	Partition coefficient, $(-)$
L	=	Length, (m)
$\dot{m}$	=	Mass flow rate, $\left(\frac{kg}{h}\right)$
M	=	Molar mass, $\left(\frac{kg}{kmol}\right)$
N	=	Number of equilibrium stages, $(-)$
$\dot{n}$	=	Molar flow rate, $\left(\frac{kmol}{h}\right)$
n_i	=	Amount of substance, $(kmol)$
p_i	=	Partial pressure, (MPa)
P	=	Total pressure, (MPa)
p^{vap}	=	Vapor pressure, (MPa)
$\dot{Q}$	=	Heat flux, $\left(\frac{kJ}{h}\right)$
R	=	Gas constant, $\left(\frac{kJ}{mol \cdot K}\right)$, Reflux ratio, $(-)$
S	=	Boilup ratio, $(-)$
T	=	Temperature, (K)
TAC	=	Total annualized cost, $\left(\frac{\$}{kmol}\right)$
u_{fl}	=	Flooding velocity, $\left(\frac{m}{s}\right)$
U		Heat transfer coefficient, $\left(\frac{W}{m^2 \cdot K}\right)$
V	=	Volume, (m^3)
w	=	Mass fraction, $(-)$
x	=	Mole fraction, $(-)$
X	=	Conversion, $(-)$
Y	=	Yield, $(-)$

Greek symbols

α = Relative volatility, $(-)$
$\bar{\alpha}$ = Mean relative volatility, $(-)$
Δp = Pressure drop, (MPa)
ϵ_{vap} = Vapor efficiency, $(-)$
η_N = Tray efficiency, $(-)$
η_{fl} = Flooding efficiency, $(-)$
Θ = Underwood factor, $(-)$
θ = Partition Coefficient, $(-)$
μ = Chemical Potential, $\left(\frac{J}{mol}\right)$

ξ = Recovery ratio, $(-)$
ρ = Density, $\left(\frac{kg}{m^3}\right)$
σ = Surface tension, $\left(\frac{mN}{m}\right)$
Φ = Cost, $\left(\frac{\$}{kmol}, \frac{\$}{kJ}, \frac{\$}{kg}\right)$
Ψ = Mass fraction of DMF in TMS
ω = Mass fraction, $(-)$

Indices

0 = Initial value
B = Bottoms
base = Base value
bub = Bubble point
c = Cold stream
cat = Catalyst
cd = Coolant
con = Condenser
cw = Cooling water
D = Distillate
d = Decanter
dew = Dewpoint
h = Hot stream
HK = Heavy key
i, j = Component index
in = Inlet
liq = Liquid phase in the reactor
LK = Light key
lm = Log mean
np = Nonpolar phase
out = Outlet
p = Polar phase
r = Reactor
reb = Reboiler
ref = Refrigeration
s = Stream index
st = Steam
V = Vapor phase
vap = Vapor

Abbreviations

ALAMO	Automated Learning of Algebraic Models for Optimization
AMPL	A Modeling Language for Mathematical Programming
API	Active Pharmaceutical Ingredient
BC	Bare Cost
CAMD	Computer-Aided Molecular Design
CE	Chemical Engineering Index
CFC	Chlorofluorocarbon
COSMO	Conductor-like Screening Model
COSMO-RS	Conductor-like Screening Model for Real Solvents
COSMO-SAC	Conductor-like Screening Model – Segment Activity Coefficient
CSTR	Continuously Stirred Tank Reactor
DEF	N,N-diethylformamide
DMA	N,N-dimethylacetamide
DMF	N,N-dimethylformamide
DSR	Dosing Side-stream Reactor
EPF	Elementary Process Functions
GC	Gas Chromatography
HAM	Hydroaminomethylation
HRSC	High Relative Solubility of the Catalyst
HTMC	Homogeneous Transition Metal Catalyst
ICP-MS	Induced Coupled Plasma Mass Spectrometry
ICP-OES	Induced Coupled Plasma Optical Emission Spectrometry
LLE	Liquid-Liquid Equilibrium
LRSC	Low Relative Solubility of the Catalyst
MAE	Mean Average Error
MAPE	Mean Average Pecent Error
MF	Module Factor
MSS	Micellar Solvent Systems
MPF	Material and Pressure Factor
NMP	N-Methyl-2-pyrrolidone
NRTL	Non-Random Two Liquid
NRTL-SAC	Non-Random Two Liquid Segment Activity Coefficient
OSN	Organic Solvent Nanofiltration
PC-SAFT	Perturbed-Chain Statistical Association Fluid Theory
PCP-SAFT	Perturbed-Chain Polar Statistical Association Fluid Theory
PDMS	Polydimethylsiloxane
POSS	Polyhedral Oligomeric Silsesquioxane
PSE	Process Systems Engineering
QSPR	Quantitative Structure—Property Relationships
RI-DFT	Resolution of the Identity Density Functional Theory
SCF-IL	Supercritical Fluid-Ionic Liquid
SFB TRR 63	Sonderforschungsbereich Transregio 63
SILP	Supported Ionic Liquid Phase
SLE	Solid-Liquid Equilibrium
TAC	Total Annualized Cost
TMS	Thermomorphic Solvent System
UCST	Upper Critical Solution Temperature
UF	Update Factor
UNIFAC	UNIQUAC Functional-group Activity Coefficients
UNIQUAC	UNIversal QUAsiChemical

Bibliography

[1] http://www2.imm.dtu.dk/projects/dace/.   (cited on Page 99)

[2] http://www.inprompt.tu-berlin.de.   (cited on Page 1)

[3] http://www.epa.gov/ozone/mbr/index.html, 2014.   (cited on Page 78)

[4] D. S. Abrams and J. M. Prausnitz. Statistical thermodynamics of liquid mixtures: a new expression for the excess gibbs energy of partly or completely miscible systems. 21(1), *AIChE Journal*, 1975, pp. 116–128.   (cited on Page 64)

[5] N. D. Austin, N. V. Sahinidis, and D. W. Trahan. A cosmo-based approach to computer-aided mixture design. *Chem. Eng. Sci.*, 2017 159, pp. 93–105.   (cited on Page 141)

[6] A. Bardow, K. Steur, and J. Gross. Continuous-molecular targeting for integrated solvent and process design. 49(6), *Ind. Eng. Chem. Res.*, 2010, pp. 2834–2840.   (cited on Page 141)

[7] A. Behr and C. Fängewisch. Temperature-dependent multicomponent solvent systems–an alternative concept for recycling homogeneous catalysts. 25(2), *Chem. Eng. Technol.*, 2002, pp. 143–147.   (cited on Page 12 and 16)

[8] A. Behr and C. Fängewisch. Rhodium-catalysed synthesis of branched fatty compounds in temperature-dependent solvent systems. *J. Mol. Catal. A: Chem.*, 2003 197(1-2), pp. 115–126.   (cited on Page 17)

[9] A. Behr and L. Johnen. *Alternative Feedstocks for Synthesis*. Wiley-VCH Verlag GmbH & Co. KGaA, 2010. ISBN 9783527628698.   (cited on Page 1 and 9)

[10] A. Behr and P. Neubert. *Applied Homogeneous Catalysis*. Wiley-VCH, 2012. ISBN 3527326332.   (cited on Page 2, 12, and 63)

[11] A. Behr and R. Roll. Hydroaminomethylation in thermomorphic solvent systems. 239(1), *J. Mol. Catal. A: Chem.*, 2005, pp. 180–184.   (cited on Page 17)

[12] A. Behr and R. Roll. Temperaturgesteuerte Mehrkomponenten-lösungsmittelsysteme für homogene übergangsmetallkatalysierte Reaktionen. *Chem. Ing. Tech.*, 2005 77(6), pp. 748–752.   (cited on Page 17, 21, and 61)

[13] A. Behr and A. Wintzer. Baukastensystem zur Auswahl von Lösungsmitteln in homogenkatalytischen Reaktionen. *Chem. Ing. Tech.*, 2011 9, pp. 1356–1370. (cited on Page 22)

[14] A. Behr, G. Henze, L. Johnen, and C. Awungacha. Advances in thermomorphic liquid/liquid recycling of homogeneous transition metal catalysts. 285(1), *J. Mol. Catal. A: Chem.*, 2008, pp. 20–28. (cited on Page 16, 17, 21, 61, and 63)

[15] A. Behr, L. Johnen, and N. Rentmeister. Novel palladium-catalysed hydroamination of myrcene and catalyst separation by thermomorphic solvent systems. 352 (11-12), *Adv. Synth. Catal.*, 2010, pp. 2062–2072. (cited on Page 18)

[16] A. Behr, L. Johnen, and A. J. Vorholt. Telomerization of myrcene and catalyst separation by thermomorphic solvent systems. 2(10), *ChemCatChem*, 2010, pp. 1271–1277. (cited on Page 10 and 18)

[17] A. Behr, Y. Brunsch, and A. Lux. Rhodium nanoparticles as catalysts in the hydroformylation of 1-dodecene and their recycling in thermomorphic solvent systems. *Tetrahedron Lett.*, 2012 53(22), pp. 2680–2683. (cited on Page 2, 10, 11, and 24)

[18] A. Behr, A. Kleyensteiber, and M. Becker. A novel approach to selecting thermomorphic multicomponent solvent systems (tms) for hydroaminomethylation reactions. *Chem. Eng. Process.*, 2013 69, pp. 15–23. (cited on Page 22)

[19] A. Behr, A. J. Vorholt, and N. Rentmeister. Recyclable homogeneous catalyst for the hydroesterification of methyl oleate in thermomorphic solvent systems. 99 (0), *Chem. Eng. Sci.*, 2013, pp. 38–43. (cited on Page 19, 61, and 75)

[20] A. Behr, A. J. Vorholt, and T. Seidensticker. An old friend in a new guise-recent trends in homogeneous transition metal catalysis. *ChemBioEng Rev.*, 2015 2(1), pp. 6–21. (cited on Page 1, 9, and 11)

[21] D. E. Bergbreiter, S. D. Sung, J. Li, D. Ortiz, and P. N. Hamilton. Designing polymers for biphasic liquid/liquid separations after homogeneous reactions. *Org. Process. Res. Dev.*, 2004 8(3), pp. 461–468. (cited on Page 17)

[22] M. Bergez-Lacoste, S. Thiebaud-Roux, P. De Caro, J.-F. Fabre, V. Gerbaud, and Z. Mouloungui. From chemical platform molecules to new biosolvents: Design engineering as a substitution methodology. *Biofuels Bioprod. Bior.*, 2014 8(3), pp. 438–451. (cited on Page 141)

[23] L. T. Biegler, I. E. Grossmann, and A. W. Westerberg. *Systematic methods of chemical design process.* Prentice Hall PTR, 1997. (cited on Page xviii, 48, 114, 116, and 120)

[24] H.-W. Bohnen and B. Cornils. Hydroformylation of alkenes: An industrial view of the status and importance. 47, *Adv. Catal.*, 2002, pp. 1–64.   (cited on Page 10)

[25] B. Bouillot, S. Teychené, and B. Biscans. An evaluation of thermodynamic models for the prediction of drug and drug-like molecule solubility in organic solvents. *Fluid Phase Equilib.*, 2011 309(1), pp. 36–52.   (cited on Page 65)

[26] B. Bouillot, S. Teychené, and B. Biscans. An evaluation of cosmo-sac model and its evolutions for the prediction of drug-like molecule solubility: Part 1. *Ind. Eng. Chem. Res.*, 2013 52(26), pp. 9276–9284.   (cited on Page 65)

[27] B. Bouillot, S. Teychené, and B. Biscans. Discussion and improvement of the refined cosmo-sac parameters for solubility predictions: Part 2. *Ind. Eng. Chem. Res.*, 2013 52(26), pp. 9285–9294.   (cited on Page 65)

[28] Y. Brunsch. *Temperaturgesteuertes Katalysatorrecycling für die homogen katalysierte Hydroformylierung langkettiger Alkene.* PhD thesis, TU Dortmund, Germany, 2013.   (cited on Page 11, 20, 26, 29, 32, 33, 43, 48, 63, 83, and 108)

[29] Y. Brunsch and A. Behr. Temperature-controlled catalyst recycling in homogeneous transition-metal catalysis: Minimization of catalyst leaching. *Angew. Chem. Int. Ed.*, 2013 52(5), pp. 1586–1589.   (cited on Page 11, 20, 26, 29, 40, 53, 67, 74, 84, and 97)

[30] J. Burger, V. Papaioannou, S. Gopinath, G. Jackson, A. Galindo, and C. S. Adjiman. A hierarchical method to integrated solvent and process design of physical co2 absorption using the saft- mie approach. 61(10), *AIChE J.*, 2015, pp. 3249–3269. Cq7ed Times Cited:0 Cited References Count:99.   (cited on Page 141)

[31] J. A. Caballero and I. E. Grossmann. An algorithm for the use of surrogate models in modular flowsheet optimization. 54(10), *AIChE J.*, 2008, pp. 2633–2650.   (cited on Page 95)

[32] C. Capello, U. Fischer, and K. Hungerbühler. What is a green solvent? A comprehensive framework for the environmental assessment of solvents. 9(9), *Green Chem.*, 2007, pp. 927.   (cited on Page 73)

[33] L. M. Casás, B. Orge, C. Díaz, and J. Tojo. Liquid-liquid equilibria for mixtures of methyl acetate+methanol+n-alkane (C10-C12) at several temperatures and 1 atm. *J. Chem. Thermodyn.*, 2004 36(3), pp. 237–243.   (cited on Page 86)

[34] C.-C. Chen and Y. Song. Solubility modeling with a nonrandom two-liquid segment activity coefficient model. *Ind. Eng. Chem. Res.*, 2004 43(26), pp. 8354–8362.   (cited on Page 65)

[35] D. J. Cole-Hamilton. Homogeneous catalysis–new approaches to catalyst separa-
      tion, recovery, and recycling. 299(5613), *Science*, 2003, pp. 1702–1706. (cited on
      Page 13)

[36] B. Cornils and W. A. Herrmann. Concepts in homogeneous catalysis: the indus-
      trial view. 216(1), *J. Catal.*, 2003, pp. 23–31. (cited on Page 11)

[37] A. Cozad, N. V. Sahinidis, and D. C. Miller. Learning surrogate models for
      simulation-based optimization. 60(6), *AIChE J.*, 2014, pp. 2211–2227. Ag1sr
      Times Cited:3 Cited References Count:52. (cited on Page 100)

[38] A. Cozad, N. V. Sahinidis, and D. C. Miller. A combined first-principles and data-
      driven approach to model building. 73, *Comput. Chem. Eng.*, 2015, pp. 116–127.
      (cited on Page 100)

[39] J. Dreimann, P. Lutze, M. Zagajewski, A. Behr, A. Górak, and A. J. Vorholt.
      Highly integrated reactor-separator systems for the recycling of homogeneous cat-
      alysts. *Chem. Eng. Process.*, 2016 99, pp. 124–131. (cited on Page 93 and 94)

[40] J. M. Dreimann, M. Skiborowski, A. Behr, and A. J. Vorholt. Recycling homo-
      geneous catalysts simply by organic solvent nanofiltration: New ways to efficient
      catalysis. 8(21), *ChemCatChem*, 2016, pp. 3330–3333. (cited on Page 93 and 141)

[41] F. Eckert and A. Klamt. COSMOtherm, version C16, COSMOlogic GmbH & Co.
      KG, Leverkusen, Germany, 2016. (cited on Page 66, 69, and 97)

[42] K. Eichkorn, F. Weigend, O. Treutler, and R. Ahlrichs. Auxiliary basis sets for
      main row atoms and transition metals and their use to approximate coulomb
      potentials. 97, *Theor. Chem. Acc.*, 1997, pp. 119–124. (cited on Page 69 and 97)

[43] J. Fang, H. Jin, T. Ruddy, K. Pennybaker, D. Fahey, and B. Subramaniam.
      Economic and environmental impact analyses of catalytic olefin hydroformylation
      in co 2 -expanded liquid (cxl) media. *Ind. Eng. Chem. Res.*, 2007 46(25), pp. 8687–
      8692. (cited on Page 2, 12, 16, 29, and 53)

[44] J. Fang, R. Jana, J. A. Tunge, and B. Subramaniam. Continuous homogeneous hy-
      droformylation with bulky rhodium catalyst complexes retained by nano-filtration
      membranes. 393(1), *Appl. Catal. A-Gen.*, 2011, pp. 294–301. (cited on Page 14)

[45] M. R. Fenske. Fractionation of straight-run pennsylvania gasoline. *Ind. Eng.
      Chem.*, 1932 24(5), pp. 482–485. (cited on Page 108 and 150)

[46] R. Franke, D. Selent, and A. Börner. Applied hydroformylation. *Chem. Rev.*,
      2012 112(11), pp. 5675–5732. (cited on Page 10 and 11)

[47] A. Fredenslund, R. L. Jones, and J. M. Prausnitz. Group-contribution estima-
      tion of activity coefficients in nonideal liquid mixtures. 21(6), *AIChE J.*, 1975,
      pp. 1086–1099. (cited on Page 65)

[48] H. Freund and K. Sundmacher. Towards a methodology for the systematic analysis and design of efficient chemical processes. *Chem. Eng. Process.*, 2008 47(12), pp. 2051–2060.   (cited on Page 7)

[49] H. Freund and K. Sundmacher. *Process Intensification, 2. Phase Level.* Wiley Online Library, 2008.   (cited on Page 26)

[50] H. Freund, A. Peschel, and K. Sundmacher. Model-based reactor design based on the optimal reaction route. 83(4), *Chem. Ing. Tech.*, 2011, pp. 420–426.   (cited on Page 103)

[51] E. R. Gilliland. Multicomponent rectification estimation of the number of theoretical plates as a function of the reflux ratio. *Ind. Eng. Chem.*, 1940 32(9), pp. 1220–1223.   (cited on Page 108 and 150)

[52] E. L. Goetheer, A. W. Verkerk, L. J. van den Broeke, E. de Wolf, B.-J. Deelman, G. van Koten, and J. T. Keurentjes. Membrane reactor for homogeneous catalysis in supercritical carbon dioxide. *J. Catal.*, 2003 219(1), pp. 126–133.   (cited on Page 14)

[53] H. Grensemann and J. Gmehling. Performance of a conductor-like screening model for real solvents model in comparison to classical group contribution methods. *Ind. Eng. Chem. Res.*, 2005 44(5), pp. 1610–1624.   (cited on Page 65)

[54] J. Gross and G. Sadowski. Perturbed-chain saft: An equation of state based on a perturbation theory for chain molecules. *Ind. Eng. Chem. Res.*, 2001 40(4), pp. 1244–1260.   (cited on Page 64, 102, and 141)

[55] J. Gross and J. Vrabec. An equation-of-state contribution for polar components: Dipolar molecules. 52(3), *AIChE J.*, 2006, pp. 1194–1204.   (cited on Page 20 and 35)

[56] K. M. Guthrie. *Data and techniques for preliminary capital cost estimating.* McGraw-Hill, 1969.   (cited on Page 47, 49, 116, 117, 119, and 120)

[57] I. Hahnenkamp, G. Graubner, and J. Gmehling. Measurement and prediction of solubilities of active pharmaceutical ingredients. *Int. J. Pharm.*, 2010 388(1-2), pp. 73–81.   (cited on Page 65)

[58] T. Hamerla, A. Rost, Y. Kasaka, and R. Schomäcker. Hydroformylation of 1-Dodecene with water-soluble rhodium catalysts with bidentate ligands in multiphase systems. *ChemCatChem*, 2013 5(7), pp. 1854–1862.   (cited on Page 15)

[59] C. M. Hansen. *Hansen solubility parameters: a user's handbook.* CRC press, 2007.   (cited on Page 21, 61, and 64)

[60] B. Hentschel, H. Freund, and K. Sundmacher. Modellbasierte Ermittlung der op-
timalen Reaktionsführung für integrierte Mehrphasenprozesse. *Chem. Ing. Tech.*,
2014 86(7), pp. 1080–1087.   (cited on Page 8 and 122)

[61] B. Hentschel, A. Peschel, H. Freund, and K. Sundmacher. Simultaneous design
of the optimal reaction and process concept for multiphase systems. 115, *Chem.
Eng. Sci.*, 2014, pp. 69–87.   (cited on Page 8, 26, 29, 31, 32, 35, 37, 40, 42, 44, 45, 48, 50,
52, 57, 94, 103, 106, 108, 120, and 130)

[62] B. Hentschel, G. Kiedorf, M. Gerlach, C. Hamel, A. Seidel-Morgenstern, H. Fre-
und, and K. Sundmacher. Model-based identification and experimental validation
of the optimal reaction route for the hydroformylation of 1-dodecene. *Ind. Eng.
Chem. Res.*, 2015 54(6), pp. 1755–1765.   (cited on Page xiv, xviii, 8, 26, 32, 88, 102,
103, 131, 133, 146, and 147)

[63] U. Hintermair, G. Zhao, C. C. Santini, M. J. Muldoon, and D. J. Cole-Hamilton.
Supported ionic liquid phase catalysis with supercritical flow. (14), *Chem. Com-
mun.*, 2007, pp. 1462–1464.   (cited on Page 14)

[64] U. Hintermair, Z. Gong, A. Serbanovic, M. J. Muldoon, C. C. Santini, and D. J.
Cole-Hamilton. Continuous flow hydroformylation using supported ionic liquid
phase catalysts with carbon dioxide as a carrier. 39(36), *Dalton Trans.*, 2010,
pp. 8501.   (cited on Page 14)

[65] U. Hintermair, G. Franciò, and W. Leitner. A fully integrated continuous-flow
system for asymmetric catalysis: Enantioselective hydrogenation with supported
ionic liquid phase catalysts using supercritical CO_2 as the mobile phase. *Chem.-
Eur. J.*, 2013 19(14), pp. 4538–4547.   (cited on Page 14)

[66] H. Hugl and M. Nobis. Multiphase catalysis in industry. , *Topics in Organometal-
lic Chemistry*, 2006, pp. 1–17.   (cited on Page 21)

[67] M. Janssen, J. Wilting, C. Müller, and D. Vogt. Continuous rhodium-catalyzed
hydroformylation of 1-octene with polyhedral oligomeric silsesquioxanes (POSS)
enlarged triphenylphosphine. *Angew. Chem. Int. Edit.*, 2010 49(42), pp. 7738–
7741.   (cited on Page 15)

[68] R. Jennerjahn, I. Piras, R. Jackstell, R. Franke, K.-D. Wiese, and M. Beller.
Palladium-catalyzed isomerization and hydroformylation of olefins. *Chem.-Eur.
J.*, 2009 15(26), pp. 6383–6388.   (cited on Page 10)

[69] N. M. Kaiser, R. J. Flassig, and K. Sundmacher. Probabilistic reactor design in
the framework of elementary process functions. *Comput. Chem. Eng.*, 2016 94,
pp. 45–59.   (cited on Page 8, 26, and 142)

[70] G. Kiedorf, D. Hoang, A. Müller, A. Jörke, J. Markert, H. Arellano-Garcia,
A. Seidel-Morgenstern, and C. Hamel. Kinetics of 1-dodecene hydroformylation

in a thermomorphic solvent system using a rhodium-biphephos catalyst. *Chem. Eng. Sci.*, 2014 115, pp. 31–48.   (cited on Page 26, 29, 32, 33, 52, and 102)

[71] A. Klamt. Conductor-like screening model for real solvents: A new approach to the quantitative calculation of solvation phenomena. *J. Phys. Chem.-US*, 1995 99 (7), pp. 2224–2235.   (cited on Page 62 and 64)

[72] A. Klamt. *COSMO-RS From Quantum Chemistry to Fluid Phase Thermodynamics and Drug Design.* Elsevier B.V., 2005.   (cited on Page 65, 69, and 71)

[73] A. Klamt. The COSMO and COSMO-RS solvation models. *Wiley Interdisciplinary Reviews: Computational Molecular Science*, 2011 1(5), pp. 699–709.   (cited on Page 65)

[74] A. Klamt and G. Schüürmann. COSMO: a new approach to dielectric screening in solvents with explicit expressions for the screening energy and its gradient. (5), *J. Chem. Soc. Perk. T. 2*, 1993, pp. 799–805.   (cited on Page 64)

[75] A. Klamt, F. Eckert, and W. Arlt. COSMO-RS: An alternative to simulation for calculating thermodynamic properties of liquid mixtures. 1, *Annu. Rev. Chem. Biomol. Eng.*, 2010, pp. 101–122.   (cited on Page 15 and 97)

[76] J. P. Kleijnen. Kriging metamodeling in simulation: A review. *Eur. J. Oper. Res.*, 2009 192(3), pp. 707–716.   (cited on Page 95)

[77] C. W. Kohlpaintner, R. W. Fischer, and B. Cornils. Aqueous biphasic catalysis: Ruhrchemie/rhône-poulenc oxo process. *Appl. Catal., A.*, 2001 221(1-2), pp. 219–225.   (cited on Page 13)

[78] G. Koller, U. Fischer, and K. Hungerbühler. Assessing safety, health, and environmental impact early during process development. *Ind. Eng. Chem. Res.*, 2000 39(4), pp. 960–972.   (cited on Page 73)

[79] D. G. Krige. A statistical approach to some mine valuations and allied problems at the witwatersrand. Masters thesis, University of Witwatersrand, South Africa, 1951.   (cited on Page 95)

[80] T. E. Kunene, P. B. Webb, and D. J. Cole-Hamilton. Highly selective hydroformylation of long-chain alkenes in a supercritical fluid ionic liquid biphasic system. 13(6), *Green Chem.*, 2011, pp. 1476.   (cited on Page 14)

[81] K. Kunna, C. Müller, J. Loos, and D. Vogt. Aqueous-phase hydroformylation of 1-octene: Styrene latices as phase-transfer agents. *Angew. Chem. Int. Ed.*, 2006 45(43), pp. 7289–7292.   (cited on Page 15)

[82] M. Lampe, M. Stavrou, H. M. Bäcker, J. Gross, and A. Bardow. Simultaneous optimization of working fluid and process for organic rankine cycles using PC-SAFT. 53(21), *Ind. Eng. Chem. Res.*, 2014, pp. 8821–8830.   (cited on Page 141)

[83] M. Lampe, M. Stavrou, J. Schilling, E. Sauer, J. Gross, and A. Bardow. Computer-aided molecular design in the continuous-molecular targeting framework using group-contribution PC-SAFT. 81, *Comput. Chem. Eng.*, 2015, pp. 278–287. (cited on Page 141)

[84] S.-T. Lin and S. I. Sandler. A priori phase equilibrium prediction from a segment contribution solvation model. *Ind. Eng. Chem. Res.*, 2002 41(5), pp. 899–913. (cited on Page 65)

[85] P. Lutze, R. Gani, and J. M. Woodley. Process intensification: A perspective on process synthesis. *Chem. Eng. Process.*, 2010 49(6), pp. 547–558. (cited on Page 1)

[86] J. Markert, Y. Brunsch, T. Munkelt, G. Kiedorf, A. Behr, C. Hamel, and A. Seidel-Morgenstern. Analysis of the reaction network for the rh-catalyzed hydroformylation of 1-dodecene in a thermomorphic multicomponent solvent system. *Appl. Catal. A-Gen.*, 2013 462-463, pp. 287–295. (cited on Page 26 and 102)

[87] K. McBride and K. Sundmacher. Computer-aided design of solvents for the recovery of a homogeneous catalyst used for alkene hydroformylation. , *Computer Aided Chemical Engineering*, 2015, pp. 2075–2080. (cited on Page 95)

[88] K. McBride and K. Sundmacher. Data driven conceptual process design for the hydroformylation of 1-Dodecene in a thermomorphic solvent system. *Ind. Eng. Chem. Res.*, 2015 54(26), pp. 6761–6771. (cited on Page xiii, xiv, xvii, 2, 33, 34, 36, 37, 39, 41, 42, 56, 57, 58, and 108)

[89] K. McBride, T. Gaide, A. Vorholt, A. Behr, and K. Sundmacher. Thermomorphic solvent selection for homogeneous catalyst recovery based on COSMO-RS. *Chem. Eng. Process.*, 2016 99, pp. 97–106. (cited on Page xiv, 63, 69, and 84)

[90] K. McBride, N. M. Kaiser, and K. Sundmacher. Integrated reaction-extraction process for the hydroformylation of long-chain alkenes with a homogeneous catalyst. *Comput. Chem. Eng.*, 2016 . (cited on Page xiv, xv, xviii, 95, 98, 101, 102, 105, 106, 107, 111, 122, 127, and 128)

[91] Y. K. Molokanov, N. I. Mazurina, G. A. Nikiforov, and T. P. Korablina. Approximation method for calculating basic parameters of multicomponent fractionation. 12(2), *Int. Chem. Eng.*, 1972, pp. 209–212. (cited on Page 108 and 150)

[92] M. Müller, Y. Kasaka, D. Müller, R. Schomäcker, and G. Wozny. Process design for the separation of three liquid phases for a continuous hydroformylation process in a miniplant scale. *Ind. Eng. Chem. Res.*, 2013 52(22), pp. 7259–7264. (cited on Page 15)

[93] H. Nowothnick, A. Rost, T. Hamerla, R. Schomäcker, C. Müller, and D. Vogt. Comparison of phase transfer agents in the aqueous biphasic hydroformylation of higher alkenes. 3(3), *Catal. Sci. Technol.*, 2013, pp. 600–605. (cited on Page 15)

[94] F. Pereira, E. Keskes, A. Galindo, G. Jackson, and C. Adjiman. Integrated solvent and process design using a saft-vr thermodynamic description: High-pressure separation of carbon dioxide and methane. *Comput. Chem. Eng.*, 2011 35(3), pp. 474–491. (cited on Page 141)

[95] A. Peschel, H. Freund, and K. Sundmacher. Systematik zur modellgestützten Ermittlung der optimalen Reaktionsführung am Beispiel der SO_2-Oxidation. 81 (8), *Chem. Ing. Tech.*, 2009, pp. 1096–1097. (cited on Page 8)

[96] A. Peschel, H. Freund, and K. Sundmacher. Methodology for the design of optimal chemical reactors based on the concept of elementary process functions. 49(21), *Ind. Eng. Chem. Res.*, 2010, pp. 10535–10548. (cited on Page 8)

[97] A. Peschel, B. Hentschel, H. Freund, and K. Sundmacher. Design of optimal multiphase reactors exemplified on the hydroformylation of long chain alkenes. 188, *Chem. Eng. J.*, 2012, pp. 126–141. (cited on Page 8)

[98] A. Peschel, A. Jörke, K. Sundmacher, and H. Freund. Optimal reaction concept and plant wide optimization of the ethylene oxide process. *Chem. Eng. J.*, 2012 207-208, pp. 656–674. (cited on Page 8 and 26)

[99] T. Pogrzeba, D. Müller, T. Hamerla, E. Esche, N. Paul, G. Wozny, and R. Schomäcker. Rhodium-catalyzed hydroformylation of long-chain olefins in aqueous multiphase systems in a continuously operated miniplant. *Ind. Eng. Chem. Res.*, 2015 54(48), pp. 11953–11960. (cited on Page 15)

[100] J. Pospech, I. Fleischer, R. Franke, S. Buchholz, and M. Beller. Alternative Metalle für die homogen katalysierte Hydroformylierung. *Angew. Chem.*, 2013 125(10), pp. 2922–2944. (cited on Page 11)

[101] A. Pozarska, C. da Costa Mathews, M. Wong, and K. Pencheva. Application of COSMO-RS as an excipient ranking tool in early formulation development. *Eur. J. Pharm. Sci.*, 2013 49(4), pp. 505–511. (cited on Page 65)

[102] N. Quirante, J. Javaloyes, and J. A. Caballero. Rigorous design of distillation columns using surrogate models based on kriging interpolation. , *AIChE J.*, 2015, pp. 2169–2187. (cited on Page 95)

[103] D. Rappoport and F. Furche. Property-optimized Gaussian basis sets for molecular response calculations. 133(13), *J. Chem. Phys.*, 2010, pp. 134105. (cited on Page 97)

[104] H. Renon and J. M. Prausnitz. Local compositions in thermodynamic excess functions for liquid mixtures. 14(1), *AIChE J.*, 1968, pp. 135–144.   (cited on Page 64)

[105] H. Renon and J. M. Prausnitz. Estimation of parameters for the NRTL equation for excess gibbs energies of strongly nonideal liquid mixtures. *Ind. Eng. Chem. Proc. D. D.*, 1969 8(3), pp. 413–419.   (cited on Page 64)

[106] A. Riisager, R. Fehrmann, M. Haumann, and P. Wasserscheid. Supported ionic liquid phase (SILP) catalysis: An innovative concept for homogeneous catalysis in continuous fixed-bed reactors. *Eur. J. Inorg. Chem.*, 2006 2006(4), pp. 695–706. (cited on Page 14)

[107] A. Rost, M. Müller, T. Hamerla, Y. Kasaka, G. Wozny, and R. Schomäcker. Development of a continuous process for the hydroformylation of long-chain olefins in aqueous multiphase systems. *Chem. Eng. Process.*, 2013 67, pp. 130–135.   (cited on Page 15)

[108] A. Schäfer, C. Huber, and R. Ahlrichs. Fully optimized contracted gaussian basis sets of triple zeta valence quality for atoms li to kr. 100, *J. Chem. Phys.*, 1994, pp. 5829–5835.   (cited on Page 69)

[109] E. Schäfer and G. Sadowski. Liquid-liquid equilibria of systems with linear aldehydes. experimental data and modeling with PCP-SAFT. *Ind. Eng. Chem. Res.*, 2012 51(44), pp. 14525–14534.   (cited on Page xiv, 33, 35, 97, and 98)

[110] E. Schäfer, Y. Brunsch, G. Sadowski, and A. Behr. Hydroformylation of 1-dodecene in the thermomorphic solvent system dimethylformamide/decane. *Ind. Eng. Chem. Res.*, 2012 51(31), pp. 10296–10306.   (cited on Page 20, 21, 24, 26, 29, 33, 35, 40, 79, and 87)

[111] J. Scheffczyk, L. Fleitmann, A. Schwarz, M. Lampe, A. Bardow, and K. Leonhard. COSMO-CAMD: A framework for optimization-based computer-aided molecular design using COSMO-RS. *Chem. Eng. Sci.*, 2017 159, pp. 84–92.   (cited on Page 91 and 141)

[112] M. Schwarze, J. Milano-Brusco, V. Strempel, T. Hamerla, S. Wille, C. Fischer, W. Baumann, W. Arlt, and R. Schomäcker. Rhodium catalyzed hydrogenation reactions in aqueous micellar systems as green solvents. 1(3), *RSC Adv.*, 2011, pp. 474–483.   (cited on Page 15)

[113] M. Schwarze, M. Schmidt, L. A. T. Nguyen, A. Drews, M. Kraume, and R. Schomäcker. Micellar enhanced ultrafiltration of a rhodium catalyst. 421-422(0), *J. Membr. Sci.*, 2012, pp. 165–171.   (cited on Page 15)

[114] K.-C. Song, J. Y. Baek, J. A. Bae, J.-H. Yim, Y. S. Ko, D. H. Kim, Y.-K. Park, and J.-K. Jeon. Octene hydroformylation by using rhodium complexes tethered

onto selectively functionalized mesoporous silica and in situ high pressure IR study. 164(1), *Catal. Today*, 2011, pp. 561–565.   (cited on Page 14)

[115] M. Stavrou, M. Lampe, A. Bardow, and J. Gross.   Continuous molecular targeting–computer-aided molecular design (CoMT–CAMD) for simultaneous process and solvent design for CO_2 capture. 53(46), *Ind. Eng. Chem. Res.*, 2014, pp. 18029–18041. Au0jj Times Cited:0 Cited References Count:75.   (cited on Page 141)

[116] F. Steyer, D. Flockerzi, and K. Sundmacher. Equilibrium and rate-based approaches to liquid-liquid phase splitting calculations. 30(2), *Comput. Chem. Eng.*, 2005, pp. 277–284.   (cited on Page 30 and 38)

[117] B. Subramaniam, R. V. Chaudhari, A. S. Chaudhari, G. R. Akien, and Z. Xie. Supercritical fluids and gas-expanded liquids as tunable media for multiphase catalytic reactions. 115, *Chem. Eng. Sci.*, 2014, pp. 3–18.   (cited on Page 16)

[118] H.-H. Tung, J. Tabora, N. Variankaval, D. Bakken, and C.-C. Chen. Prediction of pharmaceutical solubility via NRTL-SAC and COSMO-SAC. *J. Pharm. Sci.*, 2008 97(5), pp. 1813–1820.   (cited on Page 65)

[119] TURBOMOLE. V6.5, Program packager for ab initio electronic structure calculations, COSMOlogic GmbH & Co. KG, Leverkusen, Germany, 2013.   (cited on Page 69 and 97)

[120] A. Underwood. Theory and practice ot testing stills. 10, *Trans. Inst. Chem. Eng.*, 1932, pp. 112–158.   (cited on Page 42, 108, and 150)

[121] A. Underwood. Fractional distillation of multicomponent mixtures. 44(8), *Chem. Eng. Prog*, 1948, pp. 603–614.   (cited on Page 42, 108, and 150)

[122] L. J. P. van den Broeke, E. L. V. Goetheer, A. W. Verkerk, E. de Wolf, B.-J. Deelman, G. van Koten, and J. T. F. Keurentjes. Homogeneous reactions in supercritical carbon dioxide using a catalyst immobilized by a microporous silica membrane. 40(23), *Angew. Chem. Int. Ed.*, 2001, pp. 4473–4474. (cited on Page 14)

[123] R. van Duren, J. I. van der Vlugt, H. Kooijman, A. L. Spek, and D. Vogt. Platinum-catalyzed hydroformylation of terminal and internal octenes. (10), *Dalton Trans.*, 2007, pp. 1053–1059.   (cited on Page 11)

[124] A. Vorholt, P. Neubert, and A. Behr. Katalytische Funktionalisierungen von Oleylalkohol in thermomorphen Lösungsmittelsystemen zur Synthese potenzieller Biotenside und -Monomere. *Chem. Ing. Tech.*, 2013 , pp. 1540–1547.   (cited on Page 19)

[125] P. B. Webb, M. F. Sellin, T. E. Kunene, S. Williamson, A. M. Z. Slawin, and D. J. Cole-Hamilton. Continuous flow hydroformylation of alkenes in supercritical fluid–ionic liquid biphasic systems. *J. Am. Chem. Soc.*, 2003 125(50), pp. 15577–15588.   (cited on Page 14)

[126] U. Weidlich and J. Gmehling. A modified UNIFAC model. 1. prediction of VLE, h^e, and γ^∞. 26, *Ind. Eng. Chem. Res.*, 1987, pp. 1372–1381.   (cited on Page 31, 35, 64, 65, and 96)

[127] K. Wichmann and A. Klamt. *Drug Solubility and Reaction Thermodynamics*, pages 457–476. John Wiley & Sons, Inc., 2010. ISBN 9780470882221.   (cited on Page 66)

[128] K.-D. Wiese and D. Obst. Hydroformylation. , *Catalytic Carbonylation Reactions*, 2006, pp. 1–33.   (cited on Page 11)

[129] Z. Xie, J. Fang, B. Subramaniam, S. K. Maiti, W. Snavely, and J. A. Tunge. Enhanced hydroformylation by carbon dioxide-expanded media with soluble rh complexes in nanofiltration membrane reactors. *AIChE J.*, 2013 59(11), pp. 4287–4296.   (cited on Page 16)

[130] Z. Xie, G. R. Akien, B. R. Sarkar, B. Subramaniam, and R. V. Chaudhari. Continuous hydroformylation with phosphine-functionalized polydimethylsilox-ane rhodium complexes as nanofilterable homogeneous catalysts. 54(43), *Ind. Eng. Chem. Res.*, 2015, pp. 10656–10660.   (cited on Page 15)

[131] C. Yaws. *Chemical Properties Handbook: Physical, Thermodynamics, Environmental Transport, Safety & Health Related Properties for Organic & Inorganic Chemical.* McGraw-Hill Professional, 1ˢᵗ edition, 1998.   (cited on Page xviii, 45, 99, 112, and 145)

[132] K. Ye. *Process design based on CO_2-expanded liquids as solvents.* PhD thesis, Otto-von-Guericke-Universität Magdeburg, 2013.   (cited on Page 35)

[133] M. Zagajewski, A. Behr, P. Sasse, and J. Wittmann. Continuously operated miniplant for the rhodium catalyzed hydroformylation of 1-dodecene in a thermomorphic multicomponent solvent system (TMS). *Chem. Eng. Sci.*, 2013 115, pp. 88–94.   (cited on Page 63)

[134] M. Zagajewski, J. Dreimann, and A. Behr. Verfahrensentwicklung vom Labor zur Miniplant: Hydroformylierung von 1-Dodecen in thermomorphen Lösungsmittelsystemen. *Chem. Ing. Tech.*, 2014 86(4), pp. 449–457.   (cited on Page 106)

[135] T. Zhou, K. McBride, X. Zhang, Z. Qi, and K. Sundmacher. Integrated solvent and process design exemplified for a diels-alder reaction. *AIChE J.*, 2014 61(1), pp. 147–158.   (cited on Page 142)

[136] T. Zhou, J. Wang, K. McBride, and K. Sundmacher. Optimal design of solvents for extractive reaction processes. 62(9), *AIChE J.*, 2016, pp. 3238–3249. (cited on Page 142)

[137] T. Zhou, Y. Zhou, and K. Sundmacher. A hybrid stochastic–deterministic optimization approach for integrated solvent and process design. 159, *Chem. Eng. Sci.*, 2017, pp. 207–216. (cited on Page 142)

I hereby declare that this work is original and was conducted independently by myself using the methods and sources listed above and that no part of this thesis has been submitted to another degree granting institution

Magdeburg, the 1$^{\text{st}}$ of June in the year 2017.